PLANT GROWTH AND DEVELOPMENT UNDER EXPERIMENTAL TRANSPARENT
PHOTOVOLTAIC AND RED-FLUORESCENT GREENHOUSE COVERINGS

By

Eric Joseph Stallknecht

A DISSERTATION

Submitted to
Michigan State University
in partial fulfillment of the requirements
for the degree of

Horticulture – Doctor of Philosophy

2023

ABSTRACT

While greenhouse design varies in sophistication, all greenhouses utilize covers that transmit photosynthetically active radiation (PAR; 400–700 nm) to crops grown inside. These covering materials can have different transmission characteristics including spectral distribution, photosynthetic photon flux density (PPFD; 400–700 nm), and diffuseness (i.e., light scattering). Such characteristics can independently or interactively impact the growth and development of greenhouse crops. There is increasing interest in developing and integrating advanced greenhouse covers with 1) photovoltaic (PV) materials that generate electricity to power mechanical equipment or provide an additional, passive income source for growers; and 2) fluorescent pigments that alter the solar spectrum to potentially increase crop growth and yield. Despite their potential, their short- and long-term effects on greenhouse crop yield and quality are largely unknown. Thus, the objective of this research was to evaluate the growth, flowering, and fruiting of economically important greenhouse crops under experimental transparent PV panels and red-fluorescent covers to inform further development and ultimately application in greenhouse-based horticulture.

The integration of PV panels in agriculture, commonly referred to as "agrivoltaics", is a possible solution to concurrently address the rising global energy and food demand while considering land-use efficiency. As PV materials have developed technologically, they can now be designed to selectively transmit PAR and potentially be integrated into greenhouse structures. However, a tradeoff is created where PV materials and plants compete for the same resource – solar energy. The tradeoffs of PV panel absorption (for electricity generation) and transmission (for plant growth) of various light wavebands are not well understood. Therefore, we evaluated the effects of neutral-density and experimental, photoselective PV materials that primarily absorbed photons between 400 and 850 nm on commercially important crop types of leafy greens, culinary herbs, fruiting crops, and floriculture crops. Regardless of the transmitted photon distribution, the best predictor of crop yield and quality was the average daily light integral (DLI; 400–700 nm). Over multiple years of research, leafy greens, culinary herbs, and floriculture crops exhibited greater tolerance to PV shading than fruiting crops and therefore have the greatest potential for cultivation in agrivoltaic systems. In contrast, PV shading decreased the yield of fruiting crops. Our findings collectively suggest that PV panels with the greatest PAR transmission (i.e., primarily absorb photons <400 and >700 nm) are the most suitable for greenhouse applications.

At the same PPFD, decreasing the intensity of blue (B; 400–499 nm) and green (G; 500–599 nm) light and increasing the intensity of red (R; 600–699 nm) light can potentially increase plant biomass accumulation. This can be attributed to a higher photosynthetic efficiency of R light compared to B and G light, as well as greater leaf expansion and photon interception in a low B-light environment. Spectrum-shifting films absorb B and G light and amplify R light, and to a lesser extent, far-red (FR; 700–750 nm) light. However, this spectral conversion decreases the transmitted PPFD. Our objective was to determine whether a red-fluorescent material would increase biomass accumulation of various greenhouse crops despite the reduction in DLI. In an initial study, a red-fluorescent material increased the shoot fresh mass (SFM) of lettuce (*Lactuca sativa*) by up to 45%, depending on cultivar, compared to a neutral-density (unpigmented) plastic with a 10–25% higher transmitted PPFD. Cultivars with the greatest increase in SFM also had greater leaf area, projected canopy area, and/or plant diameter. In a second study, a red-fluorescent material increased the SFM of lettuce by 17–27% compared to a neutral-density plastic with a similar transmitted DLI, but this effect was not consistent among fruiting or floriculture crops. These experimental results enhance our understanding of the interplay between light quality and intensity on crop growth and opportunities and limitations of using red-fluorescent plastics and transparent PV panels in greenhouse horticulture.

ACKNOWLEDGEMENTS

TABLE OF CONTENTS

SECTION I: OPPORTUNITIES AND CHALLENGES WITH ADVANCED

GREENHOUSE GLAZING MATERIALS

Opportunities and challenges with advanced greenhouse glazing materials

E.J. Stallknecht and E.S. Runkle[a]

Department of Horticulture, Michigan State University, East Lansing, MI, USA

[a]E-mail: runkleer@msu.edu

Keywords: agrivoltaics, diffuse glazing, photoselective films, photovoltaics, spectral-shifting films, ultraviolet-transparent films, waveband-selective films

Abstract

Greenhouse glazing is critical for extending growing seasons and protecting high-value horticultural crops from adverse environmental conditions such as excessive rainfall and low temperatures. Traditionally, greenhouse glazing was made of glass, but newer photostable plastics such as acrylic, polyethylene, and polycarbonate are now the most widely used greenhouse glazing materials. The technological advancement of plastic tensile strength and lifespan has also facilitated the incorporation of other types of plastic additives that can increase light scattering (diffuseness), improve insulation, reduce condensation formation, and alter transmission spectrum, which broaden glazing application and utility. Each greenhouse glazing material will have various combinations of these properties (i.e., different additives) and come with unique opportunities and challenges for a particular crop or location. Here, we review several of the current and futuristic greenhouse glazing technologies, focusing on their optical properties and how they can influence crop growth as well as the greenhouse environment. Among particular interest are diffuse, waveband-selective, spectral-shifting, and photovoltaic materials. These have the potential to advance the greenhouse industry by increasing crop yield and quality and possibly even create dual-purpose structures capable of generating renewable energy. However, these materials often also have trade-offs such as decreases in photosynthetically active radiation and increased capital cost.

Diffuse greenhouse materials

Diffusion occurs when largely unidirectional photons reflect off a surface and deviate from their initial trajectory, scattering them in many different directions (Fig. I-1A). The scattering of photons increases light uniformity inside a greenhouse by decreasing the intensity of shadows created by objects in a greenhouse or the greenhouse macrostructure. Diffusiveness is typically increased in an environment by seasonally applied whitewash (a shading compound applied to the exterior of a greenhouse), the incorporation of plastic additives, or through the etching or

imprinting of structures onto plastic or glass (Hemming et al., 2008b, 2014; Shen et al., 2021) (Fig. I-1A, B). Diffuse materials are commonly referred to as being "hazy" because they are not translucent like traditional greenhouse glass, but rather have differing degrees of opaqueness, with increased opaqueness corresponding to increased diffusiveness (i.e., increased haze). Haze is a unitless measure defined as the percentage of transmitted photons that deviate by more than 2.5 degrees from the direction of the incident light source (ASTM, 2003). While diffusion increases light uniformity, Hemming et al. (2008b, 2014) reported a linear correlation between increased haze and decreased light transmission for diffuse plastic, glass, and temporal coatings (Fig. I-1c). Similarly, Zhen and Bugbee (2019) reported photosynthetic photon flux density (PPFD; 400–700 nm; unit of $\mu mol \cdot m^{-2} \cdot s^{-1}$) decreased by 1 to 20% depending on the type of light diffusion panel used. Thus, increasing haze can decrease the PPFD at canopy surface, but the degree of reduction will depend on the base material, the method of diffusion, and possible secondary applications of anti-reflection treatments. Importantly, through the technological development of diffuse greenhouse materials over the past twenty years, overall transmission has increased substantially. Newer materials with an arbitrarily selected 50% haze can now have transmissions as high as ~88%, which corresponds to ~4% lower transmission than non-diffuse glass (Hemming et al., 2008b, 2014).

Opportunities

Use of diffuse glazing materials can be especially useful in the production of vertical crops including tomato (*Solanum lycopersicum*) and cucumber (*Cucumis sativus*). Vertically oriented crops create a dense-canopy environment where leaves proximal to the shoot tip shade more distal ones. Thus, each plant has a progressively greater leaf area index (LAI; unit leaf surface area per unit ground surface area) as a function of time until it reaches a plateau. Diffuse light can penetrate deeper into dense-crop canopies and increase the photosynthetic rate in lower-canopy leaves, which increases whole-plant photosynthesis (Tubiello et al., 1997; Hemming et al., 2008a; Zhen and Bugbee, 2019). During periods of high solar radiation (e.g., PPFD = 1500–2000 $\mu mol \cdot m^{-2} \cdot s^{-1}$), a decrease in the PPFD at the top of the canopy usually has negligible effects on photosynthesis because the quantum yield of photosynthesis (Φ_{PSII}; mol CO_2 fixed/O_2 evolved per mol photon absorbed) is typically close to saturation (Fig. I-1D) (Weaver and van Iersel, 2019). The scattering of light to leaves lower in the canopy that are less photosynthetically saturated increase whole-plant Φ_{PSII} and therefore the radiation-use efficiency (RUE; biomass per mol absorbed light) of a

3

crop (Tubiello et al., 1997; Zhen and Bugbee, 2019). As a result, diffuse materials have increased cucumber yield by 8–10% and tomato yield by 7–9% (Dueck et al., 2012; Holsteens et al., 2020). Diffuse greenhouse materials act similarly to intra-canopy supplemental lighting that increases cucumber yield but without the input of electrical energy (Hovi et al., 2004). Additionally, diffuse materials can increase crop water-use efficiency (WUE; carbon assimilated per unit water) and decrease air temperature inside greenhouses, which can increase crop production by preventing the thermal deactivation of ribulose 1,5-bisphosphate carboxylase/oxygenase (Rubisco) or increase the crop quality of flowering plants such as cut roses (*Rosa hybrida*) (Sharkey, 2005; Kempkes et al., 2012).

Challenges

Although diffuse greenhouse materials have targeted applications for vertically grown fruiting crops, there is less experimental data suggesting they increase growth and yield of short-stature crops such as leafy greens and floriculture crops that have a comparably lower LAI (Zhen and Bugbee, 2019; Cozzolino et al., 2020). While the best light-scattering materials have a minimal decrease in transmission, lower-quality and less expensive diffuse materials can have substantially lower transmission values, in addition to transmission losses caused by increasing haze percentage. Decreased transmission could negatively impact crop yield and quality in light-limited environments, such as temperate regions from late fall to early spring (Baeza and López, 2012). Another potential limitation of macro- or micro-structures on glass or plastic that diffuse light is the accumulation of dust on the exterior of the glazing, which decreases light transmission unless periodically cleaned (Baeza and López, 2012). Application of an anti-reflective treatment can increase the transmission of diffuse glass, but some coatings can slightly alter the transmission spectrum and possibly modify crop morphology (Kempkes et al., 2012; Hemming et al., 2014). A change to the transmission spectrum depends on the chemical composition of the anti-reflective coating. Some coatings absorb more blue (B; 400–500 nm) and green (G; 500–600 nm) light, while others absorb a disproportionate percentage of red (R; 600–700 nm) and far-red (FR; 700–800 nm) light. Finally, although diffuse materials are being increasingly used, they are often more expensive than similar but non-diffuse materials.

Ultraviolet-transparent materials

Unlike greenhouse glass that can transmit ultraviolet (UV) radiation without degradation, greenhouse plastics (e.g., acrylic, polyethylene, and polycarbonate) typically incorporate

4

stabilizers that absorb or reflect ultraviolet-A (UV-A; 315–400 nm) and ultraviolet-B (UV-B; 280–315 nm) radiation to extend their effective lifespan (Yousif and Haddad, 2013). UV stabilizers and absorbers increase the lifespan of plastics by dissipating high-energy photons into low-level heat, ensuring UV photons do not disrupt the chemical bonding of the plastic polymers (i.e., photooxidative degradation) (Yousif and Haddad, 2013). While UV-transparent materials may have greater transmission of biologically active radiation (280–800 nm) than UV-opaque plastics, they do not increase transmission in the traditional or extended wavebands of photosynthetically active radiation (PAR and ePAR; 400–700 nm and 400–750 nm, respectively) (Fig. I-2A). Consequently, while different species have varying Φ_{PSII} for UV photons, UV photons have a negligible effect on photosynthesis of individual leaves (McCree, 1971; Tsormpatsidis et al., 2010). Rather, UV-transparent materials indirectly affect whole-plant/crop photosynthesis by altering crop morphology (i.e., photon interception) and/or leaf characteristics such as pigmentation (i.e., photoprotection) (Tsormpatsidis et al., 2010). The photoreceptors UV RESISTANCE LOCUS 8 (UVR8), phototropins (PHOT), cryptochromes (CRY), and zeitlupes absorb UV radiation (and blue light) and mediate physiological and morphological responses (Fig. I-2B). UVR8 primarily absorbs UV-B while PHOT and CRY primarily absorb UV-A radiation. While UV-transparent greenhouse materials are less common than plastics that block UV transmission, they offer unique opportunities for some horticultural crops.

Opportunities

Crops such as red-leaf lettuce (*Lactuca sativa*) and purple-leaf fountain grass (*Pennisetum setaceum* 'Rubrum') derive much of their consumer appeal from high concentrations of secondary metabolites including anthocyanins, which give a red color to their leaves (Quintero-Arias et al., 2021). Anthocyanin biosynthesis is stimulated by UV radiation through the UV- and B-absorbing UVR8, PHOT, and CRY photoreceptors (Kang et al., 2008; Wu et al., 2016). As such, UV-transparent materials can increase leaf pigmentation and crop quality, thus increasing their value (Tsormpatsidis et al., 2008; Quintero-Arias et al., 2021). Additionally, secondary metabolites including flavonoids and anthocyanins have nutritional benefits to humans (Tsormpatsidis et al., 2008; Behn et al., 2010). Therefore, UV-transparent materials could also increase the nutritional density and flavor of some crops consumed for their foliage. Greater transmission of UV radiation can also inhibit extension growth, creating more compact plants with smaller leaves and shorter stems (Behn et al., 2010). Compact floriculture crops enable greater crop density during production

and are generally easier to transport to market. Finally, insects also have CRY photoreceptors that influence their ability to navigate (Raviv and Antignus, 2004; Chaves et al., 2011). Thus, UV-transparent materials can improve the navigation of beneficial pollinator species and increase fertilization of fruiting vegetable and fruit crops (Parrish et al., 2021).

Challenges

While UV-transparent materials usually increase leaf pigmentation and sometimes other quality parameters of plants, these materials also inhibit extension growth, which can decrease yield. A decrease in growth and yield under UV-transparent materials could be caused by a decrease in photon interception from a decrease in leaf surface area as well as from greater photoprotective pigments (e.g., anthocyanins) that absorb some of the light useful for photosynthesis (Tsormpatsidis et al., 2010). While quantifying increases to flavonoids is straightforward, whether consumers prefer increased flavonoid concentrations is not clear. To complicate matters, the magnitude of UV-transparent materials on morphological changes are not always consistent and depend on species, cultivar, and other environmental factors (Tsormpatsidis et al., 2008; Behn et al., 2010; Quintero-Arias et al., 2021).

Similar to how UV radiation can disrupt the chemical bonding of plastic polymers, it can also disrupt the chemical bonding of important organic molecules in humans such as nucleic acids, leading to certain skin cancers (El-Yazbi and Loppnow, 2014). Laborers working in UV-transparent environments will require additional personal protective equipment. Plastic equipment inside greenhouses may not last as long when exposed to higher doses of UV radiation. Despite UV-transparent materials aiding in the navigation of beneficial pollinator species, they can also improve the navigation of insect pests such as western flower thrips (*Frankliniella occidentalis*) (Raviv and Antignus, 2004; Chaves et al., 2011; Kigathi and Poehling, 2012). Additionally, UV-transparent materials can increase the sporulation of fungal pathogens like *Alternaria solani* in greenhouse tomato (Vakalounakis, 1991). Lastly, UV-transparent materials are typically more expensive, but can have applications for specific crops such as red-leaf lettuce.

Photoselective materials

Photoselective materials, sometimes referred to as "waveband-selective" or simply "colored," alter the solar transmission spectrum through the incorporation of various pigments into greenhouse plastics. Importantly, because waveband-selective materials decrease the transmission of PAR/ePAR, they always function as a shading material. The benefits of neutral-density shading

materials (i.e., waveband-nonselective) are well documented to decrease the temperature rise in a greenhouse and reduce evapotranspiration (increase WUE) during periods of excessive solar irradiance (Ahemd et al., 2016). How plants perceive and utilize light is fundamentally different from humans. Human vision (characterized by the photopic response) is strongest from 500–600 nm while plants utilize photons from 400–750 nm for photosynthesis and between 280–800 nm as signals for growth and development (Fig. I-2B and I-3A). As such, less attention should be given to the color of a glazing as it appears to the human eye, and more attention should be given to how the transmission spectrum influences photosynthesis and crop morphology. Typically, the most common types of waveband-selective materials are those that decrease the transmission of B, R, or FR light. Not surprisingly, these wavebands also correspond to peak absorption of CRY, PHOT, and phytochrome (PHY) photoreceptors (Fig. I-2B). Manipulating the transmission spectrum entering a greenhouse presents opportunities to influence crop morphology, yield, quality, and/or flowering.

Opportunities

Materials that selectively decrease transmission of B photons typically increase extension growth (i.e., greater leaf area and/or internode elongation) in crops including lettuce, tomato, wheat (*Triticum aestivum*) and the floriculture crops *Campanula carpatica*, and *Coreopsis ×grandiflora* (Barnes and Bugbee, 1992; Brown et al., 1995; Runkle and Heins, 2001; Shen et al., 2021). There is a positive correlation between increased leaf area and shoot biomass accumulation (Park and Runkle, 2017; Meng at al., 2020). As an additional effect, a decrease in the fraction of B photons increased the anthocyanin content of developing strawberry (*Fragaria ×ananassa*) fruit (Miao et al., 2016). This suggests B-selective materials have opportunities to increase yield and perhaps some quality attributes in some horticultural crops. In contrast, waveband-selective plastics that decrease transmission of FR photons can inhibit extension growth to create more compact plants without chemical plant growth retardants (Runkle and Heins, 2002; Cerny et al., 2003). Compact plants enable a greater plant density in greenhouses and when shipped to their markets. In addition, FR-selective materials delayed the flowering of several photoperiodic long-day plants, which can be desirable to promote vegetative growth or seedling development (Runkle and Heins, 2002). Plastics with decreased transmission of G and R light (i.e., created a high blue-light fraction) also produced more compact plants (Gmizo et al., 2011). Thus, waveband-selective greenhouse plastics offer opportunities to alter crop morphology, yield, flowering, and potentially quality.

Challenges

While B-selective materials can increase extension growth and shoot biomass accumulation in some species, responses are not consistent. For instance, a B-selective plastic increased the extension growth of several floriculture crops (Runkle and Heins, 2001), but a similar B-selective plastic had no effect on poinsettia (*Euphorbia pulcherrima*) morphology or dry shoot mass (Clifford et al., 2004). Moreover, while Miao et al. (2016) reported greater anthocyanin content in strawberry fruit, a decrease in the fraction of B photons decreased the anthocyanin content of red-leaf lettuce (Meng at al., 2020). Therefore, the unpredictable effects on morphology in low-B light environments makes implementation of B-selective materials challenging. Films that create an FR-deficient environment can delay flowering of some long-day floriculture crops, but delaying flowering is typically undesirable because it increases production time (Runkle and Heins, 2002; Cerny et al., 2003). R-selective films can increase extension growth similarly to B-selective materials, but also decrease biomass accumulation (Runkle and Heins, 2001; Cerny et al., 2003). Another unavoidable challenge with waveband-selective materials is their pigments often attenuate transmission of light beyond their target waveband, which makes their effects on diverse greenhouse crops difficult to predict. Moreover, results between studies can be difficult to compare because researchers use different types of waveband-selective films. Compared with waveband-selective shade netting, there is much less experimental data on waveband-selective greenhouse plastics and less flexibility in terms of temporal application. In sum, the higher price of waveband-selective plastics, inconsistent effects on crop growth and development, and limited experimental data have hindered commercial application.

Spectral-shifting materials

Spectral shifting refers broadly to the incorporation of fluorescent dyes or quantum dots into greenhouse covers (Parrish et al., 2021; Shen et al. 2021) (Fig. I-4A, B). Spectral-shifting materials amplify certain light wavebands while waveband-selective materials only attenuate wavebands from transmission. Fluorescence occurs when photoluminescent dyes or quantum dots (i.e., fluorophores) absorb shorter-wavelength photons and emit them with longer wavelengths, which is referred to as a down-conversion (Lamnatou and Chemisana, 2013). The incorporation of fluorophore plastic additives decreases total light transmission because 1) as an electron in the fluorophore relaxes from its excited state to its ground state, energy is dissipated as heat (rather than an emitted photon) to result in an imperfect efficiency (photon emitted per photon absorbed);

8

and 2) fluorophores can reflect (not transmit) photons or photons can become trapped in the greenhouse plastic itself. While materials that incorporate unidirectional light-extracting photonics such as that described by Shen et al. (2021) (Fig. I-1B) can improve the transmission of fluoresced photons, the overall transmission of PAR was still ~20–25% less than the unpigmented base plastic.

There are two general types of spectrum-shifting materials: 1) those that absorb UV photons and emit them in the PAR waveband; or 2) those that absorb B and G photons and emit them as R and FR photons (Espí et al., 2006). In the first type, fluorophore additives can theoretically increase available PAR because UV photons are usually too energetic to drive photosynthesis (McCree, 1971). In the second type, the photon spectrum could theoretically be tailored to increase plant Φ_{PSII} or canopy photon interception. Historically, spectrum-shifting greenhouse materials have used fluorescent dyes that were relatively photo-unstable (i.e., short lifespans) and only moderately altered transmission spectra (Espí et al., 2006; Hemming et al., 2006; Schettini and Vox, 2010; Lemarié et al., 2019). More recently developed spectral-shifting materials use more photostable fluorescent dyes or quantum dots that have much longer lifespans (Parrish et al., 2021; Shen et al., 2021). While spectral-shifting materials are not widely adopted in horticulture currently, they continue to develop technologically and could have targeted applications in horticulture in the near future.

Opportunities

Spectral-shifting materials that increase the transmission of PAR (i.e., shift UV into PAR) could theoretically increase greenhouse crop growth and yield, particularly in light-limited environments or seasons. While there is limited experimental data on this type of spectral-shifting material, Hemming et al. (2006) and Kosobryukhov et al. (2000) reported greater strawberry yields and increased carbon assimilation in tomato and broccoli (*Brassica oleracea* var. *cymosa*) under spectral-shifting films that converted UV photons into B or R photons, respectively. In separate studies, spectral-shifting materials that converted B and G photons into R photons increased yields of lettuce, radish (*Raphanus sativus*), Welsh onion (*Allium fistulosum*), cucumber, and geranium (*Pelargonium × hortorum*) (Fig. I-4C) (Hidaka et al., 2008; Minich et al., 2011; Nishimura et al., 2012; Parrish et al., 2021; Shen et al., 2021; Stallknecht and Runkle, unpublished data). In addition to yield, spectra-shifting materials that decreased the fraction of transmitted B photons altered plant morphology including greater internode and petiole elongation and increased specific leaf

area (SLA; leaf surface area per leaf dry mass). Consequently, these acclimations can increase photon interception by individual leaves as well as the entire plant canopy to increase yield and RUE. However, spectral-shifting plastic additives typically decrease the transmission of PAR. In environments with high solar irradiance, a decrease in light transmission could attenuate high-light induced physiological disorders including tip burn and midrib discoloration in leafy greens (Ilić et al., 2017).

Challenges

While the growth and yield of some crops can increase under spectral-shifting materials, there is inconsistency among crops and/or the type of materials. For example, strawberry 'Elsanta' yield increased by 11% or decreased 10% under a B or R spectral-shifting material, respectively (Hemming et al., 2006). From our research with an R spectral-shifting material that decreased transmission of PAR by ~20–25%, geranium shoot fresh mass increased by 18% but kale (*Brassica oleracea* var. *sabellica* 'Red Russian') yield was statistically similar to a neutral-density control (Fig. I-4C) (Stallknecht and Runkle, unpublished data). Consequently, spectral-shifting materials will likely have targeted, and not ubiquitous, applications considering geographic location and variation in crop response. Despite morphological acclimation such as increased SLA and internode length, which can indirectly increase whole-plant photosynthesis through increased light interception, growth responses may not always be desirable. For instance, thinner leaves (i.e., increased SLA) can be more prone to physical damage during cultivation, longer stems may need additional support to remain upright, and larger plant canopies may require a decreased planting density. Additionally, spectral-shifting materials that increase UV- and B-absorption can decrease the accumulation of leaf pigments such as anthocyanins, which can diminish their marketability and, possibly, nutritional density. Despite limited data on yield in a number of crops, there is a lack of knowledge on the morphological acclimation of plants under spectral-shifting materials and direct effects on photosynthesis. Finally, spectral-shifting materials are more expensive than traditional glazing materials on the market.

PAR-transparent photovoltaics

Photovoltaic (PV) panels absorb solar energy and convert it into electrical energy. Historically, PV panels were opaque (0% transmission), but now PV panels can be engineered with variable transmission (Traverse et al., 2017). However, increasing transparency comes at the cost of generating less electricity. Theoretically, PAR-transparent PV panels can function as a

greenhouse glazing material as a one-to-one replacement for glass, rather than opaque PV panels that would need to be installed separate from a greenhouse (Loik et al., 2017). The coupling of transparent PV installations and agriculture has been termed "agrivoltaics" and promises to create passive income from generating electricity while still producing a crop (Emmott et al., 2015; Cossu et al., 2020; Ravishankar et al., 2021). Because agrivoltaics is a relatively new field of study, many strategies are being explored. In greenhouses, these include 1) PV installations on the exterior of a greenhouse; 2) temporally applied PV screens or curtains; and 3) PV panels acting as greenhouse glazing. Initial attempts at creating an agrivoltaic greenhouse simply installed opaque PV panels on the exterior. These designs created significant, and often asymmetrical, shading effects on crops that decreased yields (Yano and Cossu, 2019). While the spatial distribution of opaque PV panels can be optimized through modeling, there is limited room for further technological advancement. Since opaque PVs do not selectively absorb certain wavebands, cannot be designed in a plant-centric manner, or cannot function as greenhouse glazing, they are not further considered here. In contrast, PAR-transparent materials offer unique opportunities to alter crop growth similar to waveband-selective, spectral-shifting, and near-infrared (NIR; 800–3000 nm) glazing materials.

Opportunities

In some seasons and geographic locations, horticultural crops can receive excessive solar irradiance that can increase physiological disorders, decrease WUE, and/or create an undesirably high temperature (Ahemd et al., 2016; Yano and Cossu, 2019). PAR-transparent glazings have the greatest opportunity in environments where shading materials are already commonly used, thus allowing PAR-transparent PVs to harvest excess solar irradiance (instead of reflecting it) for electricity and transmitting enough PAR for crop growth. Floriculture and leafy green crops that tolerate or thrive under low to moderate daily light integrals (e.g., <10–12 $mol·m^{-2}·d^{-1}$) have the greatest potential for agrivoltaic settings (Cossu et al., 2020). PAR-transparent PVs can be designed to absorb UV and NIR photons and maximize the transmission of PAR (Traverse et al., 2017). These materials would be particularly useful in light-limited environments and for high-light crops such as fruiting vegetables. PAR-transparent PVs can be designed as either non-photoselective or with a selective transmitted spectrum that can alter plant morphology similar to waveband-selective glazing materials. PAR-transparent PVs that absorb NIR could theoretically generate electricity for supplemental lighting systems and limit the greenhouse temperature rise,

11

similar to NIR-reflecting materials already used in the greenhouse industry (Sonneveld et al., 2006).

Challenges

As a fledgling technology, PAR-transparent PVs have many challenges to overcome before they are commercially viable. First, attenuating PAR transmission can decrease crop growth and yield seasonally during light-limited periods. Research is needed with agrivoltaics that focuses on the impacts of PAR-transparent PV glazings in relation to seasonal variations in light and temperature. In addition, panels that are designed without adequate plant knowledge or input from plant scientists could lead to poor design, for example using the absorption spectrum for extracted chlorophyll as the basis for light transmission, rather than more relevant information (Fig. I-3) (McCree, 1971; Meitzner et al., 2021). Moreover, agrivoltaic studies often do not consider changes in plant morphology caused by changes to the photon spectrum (Fig. I-2B). Interdisciplinary collaborations are necessary to overcome this challenge. Generating electricity can theoretically create a secondary income source for greenhouses but the quality of horticultural products cannot be diminished. A metric such as crop yield per energy generated could describe the dual benefits of an agrivoltaic system, but it ignores possible effects on crop quality (Thompson et al., 2020). Finally, PAR-transparent PVs are currently cost prohibitive, and significant price decreases are needed before commercial adoption.

LITERATURE CITED

Ahemd HA, Al-Faraj AA, Abdel-Ghany AM. 2016. Shading greenhouses to improve the microclimate, energy and water saving in hot regions: A review Sci Hortic. 201:36–45. https://doi.org/10.1016/j.scienta.2016.01.030.

American Society for Testing and Materials (ASTM). 2003. Standard test method for haze and luminous transmittance of transparent plastics. ASTM D 1003.

Baeza E, López, JC. 2012. Light transmission through greenhouse covers. Acta Hortic. 956:425–440. https://doi.org/10.17660/ActaHortic.2012.956.50.

Banerjee R, Schleicher E, Meier S, Viana RM, Pokorny R, Ahmad M, Bittl R, Batschauer A. 2007. The signaling state of *Arabidopsis* cryptochrome 2 contains flavin semiquinone. J Biol Chem. 282:14916–14922. https://doi.org/10.1074/jbc.M700616200.

Barnes C, Bugbee B. 1992. Morphological responses of wheat to blue light. J. Plant Physiol. 139:339–342. https://doi.org/10.1016/S0176-1617(11)80347-0.

Behn H, Tittman S, Walter A, Schurr U, Noga G, Ulbrich A. 2010. UV-B transmittance of greenhouse covering materials affects growth and flavonoid content of lettuce seedlings. Eur J Hortic Sci. 75:259–268.

Brown CS, Schuerger AC, Sager JC. 1995. Growth and photomorphogenesis of pepper plants under red light-emitting diodes with supplemental blue or far-red lighting. J Am Soc Hortic Sci. 120:808–813. https://doi.org/10.21273/JASHS.120.5.808.

Cerny TA, Faust JE, Layne DR, Rajapakse NC. 2003. Influence of photoselective films and growing season on stem growth and flowering of six plant species. J Am Soc Hortic Sci. 128:486–491. https://doi.org/10.21273/JASHS.128.4.0486.

Chaves I, Pokorny R, Byrdin M, Hoang N, Ritz T, Brettel K, Essen L-O, van der Horst GTJ, Batschauer A, Ahmad M. 2011. The cryptochromes: blue light photoreceptors in plants and animals. Annu Rev Plant Biol. 62:335–364. https://doi.org/10.1146/annurev-arplant-042110-103759.

Christie JM, Blackwood L, Petersen J, Sullivan S. 2015. Plant flavoprotein photoreceptors. Plant Cell Physiol. 56:401–413. https://doi.org/10.1093/pcp/pcu196.

Christie, J.M., Arvai, A.S., Baxter, K.J., Heilmann, M., Pratt, A.J., O'Hara, A., Kelly, S.M., Hothorn, M., Smith, B.O., Hitomi, K., et al. (2012). Plant UVR8 photoreceptor senses UV-B by tryptophan-mediated disruption of cross-dimer salt bridges. Science *335 (6075)*, 1492–1496. https://doi.org/10.1126/science.1218091.

Clifford SC, Runkle ES, Langton FA, Mead A, Foster SA, Pearson S, Heins RD 2004. Height control of poinsettia using photoselective filters. HortScience. 39:383–387. https://doi.org/10.21273/HORTSCI.39.2.383.

Cossu M, Yano A, Solinas S, Deligios PA, Tiloca M.T, Cossu A, Ledda L. 2020. Agricultural sustainability estimation of the European photovoltaic greenhouses. Eu. J Agron. 118:126074. https://doi.org/10.1016/j.eja.2020.126074.

Cozzolino E, Ottaiano E, Di Mola I, El-Nakhel C, Mormile P, Rouphael Y, Mori M. 2020. The potential of greenhouse diffusing cover material on yield and nutritive values of lamb's

lettuce grown under diverse nitrogen regimes. Italus Hortus 27:55–67. https://doi.org/10.26353/j.itahort/2020.1.5567.

Dueck T, Janse J, Li T, Kempkes F, Eveleens B. 2012. Influence of diffuse glass on the growth and production of tomato. Acta Hortic. 956:75–82. https://doi.org/10.17660/ActaHortic.2012.956.6.

El-Yazbi AF, Loppnow GR. 2014. Detecting UV-induced nucleic-acid damage. Trends Anal Chem. 61:83–91. https://doi.org/10.1016/j.trac.2014.05.010.

Emmott CJM, Röhr JA, Campoy-Quiles M, Kirchartz T, Urbina A, Ekins-Daukes N.J, Nelson J. 2015. Organic photovoltaic greenhouses: a unique application for semi-transparent PV? Energy Environ Sci. 8:1317–1328. https://doi.org/10.1039/C4EE03132F.

Espí E, Salmerón A, Fontecha A, García Y, Real AI. 2006. Plastic films for agricultural applications. J Plastic Film Sheeting. 22:85–102. https://doi.org/10.1177/8756087906064220.

Gmizo G, Alsiņa I, Dubova L. 2012. The effect of colour plastic films on the growth, yield and plant pigment content of tomatoes. Acta Hortic. 952:217–224. https://doi.org/10.17660/ActaHortic.2012.952.26.

Hemming S, Dueck T, Janse J, van Noort F. 2008a. The effect of diffuse light on crops. Acta Hortic. 801:1293–1300. https://doi.org/10.17660/ActaHortic.2008.801.158.

Hemming S, Mohammadkhani V, Dueck T. 2008b. Diffuse greenhouse covering materials - material technology, measurements and evaluation of optical properties. Acta Hortic. 797:469–475. https://doi.org/10.17660/ActaHortic.2008.797.68.

Hemming S, Mohammadkhani V, van Ruijven J. 2014. Material technology of diffuse greenhouse covering materials - influence on light transmission, light scattering and light spectrum. Acta Hortic. 1037:883–895. https://doi.org/10.17660/ActaHortic.2014.1037.118.

Hemming S, van Os EA, Hemming J, Dieleman JA. 2006. The effect of new developed fluorescent greenhouse films on the growth of *Fragaria* x *ananassa* 'Elsanta.' Eur J Hortic Sci. 71:145–154.

Hidaka K, Yoshida K, Shimasaki K, Murakami K, Yasutake D, Kitano M. 2008. Spectrum conversion film for regulation of plant growth. J. Faculty Agric., Kyushu Univ. 53:549–552. https://doi.org/10.5109/12872.

Holsteens K, Moerkens R, Van de Poel B, Vanlommel W. 2020. The effect of low-haze diffuse glass on greenhouse tomato and bell pepper production and light distribution properties. Plants. 9:806. https://doi.org/10.3390/plants9070806.

Hovi T, Näkkilä J, Tahvonen R. 2004. Interlighting improves production of year-round cucumber. Sci Hortic. 102:283–294. https://doi.org/10.1016/j.scienta.2004.04.003.

Ilić SZ, Milenković L, Dimitrijević A, Stanojević L, Cvetković D, Kevrešan Ž, Fallik E, Mastilović J. 2017. Light modification by color nets improve quality of lettuce from summer production. Sci Hortic. 226:389–397. https://doi.org/10.1016/j.scienta.2017.09.009.

Kang B, Grancher N, Koyffmann V, Lardemer D, Burney S, Ahmad M. 2008. Multiple interactions between cryptochrome and phototropin blue-light signalling pathways in *Arabidopsis thaliana*. Planta. 227:1091–1099. https://doi.org/10.1007/s00425-007-0683-z.

Kempkes FLK, Stanghellini C, García Victoria N, Bruins M. 2012. Effect of diffuse glass on climate and plant environment: first results from an experiment on roses. Acta Hortic. 952:255–262. https://doi.org/10.17660/ActaHortic.2012.952.31.

Kendrick RE, Kronenberg GHM. eds. 1994. Photomorphogenesis in Plants, 2nd edn (Dordrecht, The Netherlands: Springer Science & Business Media). https://doi.org/10.1007/978-94-011-1884-2.

Kigathi R, Poehling H-M. 2012. UV-absorbing films and nets affect the dispersal of western flower thrips, *Frankliniella occidentalis* (Thysanoptera: Thripidae): UV manipulation affects WFT dispersal. J App Entomol. 136:761–771. https://doi.org/10.1111/j.1439-0418.2012.01707.x.

Kosobryukhov A, Kreslavskii V, Khramov R, Bratkova L, Shchelokov R. 2000. Effect of additional low intensity luminescence radiation 625 nm on plant growth and photosynthesis. Biotronics. 29:23–31.

Lamnatou Chr, Chemisana D. 2013. Solar radiation manipulations and their role in greenhouse claddings: Fluorescent solar concentrators, photoselective and other materials. Renew. Sustain. Energy Rev. 27:175–190. https://doi.org/10.1016/j.rser.2013.06.052.

Lemarié S, Guérin V, Sakr S, Jouault A, Caradeuc M, Cordier S, Guignard G, Gardet R, Bertheloot J, Demotes-Mainard S. 2019. Impact of innovative optically active greenhouse films on melon, watermelon, raspberry and potato crops. Acta Hortic. 1252:191–200. https://doi.org/10.17660/ActaHortic.2019.1252.25.

Loik ME, Carter SA, Alers G, Wade CE, Shugar D, Corrado C, Jokerst D, Kitayama C. 2017. Wavelength-selective solar photovoltaic systems: powering greenhouses for plant growth at the food-energy-water nexus: plant growth under solar windows. Earth's Future. 5:1044–1053. https://doi.org/10.1002/2016EF000531.

Marcelis LFM, Broekhuijsen AGM, Meinen E, Nijs EMFM, Raaphorst MGM. 2006. Quantification of the growth response to light quantity of greenhouse grown crops. Acta Hortic. 711:97–104. https://doi.org/10.17660/ActaHortic.2006.711.9.

McCree KJ. 1971. The action spectrum, absorptance and quantum yield of photosynthesis in crop plants. Agric. Meteorol. 9:191–216. https://doi.org/10.1016/0002-1571(71)90022-7.

Meitzner R, Schubert US, Hoppe H. 2021. Agrivoltaics—the perfect fit for the future of organic photovoltaics. Adv Energy Mater. 11:2002551. https://doi.org/10.1002/aenm.202002551.

Miao L, Zhang Y, Yang X, Xiao J, Zhang H, Zhang Z, Wang Y, Jiang G. 2016. Colored light-quality selective plastic films affect anthocyanin content, enzyme activities, and the expression of flavonoid genes in strawberry (*Fragaria ×ananassa*) fruit. Food Chem. 207:93–100. https://doi.org/10.1016/j.foodchem.2016.02.077.

Minich AS, Minich IB, Shaitarova OV, Permyakova NL, Zelenchukova NS, Ivanitshiy AE, Ivlev GA. 2011. Vital activity of *Lactuca sativa* and soil microorganisms under fluorescent films. Tomsk State Pedagogical Univ. Bulletin 8:78–84.

Nishimura Y, Wada E, Fukumoto Y, Aruga H, Shimoi Y. 2012. The effect of spectrum conversion covering film on cucumber in soilless culture. Acta Hortic. 956:481–487. https://doi.org/10.17660/ActaHortic.2012.956.56.

Park Y, Runkle ES. 2017. Far-red radiation promotes growth of seedlings by increasing leaf expansion and whole-plant net assimilation. Environ Exp Bot. 136:41–49. https://doi.org/10.1016/j.envexpbot.2016.12.013.

Parrish CH, Hebert D, Jackson A, Ramasamy K, McDaniel H, Giacomelli GA, Bergren MR. 2021. Optimizing spectral quality with quantum dots to enhance crop yield in controlled environments. Commun Biol. 4:124. https://doi.org/10.1038/s42003-020-01646-1.

Quintero-Arias DG, Acuña-Caita JF, Asensio C, Valenzuela JL. 2021. Ultraviolet transparency of plastic films determines the quality of lettuce (*Lactuca sativa* L.*)* grown in a greenhouse. Agron. 11:358. https://doi.org/10.3390/agronomy11020358.

Ravishankar E, Charles M, Xiong Y, Henry R, Swift J, Rech J, Calero J, Cho S, Booth RE, Kim T. 2021. Balancing crop production and energy harvesting in organic solar-powered greenhouses. Cell Reports Phys Sci. 2:100381. https://doi.org/10.1016/j.xcrp.2021.100381.

Raviv M, Antignus Y. 2004. UV radiation effects on pathogens and insect pests of greenhouse-grown crops. Photochem Photobiol. 79:219–226. https://doi.org/10.1111/j.1751-1097.2004.tb00388.x.

Runkle ES, Heins RD. 2001. Specific functions of red, far red, and blue light in flowering and stem extension of long-day plants. J Am Soc Hortic Sci. 126:275–282. https://doi.org/10.21273/JASHS.126.3.275.

Runkle ES, Heins RD. 2002. Stem extension and subsequent flowering of seedlings grown under a film creating a far-red deficient environment. Sci Hortic. 96:257–265. https://doi.org/10.1016/S0304-4238(02)00055-9.

Schettini E, Vox G. 2010. Greenhouse plastic films capable of modifying the spectral distribution of solar radiation. J Agric Eng. 41:19–24. https://doi.org/10.4081/jae.2010.1.19.

Sharkey TD. 2005. Effects of moderate heat stress on photosynthesis: importance of thylakoid reactions, rubisco deactivation, reactive oxygen species, and thermotolerance provided by isoprene. Plant Cell Environ. 28:269–277. https://doi.org/10.1111/j.1365-3040.2005.01324.x.

Sonneveld PJ, Swinkels GLAM, Kempkes F, Campen JB, Bot GPA. 2006. Greenhouse with an integrated NIR filter and a solar cooling system. Acta Hortic. 719:123–130. https://doi.org/10.17660/ActaHortic.2006.719.11.

Strain HH, Thomas MR, Katz JJ. 1963. Spectral absorption properties of ordinary and fully deuteriated chlorophylls *a* and *b*. Biochim et Biophys Acta. 75:306–311. https://doi.org/10.1016/0006-3002(63)90617-6.

Thompson EP, Bombelli EL, Shubham S, Watson H, Everard A, D'Ardes V, Schievano A, Bocchi S, Zand N, Howe CJ. 2020. Tinted semi-transparent solar panels allow concurrent production of crops and electricity on the same cropland. Adv Energy Mater. 10:2001189. https://doi.org/10.1002/aenm.202001189.

Traverse CJ, Pandey R, Barr MC, Lunt RR 2017. Emergence of highly transparent photovoltaics for distributed applications. Nat Energy 2:849–860. https://doi.org/10.1038/s41560-017-0016-9.

Tsormpatsidis E, Henbest RGC, Battey NH, Hadley P. 2010. The influence of ultraviolet radiation on growth, photosynthesis and phenolic levels of green and red lettuce: potential for exploiting effects of ultraviolet radiation in a production system. Ann Appl Biol. 156:357–366. https://doi.org/10.1111/j.1744-7348.2010.00393.x.

Tsormpatsidis E, Henbest RGC, Davis FJ, Battey NH, Hadley P, Wagstaffe A. 2008. UV irradiance as a major influence on growth, development and secondary products of commercial importance in Lollo Rosso lettuce 'Revolution' grown under polyethylene films. Environ Exp Bot. 63:232–239. https://doi.org/10.1016/j.envexpbot.2007.12.002.

Tubiello F, Volk T, Bugbee B. 1997. Diffuse light and wheat radiation-use efficiency in a controlled environment. Life Support Biosphere Sci. 4:77–85.

Vakalounakis DJ. 1991. Control of early blight of greenhouse tomato, caused by *Alternaria solani*, by inhibiting sporulation with ultraviolet-absorbing vinyl film. Plant Dis. 75:795-797. https://doi.org/10.1094/PD-75-0795.

Vernon LP, Seely GR. 2014. The Chlorophylls (New York, NY, USA: Academic Press).

Watanabe K, Yasugi E, Oshima M. 2000. How to search the glycolipid data in "LIPIDBANK for Web" the newly developed lipid database in Japan. Trends Glycosci Glycotechnol. 12:175–184. https://doi.org/10.4052/tigg.12.175.

Weaver G, van Iersel MW. 2019. Photochemical characterization of greenhouse-grown lettuce (*Lactuca sativa* L. 'Green Towers') with applications for supplemental lighting control. HortScience. 54:317–322. https://doi.org/10.21273/HORTSCI13553-18.

Wu Q, Su N, Zhang X, Liu Y, Cui J, Liang Y. 2016. Hydrogen peroxide, nitric oxide and UV RESISTANCE LOCUS8 interact to mediate UV-B-induced anthocyanin biosynthesis in radish sprouts. Sci Rep. 6:29164. https://doi.org/10.1038/srep29164.

Yano A, Cossu M. 2019. Energy sustainable greenhouse crop cultivation using photovoltaic technologies. Renew Sustain Energy Rev. 109:116–137. https://doi.org/10.1016/j.rser.2019.04.026.

Yousif E, Haddad R. 2013. Photodegradation and photostabilization of polymers, especially polystyrene: review. SpringerPlus. 2:398. https://doi.org/10.1186/2193-1801-2-398.

Zhen S, Bugbee B. 2019. Diffuse light panels slightly increase canopy light use efficiency but decrease light intensity and canopy photosynthesis of lettuce. Controlled Environ. Paper 12. (Logan, UT, USA: Utah State Uni.)

Zhen S, Bugbee B. 2020a. Far-red photons have equivalent efficiency to traditional photosynthetic photons: Implications for redefining photosynthetically active radiation. Plant Cell Environ. 43:1259–1272. https://doi.org/10.1111/pce.13730.

Zhen S, Bugbee B. 2020b. Substituting far-red for traditionally defined photosynthetic photons results in equal canopy quantum yield for CO2 fixation and increased photon capture during long-term studies: implications for re-defining PAR. Front Plant Sci. 11:581156. https://doi.org/10.3389/fpls.2020.581156.

Zoltowski BD, Imaizumi T. 2014. Structure and function of the ZTL/FKF1/LKP2 group proteins in *Arabidopsis*. In the Enzymes: Signaling Pathways in Plants, 1st edn, Y. Machida, C. Lin, and T. Fuyuhiko, eds. (San Diego, CA, USA: Academic Press). 213–239. https://doi.org/10.1016/B978-0-12-801922-1.00009-9.
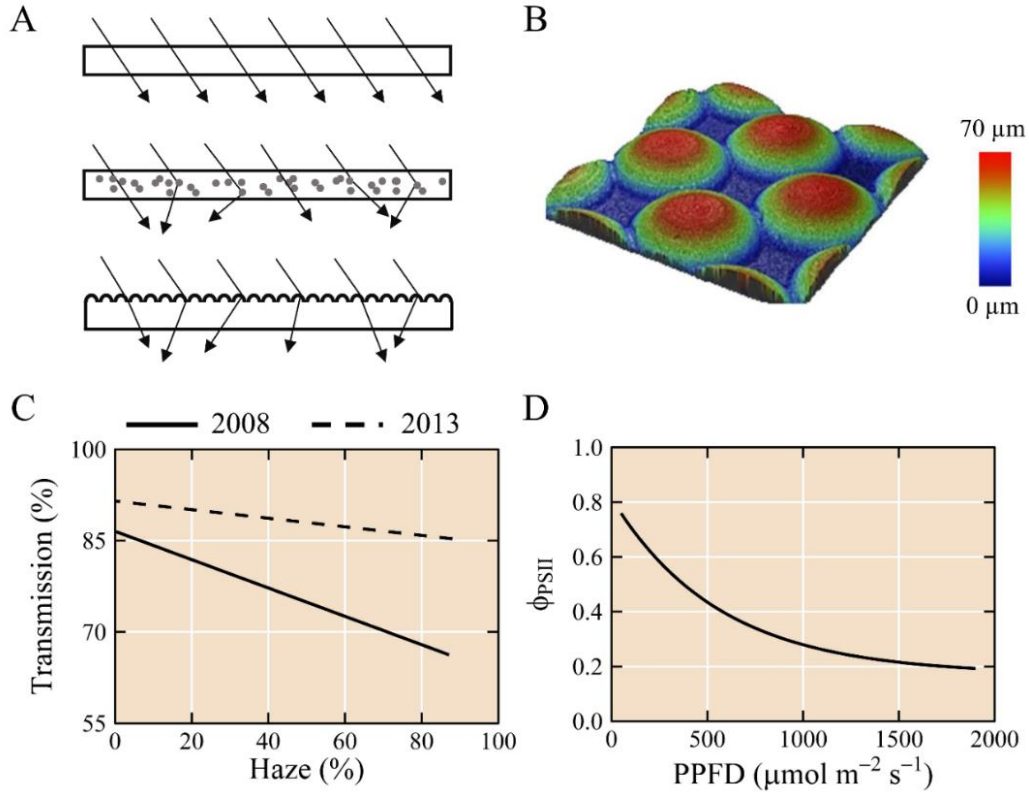
Figure I-1. A) Conceptualization of light transmitting through (top) a non-diffuse material, (middle) a plastic with additives or temporal coating, and (bottom) a material with micro- or macrostructures. While not depicted in the conceptualization, all of the incident light cannot be transmitted through a material because some light is always reflected or absorbed, and the degree of transmission lost through reflection and absorption will depend on the incident light angle and material composition, respectively. B) The design of symmetrical microstructures imprinted on the surface of a novel greenhouse plastic (Shen et al., 2021). C) Increasing the haze percentage of a material decreased the light transmission for various diffuse glass, plastic, and temporal coatings (solid line) (Hemming et al., 2008b). Similarly, increasing haze percentage decreased light transmission through diffuse glass (dashed line). However, the technological development of diffuse materials over time has increased the average transmission to be comparable to common non-diffuse materials (Hemming et al., 2014). D) the quantum efficiency of photosystem II (Φ_{PSII}) decreases nonlinearly as a function of increasing photosynthetic photon flux density (PPFD; 400–700 nm) for lettuce (Lactuca sativa) and is close to saturation when PPFD is >1500 $\mu mol \cdot m^{-2} \cdot s^{-1}$ (Weaver and van Iersel, 2019).
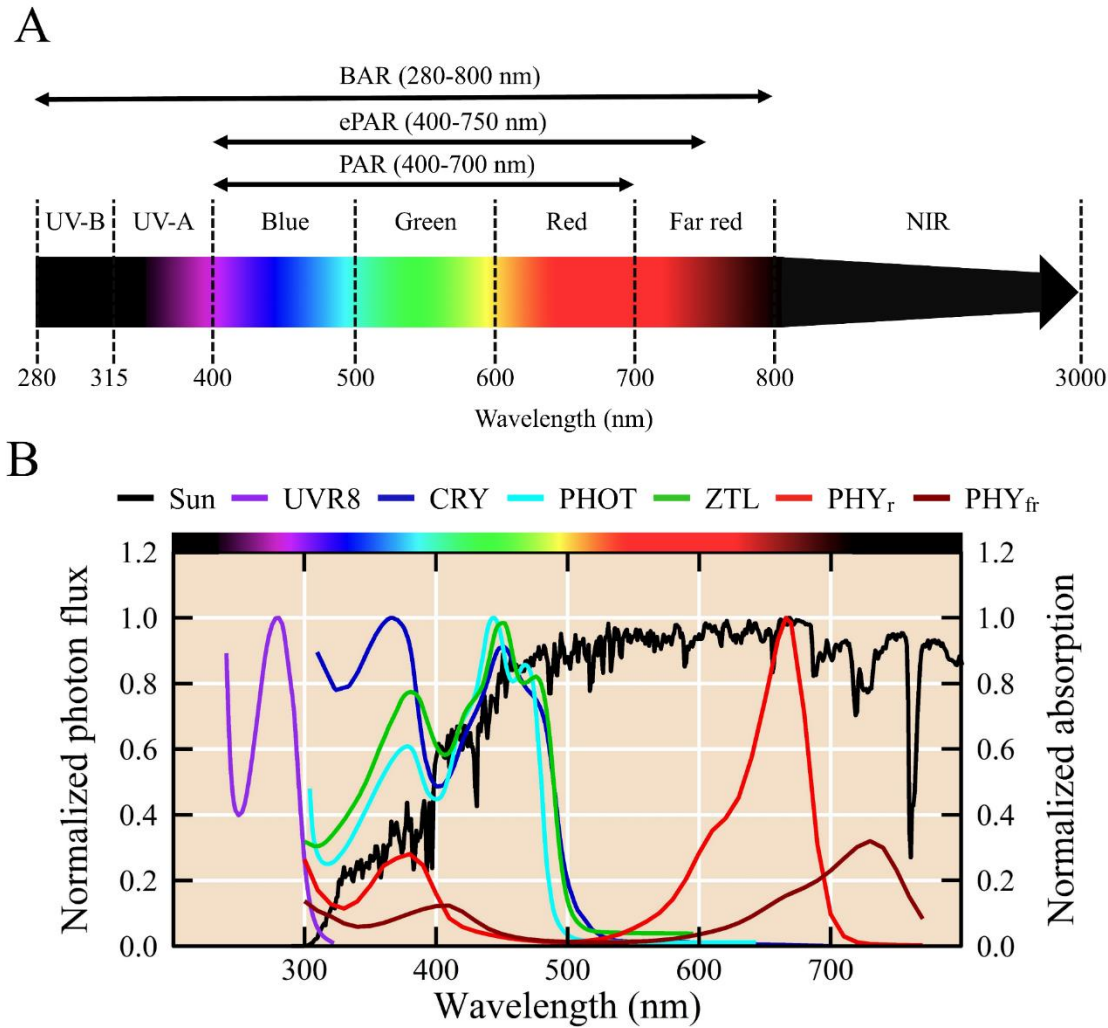
Figure I-2. A) The electromagnetic spectrum from 280 to 3000 nm and the commonly defined wavebands of ultraviolet-B (UV-B; 280–315 nm), ultraviolet-A (UV-A; 315–400 nm), blue (B; 400–499 nm), green (G; 500–599 nm), red (R; 600–699 nm), far-red (FR; 700–799 nm), and near-infrared (NIR; 800–3000 nm) radiation. PAR, ePAR, and BAR refer to photosynthetically active radiation (400–700 nm), the extended waveband of photosynthetically active radiation (400–750 nm), and biologically active radiation (280–800 nm), respectively (Zhen and Bugbee, 2020a, 2020b). B) Normalized photon flux of solar radiation (sun) and the normalized absorption spectrum of UV RESISTANCE LOCUS 8 (UVR8), phototropins (PHOT), cryptochromes (CRY), zeitlupes (ZTL), red-absorbing phytochrome (PHY$_r$) and far red-absorbing phytochrome (PHY$_{fr}$) as a function of photon wavelength. Absorption spectra were adapted from Christie et al. (2012), Christie et al. (2015), Banerjee et al. (2007), Zoltowski and Imaizumi (2014), and Kendrick and Kronenberg (1994), respectively.
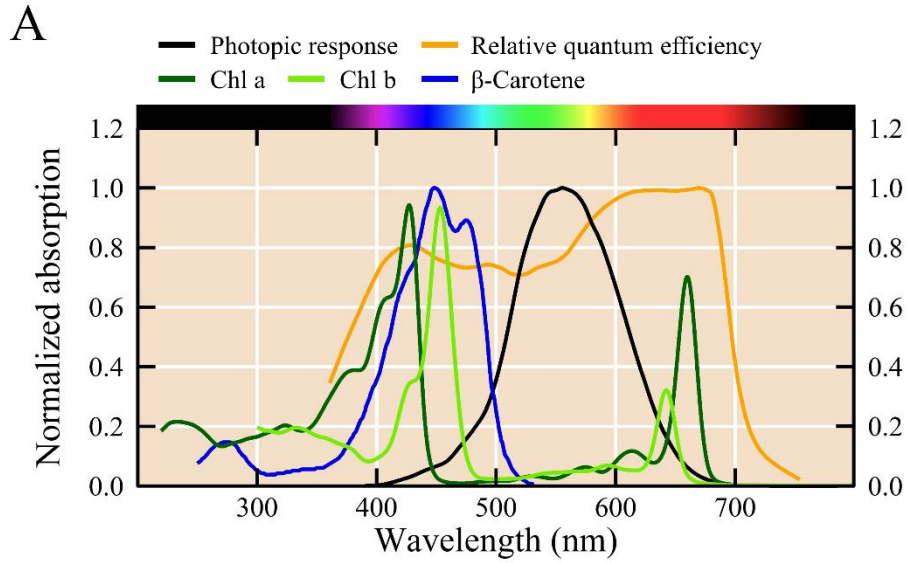
Figure I-3. The normalized absorption of some pigments used for photosynthesis including chlorophyll a (Chl a), Chl b, and β-Carotene (Strain et al., 1963; Vernon and Seely, 1966; Watanabe et al., 2000). The average normalized quantum efficiency for several species derived from McCree (1971). The photopic response characterizes human vision and peaks at ~555 nm. The differences between the photopic response and the McCree curve illustrates the difficulty in relating human perception of light to plant utilization for photosynthesis and photomorphogenesis.
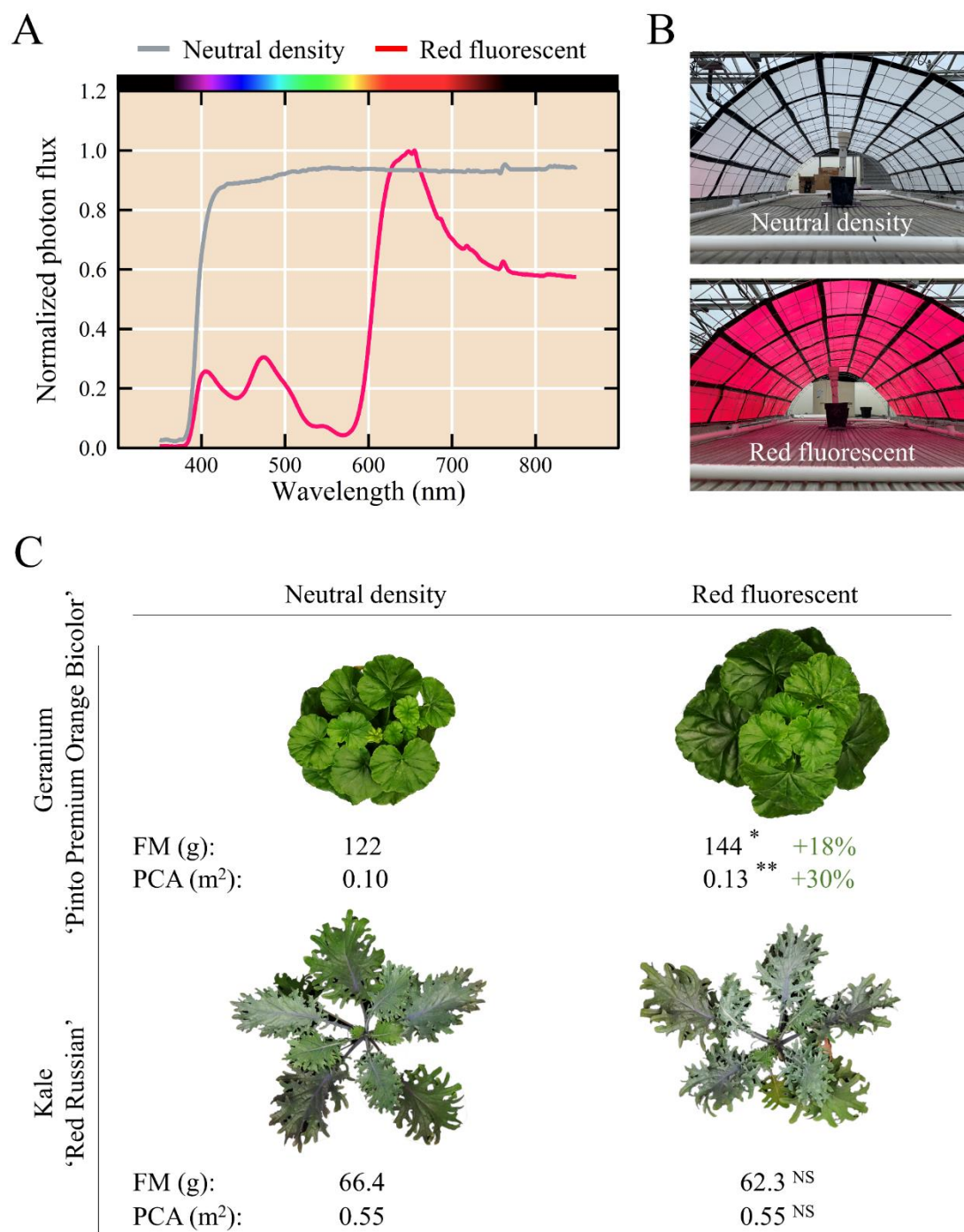
Figure I-4. A) Normalized transmission spectra of a neutral-density plastic and the same plastic with a red-fluorescent plastic additive. The red-fluorescent additive primarily absorbed B and G photons and emitted R and FR photons (Shen et al., 2021; Stallknecht and Runkle, unpublished data). B) A highly diffuse, neutral-density plastic (top) and the same plastic with a red-fluorescent dye (bottom) inside a glass-glazed research greenhouse at Michigan State University. C) Geranium (*Pelargonium × hortorum* 'Pinto Premium Orange Bicolor') (top) and kale (*Brassica oleracea* var. sabellica 'Red Russian') (bottom) grown inside the chambers depicted in panel B (Stallknecht and

Figure I-4 (cont'd)

Runkle, unpublished data). Fresh mass (FM; g) and projected canopy area (PCA; m^2) were measured on ten plants (n=10). NS, *, and ** indicate t-test significance at $P > 0.05$ (not significant), $P < 0.05$, and $P < 0.01$, respectively.

SECTION II: DESIGNING PLANT-TRANSPARENT AGRIVOLTAICS

Designing plant-transparent agrivoltaics

Eric J. Stallknecht, Christopher K. Herrera[†], Chenchen Yang, Isaac King, Thomas D. Sharkey, Richard R. Lunt, and Erik S. Runkle*

E.J.S., Prof. E.S.R.

Department of Horticulture, Michigan State University, East Lansing, MI, USA

*Corresponding author; Email: runkleer@msu.edu

C.K.H., C.Y., I.K., Prof. R.R.L.

Department of Chemical Engineering and Materials Science, Michigan State University, East Lansing, MI, USA

Prof. T.D.S.

MSU-DOE Plant Research Laboratory and Department of Biochemistry and Molecular Biology, Michigan State University, East Lansing, MI, USA

Keywords: greenhouses, agrivoltaics, photovoltaics, transparent photovoltaics

Abstract

Covering greenhouses and agricultural fields with photovoltaics has the potential to create multipurpose agricultural systems that generate revenue through conventional crop production as well as sustainable electrical energy. In this work, we evaluate the effects of wavelength-selective cutoffs of visible and near-infrared (biologically active) radiation using transparent photovoltaic (TPV) absorbers on the growth of three diverse, representative, and economically important crops: petunia, basil, and tomato. Despite the differences in TPV harvester (panel) absorption spectra, photon transmission of photosynthetically active radiation (PAR; 400-700 nm) is the most dominant predictor of crop yield and quality. This indicates that different wavebands of blue, red,

and green are essentially equally important to these plants. When the average photosynthetic daily light integral is >12 mol m^{-2} d^{-1}, basil and petunia yield and quality is acceptable for commercial production. However, even modest decreases in TPV transmission of PAR reduces tomato growth and fruit yield. These results identify crop-specific design requirements that exist for TPV panel transmission and the necessity to maximize transmission of PAR to create the most broadly applicable TPV greenhouse panels for diverse crops and geographic locations. We determine that the deployment of 10% power conversion efficiency (*PCE*) plant-optimized TPVs over approximately 10% of total agricultural and pasture land in the U.S. would generate 7 TW, nearly double the entire energy demand of the U.S.

Introduction

The incorporation of photovoltaics (PV) into agriculture has drawn significant interest recently to address increased food insecurity and energy demand (Proctor et al. 2021). Agrivoltaics is the utilization of sunlight for both plant production and solar energy harvesting (Dinesh and Pearce 2016; Timmermans et al. 2020). These two fields are often seen as competitive rather than cooperative because they can both occupy large areas of land to maximize sunlight utilization. Indeed, most agrivoltaic-based efforts have looked to integrate opaque solar panels (such as Si modules) over and around agricultural spaces so that there is often a strong tradeoff between allowing light to penetrate to the plants or be utilized for solar electricity generation. Despite this, photovoltaics have potential synergistic benefits with plant production. In addition to generating electricity to power greenhouse load (e.g., lights, fans, and other equipment), PV modules can also decrease water consumption by reducing the rate of evaporation from soil and transpiration from plants (AL-agele et al. 2021; Barron-Gafford et al. 2019). Both plant responses and PV power generation are key considerations in designing agrivoltaic systems. One way to overcome the severe limitation of opaque agrivoltaics is to design new PVs that can maintain plant yield and quality by minimizing PV impact on transmission of photons with wavelengths between 400 and 700 nm, which is referred to as photosynthetically active radiation (PAR). Fig. II-1a illustrates the progression and outlook of agrivoltaic approaches, including current approaches shown here, based on increasing transparency, starting with opaque PV modules, and moving towards PAR-transparent PV devices.

Plant productivity typically increases with photon flux density of PAR (Bruggink and Heuvelink 1987; Colonna et al. 2016; Faust et al. 2005; Gao et al. 2020; Sivakumar and Virmani

2984; Touil et al. 2021). This is measured instantaneously as the photosynthetic photon flux density ($PPFD$, with units of μmol m^{-2} s^{-1}) or, more appropriately for plant growth, integrated on a daily basis as the daily light integral (DLI, with units of mol m^{-2} d^{-1}). PAR is commonly divided into three wavebands: blue (B; 400–500 nm), green (G; 500–600 nm), and red (R; 600–700 nm) light. Each waveband independently and interactively regulates plant growth and development (Fig. II-1b) with additional contributions coming from UV (280–400 nm), near-infrared (NIR) or far-red (FR; 700–750 nm) wavebands (McCree 1972; Zhen and Bugbee 2020a; Zhen and Bugbee 2020b). Of these, B and FR light strongly regulate plant morphology and development, altering characteristics such as leaf area, stem length, and flowering (Meng et al. 2019; Meng et al. 2020; Park and Runkle 2017; Runkle and Heinz 2001). Although there can be benefits to decreasing incoming solar radiation in some cases (e.g., reducing water consumption or soil temperature), adoption of this hybrid field will rely on being broadly applicable by transmitting as much PAR as possible, particularly in temperate climates (AL-agele et al. 2021; Dou et al. 2018; Ravishankar et al. 2021; Weselek et al. 2021). In some agrivoltaic approaches, G light has been considered to have less impact on plant growth because of low absorption by chlorophyll and carotenoids, causing it to be a target wavelength for absorption (Ravishankar et al. 2021; Liu et al. 2019; Thompson et al. 2020; Wang et al. 2021). However, as shown in Fig. II-1b, metrics such as relative action and quantum yield show that plants utilize G light quite efficiently in photosynthesis (McCree 1972; Hogewoning et al. 2012). Green light is particularly useful in penetrating deeper into leaves under high-light conditions and reaching leaves that are shaded by others (Wang and Folta 2013; Terashima et al. 2009). Thus, spectral manipulation by absorbing specific wavebands within PAR (Fig. II-1c) will alter plant growth and yield, which will vary among species and cultivars of plants. Allowing growers to maintain control of how plants grow and develop while still providing the benefits of agrivoltaics will be essential to enable future widespread adoption.

Recent efforts have been made to introduce and improve visible transparency of PV cells, either broadband or with selectively absorbing materials, to increase application to a greater number of surfaces (Cossu et al. 2018; Hassanien et al. 2018; Saifullah et al. 2016; Traverse et al. 2018). We can evaluate these approaches in the context of agrivoltaics, from spatially segmenting opaque solar cells to wavelength-selective active materials (Ravishankar et al. 2021; Weselek et al. 2021; Liu et al. 2019; Wang et al. 2021; Detweiler et al. 2015; Kadowaki et al. 2012; Marrou et al. 2012; Trypanagnostopoulos et al. 2017). This is a key distinction because they offer

fundamentally different theoretical limits as a function of transparency. The theoretical limit of a spatially segmented cell is 0% at 100% transparency and around 21% for wavelength-selective transparent photovoltaics (TPVs) at 100% transparency. Agrivoltaic implementations based on opaque or visibly absorbing materials will always have a tradeoff between power generation and plant productivity. As a result, agrivoltaic studies have primarily focused on the financial tradeoff of power generation over reduced crop yield (Touil et al. 2021; Weselek et al. 2021; Thompson et al. 2020). While financially the tradeoff is of slight benefit, notable losses in crop yield will limit the implementation of agrivoltaics for locations or seasons with limited or moderate PAR availability. Each study also typically focused on only one type of plant under an exceedingly small area of PVs, limiting the translatability as to how these different agrivoltaic approaches will affect a variety of species.

In this work, we evaluate the effects of TPVs with neutral shading and with wavelength-selective shading on three diverse and highly representative and commercially important species of plants grown in greenhouses: the culinary herb basil (*Ocimum basilicum*), the flowering ornamental petunia (*Petunia ×hybrida*), and the fruit-bearing tomato (*Solanum lycopersicum*). Emphasis is placed around the VIS and NIR edge to better understand where it is appropriate to absorb light for TPV without affecting plant growth and development. We show that overall DLI has particularly important ramifications for growth, yield, and morphology across species and that weighted DLI further impacts these metrics, indicating wavelength-specific phenomena should be studied further. This work will enable the design of agrivoltaic approaches to ensure greater compatibility with existing agricultural infrastructure across a large range of crop types and in regions with different solar availability.

Materials and Methods

Preparation of wavelength-selective panels (CO550a, CO700, CO770). 2-[2-[2-Chloro-3-[(1,3-dihydro-1,3,3-trimethyl-2H-indol-2-ylidene)ethylidene]-1-cylcohexen-1-yl]-ethenyl]-1,3,3-trimethyl-1H-indolium iodide (IR775-I, Few Chemicals) and 2-[2-[2-chloro-3-[2-(1,3-dihydro-3,3-dimethyl-1-ethyl-2H-benz[e]indol-2-ylidene)ethylidene]-1-cylohexen-1-yl]-ethenyl]-3,3-dimethyl-1-ethyl-1H-benz[e]indolium iodide (Cy-I, American Dye Source). Cy-I and IR775-Cl were mixed with potassium tetrakis(pentafluorophenyl)borate (K-TPFB) as described elsewhere to create Cy-TPFB (CO770) and IR775-TPFB (CO700) (Suddard-Bangsund et al. 2016). Lumogen F Red 305 (CO550a) was purchased from BASF. The dyes were dissolved

28

in ethanol and mixed with Shandon mounting media (CAS#9990435, Thermo Fisher Scientific) in a solution to mountant volume ratio of 1:2. This mixture was drop-cast onto acrylic sheets and allowed to dry in a fume hood for 6 hours. The dried panels were transferred into a glovebox under nitrogen. A layer of epoxy (KATIOBOND) was applied to the outer edge of the film, and a glass sheet was placed on top of the epoxy layer. The epoxy was treated with UV light until cured, and the active area of the panel was covered with a mask to reduce UV exposure prior to the study.

Preparation of wavelength-selective panel of CO550b. Copper (II) Pthalocyanine (CuPc) (CO550b) films were grown on acrylic panes in a custom thermal evaporator from Angstrom Engineering by evaporating powdered CuPc (Sigma Aldrich) in a tungsten boat. The acrylic was mounted on a rotation stage. The film was grown at a rate of 2 Å/s to a thickness of 5000 Å at room temperature and a pressure of less than 3x10-6 torr.

Preparation of neutral density treatment. The Neutral Density Gray panels were purchased from ePlastics. Two pieces were stacked on top of each other to achieve the ND33 treatment.

Chamber construction. Seven chambers were constructed, each covered by different luminescent solar concentrator panels or ND panels. These chambers were placed on the benches of a research greenhouse (Fig. II-2, Fig. II-3). Each chamber was 92 cm wide, 98 cm long, and had a total volume of 0.66 m^3 (Fig. II-2a). Chamber frames were constructed of polyvinyl chloride (PVC) pipe and enclosed on the four sides perpendicular to the base with opaque 1.3-cm thick insulation board to ensure light reaching plants passed solely through the panels. Moreover, we painted the inside of the insulation boards with flat white paint to increase light scattering. Each experimental chamber was constantly ventilated by heavily perforating the north-facing wall and installing one 120 V, 3.1 $m^3 min^{-1}$ fan (Axial 1238, AC Infinity Inc., City of Industry, CA) on the south-facing wall, which is in line with the research greenhouse airflow (Fig. II-2b). Chamber roof frames were fabricated from steel angle-bar and pitched 20 degrees toward the south to maximize sunlight transmission to plants inside.

Environmental sensing. Quantum sensors (LI-190SA; LI-COR, Inc., Lincoln, NE, or SQ-500; Apogee Instruments, Inc.) measured instantaneous PPFD and were located on the north-facing wall of each chamber and maintained level with the top of the plant canopies (Fig. II-2b). One aspirated thermocouple (Type E; Omega Engineering, Inc., Stamford, CT) per chamber measured air temperature. A CR-1000 datalogger (Campbell Scientific, Logan, UT) and

AM16/32B multiplexer (Campbell Scientific) sampled instantaneous air temperature and PPFD measurements every minute and recorded hourly averages. Average daily temperature and DLI) were calculated and recorded (Fig. II-4).

Greenhouse environment. Each chamber was in an east-to-west oriented glass-glazed research greenhouse at Michigan State University (42.7° N/84.5° W) on individual aluminum benches. A greenhouse environmental control system (Integro 725; Priva North America, Vineland Station, ON, Canada) regulated the air temperature at a set point of 21 °C. Radiant steam heating, roof vents, exhaust fans, and an evaporative cooling pad regulated air temperature. The air temperature inside the experimental chambers averaged 25, 27, and 24 °C for basil, petunia, and tomato, respectively, while air temperature differences between each chamber varied by a maximum of 2 °C (Fig. II-4a–c; Table II-1).

Basil seedling culture. Basil seeds (Johnny's Selected Seeds, Winslow, ME) were sowed directly into round 4-in pots (473 mL) filled with a greenhouse media consisting of 70% peat moss, 21% perlite, and 9% vermiculite (Suremix; Michigan Grower Products, Inc., Galesburg, MI) and placed inside experimental chambers on 12 May 2020. Each 4-in pot contained seven basil plants. Irrigation was provided as needed with a solution consisting of reverse osmosis water supplemented with 13N–1.3P–12.5K water-soluble fertilizer that contained (in mg·L^{-1}) 125 N, 13 P, 120 K, 77 Ca, 19 Mg, 1.7 Fe, 0.4 Cu, and Zn, 0.8 Mn, 0.2 B and Mo (MSU Orchid RO Water Special; GreenCare Fertilizers, Inc., Kankakee, IL).

Petunia and tomato seedling culture. Petunia seeds (Harris Seeds Co., Rochester, NY) were sown in a controlled-environment growth room on 29 May 2020 into 288-cell (8-mL individual cell volume) plug trays filled with a propagation mix consisting of 50% of greenhouse media mentioned previously (Suremix; Michigan Grower Products, Inc.) and 50% vermiculite by volume. Seeds of tomato, a dwarf variety, (Park Seed Co., Hodges, SC) were sown in the same growth room on 13 July 2020 into 128-cell (17.5-mL individual cell volume) plug trays filled with the same propagation mix as petunia. Petunia and tomato germinated under a 10-h and 18-h photoperiod, respectively, at a constant 23 ºC and a PPFD of 175 µmol m^{-2} s^{-1}. Sole source electrical lighting was provided with a white light-emitting diode (LED) fixture (RAY22; Fluence, Austin, TX). Transparent plastic humidity domes covered the germinating seedlings until cotyledon emergence (6 d). Seedlings were irrigated as needed with a solution of deionized water, hydroponic water-soluble fertilizer (12N–1.7P–13.3K RO Hydro FeED, JR Peters, Inc,

Allentown, PA), and magnesium sulfate (Epsom salt, Pennington Seed Inc., Madison GA) that provided the following nutrients (in mg L^{-1}): 125 N, 18 P, 138 K, 73 Ca, 49 Mg, 37 S, 1.6 Fe, 0.5 Mn, 0.4 Zn, 0.2 B and Cu, and 0.01 Mo. Seedling stock solution pH and electrical conductivity were measured upon formulation with a handheld meter (HI9814; Hanna Instruments, Woonsocket, RI) and adjusted to a pH of 5.8 and electrical conductivity of 1.2 mS cm^{-1}.

Mature crop culture. Ten pots of basil, petunia, and tomato were randomly placed into each chamber at a density of 10 pots m^{-2} until ready for harvest. Each pot was filled with the same peat-based greenhouse media described for basil seedling culture. Basil grew inside the chambers for 35 d until harvest on 16 June 2020. Petunia were transplanted into 4.5-in round pots on 20 June 2020, and grew inside chambers until 21 Jul. 2020 (31 d) when all plant had at least one fully open flower. Tomato seedlings were transplanted into 4.5-in round posts on 30 Jul. 2020. Tomato seedlings were transplanted when they developed a good root system (17 d) and grew inside experimental chambers for 75 d until harvest on 13 Oct. 2020, which is when plants in the ND91 chamber had ripe fruit. Basil, petunia, and tomato were irrigated as needed with the identical solution described in the basil seedling culture.

Plant data collection. At harvest, the following data were measured for both basil, petunia, and tomato: stem length (from the substrate to the apical meristem); fresh and dry above-ground biomass using scales (GR-200 and GX-1000; A&D Store, Inc., Wood Dale, IL); the length, width, area, and relative chlorophyll content of the youngest fully expanded leaf using a ruler, leaf area meter (LI-3100 Area Meter; LI-COR, Inc.), and relative chlorophyll content with hand-held meter (MC-100; Apogee Instruments, Inc., Logan, UT). Basil, petunia, and tomato fresh samples were dried for at least four days in parchment bags at 60 ºC in a drying oven (Blue M, Blue Island, IL) before dry mass was measured. In addition to the measurements taken for both species, independent measurements were taken for basil, petunia, and tomato. For basil, we also measured the total number of expanded leaves, expanded nodes, and branches >5 cm long; total leaf area of all expanded leaves; stem diameter at substrate level with a digital caliper (41101 DigiMax; Wiha Switzerland, Monticello, MN, USA); and fresh and dry mass of just the leaves or stems. Because each basil pot contained seven plants, we selected three plants from each pot that excluded the two tallest and two shortest plants and averaged their growth metrics. For petunia we counted the time to visible bud and flower since seed sow, number of branches > 10 cm, inflorescence, and nodes under the first flower; and measured the longest lateral branch. For tomato, we also measured fruit

number (ripe and unripe); fruit fresh and dry mass; and the date on which the first flower had fully reflexed petals. Specific leaf area (*SLA*) was calculated by dividing the youngest fully expanded leaf's area by its dry mass, and plant compactness by dividing its above-ground dry mass (excluding fruit for tomato) by its stem length according to Burnett et al. (Burnett et al. 2006). Two-dimensional projected canopy area (*PCA*) was recorded for each tomato plant with an overhead photograph and analyzed in ImageJ software (http://imagej.nih.gov/ij).

      Experimental design and statistics. The experiment was organized as a completely randomized design where treatments (7 levels) and plants were assigned to random chambers (experimental units) inside the research greenhouse. Data were analyzed in R software (Version 4.0.3, The R Foundation, Vienna, Austria) using analysis of variance (ANOVA) and Tukey's honestly significant difference test at $\alpha = 0.05$. Regression analysis comparing basil and tomato growth parameters (i.e., dry mass, stem length, or leaf area) as a function of the average DLI was first evaluated as a linear or quadratic function, but often trends appeared sigmoidal, in which the following Gompertz function was used:

$$y = a \exp\left(-b\, c^x\right), \tag{1}$$

where y = response variable (growth parameter), a = asymptote, b = displacement on the x-axis, c = growth rate, and x = predictor variable (DLI). The Gompertz function is an asymmetrical logistic function where the right-hand portion of the curve approaches the upper asymptote more gradually than the left-hand portion approaches the lower asymptote. Past studies have used the Gompertz function to describe the growth of biological organisms as a function of time and plant growth responses as a function of cumulative thermal energy and DLI (Carini et al. 2019; Yasin et al. 2019). The Gompertz function was selected over the symmetrical logistic function because curves visually fit the data better and typically had higher r^2 values.

Results

      We constructed seven ventilated chambers (each a roof area of ~0.96 m^2) that were each covered with a different experimental TPV glazing material (Fig. II-3). We provided three neutral-shading treatments to quantify the effects of PAR loss on crop production: 91% (ND91), 58% (ND58), and 33% (ND33) transmittance across PAR (Fig. II-5a). We also developed four wavelength-selective treatments based on luminescent solar concentrator (LSC) molecule platforms designed with different cutoffs to determine how removing specific wavebands and overall DLI affect plant growth, development, and yield (Fig. II-5b and II-5c): two in the NIR

(CO700 and CO770) and two in the PAR wavebands (CO550a and CO550b) (Debije and Verbunt 2012). We note that the absorption profiles of these panels have the same absorption profile of complete transparent luminescent solar concentrator modules but do not have PV strips mounted around the edge.

Fig. II-6 depicts selected growth attributes of basil, petunia, and tomato as a function of the DLI transmitted through the different glazing treatments. Each yield or quality parameter is plotted as a function of the average treatment DLI, since DLI is strongly correlated with plant growth and yield for many greenhouse crops; regression equations are displayed in Tables II-2–4 (Marcelis et al. 2006). We selected these attributes because they are important to the yield and quality of each crop and vary among crop types. Basil yield reflects the biomass accumulation of leaves and stems whereas stem length, leaf size, and color are quality parameters (Fig. II-6a–d). While it is important to quantify the biomass accumulation of petunia, floriculture crops derive more of their marketability from aesthetic qualities such as stem length (preference for compactness) and number of flowers (floral display) (Fig. II-6e–h). Unlike basil and petunia, tomato yield reflects fruit fresh mass and number (Fig. II-3i–l).

Basil growth

Basil growth and development parameters measured were highly correlated with the average transmission DLI. We characterized basil yield as the average shoot dry mass per plant (leaves plus stems). Regardless of the spectral transmission differences among treatments, there was a sigmoidal relationship between the yield of basil and the average DLI (Fig. II-6a; equation Table II-2), where yield increased linearly when the DLI was between ~6 and ~12 mol m^{-2} d^{-1}. Yield did not increase much further when the DLI exceeded ~12 mol m^{-2} d^{-1}. Basil yield was similar when grown under the ND91, CO770, and CO700 treatments, corresponding to treatments with a transmitted DLI typically ≥12 mol m^{-2} d^{-1} (Table II-5). Basil grown between a DLI of ~10 and ~14 mol m^{-2} d^{-1} (i.e., CO770, CO700, and CO550a) had statistically similar stem lengths compared to the ND91 treatment (DLI = ~20 mol m^{-2} d^{-1}) but produced fewer nodes and thinner stems at the substrate surface (Fig. II-6b; Table II-5). Elongation and narrowing of basil stems (Fig. II-7) caused plants to become progressively less upright compared to the ND91 treatment, which could negatively affect basil consumer appeal or ease of production (i.e., harvest and shipping). In addition to yield, leaf morphology is important to basil cultivation. Similar to basil yield and stem morphology, leaf morphology was correlated with treatment DLI (Table II-1). Basil

leaf length, width, and total surface area were similar when the average DLI was ≥ 12 mol m^{-2} d^{-1}, which typically occurred in the ND91, CO770, and CO700 treatments (Fig. II-6c; Table II-2). However, the relative chlorophyll content (*SPAD*) of basil decreased with any amount of shading, resulting in leaves with a lighter green color (Fig. II-6d). Reduced pigmentation could negatively affect the aesthetic appeal of basil products. In summation, when DLI was ≥ 12 mol m^{-2} d^{-1}, basil yield was statistically similar across treatments but came at the consequence of altered stem and leaf morphology.

Petunia growth

We characterized petunia yield as the average shoot dry mass per plant (leaves plus stems), and regardless of the spectral transmission differences among treatments, there was a sigmoidal relationship between biomass and the average DLI (Fig. II-6e; equations in Table II-3). Yield increased linearly when the DLI was between ~6 and ~12 mol m^{-2} d^{-1}. When the DLI exceeded ~12 mol m^{-2} d^{-1}, the yield response was at or near saturation. Thus, petunia yield was similar when grown under the ND91, CO770, CO700, and CO550a treatments when the transmitted DLI was typically ≥ 12 mol m^{-2} d^{-1} (Table II-6). While shoot biomass is not inconsequential to floriculture crops, floriferousness, time to flower, and overall canopy size can have a larger role in the marketability of a crop. Petunia grown under a DLI >13 mol m^{-2} d^{-1} (i.e., CO770 and CO700) had statistically similar central stem lengths compared to the ND91 treatment (DLI = ~20 mol m^{-2} d^{-1}) (Fig. II-6f; Table II-6). As seen in Fig. II-7, when the DLI was <13 mol m^{-2} d^{-1}, apical dominance increased in a dose-dependent manner, to the point that lateral branching was completely inhibited in the lowest DLI treatment (CO550b, DLI = ~7 mol m^{-2} d^{-1}). Petunia lateral branch length was statistically similar under treatments with DLIs between ~10 and ~20 mol m^{-2} d^{-1}, but petunia lateral branches were significantly longer under the CO550a (DLI = 12.8 mol m^{-2} d^{-1}) treatment compared to the ND91 treatment. This suggested the CO550a photoselective material that removed many of the B and G photons from transmission increased extension growth. However, the CO550a treatment did not comparably increase leaf area, and petunia that received a DLI between ~12 and 20 mol m^{-2} d^{-1} had a statistically similar individual leaf size (Fig. II-6h). The time to first open flower after transplant was statistically similar for petunia in the ND91, ND58, CO770, CO700, and CO550a treatments, which all had an average DLI >7 mol m^{-2} d^{-1} (Table II-6). When DLI was ≤ 7 mol m^{-2} d^{-1}, petunia flowered ~3 days later than those in the ND91 treatment. Petunia produced fewer total flowers when the DLI was <12 mol m^{-2} d^{-1} (Fig. II-6g).

Tomato growth

As a fruiting crop, tomato usually has a longer production time than basil or petunia. We characterized tomato yield as the total fresh mass of all fruits (ripe and unripe) per plant at a single destructive harvest. While most growth parameters for basil and petunia were best described as sigmoidal functions of DLI, tomato yield increased linearly with DLI and never approached an upper asymptote (Table II-4). This indicated that any decrease in PAR transmission negatively influenced yield, and even the coverings with the highest PAR transmission (CO770 and CO700) had 25% and 37% less yield than the ND91 treatment (Fig. II-6i). Total number of fruit and fruit dry mass in these three treatments were similar, indicating a decrease in DLI decreased fruit size, delayed fruit ripening, or both (Fig. II-6k). As such, tomato in the CO770 and CO700 treatments had 52% and 74% fewer ripe fruit at harvest than the ND91 treatment, respectively (Fig. II-6i). Tomato leaf morphology was not influenced by the average DLI or specific absorption bandwidths. However, tomato stem length increased and stem diameter decreased with decreasing DLI (Fig. II-6j, II-7). As a result, tomato required physical support to remain upright under low DLI conditions. The time to first open flower after transplant was statistically similar for tomato in the ND91, ND58, CO770, CO700, and CO550a treatments, which all had an average DLI ≥ 6 mol m^{-2} d^{-1} (Table II-7). When DLI was <6 mol m^{-2} d^{-1}, tomato flowered ~14 days later than those in the ND91 treatment.

Discussion

Quantum units in agrivoltaics

The field of agrivoltaics is relatively new and being pursued by several interested disciplines in engineering and plant sciences. In this work, we first describe plant responses to DLI because it is a quantum unit that drives photosynthesis, is highly correlated with crop yield and quality, and responses have been characterized in a wide range of greenhouse crops (Colonna et al. 2016; Cossu et al. 2020). Radiometric units (Watts or Joules) that integrate over a wider waveband of electromagnetic radiation are still important to the field of agrivoltaics because they can better describe the effect of building-integrated (BIPV) panels on the microclimate around plants (e.g., air temperature) or plant process such as transpiration that can ultimately influence crop growth.

Definitions for *PPFD* and DLI assume any photon with a wavelength between 400 and 700 nm equally powers photosynthesis (i.e., it has the same quantum yield). However, photons can have different quantum efficiencies (the yellow line in Fig. II-1b) based on their relative action

35

and leaf absorption (McCree 1972; Hogewoning et al. 2012). Thus, a weighted description of PAR was created to give a more accurate representation of the instantaneous photosynthetic rate based on the spectral distribution of a light source, which is termed yield photon flux density (YPFD) (Sager et al. 1988). In this case, YPFD is not restricted to just PAR; photons <400 nm and >700 nm are included, although their efficacy decreases rapidly as photon wavelengths decrease below 400 nm and increase above 700 nm. Recently, there has been a proposed definition change of PAR to consider photons between 400 and 750 nm as photosynthetically active, which has been termed extended PAR or ePAR (Zhen and Bugbee 2020a; Zhen and Bugbee 2020b). ePAR is relevant to the current study because whether TPVs begin to cutoff around 700 nm or closer to 750 nm could impact plant growth and energy generation. Regardless of which waveband is used to describe the photometric transmission of a photovoltaic material, reporting at least one of these plant-centric parameters is required to characterize the plant environment appropriately and to make plant growth and yield comparisons among treatments and studies meaningful. While meaningful differences between DLI, eDLI, and YPFD as predictor variables for several basil growth parameters were not observed in the current study, large transmission differences may have attenuated the effect (Appendix C). Further research into the most applicable quantum unit is still required in the field of agrivoltaics.

Crop growth and yield

Crop yield (crop biomass per unit area) and quality (e.g., metrics of aesthetics or nutritional density) influence revenue generated from horticultural crops whether grown in a field or controlled environment such as a greenhouse. While yield has a simple mathematical definition, crop quality is subjective and can consider consumer preferences for, and interactions with, an agricultural product. Examples include crop nutrition and flavor and physical qualities that make a crop easier to manage, harvest, ship, or market. Ideally, agrivoltaic systems would have no negative effect on crop yield or quality while creating passive income through electrical generation. An inescapable challenge for designing and using agrivoltaic systems is accounting for the many different crops and growing systems used in plant-based agriculture. The diversity of uses for the same land area should emphasize the need for flexible agrivoltaic systems, since each crop, and even diversity within a crop species, could have specific tolerances to DLI reductions and/or removed wavebands of radiation.

36

To strive towards broad agricultural application of BIPV cover, namely one that would have negligible impact on the yield and quality of different crops, we grew three economically important greenhouse crops that offered diverse comparisons among plants primarily grown for their leaves and stems (basil), flowers (petunia), and fruits (tomato). Generally, basil and petunia are commercially grown under moderate DLIs, while light is usually maximized for fruiting crops such as tomato (Cossu et al. 2020). However, in regions in which light is seasonally limiting, such as > 35 °N or S latitude, most commercial greenhouse growers cannot tolerate more than slight reductions in the DLI, even for crops such as basil and petunia.

For broad comparison, we plotted relative growth parameters for the three greenhouse crops as a function of the average DLI in each treatment (Fig. II-8). Data were converted to that relative to the average value of the control treatment for each growth parameter and species. This facilitates more direct response comparisons for the three representative crops commonly produced by greenhouse growers in terms of growth and yield (Fig. II-8a), as well as leaf (Fig. II-8b, 8c), stem (Fig. II-8d, 8e), and plant (Fig. II-8f) morphological responses. The three crops generally responded similarly to DLI, with two notable exceptions: 1) relative yield approached or reached a saturating DLI for basil and petunia, but not for tomato; 2) stem length of basil increased with DLI until a saturating value, whereas it decreased with DLI for petunia and tomato.

Direct comparisons between our results and past agrivoltaic studies are challenging because many of those studies reported shading factors or percentage roof cover of experimental BIPV materials, but actual light conditions would depend on geographic location and time of year, among other factors. For example, lettuce grown under PV panels that decreased *PPFD* by as much as 50% caused limited yield reductions in some studies (Touil et al. 2021; Ravishankar et al. 2021; Kadowaki et al. 2012; Marrou et al. 2013; Trypanagnostopoulos et al. 2017; Hassanien et al. 2017; Kavga et al. 2018; Valle et al. 2017). In contrast, other studies reported that basil, spinach, lettuce, and arugula yield decreased under PV panels that decreased *PPFD* by 25–60% (Thompson et al. 2020; Kavga et al. 2018; Valle et al. 2017). Reporting common quantum units and DLI, not just reduction in quantum flux, would aid in comparing studies. Many of these studies were conducted in the summer with very high incident DLIs, which may have resulted in relatively little yield loss. However, during winter greenhouse conditions, when DLIs may be at or below 10 mol m^{-2} d^{-1}, any shading may reduce yields and thus a decrease in DLI may not be tolerable. Inconsistencies among studies as well as seasonal and geographic differences in solar radiation

attest to the challenges of providing consistent shading tolerances for non-fruiting crops. Nonetheless, Touil et al. (2021) concluded that up to 25% shading was generally tolerable to crops, but this would still depend on location and crops grown (Touil et al. 2021). In addition to measuring and reporting quantum units, the use of benchmark plant species would help advance agrivoltaic development.

Fig. II-8a indicates a near-saturating DLI for production of high-quality basil and petunia is ~12 mol m^{-2} d^{-1}, which is consistent with previous studies on sweet basil and petunia, as well as other floriculture crops including impatiens (*Impatiens wallerana*), begonia (*Begonia ×semperflorens-cultorum*), and ageratum (*Ageratum houstonianum*) (Faust et al. 2005; Dou et al. 2018; Blanchard et al 2011; Torres and Lopez 2011). This indicates agrivoltaic panels that decrease the DLI by up to 40% (maintaining DLI $\geq$ 12 mol m^{-2} d^{-1}) can be useful for greenhouse systems during late spring and summer. However, when the ambient solar DLI is lower, such as during the winter and early spring, these reductions would negatively impact growth. Thus, for BIPV panels acting as a permanent greenhouse glazing, acceptable transmissions should heavily consider often suboptimal seasonal conditions for a particular geographical location.

Tomato did not tolerate even modest shading (e.g. a DLI < 12 mol m^{-2} d^{-1} or a decrease of 4 mol m^{-2} d^{-1} in the current work) without a decrease in yield or number of ripe fruits at harvest (Fig. II-8a), which is consistent with previous literature on tomato and other fruiting crops such as pepper (*Capsicum annuum*) and cucumber (*Cucumis sativus*) (Cossu et al. 2020). Moreover, it is likely our dwarf tomato cultivar was more tolerant of less light than much larger indeterminate tomato varieties typically grown in greenhouses with DLIs >20 mol m^{-2} d^{-1} (Dorais 2003). Decreased yield and delayed ripening were previously observed as a consequence of BIPV and traditional shading (Cossu et al. 2020; Gent 2007; Kläring and Krumbein 2013; López-Díaz et al. 2020; Waller et al. 2021). Therefore, for tomato and other fruiting crops, BIPV panels used for greenhouse applications should maximize transmission of PAR in temperate regions, but modest decreases in PAR transmission may be tolerable in subtropical, tropical, and especially arid regions.

There was a clear relationship between DLI and yield of the three crops studied, yet there is also the potential to manipulate the solar spectrum to increase the yield of at least some species. For example, lettuce, kale (*Brassica oleracea*), geranium (*Pelargonium × hortorum*), and snapdragon (*Antirrhinum majus*) had greater shoot dry mass when grown under higher fractions

of R and FR photons compared to B and G photons (Meng et al. 2019; Meng et al. 2020; Park and Runkle 2017). Substituting shorter-wavelength B and G photons for longer wavelength R and FR photons increased leaf area and light interception, which increased biomass accumulation. Thus, semi-transparent PV panels could theoretically be designed to absorb more B and G photons (for greater energy generation) than R and perhaps FR photons (for greater quantum yield) if the altered crop morphology was tolerable. However, for high-light crops such as fruiting vegetables, PV panels with maximal transmission of PAR may be needed, particularly in temperate climates. While the transmission (i.e., DLI) differences observed between treatments in the current study likely attenuated spectral effects, more research is needed to elucidate how waveband-selective absorption of B, G, R, and/or FR light influences both energy output and growth of diverse crops.

Crop morphology and quality

In addition to yield, shading can negatively impact crop quality, but such effects are often not reported in agrivoltaics research. The marketability and quality of many floriculture crops, as well as other ornamentals, is influenced more by their appearance and physical qualities (e.g., flower number and size) than biomass accumulation. Therefore, application of BIPV materials to greenhouses must also consider morphological acclimation, leaf and flower pigmentation, branching, time to flower, and floriferousness of crops. Striking a balance between crop quality, yield, and electrical generation by BIPV panels necessitates a comprehensive approach to crop evaluation in agrivoltaic systems.

Leaf morphology, pigmentation, and in some cases flavor, are important quality attributes for greenhouse crops sold for their vegetative growth. Fig. II-8b shows SLA was inversely and linearly related to the treatment DLI for each species, especially for tomato. Increased SLA (i.e., increase leaf surface area at the expense of leaf thickness) is a common plant response to increase light interception (Franklin 2008). Marrou et al. (2013) suggested that certain plant species that acclimate to shading by increasing their light interception could be more desirable for agrivoltaic systems (Marrou et al 2013). However, the thinning of leaves could make them more susceptible to stressors (e.g., pathogens) and physical damage during production and harvest. Leaf pigmentation, which we quantified by relative chlorophyll content (SPAD) measurements, increased as a function of the average DLI for each crop (Fig. II-8c). Among the three crops grown, basil quality could be the most negatively affected by lower chlorophyll concentration (i.e., lighter green color) because its quality is heavily dependent on leaf appearance. In addition to morphology

and color, the concentration of flavonoids decreased as DLI decreased (Walters et al. 2021). Therefore, although leaf morphology and yield of basil, petunia, and tomato were similar when the DLI decreased from ~20 to ~12 mol m^{-2} d^{-1}, there were some negative effects on metrics of plant quality.

Stem morphology (e.g., stem length and diameter) can influence the marketability of greenhouse crops. In most cases, commercial growers strive to produce containerized crops that are branched and compact (e.g., short and thick stems) to facilitate shipping and handling. A decrease in DLI increased stem elongation of tomato and decreased stem diameter of basil and tomato (Fig. II-8d and e). The thinner and longer stems of basil and tomato plants necessitated physical support to remain upright. While this may not influence tomato production because string typically provides support during commercial greenhouse production, it can reduce the quality of potted horticultural crops like basil or increase lodging of agronomic crops like soybean (Glycine max), which should remain upright without support. Calculations for compactness (plant mass per unit height) or the ratio of plant height to plant diameter help estimate the space an individual plant occupies during production. Compactness decreased (i.e., each plant occupied more space) as DLI decreased in all crop species, suggesting cropping density may need adjustment under some agrivoltaic systems, and this could ultimately influence crop yield (Fig. II-8f). Excessive extension growth is usually undesirable for floriculture crops, so the increase in stem elongation and decrease in plant compactness under lower DLIs decreased their quality, or would necessitate increased use of plant growth retardants in their management (Runkle and Heinz 2002). Similar to leaf morphology, greenhouse crop quality decreased with the transmitted DLI, which highlights the nuanced trade-offs that exist between crop yield and quality and the need for BIPV covers with high transmission of PAR.

Commercial greenhouse growers of ornamentals strive to produce crops in the shortest time possible while maintaining at least acceptable plant quality, while growers of fruiting crops seek to maximize yield per unit area and time (Kaczperski et al. 1991). We observed delayed flowering of petunia and tomato when the treatment DLI was <7 and 6 mol m^{-2} d^{-1}, respectively. Importantly, we started to observe morphological differences and reduced floriferousness when the DLI was <12 mol m^{-2} d^{-1}. Our results indicate petunia, and likely other floriculture crops, could tolerate moderate shading without decreasing yield or quality, which makes ornamentals more suitable

than fruiting vegetable crops for agrivoltaic systems located in temperate regions. To date, however, few studies have focused on ornamental crops in agrivoltaic systems.

Similar to yield, DLI was the predominate factor influencing crop quality parameters. In addition to DLI, the light spectrum also influences plant morphology and acclimation responses (Meng et al. 2019, Meng et al. 2020; Park and Runkle 2017). Responses to light spectrum include: 1) B-light mediated inhibition of cellular expansion and thus leaf area and internode elongation, as well as increased accumulation of secondary metabolites; 2) G-light promotion of *SLA* and stem elongation; and 3) shade-avoidance responses (e.g., increase in extension growth and *SLA*) triggered by a decrease in the ratio of R to FR light. In this study, basil and petunia tolerated some degree of shading without triggering shade-avoidance responses such as thinner leaves and stem elongation, which would decrease crop quality. As with biomass accumulation, the potential exists to develop PVs that modify the solar spectrum to increase crop quality of greenhouse crops. For example, PVs that transmit B light and absorb FR light would likely increase crop compactness, branching, and leaf pigmentation, but could delay flowering of some crops. Additional research is needed to understand how manipulation of the solar spectrum influences quality parameters of various species, as well as qualify trade-offs that may exist with crop growth and biomass accumulation.

Potential power output of transparent agrivoltaics

Translating semitransparent and TPV modules to plant- and agriculture-based applications requires re-defining key metrics. Typically for TPVs in the window industry, the average visible transmittance (AVT) is the most important reported parameter. It is a measure of how much incident solar photon flux passes through the panel or window weighted by the average response of the human eye (i.e., the photopic response). To translate this definition to agrivoltaics systems, we introduce a new metric, the average photosynthetic transmittance (APT), which is analogous to AVT for the window industry. Replacing the photopic response, we utilize the relative quantum efficiency of plants from McCree (1972), which is defined as the instantaneous CO_2 consumption rate per photon absorbed that is averaged among 22 varieties of plants and remains the broadest plant quantum efficiency study to date. Thus, APT is defined as:

$$APT = \frac{\int T(\lambda)S(\lambda)P(\lambda)d\lambda}{\int S(\lambda)P(\lambda)d\lambda},$$ (2)

where $S(\lambda)$ is the AM1.5G photon flux, $T(\lambda)$ is the photon transmittance of the panel, and $P(\lambda)$ is now the average photosynthetic quantum yield (McCree 1972; Reference Air Mass 1.5 Spectra).

Thus, APT is a property of the panels placed above plants that ultimately impacts and imparts a particular quantum unit (e.g., DLI, YPFD, etc.) based on the location and position-dependent solar flux.

We first utilize the definition of APT and PAR to define the upper limit for TPVs in agrivoltaics with maximum transparency. For this work, we assume the use of single-junction modules and perfectly sharp cutoffs where the transmittance is 1 between 395-715 nm (a wavelength range dictated by setting an APT of 95%) and 0 outside that range. The theoretical power conversion efficiency (PCE) of PVs is limited by the radiative recombination dark current in the detailed balance limit. This can be calculated via the Shockley ideal diode equation with the dark saturation current as:

$$J_S \cong qg \int_{E_G}^{\infty} \frac{E^2}{\exp\left(\frac{E}{nkT}\right)-1} dE, \tag{3}$$

where $g = 2\pi/(c^2h^3)$, n is the ideality factor ($n = 1$ in this case), c is the speed of light, h is Planck's constant, and E_G is the band gap of the active material in the PV. The thermodynamic single-junction Shockley-Queisser (SQ) limit also assumes: one hundred percent internal quantum efficiency, parallel resistance is infinite, series resistance is negligible, only photons with energy equal to or greater than the bandgap are absorbed, and each photon corresponds to exactly one electron. For an opaque single-junction PV module, the PCE limit is 33.7%, meaning that 33.7% of the total energy from incident solar irradiance can be converted to electricity. The limit is 20.6% for modules that transmit all light between 435-670 nm (Lunt 2012). When expanding the transmission range to 395-715 nm, the resulting theoretical limit is 17.4%. When we apply practical constraints for device operation such as device resistance (assuming 80% voltage limit, 85% maximum external quantum efficiency, and 80% fill factor), the PCE limit is around 9.5% for a device transmitting light between 395-715 nm. The thermodynamic limits we define here for standard TPV modules also translate equivalently to the limits for visibly transparent luminescent solar concentrators (TLSCs) (Yang and Lunt 2017). TLSCs are capable of higher APT values (~90%) because TPV modules are limited by multiple transparent electrodes to an APT of ~80%; however, TLSCs have lagged behind TPVs in PCE (Yang et al. 2021).

We use these limits to project forward and estimate the total potential energy output for transparent agrivoltaics that maintain maximum transparency and minimal plant impact. In the U. S., the total amount of area under protected surfaces (e.g., glass and plastic greenhouses) is

approximately $1.1 \ 10^7 \ m^2$ for fruit, vegetable, and herb production and $7.0 \ 10^7 \ m^2$ for floriculture crop production (for the 17 states surveyed) (USDA 2021). Assuming 50% of this covered area is permanent greenhouses, this gives an area of $\sim 4.0 \ 10^7 \ m^2$. Given that the annual average incident solar insolation across the US is 4.5 kWh $m^{-2} \ d^{-1}$, we then use benchmark efficiencies up to the calculated limits to show the potential annual energy output (Table II-8) (National Renewable Energy Laboratory). Assuming 5%-efficient modules, this translates to 3 TWh annually. While the greenhouse energy output value is modest, it can provide important power generation to cover much of the energy demands of greenhouse operation and produce excess energy in high solar flux regions. This effect could become increasingly important as the use of greenhouses expands to enable growth in regions that are less favorable for plant growth, and indeed could hasten greenhouse adoption. In contrast, the total area of farmland (including pastureland) in the US is $3.6 \ 10^{12} \ m^2$ (USDA 2019). Agrivoltaics could further be integrated more widely into fields and farmland, particularly if the tradeoffs between plant productivity and power generation can be minimized with the proposed TPV design approaches. In this case, array support structures that enable operating equipment (e.g., tractors and irrigation systems) to function as necessary would be important. Indeed, such solar installations could be synergistically and simultaneously installed with irrigation systems (and perhaps fertilizer and pesticide solutions too) such that the PV mounting systems double as conduit for subsurface, drip, or spray irrigation. At the theoretical limit, the total output would approach $1.0 \ 10^6$ TWh ($\sim$3,500 quadrillion British thermal units, quads), which is more than the entire energy demand of the U.S. across all sectors. We estimate TPV agrivoltaic panels could reasonably cover upwards of 1-10% of farmland area, translating to a minimum of $3.6 \ 10^{10} \ m^2$ in this case. The use of 5% efficient TPV modules over 1% of farmland results in 3,000 TWh annually, enough energy to account for 75% of the U.S. electricity consumption ($\sim$4000 TWh), and 10%-efficient TPVs would provide 6,000 TWh annually, surpassing the entire electricity consumption (US Energy Information Administration 2021). Scaling up to 10% of farmland and utilizing practically achievable 10%-efficient TPVs, the total power output would be 60,000 TWh ($\sim$200 quads), which would more than double the 27,000 TWh ($\sim$93 quads) of total power generated in the U.S. from all sources in 2020 (Fig. II-9) (US Energy Information Administration 2021). Thus, even with minimal use of PAR for solar harvesting there remains exceptional opportunity for power generation in transparent agrivoltaics enabling efficient dual land use that can power the entire country and the world.

Conclusions

In this work, we have presented an unprecedented and comprehensive approach to determine the applicability of TPV greenhouse glazings for diverse and economically important greenhouse crops. Unique to agrivoltaic greenhouse systems is the demand for growing many different crops continuously throughout the year. Currently, more comprehensive agrivoltaics research is necessary to understand what materials are most applicable to the broad range of crops grown in greenhouses while considering agricultural practices and geographical locations. The current work offers a novel plant-centric focus where TPV materials are investigated to minimize the impact on plant growth, productivity, and yield.

Despite the often-dramatic differences in PV panel photon distribution, panel transmission was the most significant predictor of crop yield and quality. Basil and petunia yield and quality responses were saturated when the average DLI was >12 mol m^{-2} d^{-1}, which corresponded to $\sim$35–40% shading ($\sim$60-65% APT). This indicates tremendous potential for herbs and floriculture crops in agrivoltaic systems from late spring to early fall when solar irradiance is high. However, the fruiting crop tomato experienced reduced yield with even moderate BIPV shading, and thus APT $>65\%$, is even more strongly desired. Additional studies are necessary to determine a more precise red, far-red, near-infrared cutoff for fruiting crops under a variety of total DLIs to provide greater context for more diverse geographical locations. Pushing the absorption edge deeper into the NIR (>750nm) increases the transmitted DLI and therefore should reduce the impact of TPVs on fruiting crops, resulting in productivity more comparable to the control of single-pane glass. Lastly, this work identifies the need for consistent quantum unit reporting in agrivoltaics to improve study reproducibility and applicability for future agrivoltaic systems, whether building- or field-based. Establishing appropriate APT, DLI, and wavelength cutoffs for different types of crops is a necessary step towards developing TPVs for a range of truly synergistic agrivoltaic implementations.

LITERATURE CITED

AL-agele HA, Proctor K, Murthy G, Higgins C. 2021. A case study of tomato (Solanum lycopersicon var. legend) production and water productivity in agrivoltaic systems. Sustainability. 13:2850. https://doi.org/10.3390/su13052850.

Barron-Gafford GA, Pavao-Zuckerman MA, Minor RL, Sutter LF, Barnett-Moreno I, Blackett DT, Thompson M, Dimond K, Gerlak AK, Nabhan GP, Macknick JE. 2019. Agrivoltaics provide mutual benefits across the food–energy–water nexus in drylands. Nature Sustainability. 2:848–855. https://doi.org/10.1038/s41893-019-0364-5.

Blanchard MG, Runkle ES, Fisher PR. 2011. Modeling plant morphology and development of petunia in response to temperature and photosynthetic daily light integral. Sci Hortic. 129:313–320. https://doi.org/10.1016/j.scienta.2011.03.044.

Bruggink GT, Heuvelink E. 1987. Influence of light on the growth of young tomato, cucumber and sweet pepper plants in the greenhouse: Effects on relative growth rate, net assimilation rate and leaf area ratio. Sci Hortic. 31:161–174. https://doi.org/10.1016/0304-4238(87)90043-4.

Burnett SE, van Iersel MW, Thomas PA. 2006. Medium-incorporated PEG-8000 reduces elongation, growth, and whole-canopy carbon dioxide exchange of marigold. HortScience. 41:124–130. https://doi.org/10.21273/hortsci.41.1.124.

Carini F, Cargnelutti Filho A, Bandeira CT, Neu IMM, Pezzini RV, Pacheco M, Tomasi RM. 2019. Growth models for lettuce cultivars growing in spring. J. Agric. Sci, 11:147–159. https://doi.org/10.5539/jas.v11n6p147.

Colonna E, Rouphael Y, Barbieri G, De Pascale, S. 2016. Nutritional quality of ten leafy vegetables harvested at two light intensities. Food Chem. 199:702–710. https://doi.org/10.1016/j.foodchem.2015.12.068.

Cossu M, Cossu A, Deligios PA, Ledda L, Li Z, Fatnassi H, Poncet C, Yano A. 2018. Assessment and comparison of the solar radiation distribution inside the main commercial photovoltaic greenhouse types in Europe. Renew Sustain Energy Rev. 94:822–834. https://doi.org/10.1016/j.rser.2018.06.001.

Cossu M, Yano A, Solinas S, Deligios PA, Tiloca M.T, Cossu A, Ledda L. 2020. Agricultural sustainability estimation of the European photovoltaic greenhouses. Eu. J Agron. 118:126074. https://doi.org/10.1016/j.eja.2020.126074.

Debije MG, Verbunt PP. 2012. Thirty years of luminescent solar concentrator research: solar energy for the built environment. Adv Energy Mats. 2:12–35. https://doi.org/10.1002/aenm.201100554.

Detweiler AM, Mioni CE, Hellier KL, Allen JJ, Carter SA, Bebout BM, Fleming EE, Corrado C, Prufert-Bebout LE. 2015. Evaluation of wavelength selective photovoltaic panels on microalgae growth and photosynthetic efficiency. Algal res. 9:170–177. https://doi.org/10.1016/j.algal.2015.03.003.

Dinesh, H. and Pearce, J.M., 2016. The potential of agrivoltaic systems. Renewable and Sustainable Energy Reviews, 54, pp.299–308. https://doi.org/10.1016/j.rser.2015.10.024.

Dorais M. 2003. The use of supplemental lighting for vegetable crop production: Light intensity, crop response, nutrition, crop management, cultural practices. Canadian Greenhouse Conference. 9.

Dou H, Niu G, Gu M, Masabni JG. 2018. Responses of sweet basil to different daily light integrals in photosynthesis, morphology, yield, and nutritional quality. HortScience. 53:496–503. https://doi.org/10.21273/hortsci12785-17.

Faust JE, Holcombe V, Rajapakse NC, Layne D.R. 2005. The effect of daily light integral on bedding plant growth and flowering. HortScience. 40:645–649. https://doi.org/10.21273/hortsci.40.3.645.

Franklin KA. 2008. Shade avoidance. New Phytol. 179:930–944. https://doi.org/10.1111/j.1469-8137.2008.02507.x.

Gao, W., He, D., Ji, F., Zhang, S. and Zheng, J., 2020. Effects of daily light integral and LED spectrum on growth and nutritional quality of hydroponic spinach. Agron. 10:1082. https://doi.org/10.3390/agronomy10081082.

Gent MP. 2007. Effect of degree and duration of shade on quality of greenhouse tomato. HortScience. 42:514–520. https://doi.org/10.21273/hortsci.42.3.514.

Hassanien RHE, Li M, Yin F. 2018. The integration of semi-transparent photovoltaics on greenhouse roof for energy and plant production. Renew Energy. 121:377–388. https://doi.org/10.1016/j.renene.2018.01.044.

Hassanien, R.H.E. and L. Ming. 2017. Influences of greenhouse-integrated semi-transparent photovoltaics on microclimate and lettuce growth. Int. J. Agri. Biol. Eng. 10:11–22. https://doi.org/10.25165/j.ijabe.20171006.3407.

Hogewoning SW, Wientjes E, Douwstra P, Trouwborst G, van Ieperen W, Croce R, Harbinson J. 2012. Photosynthetic quantum yield dynamics: from photosystems to leaves. Plant Cell 24:1921–1935. https://doi.org/10.1105/tpc.112.097972.

Kaczperski, M.P., Carlson, W.H. and Karlsson, M.G., 1991. Growth and development of Petunia× hybrids as a function of temperature and irradiance. J Am Soc Hortic Sci. 116:232–237. https://doi.org/10.21273/jashs.116.2.232.

Kadowaki, M., Yano, A., Ishizu, F., Tanaka, T. and Noda, S., 2012. Effects of greenhouse photovoltaic array shading on Welsh onion growth. Biosystems Eng. 111:290–297. https://doi.org/10.1016/j.biosystemseng.2011.12.006.

Kavga A, Trypanagnostopoulos G, Zervoudakis G, Tripanagnostopoulos Y. 2018. Growth and physiological characteristics of lettuce (*Lactuca sativa* L.) and rocket (*Eruca sativa* Mill.) plants cultivated under photovoltaic panels. Notulae Bot Hortic Agrobot Cluj-Napoca. 46:206–212. https://doi.org/10.15835/nbha46110846.

Kläring HP, Krumbein A. 2013. The effect of constraining the intensity of solar radiation on the photosynthesis, growth, yield and product quality of tomato. J Agron Crop Sci. 199:351–359. https://doi.org/10.1111/jac.12018.

Liu Y, Cheng, P, Li T, Wang R, Li Y, Chang SY, Zhu Y, Cheng HW, Wei KH, Zhan X, Sun B. 2019. Unraveling sunlight by transparent organic semiconductors toward photovoltaic and photosynthesis. ACS nano. 13:1071–1077. https://doi.org/10.1021/acsnano.8b08577.s001.

Lopez-Diaz G, Carreño-Ortega A, Fatnassi H, Poncet C, Diaz-Perez M. 2020. The effect of different levels of shading in a photovoltaic greenhouse with a north–south orientation. Appl Sci. 10:882. https://doi.org/10.3390/app10030882.

Lunt RR, Osedach TP, Brown PR, Rowehl JA, Bulović V. 2011. Practical roadmap and limits to nanostructured photovoltaics. Adv Mats. 23:5712–5727. https://doi.org/10.1002/adma.201103404.

Lunt RR. 2012. Theoretical limits for visibly transparent photovoltaics. App Phys Letters. 101:043902. https://doi.org/10.1063/1.4738896.

Marcelis, L.F.M., A.G.M. Broekhuijsen, E. Meinen, E.M.F.M. Nijs, and M.G.M. Raaphorst. 2005. Quantification of the growth response to light quantity of greenhouse grown crops. Acta. Hortic. 711:97–104. https://doi.org/10.17660/actahortic.2006.711.9.

Marrou, H., J. Wéry, L. Dufour, and C. Dupraz. 2013. Productivity and radiation use efficiency of lettuces grown in the partial shade of photovoltaic panels. Eur. J. Agron. 44:54–66.

McCree KJ. 1971. The action spectrum, absorptance and quantum yield of photosynthesis in crop plants. Agric Meteorol. 9:191–216. https://doi.org/10.1016/0002-1571(71)90022-7.

Meng, Q., J. Boldt, and E.S. Runkle. 2020. Blue radiation interacts with green radiation to influence growth and predominantly controls quality attributes of lettuce. J. Am. Soc. Hortic. Sci. 145:75–87. https://doi.org/10.21273/jashs04759-19.

Meng, Q., Kelly, N. and Runkle, E.S., 2019. Substituting green or far-red radiation for blue radiation induces shade avoidance and promotes growth in lettuce and kale. Environ exp bot. 162:383–391. https://doi.org/10.1016/j.envexpbot.2019.03.016.

National Renewable Energy Laboratory, "Reference Air Mass 1.5 Spectra," can be found under https://www.nrel.gov/grid/solar-resource/spectra-am1.5.html, n.d.

National Renewable Energy Laboratory, "Solar Resource Data, Tools, and Maps," can be found under https://www.nrel.gov/gis/solar.html.

Park Y, Runkle ES. 2017. Far-red radiation promotes growth of seedlings by increasing leaf expansion and whole-plant net assimilation. Environ Exp Bot. 136:41–49. https://doi.org/10.1016/j.envexpbot.2016.12.013.

Proctor KW, Murthy GS, Higgins CW. 2020. Agrivoltaics align with green new deal goals while supporting investment in the US'rural economy. Sustainability, 13:137. https://doi.org/10.3390/su13010137.

Ravishankar E, Charles M, Xiong Y, Henry R, Swift J, Rech J, Calero J, Cho S, Booth RE, Kim T. 2021. Balancing crop production and energy harvesting in organic solar-powered greenhouses. Cell Reports Phys Sci. 2:100381. https://doi.org/10.1016/j.xcrp.2021.100381.

Runkle ES, Heins RD. 2001. Specific functions of red, far red, and blue light in flowering and stem extension of long-day plants. J Am Soc Hortic Sci. 126:275–282. https://doi.org/10.21273/JASHS.126.3.275.

Runkle ES, Heins RD. 2002. Stem extension and subsequent flowering of seedlings grown under a film creating a far-red deficient environment. Sci Hortic. 96:257–265. https://doi.org/10.1016/S0304-4238(02)00055-9.

Sager JC, Smith WO, Edwards JL, Cyr KL. 1988. Photosynthetic efficiency and phytochrome photoequilibria determination using spectral data. Trans Am Soc Agric Eng. 31:1882–1889. https://doi.org/10.13031/2013.30952.

Saifullah M, Ahn S, Gwak J, Ahn S, Kim K, Cho J, Park JH, Eo YJ, Cho A, Yoo JS, Yun JH. 2016. Development of semitransparent CIGS thin-film solar cells modified with a sulfurized-AgGa layer for building applications. J Mats Chem A. 4:10542–10551. https://doi.org/10.1039/c6ta01909a.

Shockley W, Queisser HJ. 1961. Detailed balance limit of efficiency of p-n junction solar cells. J app phys. 32:510-519. https://doi.org/10.1063/1.1736034.

Sivakumar MVK, Virmani SM. 1984. Crop productivity in relation to interception of photosynthetically active radiation. Agric Forest Meteorol. 31:131–141. https://doi.org/10.1016/0168-1923(84)90015-7.

Suddard-Bangsund J, Traverse CJ, Young M, Patrick TJ, Zhao Y, Lunt RR. 2016. Organic Salts as a Route to Energy Level Control in Low Bandgap, High Open-Circuit Voltage Organic and Transparent Solar Cells that Approach the Excitonic Voltage Limit. Adv Energy Mats. 6:1501659. https://doi.org/10.1002/aenm.201501659.

Terashima I, Fujita T, Inoue T, Chow WS, Oguchi R. 2009. Green light drives leaf photosynthesis more efficiently than red light in strong white light: revisiting the enigmatic question of why leaves are green. Plant cell physiol. 50:684–697. https://doi.org/10.1093/pcp/pcp034.

Thompson EP, Bombelli EL, Shubham S, Watson H, Everard A, D'Ardes V, Schievano A, Bocchi S, Zand N, Howe CJ. 2020. Tinted semi-transparent solar panels allow concurrent production of crops and electricity on the same cropland. Adv Energy Mater. 10:2001189. https://doi.org/10.1002/aenm.202001189.

Timmermans GH, Hemming S, Baeza E, Van Thoor EA, Schenning AP, Debije MG. 2020. Advanced optical materials for sunlight control in greenhouses. Advanced Optical Materials. 8:2000738. https://doi.org/10.1002/adom.202000738.

Torres AP, Lopez RG. 2011. Commercial greenhouse production. Measuring Daily Light Integral in a Greenhouse. Purdue Extension.

Touil S, Richa A, Fizir M, Bingwa B. 2021. Shading effect of photovoltaic panels on horticulture crops production: A mini review. Rev Environ Sci Bio/Tech. 20:281–296. https://doi.org/10.1007/s11157-021-09572-2.

Traverse CJ, Pandey R, Barr MC, Lunt RR. 2018. Emergence of highly transparent photovoltaics for distributed applications. Nat Energy. 2:849–860. https://doi.org/10.1038/s41560-017-0016-9.

Trypanagnostopoulos G, Kavga A, Souliotis M, Tripanagnostopoulos Y. 2017. Greenhouse performance results for roof installed photovoltaics. Renew Energy. 111:724–731. https://doi.org/10.1016/j.renene.2017.04.066.

United States Department of Agriculture (USDA). 2019. 2017 census of agriculture. https://www.nass.usda.gov/Publications/AgCensus/2017/Full_Report/Volume_1,_Chapter_1_US/usv1.pdf.

US Energy Information Administration. 2021. "Electricity explained: Use of electricity," can be found under https://www.eia.gov/energyexplained/electricity/use-of-electricity.php.

USDA National Agricultural Statistics Service, 2021, 63.

Valle B, Simonneau T, Sourd F, Pechier P, Hamard P, Frisson T, Ryckewaert M, Christophe A. 2017. Increasing the total productivity of a land by combining mobile photovoltaic panels and food crops. App Energy. 206:1495–1507. https://doi.org/10.1016/j.apenergy.2017.09.113.

Waller R, Kacira M, Magadley E, Teitel M, Yehia I. 2021. Semi-transparent organic photovoltaics applied as greenhouse shade for spring and summer tomato production in arid climate. Agron. 11:1152. https://doi.org/10.3390/agronomy11061152.

Walters KJ, Lopez RG, Behe BK. 2021. Leveraging controlled-environment agriculture to increase key basil terpenoid and phenylpropanoid concentrations: The effects of radiation intensity and CO_2 concentration on consumer preference. Front Plant Sci. 11:598519. https://doi.org/10.3389/fpls.2020.598519.

Wang D, Liu H, Li Y, Zhou G, Zhan L, Zhu H, Lu X, Chen H, Li CZ. 2021. High-performance and eco-friendly semitransparent organic solar cells for greenhouse applications. Joule. 5:945–957. https://doi.org/10.1016/j.joule.2021.02.010.

Wang Y, Folta KM. 2013. Contributions of green light to plant growth and development. Amer J Bot. 100:70–78. https://doi.org/10.3732/ajb.1200354.

Weselek A, Bauerle A, Zikeli S, Lewandowski I, Högy P. 2021. Effects on crop development, yields and chemical composition of celeriac (apium graveolens l. Var. Rapaceum) cultivated underneath an agrivoltaic system. Agron. 11:733. https://doi.org/10.3390/agronomy11040733.

Yang C, Sheng W, Moemeni M, Bates M, Herrera CK, Borhan B, Lunt RR. 2021. Ultraviolet and near-infrared dual-band selective-harvesting transparent luminescent solar concentrators. Adv Energy Mats. 11:2003581. https://doi.org/10.2139/ssrn.3699147.

Yasin M, Rosenqvist E, Jensen SM, Andreasen C. 2019. The importance of reduced light intensity on the growth and development of six weed species. Weed Res. 59:130–144. https://doi.org/10.1111/wre.12352.

Zhang J, Moemeni M, Yang C, Liang F, Peng WT, Levine BG, Lunt RR, Borhan B. 2020. General strategy for tuning the Stokes shifts of near infrared cyanine dyes. J Mats Chem C. 8:16769–16773. https://doi.org/10.1039/d0tc03615c.

Zhen S, Bugbee B. 2020a. Far-red photons have equivalent efficiency to traditional photosynthetic photons: Implications for redefining photosynthetically active radiation. Plant Cell Environ. 43:1259–1272. https://doi.org/10.1111/pce.13730.

Zhen S, Bugbee B. 2020b. Substituting far-red for traditionally defined photosynthetic photons results in equal canopy quantum yield for CO_2 fixation and increased photon capture during long-term studies: implications for re-defining PAR. Front Plant Sci. 11:581156. https://doi.org/10.3389/fpls.2020.581156.

Table II-1. Environmental conditions inside chambers. Average daily air temperature (ºC) and daily light integral (DLI; 400–700 nm; mol m^{-2} d^{-1}) inside each chamber roofed with experimental glazing materials. ND91 (91% transmission), ND58 (58% transmission), and ND33 (33% transmission) were acrylic sheets with different PPFD transmissions. CO770, CO700, and CO550b experimental photoselective glazing materials with different transmission cutoffs. The CO550a glazing contained a fluorophore dye that absorbed blue and green photons and fluoresced red and far-red photons. Values represent daily averages ± SD for basil, petunia, and tomato grown inside each chamber.

Glazing material	Air temperature (ºC)			DLI (mol m^{-2} d^{-1})		
	Basil	Petunia	Tomato	Basil	Petunia	Tomato
ND91	24.9 ± 2.2	26.6 ± 1.8	23.5 ± 2.1	19.8 ± 9.0	19.5 ± 7.0	16.0 ± 7.6
ND58	24.7 ± 2.0	26.9 ± 1.8	23.6 ± 2.5	9.8 ± 4.2	10.3 ± 3.6	8.6 ± 4.3
ND33	24.8 ± 2.2	26.7 ± 1.8	23.5 ± 2.3	7.1 ± 3.3	7.4 ± 2.7	6.1 ± 2.8
CO770	24.8 ± 2.0	26.7 ± 1.8	23.6 ± 2.1	13.0 ± 5.8	13.3 ± 4.7	11.6 ± 5.5
CO700	24.1 ± 2.0	25.7 ± 1.5	23.0 ± 2.1	13.7 ± 6.0	14.1 ± 4.9	12.1 ± 5.8
CO550a	24.9 ± 2.1	27.1 ± 1.8	23.9 ± 2.4	11.5 ± 5.0	12.8 ± 4.4	10.3 ± 4.8
CO550b	24.3 ± 2.0	26.3 ± 1.6	23.5 ± 2.2	5.9 ± 2.6	6.5 ± 2.2	5.6 ± 2.7

Table II-2. Basil growth response regressions. Regression analysis of basil growth parameters (y) as a function of daily light integral (DLI; mol m^{-2} d^{-1}; 400–700 nm) (x). The regression type with the highest r^2 value was selected to describe the data. Sigmoidal regressions were always Gompertz functions (Equation 2). Specific leaf area (SLA) was calculated by dividing leaf area (cm^2) by leaf mass (g). Compactness was calculated by dividing the total above-ground dry mass by stem length (cm).

Growth parameter	Regression type	Equation	r^2
Leaf fresh mass (g)	Sigmoidal	$y = 6.90 * \exp(-20.8 * 0.647^X)$	0.92
Leaf dry mass (g)	Sigmoidal	$y = 0.507 * \exp(-14.6 * 0.701^X)$	0.90
Stem fresh mass (g)	Sigmoidal	$y = 4.22 * \exp(-81.4 * 0.556^X)$	0.90
Stem dry mass (g)	Sigmoidal	$y = 0.267 * \exp(-43.4 * 0.615^X)$	0.89
Total leaf area (cm^2)	Sigmoidal	$y = 186 * \exp(-15.9 * 0.670^X)$	0.91
Individual leaf area (cm^2)	Quadratic	$y = 5.43 - 0.190x^2 - 12.7$	0.83
Leaf length (cm)	Sigmoidal	$y = 9.80 * \exp(-9.91 * 0.575^X)$	0.72
SPAD	Sigmoidal	$y = 32.5 * \exp(-1.11 * 0.855^X)$	0.81
SLA (cm^2 g^{-1})	Sigmoidal	$y = 276 * \exp(1.13 * 0.909^X)$	0.72
Stem length (cm)	Sigmoidal	$y = 30.4 * \exp(-55.2 * 0.529^X)$	0.94
Stem diameter (mm)	Sigmoidal	$y = 3.61 * \exp(-3.76 * 0.735^X)$	0.85
Node no.	Sigmoidal	$y = 5.24 * \exp(-1.60 * 0.829^X)$	0.81
Branch no.	Linear	$y = 0.0554x - 0.302$	0.27
Compactness (g cm^{-1})	Sigmoidal	$y = 0.0316 * \exp(-1.84 * 0.860^X)$	0.78

Table II-3. Petunia growth response regressions. Regression analysis of petunia growth parameters (y) as a function of daily light integral (DLI; mol m^{-2} d^{-1}; 400–700 nm) (x). The regression type with the highest r^2 value was selected to describe the data. Sigmoidal regressions were always Gompertz functions (Equation 2). Time to flower was recorded as the number of days from seed sow to first open flower. Specific leaf area (SLA) is calculated by dividing leaflet area (cm^2) by leaf mass (g). Compactness is calculated by dividing the total above-ground dry mass by central stem length (cm). Sigmoidal regressions were Gompertz functions (Equation 2).

Growth parameter	Regression type	Equation	r^2
Shoot fresh mass (g)	Sigmoidal	$y = 93.3 * \exp(-53.2 * 0.565^X)$	0.88
Shoot dry mass (g)	Sigmoidal	$y = 5.76 * \exp(-26.1 * 0.629^X)$	0.90
Leaf length (cm)	Sigmoidal	$y = 6.83 * \exp(2.80 * 0.710^X)$	0.54
Leaf width (cm)	Sigmoidal	$y = 3.51 * \exp(1.47 * 0.858^X)$	0.60
Leaf area (cm^2)	Sigmoidal	$y = 15.3 * \exp(4.58 * 0.758^X)$	0.78
SPAD	Linear	$y = 0.622x + 19.5$	0.47
SLA (cm^2 g^{-1})	Linear	$y = -6.64x + 304$	0.55
Central stem length (cm)	Sigmoidal	$y = 13.6 * \exp(3.31 * 0.862^X)$	0.89
Longest branch (cm)	Sigmoidal	$y = 30.2 * \exp(-1.13e^4 * 0.196^X)$	0.79
Branch no.	Sigmoidal	$y = 8.81 * \exp(-61.9 * 0.603^X)$	0.91
Compactness (g cm^{-1})	Sigmoidal	$y = 0.357 * \exp(-22.2 * 0.718^X)$	0.84
Time to visible bud (d)	Sigmoidal	$y = 15.0 * \exp(54.5 * 0.373^X)$	0.38
Time to flower (d)	Sigmoidal	$y = 24.6 * \exp(1.53 * 0.649^X)$	0.34
Total inflorescence no.	Sigmoidal	$y = 62.8 * \exp(-17.6 * 0.703^X)$	0.93
Nodes under first flower no.	Sigmoidal	$y = 7.51 * \exp(104 * 0.407^X)$	0.43

Table II-4. Tomato growth response regressions. Regression analysis for various tomato growth parameters (y) as a function of daily light integral (DLI; mol m^{-2} d^{-1}; 400–700 nm) (x). The regression type with the highest r^2 value was selected to describe the data. Sigmoidal regressions were always Gompertz functions (Equation 2). Projected canopy area (PCA) was measured perpendicular to the top of the canopy. Time to flower was recorded as the number of days from seed sow to first open floret. Specific leaf area (SLA) was calculated by dividing leaflet area (cm^2) by leaf mass (g). Compound leaflets from a representative leaf of each sample were excised from the petiole before the area and dry mass were measured. Compactness was calculated by dividing the total above-ground dry mass by central stem length (cm). Sigmoidal regressions were Gompertz functions (Equation 2).

Growth parameter	Regression type	Equation	r^2
Shoot fresh mass (g)	Sigmoidal	$y = 116 * \exp(-4.92e^6 * 0.0566^X)$	0.33
Shoot dry mass (g)	Rectangular hyperbola	$y = \dfrac{17.9 * x}{6.25 + x}$	0.19
fruit fresh mass (g)	Linear	$y = 30.4x - 121$	0.80
Fruit dry mass (g)	Sigmoidal	$y = 16.1 * \exp(-13.7 * 0.704^X)$	0.75
Total fruit no.	Sigmoidal	$y = 30.6 * \exp(-34.0 * 0.593^X)$	0.75
Ripe fruit no.	Linear	$y = 1.53x - 9.30$	0.64
Unripe fruit no.	Sigmoidal	$y = 19.1 * \exp(-292 * 0.392^X)$	0.41
Leaf length (cm)	-	NS	-
Leaf width (cm)	-	NS	-
Leaflet area (cm^2)	Linear	$y = 3.19x + 98.0$	0.14
SPAD	Linear	$y = 0.252x + 31.5$	0.07
PCA (cm^2)	Sigmoidal	$y = 6.38 * \exp(4.47 * 0.980^X)$	0.40
SLA (cm^2 g^{-1})	Linear	$y = -23.2x + 671$	0.67
Stem length (cm)	Sigmoidal	$y = 6.09 * \exp(2.42 * 0.957^X)$	0.45
Stem diameter (mm)	Sigmoidal	$y = 10.9 * \exp(-2.74 * 0.680^X)$	0.41
Compactness (g cm^{-1})	Linear	$y = 0.0409x - 0.0150$	0.64
Flower time (d)	Sigmoidal	$y = 40.4 * \exp(11.0 * 0.529^X)$	0.68

Table II-5. Basil growth under various glazing materials. Materials had differing photosynthetic photon flux density (PPFD; 400–700 nm) transmissions and photon distributions. ND91 (91% transmission), ND58 (58% transmission), and ND33 (33% transmission) were acrylic sheets with different PPFD transmissions. CO770, CO700, and CO550b were experimental photoselective glazing materials with different transmission cutoffs. The CO550a glazing contained a fluorophore dye that absorbed blue and green photons and fluoresced red and far-red photons. Specific leaf area (SLA) was calculated by dividing the leaf area (cm^2) by leaf mass (g) of a representative leaf. Compactness is calculated by dividing the total above-ground dry mass by stem length (cm). Data represent means with ten samples. Means with different letters are significant according to Tukey's honestly significant difference test ($P<0.05$) and correspond to each row. Darker shaded cells correspond to each parameter's highest values, and lighter shaded cells the lowest values and reflect pair-wise comparisons.

Growth parameter	Glazing material						
	ND91	ND58	ND33	CO770	CO700	CO550a	CO550b
Leaf fresh mass (g)	6.8 **a**	5.5 **c**	2.3 **d**	6.7 **a**	6.5 **ab**	5.7 **bc**	1.7 **d**
Leaf dry mass (g)	0.51 **a**	0.35 **d**	0.14 **e**	0.45 **ab**	0.43 **bc**	0.38 **cd**	0.093 **e**
Stem fresh mass (g)	4.0 **ab**	3.3 **c**	1.1 **d**	4.4 **a**	4.1 **ab**	3.7 **bc**	0.5 **d**
Stem dry mass (g)	0.28 **a**	0.20 **c**	0.061 **d**	0.26 **ab**	0.23 **bc**	0.22 **bc**	0.027 **d**
Individual leaf area (cm^2)	20 **c**	23 **bc**	16 **d**	27 **a**	26 **ab**	24 **b**	13 **d**
Total leaf area (cm^2)	186 **a**	143 **c**	68 **d**	177 **ab**	166 **ab**	156 **bc**	47 **d**
Leaf length (cm)	9.1 **b**	9.9 **a**	7.5 **c**	10.0 **a**	9.8 **ab**	9.8 **ab**	7.0 **c**
SPAD	30.2 **a**	25.0 **c**	21.7 **d**	27.9 **b**	26.4 **bc**	26.6 **bc**	20.3 **d**
SLA (cm^2 g^{-1})	329 **c**	414 **b**	525 **a**	407 **b**	368 **bc**	389 **b**	509 **a**
Stem length (cm)	29.9 **ab**	27.9 **b**	15.7 **c**	31.2 **a**	28.5 **b**	30.1 **ab**	9.0 **d**
Stem diameter (mm)	3.4 **a**	3.1 **b**	2.1 **c**	3.6 **a**	3.5 **a**	3.1 **b**	2.1 **c**
Node no.	5.2 **a**	4.3 **b**	3.4 **c**	4.5 **b**	4.3 **b**	4.4 **b**	3.1 **c**
Branch no.	0.7 **a**	0.3 **ab**	0.0 **b**	0.6 **a**	0.4 **ab**	0.4 **ab**	0.0 **b**
Compactness (g cm^{-1})	0.029 **a**	0.022 **d**	0.015 **e**	0.25 **bc**	0.026 **ab**	0.022 **cd**	0.016 **e**

Table II-6. Petunia growth response under various glazing materials. Glazing materials have differing photosynthetic photon flux density (PPFD; 400–700 nm) transmissions and photon distributions. ND91 (91% transmission), ND58 (58% transmission), and ND33 (33% transmission) were acrylic sheets with different PPFD transmissions. CO770, CO700, and CO550b were experimental photoselective glazing materials with different transmission cutoffs. The CO550a glazing contained a fluorophore dye that absorbed blue and green photons and fluoresced red and far-red photons. Time to flower was recorded as the number of days from seed sow to first open flower. Specific leaf area (SLA) is calculated by dividing leaflet area (cm^2) by leaf mass (g). Compactness is calculated by dividing the total above-ground dry mass by central stem length (cm). Data represent means with ten samples. Means with different letters are significant according to Tukey's honestly significant difference test ($P<0.05$) and correspond to each row. Darker shaded cells correspond to each parameter's highest values, and lighter shaded cells the lowest values and reflect pair-wise comparisons.

Growth parameter	Treatment						
	ND91	ND58	ND33	CO770	CO700	CO550a	CO550b
Shoot fresh mass (g)	81.1 **cd**	74.6 **d**	43.8 **e**	102.8 **a**	97.7 **ab**	89.3 **bc**	25.6 **f**
Shoot dry mass (g)	5.5 **ab**	4.5 **c**	2.4 **d**	5.9 **a**	5.7 **ab**	5.1 **bc**	1.7 **e**
Leaf length (cm)	6.9 **b**	7.4 **b**	8.6 **a**	6.7 **b**	7.2 **b**	7.3 **b**	9.2 **a**
Leaf width (cm)	3.6 **c**	4.3 **bc**	5.8 **a**	4.4 **bc**	4.5 **b**	4.5 **b**	6.1 **a**
Leaf area (cm^2)	14.7 **b**	17.7 **b**	28.7 **a**	16.7 **b**	18.3 **b**	18.8 **b**	32.1 **a**
SPAD	30.8 **ab**	24.5 **d**	24.4 **d**	28.1 **bc**	31.4 **a**	26.0 **cd**	23.7 **d**
SLA ($cm^2\,g^{-1}$)	168 **d**	251 **a**	253 **a**	215 **bc**	198 **cd**	242 **ab**	247 **a**
Central stem length (cm)	16.9 **d**	28.9 **c**	38.8 **b**	18.2 **d**	17.8 **d**	27.0 **c**	48.6 **a**
Longest branch (cm)	27.3 **bc**	31.2 **ab**	23.7 **c**	29.5 **ab**	29.5 **ab**	33.3 **a**	10.7 **d**
Branch no.	8.3 **ab**	5.6 **c**	3.0 **d**	9.0 **a**	8.7 **ab**	7.8 **b**	0.0 **e**
Compactness ($g\,cm^{-1}$)	0.33 **a**	0.16 **b**	0.06 **c**	0.33 **a**	0.33 **a**	0.19 **b**	0.04 **c**
Time to visible bud (d)	15.3 **b**	14.9 **b**	15.6 **ab**	14.9 **b**	15.0 **b**	14.9 **b**	16.4 **a**
Time to flower (d)	24.4 **cd**	25.0 **bd**	26.4 **ab**	24.6 **cd**	25.9 **ac**	23.9 **d**	26.9 **a**
Inflorescence no.	60.8 **a**	39.0 **c**	17.4 **d**	53.9 **ab**	58.1 **ab**	49.9 **b**	10.7 **d**

Table II-6 (cont'd)

Nodes under first flower no.	7.9 **bd**	6.9 **cd**	8.8 **ab**	7.9 **bd**	8.2 **bc**	6.6 **d**	10.1 **a**

Table II-7. Tomato growth response under various glazing materials. Glazing materials had differing photosynthetic photon flux density (PPFD; 400–700 nm) transmissions and photon distributions. ND91 (91% transmission), ND58 (58% transmission), and ND33 (33% transmission) were acrylic sheets with different PPFD transmissions. CO770, CO700, and CO550b were experimental photoselective glazing materials with different transmission cutoffs. The CO550a glazing contained a fluorophore dye that absorbed blue and green photons and fluoresced red and far-red photons. Projected canopy area (PCA) was measured perpendicular to the top of the canopy. Time to flower was recorded as the number of days from seed sow to first open floret. Specific leaf area (SLA) is calculated by dividing leaflet area (cm^2) by leaf mass (g). Compound leaflets from a representative leaf of each sample were excised from the petiole before the area, and dry mass was measured. Compactness is calculated by dividing the total above-ground dry mass by central stem length (cm). Data represent means with ten samples. Means with different letters are significant according to Tukey's honestly significant difference test (P<0.05) and correspond to each row. Darker shaded cells correspond to each parameter's highest values, and lighter shaded cells the lowest values and reflect pair-wise comparisons.

Growth parameter	Glazing material						
	ND91	ND58	ND33	CO770	CO700	CO550a	CO550b
Shoot fresh mass (g)	119 a	108 a	103 a	116 a	122 a	115 a	70 b
Shoot dry mass (g)	12.5 a	10.7 ab	9.9 ab	11.8 a	11.7 a	11.4 a	7.0 b
Fruit fresh mass (g)	352 a	182 c	45 d	263 b	223 bc	189 c	36 d
Fruit dry mass (g)	15.8 a	9.6 b	1.7 c	13.0 ab	12.3 ab	10.5 b	2.3 c
Total fruit no.	31.1 a	23.2 b	6.4 c	30.5 ab	27.4 ab	23.0 b	5.6 c
Ripe fruit no.	17.9 a	4.9 bc	0.6 cd	8.5 b	4.7 bd	5.7 b	0 d
Unripe fruit no.	13.2 bc	18.3 ab	5.8 c	22.0 ab	22.7 a	17.3 ab	5.6 c
Leaf length (cm)	20.7 a	18.7 ab	20.4 a	17.1 b	19.5 ab	19.7 ab	18.3 ab
Leaf width (cm)	17.2	16.4	16.4	15.1	17.0	17.3	15.1
Leaflet area (cm^2)	159 a	122 b	125 ab	111 b	132 ab	144 ab	114 b
SPAD	24.7 ab	34.6 ab	31.2 b	35.0 ab	35.8 a	33.3 ab	33.8 ab
PCA (cm^2)	177 c	291 ab	382 a	199 bc	189 c	237 bc	293 ab

57

Table II-7 (cont'd)

SLA (cm^2 g^{-1})	323 **d**	372 **bc**	367 **ab**	551 **d**	475 **d**	446 **c**	530 **a**
Stem length (cm)	20.4 **c**	29.8 **bc**	44.6 **a**	26.3 **bc**	24.4 **c**	28.6 **bc**	35.7 **ab**
Stem diameter (mm)	10.6 **ab**	9.4 **b**	9.2 **b**	11.2 **a**	10.9 **ab**	9.9 **ab**	7.4 **c**
Compactness (g cm^{-1})	0.63 **a**	0.46 **bc**	0.49 **cd**	0.20 **d**	0.37 **ab**	0.40 **b**	0.23 **d**
Flower time (d)	39.1 **b**	41.6 **b**	50.7 **a**	40.3 **b**	42.1 **b**	42.0 **b**	55.1 **a**

Table II-8. Potential energy output of agrivoltaic systems in the US. Land-area availability was approximated where agrivoltaic greenhouses account for 50% of covered growing area in the US and 1% of farmland area is covered for agrivoltaics purposes. The average daily solar insolation in the US ($4.5 kWh/m^2/day$) was used as the incident power on the TPV modules, which were assigned efficiencies based on current and prospective TPV benchmarks.

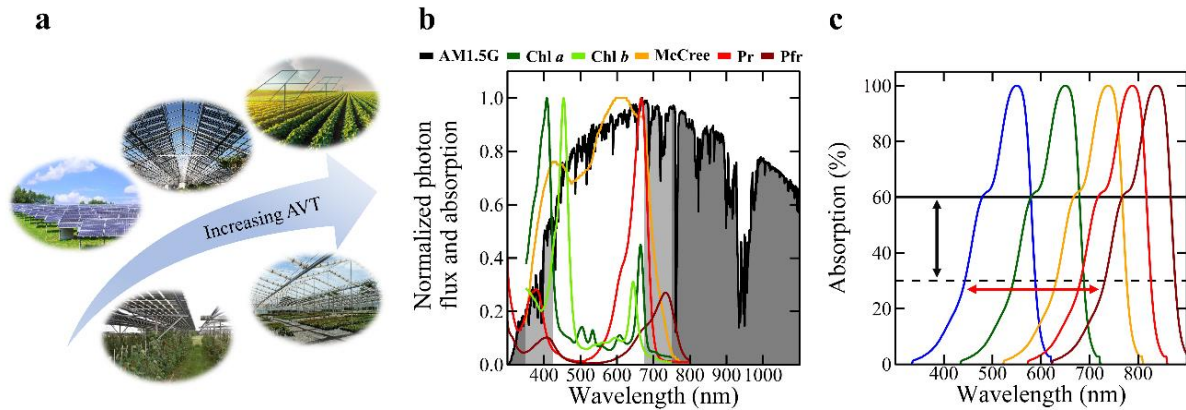| TPV Efficiency (%)	Greenhouse energy output (TWh/year)	Farmland energy output (TWh/year)
1	0.6	600
2	1	1200
5	3	3000
10	6	6000
15	10	9000

Figure II-1. Conceptualization of key agrivoltaic principles. a) Ideally, agrivoltaic systems would have high transmission of photosynthetically active radiation (PAR; photons between 400–700 nm). The simplest implementation of agrivoltaics is by deploying opaque modules over or adjacent to crops. Higher average photosynthetic transmittance (APT) can be achieved by moving to wavelength-selective modules that do not absorb PAR. Image credit (clockwise starting from the left-most picture): "Poultry Field Day Solar Panel" by Delaware Cooperative Extension (via creativecommons.org); "Beaulieu Abbey, Palace & Gardens 22-09-2012" by Karen Roe (via creativecommons.org), modified to add representative solar cells; "Garage of Green Furrows" by Ian Sane (via creativecommons.org), modified to add representative TPV modules over the field; "20120625-OSEC-RH-0019" by USDA.gov (via creativecommons.org); credit: Groen Leven (via hortidaily.com). b) Having a high PAR transmission is important because plants use photons from this waveband for photosynthesis and as signals for photomorphogenesis. To characterize this window, we have plotted the absorption spectra of chlorophyll (Chl) a and b, red-absorbing phytochrome (Pr) and far-red-absorbing phytochrome (Pfr), and the averaged quantum yield (mol CO_2 fixed per mol photon absorbed as a function of wavelength; denoted as McCree) of many plants (McCree 1972). Absorbing visible radiation (VIS) would be energetically advantageous for building-integrated PV (BIPV) panels but could negatively influence greenhouse crop growth and development. c) Thus, in this research we look at plant growth and productivity as a function of cutoffs of VIS and near infra-red wavebands and of overall transmission using neutral-density treatments.
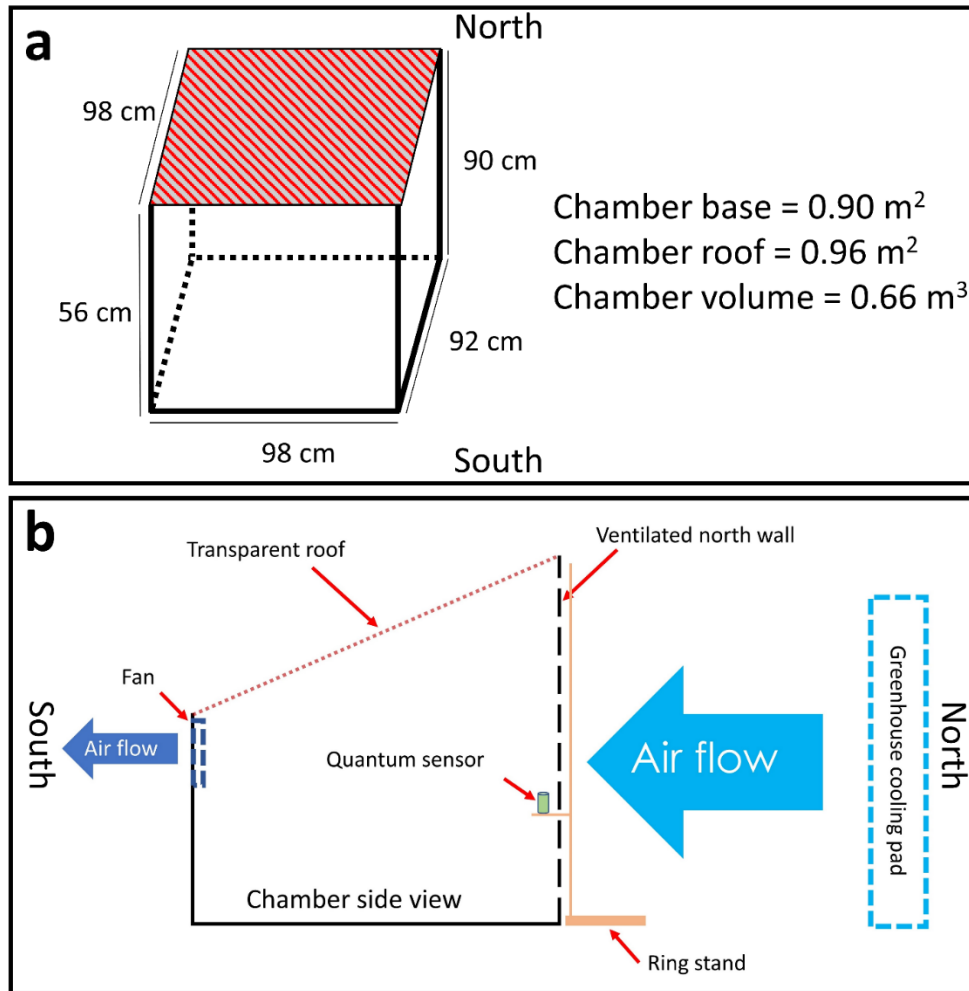
Figure II-2. a) Experimental chamber dimensions and b) greenhouse orientation schematic.
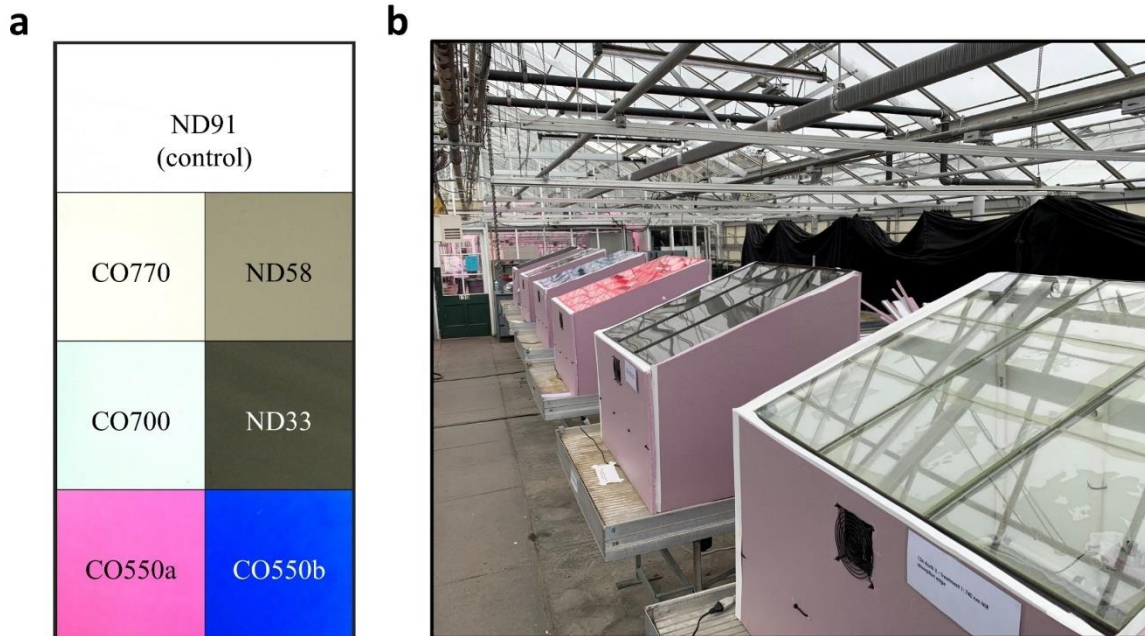
Figure II-3. Visual representation of glazing materials and chambers inside the greenhouse. Photographs of various materials used for experimentation. a) ND91 (91% transmission), ND58 (58% transmission), and ND33 (33% transmission) were acrylic sheets with different PPFD transmissions. CO770, CO700, and CO550b were experimental photoselective glazing materials with different transmission cutoffs. The CO550a glazing contained a fluorophore dye that absorbed blue and green photons and fluoresced red and far-red photons. b) Experimental chambers were roofed with various experimental glazing materials inside a Michigan State University research greenhouse.

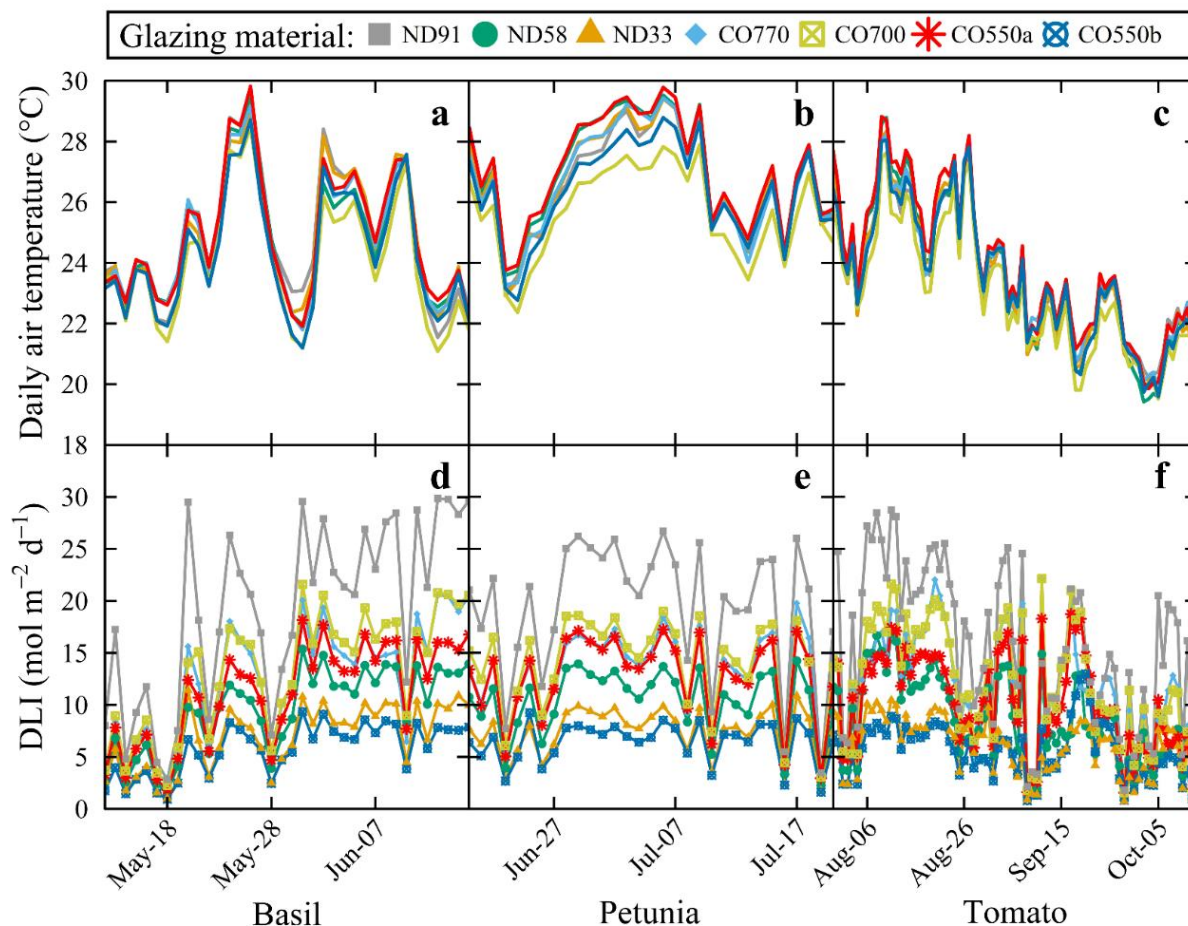Figure II-4. Chamber environmental conditions time series. a–c) Average daily air temperature (ºC), and d–f) daily light integral (DLI; 400–700 nm; mol m^{-2} d^{-1}) inside each chamber roofed with experimental glazing materials for basil (a and d), petunia (b and e), and tomato (c and f). ND91 (91% transmission), ND58 (58% transmission), and ND33 (33% transmission) were acrylic sheets with different PPFD transmissions. CO770, CO700, and CO550b were experimental photoselective glazing materials with different transmission cutoffs. The CO550a glazing contained a fluorophore dye that absorbed blue and green photons and fluoresced red and far-red photons. Instantaneous photosynthetic photon flux density (400–700 nm) was measured at canopy height every minute and integrated over 24 h to calculate DLI. Differences between chamber DLIs reflect differences between experimental glazing transmissions that ranged from 91% (ND91) to 34% (VIS550b) of incident sunlight directly above the chambers.
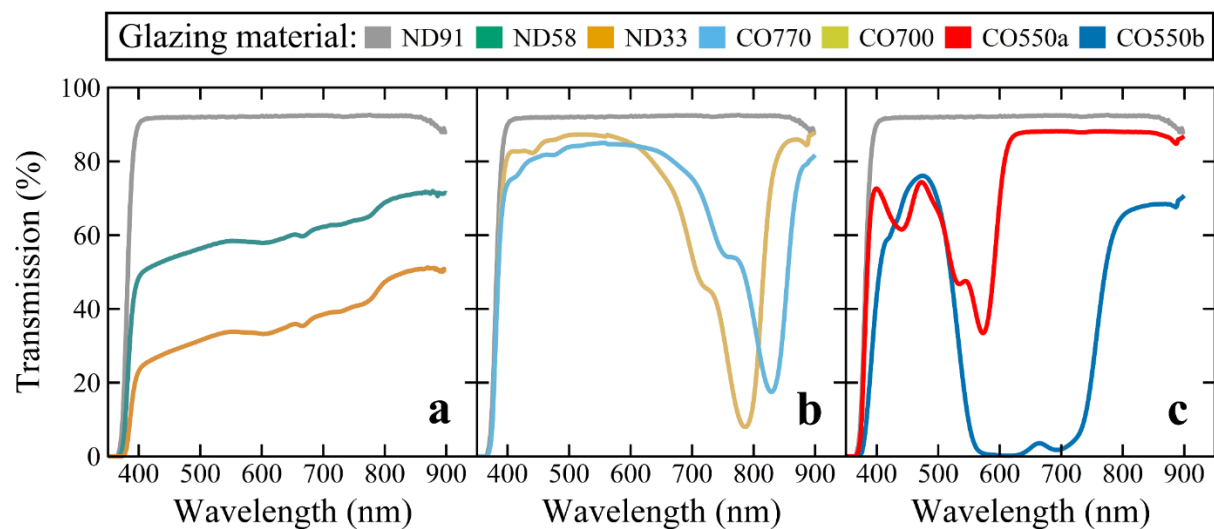
Figure II-5. Transmitted photon spectra of glazing materials. Measurements were made inside chambers covered with various glazing materials with different spectral transmissions on a clear day around solar noon. a) ND91 (91% transmission) (repeated in b and c), ND58 (58% transmission), and ND33 (33% transmission) were acrylic sheets with different photon transmissions. b) CO770, CO700, and c) CO550a, and CO550b were experimental photoselective glazing materials with different wavelength transmission cutoffs in the photosynthetically active radiation (PAR; photons between 400 and 700 nm) and the near-infrared (NIR) wavebands.
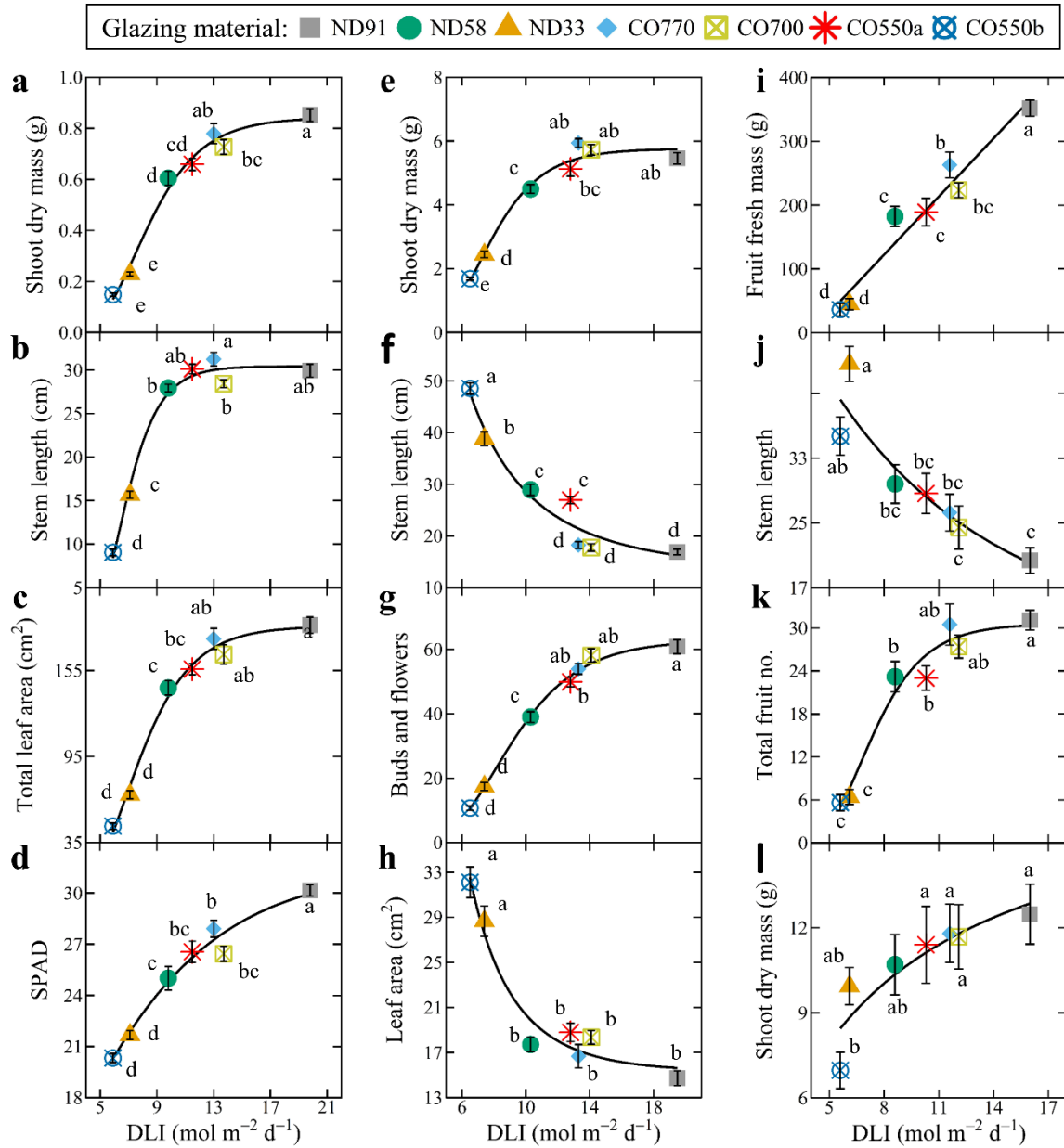
Figure II-6. Selected growth response regressions from basil, petunia, and tomato. Growth parameters of basil (a–d), petunia (e–h), and tomato (i–l) under various glazing materials with different spectral transmissions. The transmission spectra for the different glazing materials are given in Figure II-5. Shoot dry mass for basil and tomato refers to both leaves and stems. Data represent means ±SE with ten samples. Means with different letters are significant according to Tukey's honestly significant difference test (P<0.05). Regression equations for basil, petunia, and tomato are presented in Table II-1–3, respectively.

Glazing material:

Figure II-7. Representative plants under each glazing material. Photos of basil, petunia, and tomato plants representative of those grown under various experimental glazing materials on 16 June 2020, 21 July 2020, and 13 Oct. 2020, respectively. The transmission spectra for the different glazing materials are given in Figure II-5.

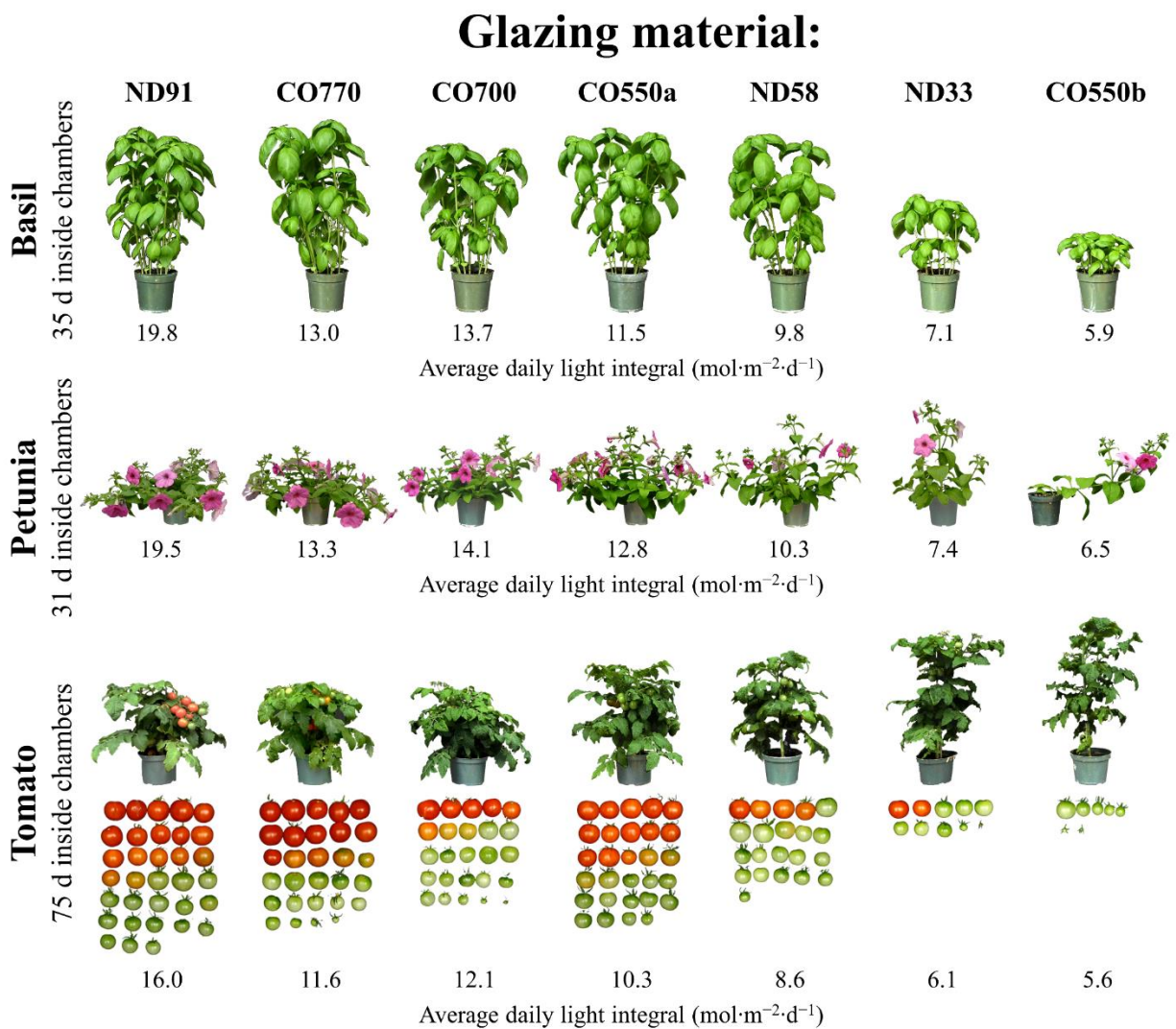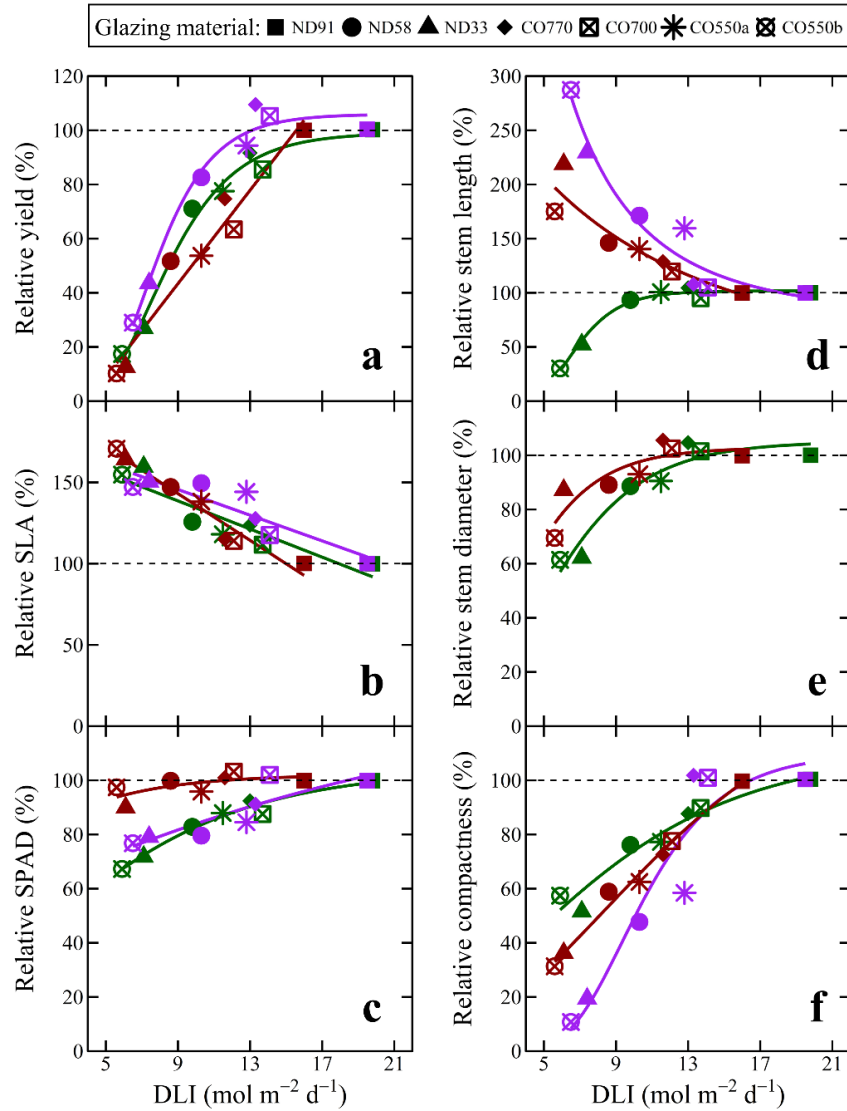Figure II-8. Relative growth response of basil, petunia, and tomato. Relative growth of basil (green symbols and regression lines), petunia (purple symbols and regression lines), and tomato (red symbols and regression lines) under various glazing materials with different spectral characteristics. The transmission spectra for the different glazing materials are given in Figure II-5. Each growth parameter is relative to the average value of the control treatment according to species and represents the average of ten samples. a) Relative yield refers to basil and petunia shoot dry mass (leaves and stems) and tomato fresh fruit mass. b) Specific leaf area (SLA) was calculated by dividing leaf area (cm^2) by leaf mass. c) SPAD reflects the relative chlorophyll concentration of leaves. d) Stem length was measured from the substrate surface to the apical meristem. e) Stem diameter was measured at the substrate surface. f) Compactness was calculated by dividing the total above-ground dry mass (g) by stem length (cm).
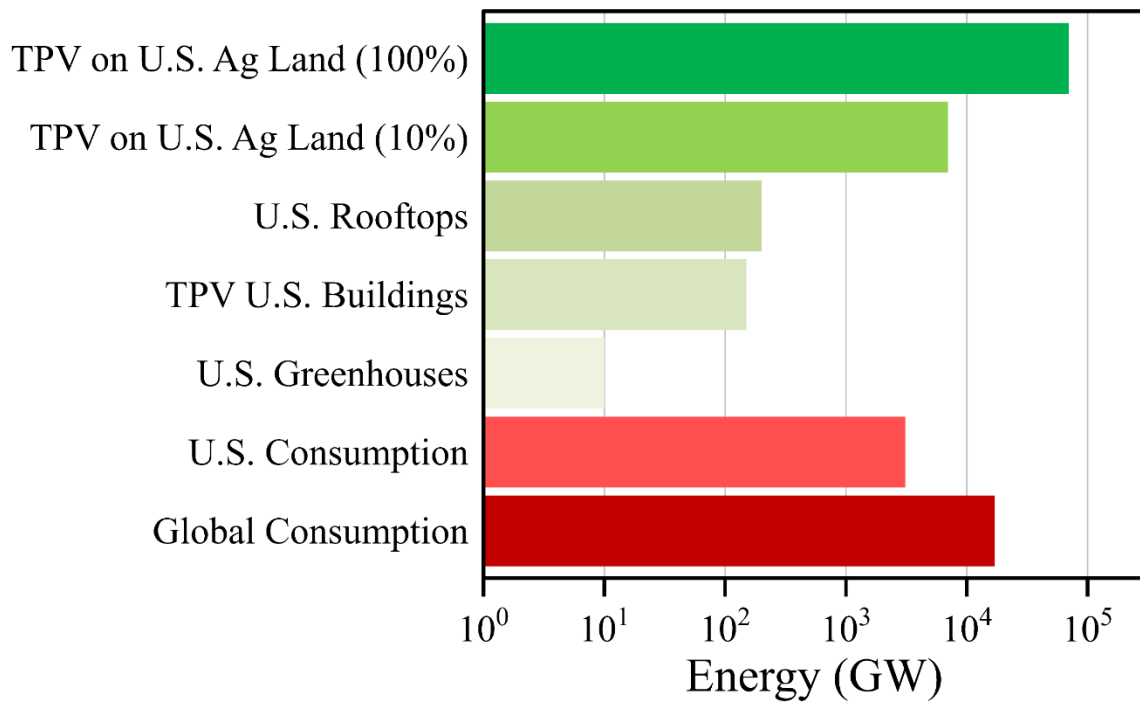
Figure II-9. Potential Energy Output of Agrivoltaics. The potential energy output of agrivoltaics on US agricultural land significantly surpasses the energy generation of rooftop solar and other integrated solar approaches. Agrivoltaics with 10%-efficient panels would produce more than double the US energy consumption with only 10% coverage of US agricultural land, and more than quadruple the global energy consumption with 100% coverage of US agricultural land.

APPENDIX C: ASSESSING CROP GROWTH WITH VARIOUS QUANTUM UNITS

To determine the applicability of additional plant-centric quantum units like YPFD and eDLI to predict crop growth, we transformed our treatment DLIs to reflect the YPFD and ePAR using spectroradiometer measurements. Then, we compared the transformed predictor variables to a subset of our basil growth metrics (shoot dry mass, stem length, total leaf area, and relative chlorophyll content) to determine if one parameter was preferable for agrivoltaic reporting (Fig. II-10).

The sigmoidal curves shifted to lower mol m^{-2} d^{-1} values when DLI was transformed into YPFD, a result of quantum efficiencies less than one for most PAR wavelengths. Curves shifted to higher mol m^{-2} d^{-1} values when transformed into eDLI, the result of integrating photons from a wider waveband. Each regression using the transformed predictor variables had an almost identical sigmoidal shape and similar ability to function as the DLI predictor variable for the entire subset of basil growth metrics selected. The observed critical illumination threshold (the mol m^{-2} d^{-1} required to grow a crop with similar yield and quality to the ND91 treatment) for basil was an average DLI of ~12 mol m^{-2} d^{-1}. After transformation, the critical illumination threshold became ~10 mol m^{-2} d^{-1} and ~14 mol m^{-2} d^{-1} for YPFD and eDLI, respectively. Generally, these values appropriately reflect the imperfect quantum efficiency of YPFD (lower values) and the extended waveband integral of eDLI (higher values). However, the magnitude of change upon the x-axis will inevitably depend on the transmission spectra and transformation. For instance, because the CO700 treatment absorbed a large fraction of the FR photons, its DLI and eDLI should be closer (lower magnitude of change) compared to a neutral-density TPV that does not absorb FR photon (higher magnitude of change). Regardless, even though the magnitude of transformation existed between our treatments, due to the larger magnitude of difference between treatment DLIs, the effect of the x-axis transformations were likely minimized.

These results suggest that YPFD and eDLI were comparable to the traditional, unweighted DLI definition to predict plant yield and growth, despite spectral differences being utilized in the agrivoltaic design. As such, it may be beneficial to the field of agrivoltaics to use eDLI (the integration of photons between 400 and 750 nm) as the benchmark quantum unit as explained by Zhen and Bugbee (2020a and 2020b) (Zhen and Bugbee 2020a; Zhen and Bugbee 2020b). Yet, regardless of the quantum unit, these results emphasize the necessity for the use of at least one quantum unit in agrivoltaic reporting but leaves room for further research into a common quantum

metric that best describes PV panel transmission relative to crops grown underneath them. Furthermore, the use of DLI transformations such as these may be more important and meaningful when the average panel transmissions are more similar.
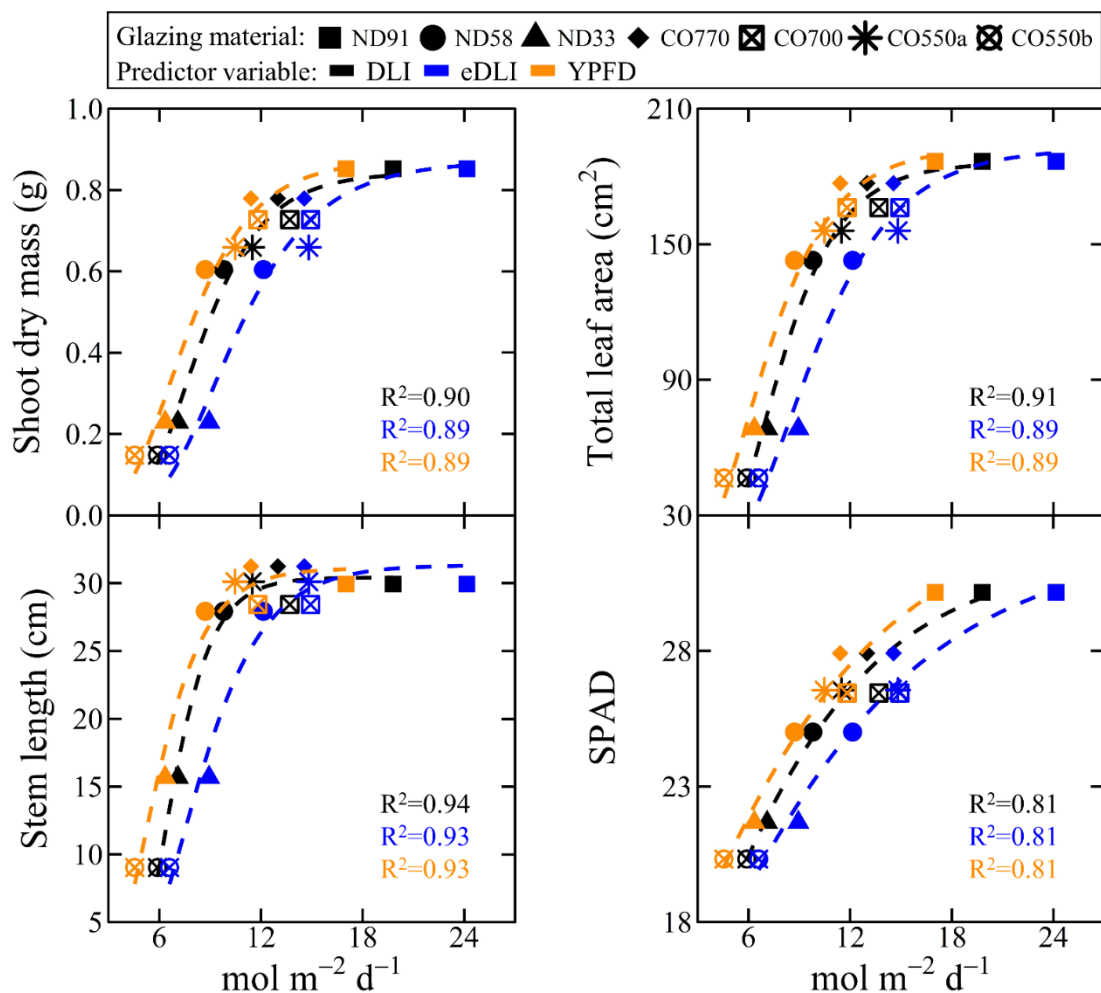
Figure II-10. Basil growth parameters as a function of three predictor variables. Growth parameters of basil as a function of daily light integral (DLI; 400–700 nm), extended daily light integral (eDLI; 400–750 nm) and average photosynthetic transmission (APT; synonymous with yield photon flux density according to McCree, 1972). Average treatment DLI was recorded throughout the duration of the experiment and then transformed into eDLI and APT using spectroradiometric data. Typically, APT values are lower and eDLI values are greater than DLI.

SECTION III: GROWTH OF SNAPDRAGON UNDER SIMULATED TRANSPARENT PHOTOVOLTAIC PANELS FOR GREENHOUSE APPLICATIONS

Growth of snapdragon under simulated transparent photovoltaic panels for greenhouse applications

Eric J. Stallknecht[1], Christopher K. Herrera[2], Thomas D. Sharkey[3], Richard R. Lunt[2], and Erik S. Runkle[1,*]

[1]Department of Horticulture, Michigan State University, East Lansing, MI, USA

[2]Department of Chemical Engineering and Materials Science, Michigan State University, East Lansing, MI, USA

[3]MSU-DOE Plant Research Laboratory and Department of Biochemistry and Molecular Biology, Michigan State University, East Lansing, MI, USA

[*]Corresponding author: runkleer@msu.edu

Index words: Agrivoltaics, *Antirrhinum majus*, floriculture, greenhouse glazing

Species used in the study: Snapdragon (*Antirrhinum majus*)

Abstract

Transparent photovoltaic (PV) materials can be used as greenhouse coverings that selectively transmit photosynthetically active radiation (PAR). Despite the economic importance of the floriculture industry, research on floriculture crops has been limited in these dual-purpose, agrivoltaic greenhouses. We grew snapdragon under simulated photoselective and neutral-density panels with transmissions ranging from ~30 to 90%, and absorption edges in the green (G; 500–599 nm), red (R; 600–699 nm), far-red (FR, 700–750 nm), and near-infrared (NIR) wavebands. We hypothesized that snapdragon could tolerate some degree of PV shading without reducing growth and flower number or delaying flowering time. Biomass accumulation, compactness, time to flower, and crop quality under 1) a clear acrylic control, 2) a FR-absorbing, and 3) a NIR-absorbing PV panel were not statistically different when the average daily light integral was between 17 and 20 $mol \cdot m^{-2} \cdot d^{-1}$. Crop quality progressively diminished below 17 $mol \cdot m^{-2} \cdot d^{-1}$. These results indicate that snapdragon tolerated ~15% PV shading during summer months without reduced growth or quality.

Significance to the Horticulture Industry

An agrivoltaic greenhouse has the potential to synergistically co-localize energy and agricultural crop production. The development of transparent photovoltaics (PV) that selectively transmit photosynthetically active radiation could potentially be incorporated into greenhouse glazing materials with little to no effect on crop growth. The representative floriculture crop snapdragon grown under simulated semitransparent PV panels that absorbed far-red and near-infrared radiation had similar biomass accumulation, compactness, time to flower, and morphology compared to plants grown under a clear acrylic plastic during the summer. While agrivoltaic production is still early in development and has many unanswered questions, these promising results warrant further research on additional specialty crop types, at greenhouse locations, and especially on the economics of such a system before commercial greenhouse adoption.

Introduction

The current challenge to increase global food production and renewable energy sources paired with diminishing arable land requires reimagining contemporary agricultural production systems (Weselek et al. 2019). Incorporating photovoltaic (PV) panels into an agricultural system, often termed agrivoltaics, offers a unique opportunity to couple the production of agricultural crops and electrical generation to increase arable land-use efficiency (Amaducci and Colauzzi 2018, Dinesh and Pearce 2016, Proctor et al. 2020). However, crops and PV panels compete for a common resource: solar radiation. Consequently, a successful agrivoltaic system must prioritize crop yield and quality while also considering electrical generation. Furthermore, incorporating an agrivoltaic system into a greenhouse necessitates additional design considerations to account for year-round production. Therefore, a greenhouse-based agrivoltaic system must be designed using plant-centric principles to conserve crop yield and quality. For example, an agrivoltaic system must consider how PVs affect the greenhouse microclimate such as air temperature, canopy temperature, photosynthetic photon flux density (PPFD; 400-700 nm), transmission spectrum, and light uniformity, and how altered microclimate conditions influence crop yield and quality (Weselek et al. 2019).

Photovoltaic materials can range from opaque to semitransparent to visually transparent with controllable degrees of transmission (Traverse et al., 2017). The flexibility to control PV transmission is critical because greenhouse locations and the crops grown inside are extremely

diverse. While opaque agrivoltaic materials are typically used for field-based installations, pilot studies in PV greenhouses have successfully used opaque to semitransparent materials covering roughly 10 to 30% of the greenhouse roof area to grow a diverse range of greenhouse crops including lettuce (*Lactuca sativa*), pepper (*Capsicum annuum*), tomato (*Solanum lycopersicum*), strawberry (*Fragaria × ananassa*), and petunia (*Petunia × hybrida*) without significantly decreasing crop yield or quality (Aroca-Delgado et al. 2019, Colantoni et al. 2018, Hassanien and Ming 2017, Kavga et al. 2019, Tang et al. 2020, Toledo and Scognamiglio 2021). Opaque and semitransparent PVs most often function as shading materials that decrease the transmission of photosynthetically active radiation (PAR; 400–700 nm) or extended photosynthetically active radiation (ePAR; 400–750 nm). Within a certain range, a 1% decrease in PAR transmission typically decreases crop yields by 0.75–1% (Marcelis et al. 2005). However, in high radiation environments shading can decrease crop stress and increase the harvestable yield, partly by decreasing air temperature, and increase water-use efficiency (Barron-Gafford et al. 2019). In contrast, in lower radiation environments, permanent shading caused by PV installations could increase production time, decrease plant quality, or both, and necessitate supplemental lighting and more heating during the winter. To mitigate seasonal shading limitations, transparent PVs can be developed that transmit most of the incident (e)PAR, favorably modify transmission of the solar spectrum, or both.

Nearly all agrivoltaic research conducted in experimental PV-covered greenhouses has focused on growing leafy greens, culinary herbs, and fruiting crops such as lettuce, spinach (*Spinacia oleracea*), basil (*Ocimum basilicum*), tomato, and pepper. However, floriculture crops are a major segment of greenhouse crop production; it was valued at 6.4 and 50 billion USD in the US and globally in 2021, respectively (USDA 2021). Leafy greens and many floriculture crops can be produced under a moderate average daily light integral (DLI; $mol \cdot m^{-2} \cdot d^{-1}$) whereas the harvestable yield of fruiting crops such as tomato usually decreases with the average DLI (Cossu et al. 2020). Research focusing on floriculture crops produced inside a simulated agrivoltaic greenhouse is needed to quantify trade-offs that may exist between energy generation and crop timing and quality attributes. Here, we investigated the growth and flowering responses of snapdragon (*Antirrhinum majus*), which is a relatively commonly grown species of economic importance, and whose flowering response is influenced by day length, DLI, and the light

spectrum. We hypothesized that snapdragon could tolerate some degree of PV shading with little to no decrease in growth or flower number, or delay in flowering time. We grew snapdragon under a range of experimental PV panels with different transmission spectra and quantified growth and flowering responses.

Materials and Methods

Chamber design. We constructed eight identical experimental chambers inside a glass-glazed research greenhouse at Michigan State University (42.7° N lat.) (Fig. III-1A and B). Chambers were placed on aluminum benches (one per bench) that were positioned in a north-south orientation. Chamber frames were constructed of polyvinyl chloride (PVC) pipe and covered with an opaque insulation board. Each chamber provided ~0.90 m^2 of growing space and a volume of ~0.66 m^3. The interior insulation board surface was painted white to increase light scattering and uniformity. One electric 3.1 $m^3 \cdot min^{-1}$ fan (Axial 1238, AC Infinity Inc., City of Industry, CA) was installed on the south-facing wall of each chamber, which was in the same wind direction as the greenhouse evaporative cooling system. Additionally, the north-facing wall was heavily perforated to increase air movement and prevent overheating. Each chamber roof was constructed from steel angle bars and supported various experimental PV panels. To increase light transmission and reduce cast shadows, chamber roofs were pitched 20 degrees south.

Simulated transparent PV panels. Simulated semitransparent and transparent PV panel transmission spectra are shown in Fig. III-2A–C and were measured with a portable spectroradiometer at solar noon on a cloudless day (LI-180; LI-COR, Inc., Lincoln, NE). Table III-1 quantifies the total photon flux density (TPFD; 400–750 nm) transmission divided into percent blue (B; 400–499 nm), green (G; 500–599 nm); red (R; 600–699 nm); and far-red (FR; 700–750 nm). Experimental panels included three neutral-density (ND) materials with 91, 58, and 33% transmission (henceforth termed clear plastic, moderate shade, and heavy shade, respectively) (Fig. III-2A). Additionally, five wavelength-selective panels were evaluated with cutoffs close to 475, 575, 700, 770, and 850 nm (henceforth termed −G, −R, −FR1, −FR2, and −NIR, respectively) (Fig. III-2B and C).

Preparation of wavelength-selective panels. (−G, −R, −FR1, −FR2, and −NIR): 3-Ethyl-2-[3-[3-ethyl-3H-benzothiazol-2-ylidene]-1-propenyl]-benzothiazolium iodide (Cy3-I, American Dye Source), 2-[5-(1,3-Dihydro-3,3-dimethyl-1-propyl-2H-indol-2-ylidene)-1,3-pentadienyl]-3,3-dimethyl-1-propyl-3H-indolium perchlorate (Cy5-ClO$_4$, American Dye Source), 2-[2-[2-

Chloro-3-[(1,3-dihydro-1,3,3-trimethyl-2H-indol-2-ylidene)ethylidene]-1-cylcohexen-1-yl]-ethenyl]-1,3,3-trimethyl-1H-indolium iodide (IR775-I, Few Chemicals), 2-[2-[2-chloro-3-[2-(1,3-dihydro-3,3-dimethyl-1-ethyl-2H-benz[e]indol-2-ylidene)ethylidene]-1-cylohexen-1-yl]-ethenyl]-3,3-dimethyl-1-ethyl-1H-benz[e]indolium iodide (Cy-I, American Dye Source), 1-Butyl-2-(2-[3-[2-(1-butyl-1H-benzo[cd]idnol-2-ylidene)-ethylidene]-2-diphenylamino-cyclopent-1-enyl]-vinyl)-benzo[cd]indolium tetrafluoroborate (IR996-BF$_4$, Few Chemicals). Cy3-I, Cy5-ClO$_4$, IR775-Cl, Cy-I, and IR996-BF$_4$ were mixed with potassium tetrakis(pentafluorophenyl)borate (K-TPFB) as described by Suddard-Bangsund et al. (2016) to create Cy3-TPFB (−G), Cy5-TPFB (−R), IR775-TPFB (−FR1), Cy-TPFB (−FR2), and IR996-TPFB (−NIR). −G, −R, −FR1, −FR2, and −NIR were cast into a solid film using a Shandon mounting media (CAS#9990435, Thermo Fisher Scientific) and sealed in a nitrogen environment as previously described in Stallknecht et al. (2023).

Environmental sensing. Each chamber was equipped with an aspirated thermocouple (Type E; Omega Engineering, Inc., Stamford, CT) to measure air temperature. Additionally, each chamber had a quantum sensor (400–700 nm) (LI-190SA; LI-COR, Inc., or SQ-500; Apogee Instruments, Inc., Logan, UT) and ePAR quantum sensor (400–750 nm) (SQ-610; Apogee Instruments, Inc.) to measure instantaneous PPFD and TPFD at the top of the crop canopy, respectively. Thermocouples and quantum sensors were connected to a CR1000 datalogger (Campbell Scientific, Logan, UT) and AM16/32B multiplexer (Campbell Scientific) combination that sampled environmental conditions every minute and recorded hourly averages. Instantaneous PPFD and TPFD measurements were integrated daily to calculate the DLI and eDLI. Average chamber air temperature, DLI, and eDLI are depicted in Fig. III-2D–F.

Greenhouse environment. The greenhouse environment was regulated by an Integro 725 (Priva North America, Vineland Station, ON, Canada) control system. The air temperature setpoint was a constant 21 °C. Heating was provided by radiant steam and cooling was provided through roof vents, exhaust fans, and an evaporative cooling pad.

Snapdragon seedling growth. Snapdragon 'Snapshoot Yellow' (PanAmerican Seed Co., West Chicago, IL) seeds were sown on 2 June 2021 into 288-cell (8-mL individual cell volume) plug trays filled with 50% peat-based soilless substrate (Suremix; Michigan Grower Products, Inc., Galesburg, MI) and vermiculite. Plug trays were placed into a controlled-environment growth

room at 21 °C air temperature, 9-h photoperiod, and a PPFD of 180 µmol·m^{-2}·s^{-1} at canopy height (DLI = 5.8 mol·m^{-2}·d^{-1}). The light was provided by white, blue, and red light-emitting diodes (RAY 44 Physiospec Indoor; Fluence Bioengineering; Austin, TX). Plug trays were covered for one week with transparent humidity domes. Seedlings were irrigated as needed with a solution of deionized water, hydroponic water-soluble fertilizer (12N–1.7P–13.3K RO Hydro FeED, JR Peters, Inc, Allentown, PA), and magnesium sulfate (Epsom salt, Pennington Seed Inc., Madison GA). This provided the following nutrients (in mg L^{-1}): 125 N, 18 P, 138 K, 73 Ca, 49 Mg, 37 S, 1.6 Fe, 0.5 Mn, 0.4 Zn, 0.2 B and Cu, and 0.01 Mo. The fertilizer solution was adjusted to a pH of 5.8 and electrical conductivity of 1.2 mS·cm^{-1} with a handheld meter (HI9814; Hanna Instruments, Woonsocket, RI) upon formulation.

Snapdragon mature growth. Snapdragon seedlings were transplanted on 28 June 2021 into 10-cm pots filled with peat-based potting media (Suremix; Michigan Grower Products, Inc.). Plants were irrigated as needed with a solution consisting of reverse osmosis water supplemented with 13N–1.3P–12.5K water-soluble fertilizer that contained (in mg·L^{-1}) 125 N, 13 P, 120 K, 77 Ca, 19 Mg, 1.7 Fe, 0.4 Cu, and Zn, 0.8 Mn, 0.2 B and Mo (MSU Orchid RO Water Special; GreenCare Fertilizers, Inc., Kankakee, IL).

Experimental design and statistics. The experiment was organized as a completely randomized design where the most uniform snapdragon seedlings (n=15) were randomly transplanted into one of eight chambers (experimental unit) that had one randomly assigned experimental PV treatment. Data were analyzed in R software (Version 4.2.2, The R Foundation, Vienna, Austria) using analysis of variance (ANOVA) and Tukey's honestly significant difference test at $\alpha = 0.05$.

Data collection. Snapdragon grew under natural photoperiods for 36 days (after transplant) until destructive measurements were taken on 23 Aug. 2021. Time to first visible bud (VB) was recorded when a flower bud was visible with the naked eye on the terminal inflorescence, and time to first open flower was recorded when the first flower of the terminal inflorescent fully opened. At harvest, central stem length and diameter were measured with a ruler and digital calipers (41101 DigiMax; Wiha Switzerland, Monticello, MN, USA). The total number of flowers, flowers on the terminal inflorescence, and nodes under the terminal inflorescence were counted. For each plant, the length, width, and relative chlorophyll content was measured on three leaves with a ruler and SPAD meter (MC-100; Apogee Instruments, Inc., Logan, UT) and averaged for each sample.

Specific leaf area (SLA; $cm^2 \cdot g^{-1}$) was calculated by dividing the leaf area of the three representative leaves [measured by a leaf area meter (LI-3100 Area Meter; LI-COR, Inc.)] by their dry mass and averaged per sample. Shoot fresh mass was measured with a digital scale at the time of harvest (GR-200; A&D Store, Inc., Wood Dale, IL). Shoot dry mass after four days in a 60 °C drying oven (SMO28-2; Sheldon Manufacturing, Inc., Cornelius, OR) was measured with a digital scale (GX-1000; A&D Store, Inc.). Radiation-use efficiency (RUE; g shoot dry mass·mol^{-1} photon) was calculated by dividing shoot dry mass by the accumulated DLI ($mol \cdot m^{-2}$) while snapdragon plants were in the chambers. The sturdiness quotient (SQ; $cm \cdot mm^{-1}$) was calculated by dividing stem length by stem diameter (Jaenicke 1999).

Results and Discussion

Chamber environmental conditions. Average chamber air temperature, DLI, and eDLI are reported in Fig. III-2D–F and Fig. III-3. Average daily air temperature deviated by a maximum of 1.2 °C between treatments, and the largest deviation occurred between the clear-plastic and heavy-shade treatments. Air temperature variations between treatments were not correlated with DLI or eDLI ($P=0.056$ and $P=0.058$, respectively) and were likely caused by minor micro-climates within the research greenhouse. Similar to air temperature, the average DLI and eDLI were greatest under the clear-plastic treatment and lowest under the heavy-shade treatment. The DLI and eDLI were significantly correlated between treatments ($P<0.001$; $r^2=0.96$).

Biomass accumulation. Snapdragon shoot dry mass (SDM) was greatest under treatments with the highest light transmission (clear plastic, −NIR, −FR1, and −FR2) and lowest under the heavy-shade treatment (Fig. III-4A; Table III-2). Snapdragon SDM was positively correlated to treatment DLI and eDLI (Fig. III-4A; Table III-3 and III-4) and decreased by ~65% when transmission decreased by ~67% (i.e., 67% shade). At a similar average DLI (~11 $mol \cdot m^{-2} \cdot d^{-1}$), snapdragon SDM was greater under the −G and −R treatments than under the moderate-shade treatment that had no spectral manipulation between 400 and 700 nm. These results indicate that PV panel transmission and spectrum both influenced snapdragon biomass accumulation.

Radiation-use efficiency (RUE) is the ratio of accumulated dry mass to the total quantity of light intercepted by a plant (g SDM per mol PAR intercepted) and is a common plant performance metric for light utilization. Critical to agrivoltaic research, RUE is sensitive to light spectrum and PPFD (Ke et al 2022, Theekshana and van Iersel 2021, Wollaeger and Runkle 2014). Snapdragon RUE was greatest in the moderate- and heavy-shade treatments and ~55% greater than snapdragon

79

under the clear-plastic treatment (Table III-2). As DLI and eDLI increased, snapdragon RUE decreased linearly (Table III-3, III-4). Snapdragon grown during the summer under PV panels tolerated approximately a 15% decrease in DLI and eDLI transmission without significantly affecting snapdragon biomass accumulation.

Snapdragon biomass accumulation under a range of potential PV panel transmissions was consistent with the paradigm that a 1% decrease in light equates to ~0.75 to 1% decrease in SDM (Marcelis et al. 2005) when the average DLI decreased from 19.8 to 5.9 mol·m^{-2}·d^{-1}. However, snapdragon SDM was similar when the DLI decreased by 16% from 19.8 to 16.6 mol·m^{-2}·d^{-1}. In a separate study, SDM decreased by 64% as the DLI decreased from 21.8 to 10.5 mol·m^{-2}·d^{-1} (by 52%) but decreasing the DLI from 21.8 to 17.8 (18%) produced snapdragon with a similar SDM (Warner and Erwin 2005). This DLI and SDM response is consistent with other common floriculture crops including impatiens (*Impatiens wallerana*), cyclamen (*Cyclamen persicum*), and periwinkle (*Catharanthus roseus*) (Faust et al. 2005, Oh et al. 2009, Warner and Erwin 2005). In addition, biomass accumulation of petunia under transparent PV tolerated ~20–25% PV shading during summer months without decreasing SDM (Stallknecht et al. 2023). Thus, decreasing (e)DLI by 15–25% (beyond that of traditional glazing materials) is likely an acceptable shading factor for most floriculture crops grown during high-light periods, e.g., April through August in the northern hemisphere. Because snapdragon and petunia grown under experimental transparent PV panels follow the paradigm regarding biomass accumulation and light quantity, the effects of experimental PV panels on floriculture crop production can be predicted based on DLI responses already published.

Growing ornamental greenhouse crops only during high-light periods does not fully describe long-term shading effects on crop production during light-limited periods. A typical greenhouse glazing material has a solar transmission of ~70–90% and a greenhouse macro-structure can further reduce the amount of light reaching crops by an additional ~20–35% (Both 2002, Giacomelli and Roberts 1993). In sum, the average transmission of (e)PAR incident upon a greenhouse crop can range from 40–70% of that outdoors (Von Elsner 2000). In the current work, the highest light transmission panels (−NIR, −FR1, and −FR2) were similar to those of conventional greenhouse glazing materials (~75-80%) such as twin-wall polycarbonate or double-layer polyethylene (Both 2002, Giacomelli and Roberts 1993). Even with a high-transmission glazing material and minimal overhead obstructions, supplemental lighting is sometimes used

from early winter to mid-spring, which is when most annual bedding plants are produced. While PV panels that absorb (e)PAR would increase electricity generation, decreasing PAR transmission would come at the expense of crop quality and production time. Therefore, in temperate climates, transparent PV panels that maximize the transmission of PAR (yet absorb UV and NIR for electricity generation) are needed for year-round agrivoltaic greenhouse crop production.

The tolerance to light transmission decreases by PV panels depends on the greenhouse location and crops grown. For instance, the DLI outside in January typically ranges from 5–10 mol·m^{-2}·d^{-1} in Michigan but 20–25 mol·m^{-2}·d^{-1} in Arizona (Faust and Logan 2018). Consequently, transparent PV panels have greater energy generation potential in high-light areas, as well as a greater opportunity to manipulate the light spectrum to elicit desirable morphological changes. At a similar light intensity, crops grown under a light spectrum with a greater fraction of R and FR photons generally have a higher RUE from increased extension growth (e.g., leaf surface area or stem elongation) and light interception (Ke et al. 2022, Meng et al. 2019, Meng et al. 2020, Theekshana and van Iersel 2021, Wollaeger and Runkle 2014,). Thus, PV panels that target the absorption of B or G light, in addition to UV and NIR, could increase the biomass accumulation and RUE of some greenhouse crops grown in high-light regions if changes to plant morphology are tolerable.

Flowering. Time to first visible inflorescence and open flower were similar among most treatments except for the heavy-shade treatment, which occurred 2 or 5 d later (Fig. III-4B). Thus, the flowering of snapdragon was delayed when the average DLI or eDLI was ≤ 10 and 13 mol·m^{-2}·d^{-1}, respectively, which is consistent with DLI values reported by Blanchard and Runkle (2011). In contrast, there was a linear response to (e)DLI for several growth parameters. For example, snapdragon grown under the clear-plastic and −FR2 treatments had the greatest number of open flowers and buds while those grown under the heavy shade had the fewest (~62% decrease) (Fig. III-3, III-4C).

Typically, it is desirable to produce floriculture crops as quickly as possible to minimize overhead costs and maximize the number of crop cycles grown in a year. Average DLI regulates time to flower (i.e., flower development rate) in a species- and cultivar-specific manner. For example, the maximum flower development rate saturates when the average DLI is between 6–12 mol·m^{-2}·d^{-1} for a large number of economically important bedding plants, although some saturate at a much higher DLI, for example, 20–25 mol·m^{-2}·d^{-1} for regal geranium (*Pelargonium*

×*domestica*) and hibiscus (*Hibiscus cisplatinus*) (Loehrlein and Craig 2004, Runkle and Blanchard 2011, Warner and Erwin 2003). Similar to other common bedding plants, snapdragon flower development rate saturated when the DLI was >10 mol·m^{-2}·d^{-1}, and in a previous agrivoltaics study on petunia, the saturation DLI was >7 mol·m^{-2}·d^{-1} (Stallknecht et al. 2023). Therefore, flowering of most (but not all) floriculture crops would likely not be delayed if PV panel transmission was ≥50% during the summer. However, during winter and early spring, such a decrease in (e)DLI would delay the flowering of some crops grown in temperate regions, necessitating PV panels that maximize light transmission and/or greater use of supplemental photosynthetic lighting.

Because most floriculture crops are judged primarily by their visual appearance, it is usually desirable to market plants with as many flowers and flower buds as possible. Similar to SDM, DLI influences the number of flowers produced by floriculture crops and varies within and between species. For instance, increasing the DLI to 15–20 mol·m^{-2}·d^{-1} increased the number of flowers of salvia (*Salvia splendens*), impatiens, marigold (*Tegetes patula*), cyclamen, and snapdragon (Colantoni et al. 2018, Moccaldi and Runkle 2007, Oh et al. 2009, Pramuk and Runkle 2005, Warner and Erwin 2005). Snapdragon followed a similar trend and had the greatest flower number under a DLI of ~20 mol·m^{-2}·d^{-1}, and likely would have increased with higher DLI values since this response never saturated (Fig. III-4C). In another study, experimental PV panels that provided ~20% shade (DLI estimated to be ~30 mol·m^{-2}·d^{-1}) did not decrease the number of flowers produced by petunia (*Petunia grandiflora*) and candytuft (*Iberis sempervirens*) during the summer in Italy (Colantoni et al. 2018). While an average DLI of 6–12 mol·m^{-2}·d^{-1} may not delay the flowering of many common bedding plants grown in the spring, this DLI range does not produce floriculture crops with the highest quality.

Morphology. Leaf length and width were not correlated to treatment (e)DLI (Table III-3, III-4). Relative chlorophyll content (SPAD) increased linearly with (e)DLI while individual leaf surface area (SLA) decreased linearly. Stem length was quadratically correlated to treatment (e)DLI but had a low r^2 value. Stem diameter increased linearly as (e)DLI increased. However, snapdragon stem diameter under the −R treatment was similarly narrow as that under the heavy-shade treatment but had a ~50% greater average (e)DLI (Table III-1, III-2). Thus, leaf length and width were affected by treatment spectra whereas SPAD, SLA, and stem diameter were primarily

influenced by treatment (e)DLI. Similar to biomass accumulation, snapdragon tolerated a ~15% decrease in DLI and eDLI during the summer without significant changes to crop morphology.

Plants grown in low-light environments develop shade-avoidance and shade-acclimation responses such as greater stem elongation, increases in SLA, and a decrease in leaf chlorophyll concentration (Casal 2012). Increasing SLA (shade acclimation) and stem elongation (shade avoidance) can increase light interception and consequently increase RUE (Theekshana and van Iersel 2021). Snapdragon SLA and RUE were positively correlated under PV panel shading (P<0.001; r^2=0.30; data not shown). While SLA may not be a principal concern for snapdragon cultivation, floriculture crops grown for their foliage, such as coleus (*Coleus scutellarioides*), or food crops such as lettuce and basil, can be more susceptible to physical damage during production or harvest as SLA increases (Onoda et al. 2011). Many shade-avoidance and shade-acclimation responses are mediated through UV and B light-absorbing cryptochrome and R and FR light-absorbing phytochrome photoreceptors (Casal 2012, Meng et al. 2019, Park and Runkle 2018). Environments that create a phytochrome photoequilibrium (PPE) or internal phytochrome equilibrium (iPPE) <0.72 or <0.40, respectively (i.e., decreased R:FR) are indicative of plant canopy shading and the disproportionate absorption of B and R light relative to G and FR light. In this study, snapdragon stems were longer under the −R treatment (PPE=0.56, iPPE=0.25) than the moderate-shade treatment (PPE=0.69, iPPE=0.37) when the (e)DLI was similar. Therefore, consideration of (e)PAR transmittance and the light spectrum is needed when designing PV panels because of the possible effects on crop growth and morphology.

Floriculture crops grown in containers are commonly managed to have compact growth to facilitate shipping. Compactness (SDM per stem length) increased linearly with (e)DLI and was similar under the highest light transmission treatments (clear plastic, −NIR, −FR1, and −FR2) (Fig. III-4D). As an additional quality consideration, potted floriculture crops such as snapdragon should remain upright during production, shipping, and sale. Snapdragon grown under the −R and heavy-shade treatments were more likely to fall over (lodging) than those in other treatments, and this occurred when the stem length to stem diameter ratio (i.e., SQ) was ≥5.5 cm·mm^{-1}. Similarly, some nursery tree species with a SQ >6 cm·mm^{-1} were prone to lodging, resulting in diminished crop quality or survivability after transplant (Jaenicke 1999). While SQ values related to lodging are likely species- and cultivar-specific, the SQ metric has not been reported in previous agrivoltaics studies and merits consideration in future studies with ornamental crops.

While metrics such as RUE or land equivalent ratio (LER) can be mathematically optimized for an agrivoltaics system, both metrics ignore key quality parameters necessary for the marketability of floriculture crops (Toledo and Scognamiglio 2021). For instance, although snapdragon had the greatest RUE under the moderate- and heavy-shade treatments, flowering under those treatments was delayed, plants were less compact, and plants had fewer flowers. Furthermore, metrics such as LER often do not account for fluctuating commodity and energy prices with respect to time and the permanence of PV-greenhouse glazing materials. Consequently, agrivoltaic research that reports morphological attributes such as, but not limited to, compactness, SLA, branching, stem elongation, and flowering are needed to better characterize short- and long-term effects of PV materials on greenhouse crops.

In summary, snapdragon grown in the summer under simulated and experimental PV panels tolerated a decrease in average DLI and eDLI of around 15% (DLI and eDLI >17 and 19 $mol·m^{-2}·d^{-1}$, respectively) without significantly affecting biomass accumulation, compactness, number of flowers, or time to flower. This suggests floriculture production under PAR-transparent PV panels is possible when solar irradiance is high. In addition, semitransparent PV panels that absorbed (e)PAR, particularly red light, could have greater electricity generation than PAR-transparent PV panels, but at the expense of decreasing snapdragon crop quality. Despite having treatments with different transmitted light spectra, DLI or eDLI were similarly effective predictor variables for snapdragon growth and development. However, further research with additional species is needed to validate this conclusion. Given the economic importance of floriculture crops grown in greenhouses, additional agrivoltaic research on floriculture and other high-value specialty crops is needed to better understand trade-offs that can exist between electricity generation and various dimensions of plant quality.

LITERATURE CITED

Amaducci S, Yin X, Colauzzi M. 2018. Agrivoltaic systems to optimize land use for electric energy production. Appl Eng. 220:545–561. https://doi.org/10.1016/j.apenergy.2018.03.081.

Aroca-Delgado R, Pérez-Alonso J, Callejón-Ferre ÁJ, Díaz-Pérez M. 2019. Morphology, yield and quality of greenhouse tomato cultivation with flexible photovoltaic rooftop panels. Sci Hortic. 257:108768. https://doi.org/10.1016/j.scienta.2019.108768.

Barron-Gafford GA, Pavao-Zuckerman MA, Minor RL, Sutter LF, Barnett-Moreno I, Blackett DT, Thompson M, Dimond K, Gerlak AK, Nabhan GP, Macknick JE. 2019. Agrivoltaics provide mutual benefits across the food–energy–water nexus in drylands. Nat Sus. 2:848–855. https://doi.org/10.1038/s41893-019-0364-5.

Both AJ. 2002. Greenhouse glazing. Hort Eng Newsl. Rutgers Coop. Exten. 17:5–6.

Casal JJ. 2012. Shade avoidance. The Arabidopsis book. 10: e0157. ttps://doi.org/10.1199/tab.0157.

Colantoni A, Monarca D, Marucci A, Cecchini M, Zambon I, Di Battista F, Maccario D, Saporito MG, Beruto M. 2018. Solar radiation distribution inside a greenhouse prototypal with photovoltaic mobile plant and effects on flower growth. Sustainability. 10:855. https://doi.org/10.3390/su10030855.

Cossu M, Yano A, Solinas S, Deligios PA, Tiloca M.T, Cossu A, Ledda L. 2020. Agricultural sustainability estimation of the European photovoltaic greenhouses. Eu J Agron. 118:126074. https://doi.org/10.1016/j.eja.2020.126074.

Dinesh H, Pearce JM. 2016. The potential of agrivoltaic systems. Renew Sustain Energy Rev. 54:299–308. https://doi.org/10.1016/j.egyr.2021.06.017.

Faust JE, Holcombe V, Rajapakse NC, Layne D.R. 2005. The effect of daily light integral on bedding plant growth and flowering. HortScience. 40:645–649. https://doi.org/10.21273/hortsci.40.3.645.

Faust JE, Logan J. 2018. Daily light integral: A research review and high-resolution maps of the United States. HortScience. 53:1250–1257. https://doi.org/10.21273/hortsci.40.3.645.

Giacomelli GA, Roberts WJ. 1993. Greenhouse covering systems. HortTech. 3:50–58. https://doi.org/10.21273/horttech.3.1.50.

Hassanien RHE, Ming L. 2017. Influences of greenhouse-integrated semi-transparent photovoltaics on microclimate and lettuce growth. Int J Agric Biol Eng. 10:11–22. https://doi.org/10.25165/j.ijabe.20171006.3407.

Jaenicke H. 1999 Good tree nursery practices: practical guidelines for research nurseries. ICRAF, 8–15

Jayalath TC, van Iersel MW. 2021. Canopy size and light use efficiency explain growth differences between lettuce and mizuna in vertical farms. Plants. 10:704. https://doi.org/10.3390/plants10040704.

Kavga, A, Strati IF, Sinanoglou VJ, Fotakis C, Sotiroudis G, Christodoulou P, Zoumpoulakis P. 2019. Evaluating the experimental cultivation of peppers in low-energy-demand

greenhouses. An interdisciplinary study. J Sci Food Ag. 99:781–789. https://doi.org/10.1002/jsfa.9246.

Ke X, Yoshida H, Hikosaka S, Goto E. 2022. Optimization of photosynthetic photon flux density and light quality for increasing radiation-use efficiency in dwarf tomato under LED light at the vegetative growth stage. Plants. 11:121. https://doi.org/10.3390/plants11010121

Kusuma P, Bugbee B. 2021. Improving the predictive value of phytochrome photoequilibrium: Consideration of spectral distortion within a leaf. Front Plant sci. 12:596943. https://doi.org/10.3389/fpls.2021.596943.

Loehrlein MM, Craig R. 2004. The effect of daily light integral on floral initiation of *Pelargonium× domesticum* LH Bailey. HortScience. 39:529–532. https://doi.org/10.21273/hortsci.39.3.529.

Marcelis, LFM, Broekhuijsen AGM, Meinen E, Nijs EMFM, Raaphorst MGM. 2005. Quantification of the growth response to light quantity of greenhouse grown crops. Acta Hortic. 711:97–104. https://doi.org/10.17660/actahortic.2006.711.9.

Marrou H, Wéry J, Dufour L, Dupraz C. 2013. Productivity and radiation use efficiency of lettuces grown in the partial shade of photovoltaic panels. Eur J Agron. 44:54–66. https://doi.org/10.1016/j.eja.2012.08.003.

Meng Q, Boldt J, Runkle ES. 2020. Blue radiation interacts with green radiation to influence growth and predominantly controls quality attributes of lettuce. J Am Soc Hortic Sci. 145:75–87. https://doi.org/10.21273/jashs04759-19.

Meng Q, Kelly N, Runkle ES. 2019. Substituting green or far-red radiation for blue radiation induces shade avoidance and promotes growth in lettuce and kale. Environ Exp bot. 162:383–391. https://doi.org/10.1016/j.envexpbot.2019.03.016

Moccaldi LA, Runkle ES. 2007. Modeling the effects of temperature and photosynthetic daily light integral on growth and flowering of *Salvia splendens* and *Tagetes patula*. J Am Soc Hortic Sci. 132:283–288. https://doi.org/10.21273/jashs.132.3.283.

Oh W, Cheon IH, Kim KS, Runkle ES. 2009. Photosynthetic daily light integral influences flowering time and crop characteristics of *Cyclamen persicum*. HortScience. 44:341–344. https://doi.org/10.21273/hortsci.44.2.341.

Onoda Y, Westoby M, Adler PB, Choong AM, Clissold FJ, Cornelissen JH, Díaz S, Dominy NJ, Elgart A, Enrico L, Fine PV. 2011. Global patterns of leaf mechanical properties. Ecol Lett. 14:301–312. https://doi.org/10.1111/j.1558-5646.2012.01591.x.

Park Y, Runkle ES. 2018. Far-red radiation and photosynthetic photon flux density independently regulate seedling growth but interactively regulate flowering. Environ Exp Bot. 155:206–216. https://doi.org/10.1016/j.envexpbot.2018.06.033.

Pramuk LA, Runkle ES. 2005. Modeling growth and development of Celosia and Impatiens in response to temperature and photosynthetic daily light integral. J Am Soc Hortic. Sci. 130:813–818. https://doi.org/10.21273/jashs.130.6.813.

Proctor KW, Murthy GS, Higgins CW. 2020. Agrivoltaics align with green new deal goals while supporting investment in the US' rural economy. Sustainability. 13:137. https://doi.org/10.3390/su13010137.

Runkle E, Blanchard M. 2011. Saturating DLIs for flowering. Greenhouse Product News 21(2):42.

Stallknecht EJ, Herrera CK, Yang C, King I, Sharkey TD, Lunt RR, Runkle ES. 2023. Designing plant–transparent agrivoltaics. Sci Rep. 13:1903. https://doi.org/10.1038/s41598-023-28484-5.

Suddard-Bangsund J, Traverse CJ, Young M, Patrick TJ, Zhao Y, Lunt RR. 2016. Organic salts as a route to energy level control in low bandgap, high open-circuit voltage organic and transparent solar cells that approach the excitonic voltage limit. Adv Energy Mater. 6:501659. https://doi.org/10.1002/aenm.201501659.

Tang Y, Ma X, Li M, Wang Y. 2020. The effect of temperature and light on strawberry production in a solar greenhouse. Solar Energy, 195:318–328. https://doi.org/10.1016/j.solener.2019.11.070.

Toledo C, Scognamiglio A. 2021. Agrivoltaic systems design and assessment: a critical review, and a descriptive model towards a sustainable landscape vision (three-dimensional agrivoltaic patterns). Sustainability. 13:6871. https://doi.org/10.3390/su13126871.

Traverse CJ, Pandey R, Barr MC, Lunt RR. 2017. Emergence of highly transparent photovoltaics for distributed applications. Nat Energy. 2:849–860. https://doi.org/10.1038/s41560-017-0016-9.

USDA National Agricultural Statistics Service. 2022. Floriculture summary report. https://downloads.usda.library.cornell.edu/usda-esmis/files/0p0966899/s4656b62g/g445d913v/floran21.pdf.

Von Elsner B, Briassoulis D, Waaijenberg D, Mistriotis A, Von Zabeltitz C, Gratraud J, Russo G, Suay-Cortes R. 2000. Review of structural and functional characteristics of greenhouses in European Union countries: part I, design requirements. J. Ag. Eng. Res. 75:1–16. Warner, R.M. and J.E. Erwin. 2003. Effect of photoperiod and daily light integral on flowering of five *Hibiscus* sp. Sci Hortic. 97:341–351. https://doi.org/10.1006/jaer.1999.0502.

Warner RM, Erwin JE. 2005. Prolonged high temperature exposure and daily light integral impact growth and flowering of five herbaceous ornamental species. J Am Soc Hortic. Sci. 130:319–325. https://doi.org/10.21273/jashs.130.3.319.

Weselek A, Ehmann A, Zikeli S, Lewandowski I, Schindele S, Högy P. 2019. Agrophotovoltaic systems: applications, challenges, and opportunities. A review. Agron Sus Dev. 39:1–20. https://doi.org/10.1007/s13593-019-0581-3.

Wollaeger HM, Runkle ES. 2014. Growth of impatiens, petunia, salvia, and tomato seedlings under blue, green, and red light-emitting diodes. HortScience. 49:734–740. https://doi.org/10.21273/hortsci.49.6.734.

Zhen S, Bugbee B. 2020. Far-red photons have equivalent efficiency to traditional photosynthetic photons: Implications for redefining photosynthetically active radiation. Plant Cell Environ. 43:1259–1272. https://doi.org/10.1111/pce.13730.

APPENDIX D: TABLES AND FIGURES

Table III-1. The spectral characteristics of simulated semitransparent and transparent photovoltaic (PV) panels. Total photon flux density (TPFD; 400–750 nm) transmission was divided into percentages of blue (B; 400–499 nm), green (G; 500–599 nm); red (R; 600–699 nm); and far-red (FR; 700–750 nm) light. Phytochrome photoequilibrium (PPE) and internal phytochrome photoequilibrium (iPPE) were calculated according to Seger (1982) and Kusuma and Bugbee (2021), respectively. Clear plastic, moderate shade, and heavy shade correspond to neutral-density materials with 91%, 58%, and 33% transmission from 400–750 nm. Near-infrared (NIR) deficient, FR deficient 1 and 2, R deficient, and G deficient refer to experimental materials with different transmission cutoffs. Semitransparent and transparent PV panels are organized in descending order according to average (e)DLI from right to left.

Spectral characteristics	Semitransparent and transparent photovoltaic panels							
	Clear plastic	−NIR	−FR1	−FR2	−R	Moderate shade	−G	Heavy shade
B (% of TPFD)	28.4	27.9	31.3	28.6	37.9	26.2	30.0	24.0
G (% of TPFD)	28.5	29.5	32.3	30.2	31.7	28.5	0.02	28.4
R (% of TPFD)	28.6	28.6	27.9	29.1	11.1	29.4	44.5	30.3
FR (% of TPFD)	14.6	14.0	0.09	12.0	19.2	15.8	23.2	17.2
PPE	0.70	0.71	0.76	0.73	0.56	0.69	0.70	0.69
iPPE	0.38	0.39	0.52	0.44	0.25	0.37	0.36	0.35

Table III-2. Growth of snapdragon under eight different simulated semitransparent and transparent photovoltaic (PV) panels. Time to visible bud (VB) was calculated from seed sow. Radiation-use efficiency (RUE) was calculated by dividing total dry biomass accumulation (g) by accumulated daily light integral (mol photon·m^{-2}; 400–700 nm) while snapdragon was inside the experimental chambers. Specific leaf area (SLA) was calculated by dividing leaf area (cm^2) by leaf mass (g) of three representative leaves per plant. Compactness was calculated by dividing the total above-ground dry mass (g) by stem length (cm). The sturdiness quotient (SQ) was calculated by dividing stem length (cm) by the stem diameter at the substrate surface (mm). Data represent means with 15 samples. Means with different letters are significantly different according to Tukey's honestly significant difference test (P <0.05) and correspond to each row. Semitransparent and transparent PV panels are organized in descending order according to average (e)DLI from right to left.

Growth parameter	Semitransparent and transparent photovoltaic panels							
	Clear plastic	−NIR	−FR1	−FR2	−R	Moderate shade	−G	Heavy shade
Fresh mass (g)	35.5 b	32.4 c	34.7 bc	40.7 a	26.9 d	23.1 e	26.2 d	14.7 f
RUE (g·mol^{-1})	0.29 c	0.33 c	0.31 c	0.33 c	0.38 b	0.42 ab	0.40 b	0.47 a
Time to VB (d)	40 c	40 bc	40 b	40 c	40 bc	40 bc	40 bc	42 a
Leaf length (cm)	5.25 bc	5.05 c	5.56 ab	5.68 a	5.41 abc	5.23 bc	5.35 abc	5.11 c
Leaf width (cm)	1.81 ab	1.55 d	1.77 abc	1.93 a	1.75 abcd	1.57 cd	1.67 bcd	1.75 abcd
SPAD	30.9 ab	31.7 a	32.0 a	29.8 ab	26.7 d	29.3 bc	26.3 d	27.2 cd
SLA (cm^2·g^{-1})	510 e	499 e	542 de	555 cde	609 b	598 cd	659 bc	743 a
Stem length (cm)	23.0 ab	22.0 b	22.2 b	24.1 a	24.4 a	21.2 b	22.8 ab	21.8 b
Stem diameter (mm)	4.15 b	4.18 b	4.64 a	4.71 a	3.39 d	3.98 b	3.83 bc	3.49 cd
SQ (cm·mm^{-1})	5.42 cd	5.28 d	4.79 d	5.16 d	7.24 a	5.41 cd	5.96 bc	6.33 b

Table III-3. Regression coefficients for snapdragon growth parameters as a function of average daily light integral (DLI; 400–700 nm; $mol \cdot m^{-2} \cdot d^{-1}$). Radiation-use efficiency (RUE), time to visible flower bud (VB), specific leaf area (SLA), compactness, and sturdiness quotient (SQ) calculations are defined in Table 2. Linear, quadratic, and sigmoidal functions were evaluated as possible regression types. The regression with the highest r^2 value was selected, unless not meaningfully better than a linear model. In this case, a linear model was selected. Asterisks indicate significance at $P < 0.05$, $P < 0.01$, and $P < 0.001$ and are designated by *, **, and ***, respectively. N.S. = not significant. n=120.

Growth parameter	Regression type	Equation	
Fresh mass (g)	Sigmoidal	$y = 39.3 * \exp(-2.97 * 0.831^X)$	$r^2 = 0.77$***
Dry mass (g)	Linear	$y = 0.220 * x + 0.765$	$r^2 = 0.79$***
RUE ($g \cdot mol^{-1}$)	Linear	$y = -0.0115 * x + 0.525$	$r^2 = 0.66$***
Time to VB (d)	Sigmoidal	$y = 39.8 * \exp(0.914 * 0.616^X)$	$r^2 = 0.53$***
Time to flower (d)	Sigmoidal	$y = 51.4 * \exp(1.88 * 0.607^X)$	$r^2 = 0.57$***
Flowers (no.)	Linear	$y = 1.85 * x + 5.59$	$r^2 = 0.64$***
Leaf length (cm)	-	-	N.S.
Leaf width (cm)	-	-	N.S.
SPAD	Linear	$y = 0.376 * x + 24.0$	$r^2 = 0.38$***
SLA ($cm^2 \cdot g^{-1}$)	Linear	$y = -15.7 * x + 806$	$r^2 = 0.64$
Stem length (cm)	Quadratic	$y = (-0.0290 * x^2) + (0.790 * x) + 17.8$	$r^2 = 0.08$**
Stem diameter (mm)	Linear	$y = 0.0707 * x + 3.07$	$r^2 = 0.33$***
Compactness ($g \cdot m^{-1}$)	Linear	$y = 0.951 * x + 3.68$	$r^2 = 0.85$***
SQ ($cm \cdot mm^{-1}$)	Linear	$y = -0.0970 * x + 7.04$	$r^2 = 0.22$***

Table III-4. Regression coefficients for snapdragon growth parameters as a function of average extended daily light integral (eDLI; 400–750 nm; mol·m^{-2}·d^{-1}). Radiation-use efficiency (RUE), time to visible flower bud (VB), specific leaf area (SLA), compactness, and sturdiness quotient (SQ) calculations are defined in Table 2. Linear, quadratic, and sigmoidal functions were evaluated as possible regression types. The regression with the highest r^2 value was selected, unless not meaningfully better than a linear model. In this case, a linear model was selected. Asterisks indicate significance at $P < 0.05$, $P < 0.01$, and $P < 0.001$ and are designated by *, **, and ***, respectively. N.S. = not significant. n=120.

Growth parameter	Regression type	Equation	
Fresh mass (g)	Sigmoidal	$y = 44.2 * \exp(-2.93 * 0.881^{X})$	$r^2 = 0.76$***
Dry mass (g)	Linear	$y = 0.227 * x + 0.105$	$r^2 = 0.81$***
RUE (g·mol^{-1})	Linear	$y = -0.0115 * x + 0.554$	$r^2 = 0.64$***
Time to VB (d)	Sigmoidal	$y = 39.7 * \exp(0.557 * 0.734^{X})$	$r^2 = 0.54$***
Time to flower (d)	Sigmoidal	$y = 51.3 * \exp(1.26 * 0.715^{X})$	$r^2 = 0.58$***
Flowers (no.)	Linear	$y = 1.92 * x - 0.0195$	$r^2 = 0.65$***
Leaf length (cm)	-	-	N.S.
Leaf width (cm)	-	-	N.S.
SPAD	Linear	$y = 0.332 * x + 23.8$	$r^2 = 0.27$***
SLA (cm^2·g^{-1})	Linear	$y = -16.1 * x + 850$	$r^2 = 0.64$***
Stem length (cm)	Quadratic	$y = (-0.0180 * x^2) + (0.605 * x) + 18.0$	$r^2 = 0.07$***
Stem diameter (mm)	Linear	$y = 0.0631 * x + 3.02$	$r^2 = 0.25$***
Compactness (g·m^{-1})	Linear	$y = 0.967 * x + 1.12$	$r^2 = 0.84$***
SQ (cm·mm^{-1})	Linear	$y = -0.0790 * x + 6.98$	$r^2 = 0.13$***

Figure III-1. Chambers covered with simulated semitransparent and transparent photovoltaic panels inside the Michigan State University research greenhouse facility. A) Chamber frames were constructed with polyvinyl chloride pipe. Each chamber was actively ventilated with a fan and equipped with an aspirated thermocouple and quantum sensors to continually measure air temperature and instantaneous photosynthetic photon flux density. B) Chamber walls were opaque to ensure light entering each chamber was transmitted through the experimental panels.
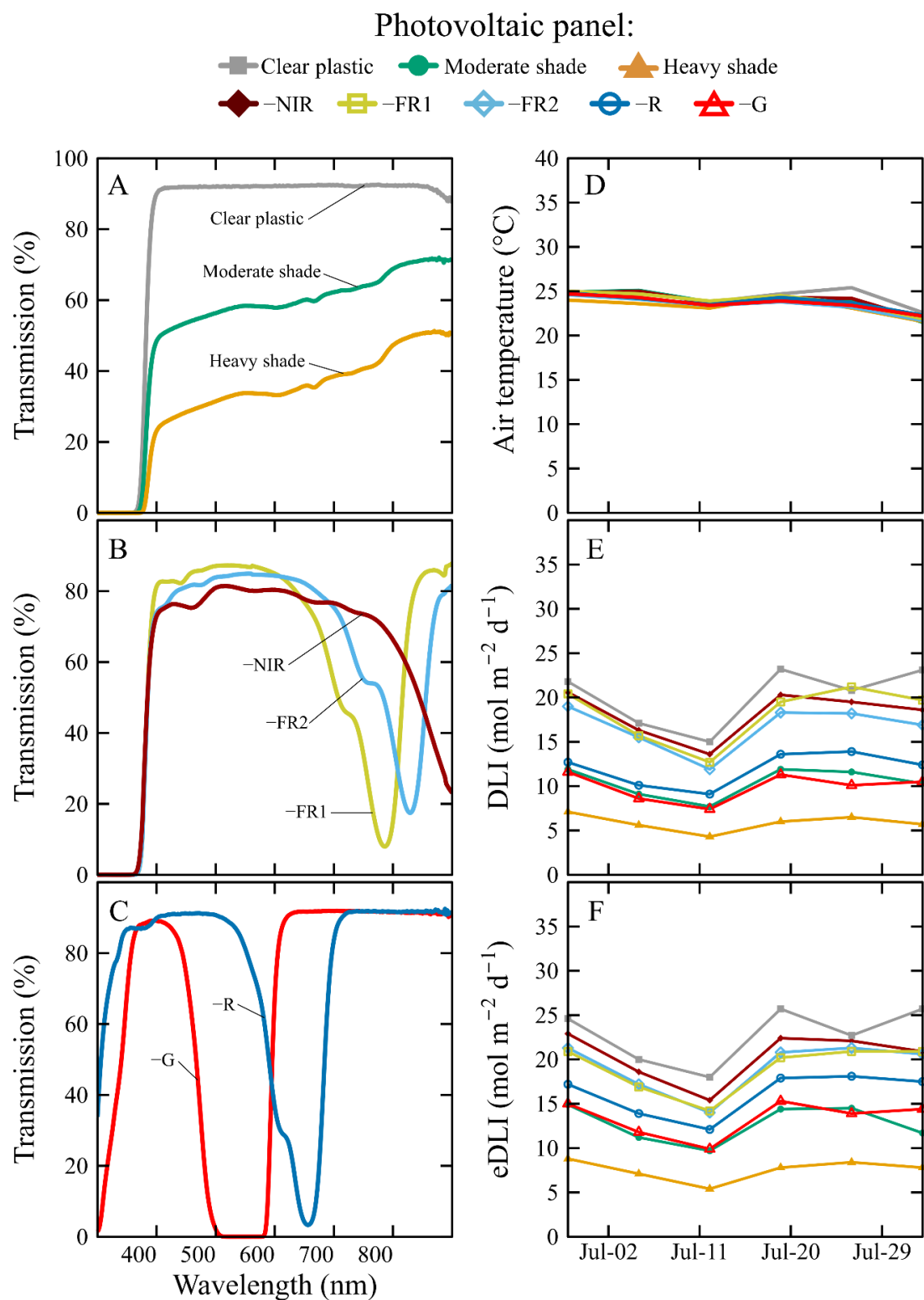
Figure III-2. The transmission spectrum and average environmental conditions inside chambers covered with simulated semitransparent or transparent photovoltaic (PV) panels. A–C) Clear

Figure III-2 (cont'd)

plastic, moderate shade, and heavy shade correspond to neutral-density materials with 91%, 58%, and 33% transmission from 400–700 nm. Near-infrared (NIR) deficient, far-red (FR; 700–750 nm) deficient 1 and 2, red (R; 600–700 nm) deficient, and green (G; 500–600 nm) deficient were simulated semitransparent or transparent PV panel with different transmission cutoffs between 400 and 850 nm. Transmission data were collected using a spectroradiometer. Transmissions were normalized to the incident photon flux density per nanometer of solar irradiance impinging on each chamber roof surface. Percentages of B, G, R, and FR light in each spectrum are displayed in Table 1. D–F) environmental conditions inside each chamber. Values represent weekly averages.

Photovoltaic panel:

Clear plastic	−NIR	−FR1	−FR2	−R	Moderate shade	−G	Heavy shade

Average daily air temperature (°C)

24.7	24.3	24.2	23.7	24.0	24.3	23.5	23.5

Average daily light integral (DLI; 400–70 nm; $mol \cdot m^{-2} \cdot d^{-1}$)

19.8	18.1	18.0	16.6	11.9	10.4	9.8	5.9

Average extended daily light integral (eDLI; 400–750 nm; $mol \cdot m^{-2} \cdot d^{-1}$)

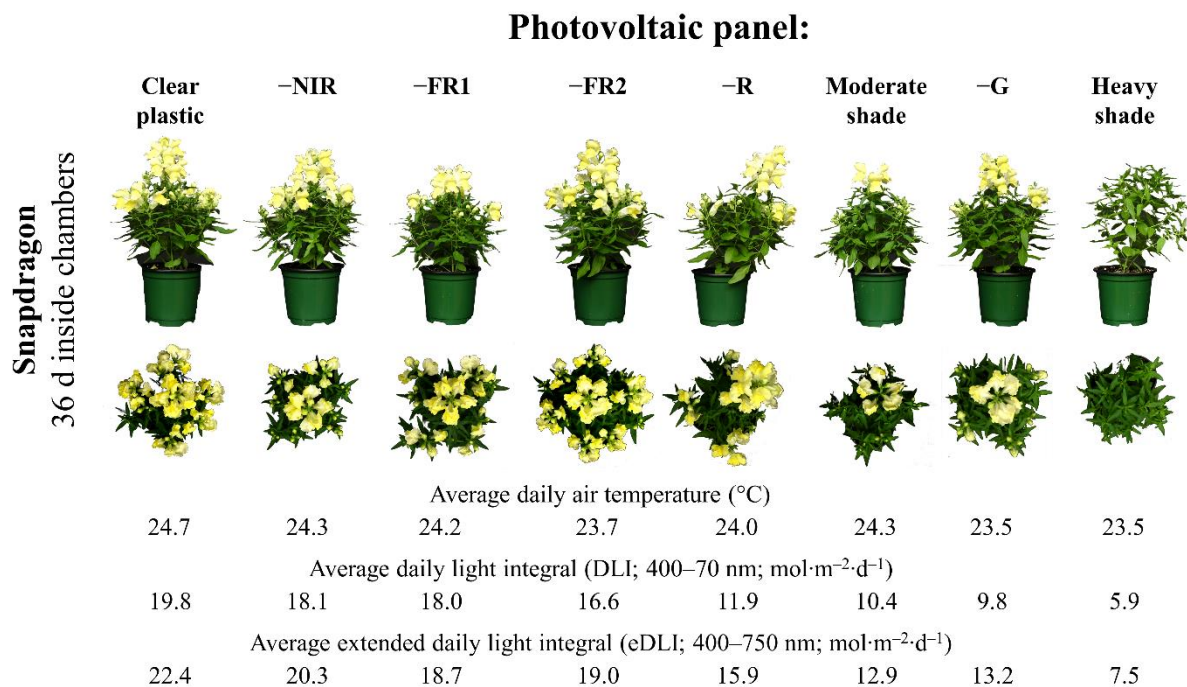| 22.4	20.3	18.7	19.0	15.9	12.9	13.2	7.5

Figure III-3. Photographs of representative snapdragon plants grown under eight different simulated semitransparent and transparent photovoltaic (PV) panels. Semitransparent and transparent PV panel spectra are displayed in Table 1 and Fig. III-2A–C. Average daily air temperature (°C), daily light integral (DLI; 400–700 nm), and extended daily light integral (eDLI; 400–750 nm) were measured at canopy height. Values represent daily means and are organized in descending order according to (e)DLI from right to left.
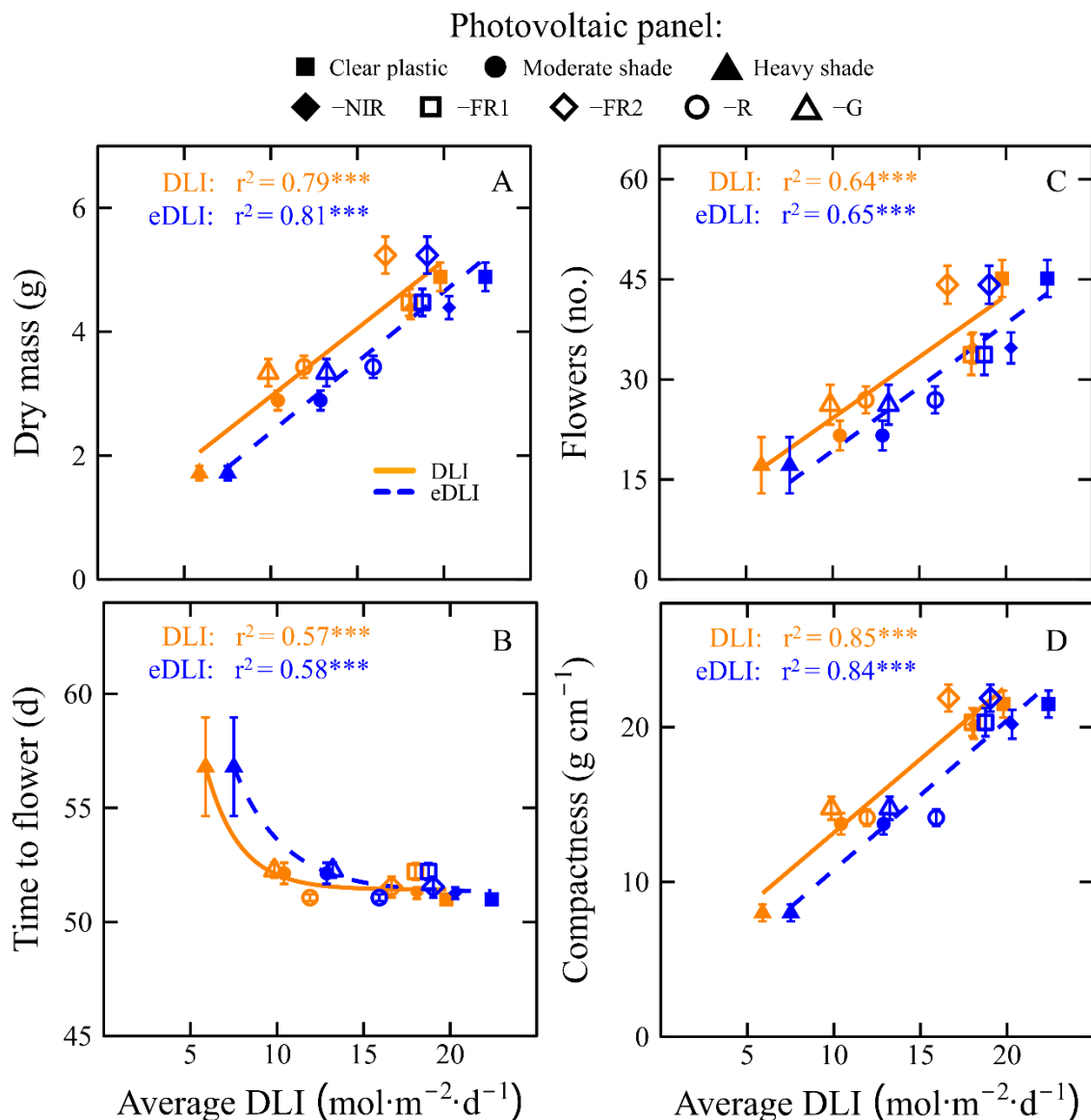
Figure III-4. Key growth metrics for snapdragon grown under eight different simulated semitransparent and transparent photovoltaic (PV) panels as a function of daily light integral (DLI; 400–700 nm) and extended daily light integral (eDLI; 400–750 nm). Simulated semitransparent and transparent PV panel transmission spectra are displayed in Table 1 and Fig. III-2A–C. Average DLI and eDLI were measured at canopy height. Time to flower was calculated from seed sow to first open floret. Flower number integrated all open florets and visible buds. Compactness was calculated according to table 2. Regression equations are displayed in Tables 3 and 4. Values represent averages ± 95% CI (n=15). Asterisks indicate significance at $P < 0.05$, $P < 0.01$, and $P < 0.001$ and are designated by *, **, and ***, respectively. Regression equations are displayed in Tables 3 and 4.

SECTION IV: LETTUCE GROWTH UNDER AN EXPERIMENTAL FLUORESCENT FILM THAT CONVERTS BLUE AND GREEN PHOTONS INTO RED AND FAR-RED PHOTONS

Lettuce growth under an experimental fluorescent film that converts blue and green photons into red and far-red photons

Eric J. Stallknecht and Erik S. Runkle[1]

Department of Horticulture, Michigan State University, 1066 Bogue Street, East Lansing, MI 48824

[1]Corresponding author. E-mail: runkler@msu.edu

Abbreviations: B, blue; DLI, daily light integral; FR, far red; G, green; LED, light-emitting diode; PC, protected cultivation; PCA, projected canopy area; PPE, phytochrome photoequilibrium; PPFD, photosynthetic photon flux density; R, red; RUE, radiation use efficiency; SAR, shade avoidance response; SDM, shoot dry mass; SFM, shoot fresh mass; SLA, specific leaf area; TPFD, total photon flux density.

Additional index words: Lactuca sativa, protected cultivation, fluorescence, spectral shifting, greenhouse film

Abstract

Glazing and covering materials used in protected cultivation are primarily selected based on cost, longevity, heat retention, and light transmission. They can also be engineered to modify transmission of the solar spectrum, including by the incorporation of fluorescent pigments. Fluorescent pigments typically absorb blue (B, 400–499 nm and/or green (G, 500–599 nm) photons and emit longer wavelength red (R, 600–699 nm) and, to a lesser extent, far-red (FR, 700–750 nm) photons. However, the incorporation of fluorescent pigments into plastics decreases its transmission of photosynthetically active radiation (PAR, 400–700 nm). In small-scale studies, lettuce (*Lactuca sativa*) 'Butter Crunch' shoot fresh mass (SFM) increased by as much as 22% when grown under a

red-fluorescent film compared to an unpigmented film with approximately 25% greater transmission of PAR. The objective of this research was to determine whether an experimental red-fluorescent film that amplified R and FR light, at the expense of B and G light and less PAR, can increase lettuce biomass accumulation in a larger-scale greenhouse experiment and whether greater biomass accumulation is cultivar specific. We grew five cultivars of lettuce under an experimental red-fluorescent film or a neutral-density shade that provided a 15–24% greater average daily light integral (DLI). The per plant SFM of lettuce increased by up to 45% and yield (SFM per m^2) by up to 37% when grown under the red-fluorescent film, and the magnitude of increase was cultivar specific. The SFM increase was linearly correlated with increased single leaf area. Despite the lower average DLI, a red-fluorescent shade material can increase lettuce yield in a cultivar-specific manner in spring if morphological changes such as greater extension growth are acceptable or desirable.

Introduction

In the protected cultivation (PC) of specialty crops, the microenvironment is managed to regulate plant growth and development (Reddy 2016; Wittwer and Castilla 1995). This encompasses a variety of agricultural covering materials, including, but not limited to, shade structures, high tunnels, and greenhouses. Covering materials are used to protect crops from unfavorable environmental conditions and are often composed of plastic, fabric, or glass (Wittwer and Castilla 1995). Advantages of PC can include increased crop yield and quality, production out of season, reductions in biotic and abiotic stresses, expanded arable land, and enhanced water-use efficiency (Wittwer and Castilla 1995). According to the USDA (2019), vegetable, fruit, culinary herb, floriculture, and propagated crops produced in the U.S. under PC totaled 13,000 ha, spread across 42,623 businesses. The production area under PC and the number of businesses increased by 6% and 5%, respectively, between 2012 and 2017 in the U.S. (USDA 2019). However, only 0.2% of the global 5.6 million ha of PC agriculture in 2019 was in the U.S. (Produce Grower 2019).

Glass, fabric, or plastic PC coverings have been engineered to transmit, reflect, absorb, and/or fluoresce solar energy (Hemming 2009). Photoselective materials differentially absorb or reflect portions of the electromagnetic spectrum (Stamps 2009). For example, photoselective coverings that absorb in the far-red [FR (700–750 nm)] waveband can inhibit the stem elongation of poinsettia (*Euphorbia pulcherrima*), pea (Pisum sativum), and pansy (*Viola ×wittrockiana*) (Clifford et al. 2004; Runkle and Heins 2001). Other photoselective covers absorb in the red [R (600–699 nm)] or

blue [B (400–499 nm)] wavebands to alter plant morphology (Lamnatou and Chemisana 2013a; Rajapakse et al. 1999). Other materials absorb ultraviolet [UV-A and UV-B (280–400 nm)] radiation to reduce disease pressure and improve plastic lifespan (Edser 2002; Lamnatou and Chemisana 2013b), while others absorb near-infrared (780–3000 nm) radiation to reduce heat transmission to plants and decrease evapotranspiration (Runkle et al. 2000; Sonneveld et al. 2006). Fluorescent PC coverings absorb high-energy, short wavelength photons and emit them at longer, less-energetic wavelengths, thus "shift" the transmission spectrum (Lamnatou and Chemisana 2013a; Pearson et al. 1995). Various approaches are used to shift photons in the UV, B, or green [G (500–599 nm)] wavebands into longer-wavelength photons, which can potentially improve crop growth (Edser 2002; Raviv 1988; Shen et al. 2021). Most commonly, fluorescent covers increase the flux of R photons that a crop receives, but at the expense of a decrease in total photosynthetically active radiation (PAR, 400–700 nm). Although these red-fluorescent coverings have increased crop biomass accumulation in some small-scale experiments, questions remain about the efficacy and economic viability of fluorescent coverings on diverse horticultural crops.

Isolated and purified chlorophyll a (Chl a) and chlorophyll b (Chl b) pigments primarily absorb R and B light and are the predominant pigments driving photosynthesis (Heldt and Piechulla 2021). At low-light intensities, R light can drive instantaneous photosynthesis by as much as 25% more efficiently than B or G light (Bugbee 1994; Inada 1976; McCree 1971). Specifically, R light more efficiently assimilates CO_2 (or evolves O_2) per photon absorbed (i.e., the quantum yield for CO2 fixation) compared to B or G light. Because of the high efficacy of R light at stimulating photosynthesis, researchers extrapolated that PC covers that increased R light at the expense of less-efficient B and G light by fluorescence could increase the photosynthetic efficiency of crops and thus, increase biomass accumulation (Raviv 1988). However, solely focusing on Chls a and b and the quantum yield of R light ignores other important photosynthetic factors. Inada (1976) and McCree (1971) quantified the relative quantum efficiency on a per nm basis for a wide range of crops using monochromatic light at low photon flux densities. Extrapolating and applying their curves to polychromatic light or higher photon flux densities is hypothetical (Bugbee 2016; Hogewoning et al. 2012). While G light may not drive photosynthesis as efficiently as R, it does better penetrate leaves and crop canopies, which can stimulate photosynthesis lower in mesophyll cells of individual leaves and lower leaves of a plant (Smith et al. 2017). Focusing on Chls a and b also ignores accessory pigments, such as carotenoids, which absorb G light and contribute energy

100

that drives photosynthesis (Ouzounis et al. 2015). Questions remain about the relative efficacy of R light compared with other photosynthetically active wavebands and thus, further research is needed to determine whether amplified R light (at the expense of less PAR) can surmount decreases in excitation energy lower in leaves and lower in the canopy, as well as other accessory pigments, to increase biomass.

The photoreceptor families of phytochrome and cryptochrome photoselectively absorb light and mediate photomorphological responses (Ouzounis et al. 2015). Phytochromes primarily absorb R and FR photons and exist in a dynamic continuum between the active form (Pfr) and inactive form (Pr) called the phytochrome photoequilibrium (PPE). Inactive Pr primarily absorbs R light and alters its conformation into the Pfr form. Alternatively, active Pfr slowly reverts into inactive Pr in darkness or by absorbing FR light. Therefore, the R:FR of an incident spectrum regulates plant PPE, with a high R:FR creating a high PPE, and vice versa (Sager et al. 1988). PPE is estimated using the equation [Pr/(Pr+Pfr)], the spectral irradiance between 300–800 nm, and the absorption spectra of Pr and Pfr (Sager et al. 1988). A low PPE (low R:FR) can promote shade-avoidance responses (SAR) such as stem and leaf elongation, hyponasty, apical dominance, early flowering, and decreased chlorophyll density (Franklin 2008; Ouzounis et al. 2015). PC covers that increase the R:FR by reflecting or absorbing FR can reduce SAR and inhibit unwanted extension growth of ornamental crops such as poinsettia and pansy (Clifford et al. 2004; Runkle and Heins 2001). Similarly, increasing the flux of R and not FR light would increase the R:FR and inhibit extension growth.

Cryptochromes primarily absorb UV and B light and inhibit stem and leaf elongation, promote anthocyanin production, and partially regulate flower initiation (Li and Yang 2007; Ouzounis et al. 2015). Low-intensity B light, indicative of vegetative shading, can also induce SAR similar to a low R:FR (Franklin 2008). For example, photoselective PC materials that decreased transmission of B light increased stem elongation of pansy, lobelia (*Lobelia × speciosa*), campanula (*Campanula carpatica*), and coreopsis (*Coreopsis × grandiflora*) compared to a neutral-density shade (Runkle and Heins 2001). Therefore, PC coverings that modify the transmitted spectral irradiance influence phytochrome and cryptochrome activity to regulate plant morphology, biomass accumulation, and crop quality.

There is growing interest in the technological advancement of PC coverings that have secondary purposes, such as harvesting solar energy to generate electricity, increase crop biomass

accumulation, or alter crop morphology (Shen et al. 2021; Stallknecht et al. 2023). Unavoidably, these coverings often reduce the photosynthetic photon flux density [PPFD (400–700 nm)] and/or alter the photon distribution reaching plants below. Because each PC material has unique transmission characteristics, research into potential applications considering crop yield and quality, geographic location, and economics is needed before widespread commercial application. Recently, a red-fluorescent plastic film that converts B and G photons into R photons was developed that increased the shoot fresh mass (SFM) of indoor-grown lettuce (*Lactuca sativa*) by 19–22% and greenhouse-grown lettuce by 22–30% compared to a non-pigmented control with 20–25% greater transmission PPFD (Shen et al. 2021). In both studies, individual lettuce leaves were larger but relative chlorophyll content was not affected. Despite promising initial results, further validation is required to determine whether red-fluorescent films can increase the biomass accumulation of other types of lettuce, whether increases in leaf area are consistent among studies, and how morphological changes may influence crop quality and overall yield.

Here, we evaluated whether increasing R light, at the expense of decreased B and G light, can improve plant biomass accumulation for multiple lettuce types, as well as conducted a larger greenhouse trial. We grew lettuce under an experimental red-fluorescent PC covering similar to that of Shen et al. (2021) and compared growth responses to those under a neutral-density PC covering. We postulated that the red-fluorescent film would 1) increase lettuce biomass accumulation because R light efficiently drives photosynthesis, at least on an instantaneous basis; 2) reduce red pigmentation of red-leaf lettuce because of decreased transmission of B light; and 3) increase the leaf size of lettuce because of the decrease in transmitted B light.

Materials and Methods

Expt. 1.

Lettuce seedling culture. Lettuce 'Rex' and 'Cherokee' seeds (Johnny's Selected Seeds, Winslow, ME) were sown in Rockwool cubes (AO 25/40 Starter Plugs; Grodan, Milton, ON, Canada) in a 23 °C controlled-environment growth room at ambient CO_2 concentration. Seedlings germinated under an 18-h photoperiod with a PPFD of 180 $\mu mol \cdot m^{-2} \cdot s^{-1}$ from warm-white light-emitting diodes (LEDs) (2700 K, PHYTOFY RL; OSRAM, Beverley, MA, USA), as controlled by proprietary software (PHYTOFY Control Software; OSRAM). Seedlings received irrigation as needed using deionized water and hydroponic water-soluble fertilizer (12N–4P–16K RO Hydro FeED, JR Peters, Inc., Allentown, PA, USA), and magnesium sulfate (Epsom salt; Pennington

Seed Inc., Madison, GA, USA) that provided the following nutrients (in mg·L^{-1}): 125 N, 42 P, 167 K, 73 Ca, 49 Mg, 39 S, 1.7 Fe, 0.52 Mn, 0.56 Zn, 0.13 B, 0.47 Cu, and 0.13 Mo. The fertilizer solution pH and electrical conductivity (EC) were measured after the formulation of a stock solution with a handheld meter (HI9814; Hanna Instruments, Woonsocket, RI, USA) and adjusted to a pH of 5.8 and EC of 1.2 mS·cm^{-1}. Transparent plastic humidity domes covered the germinating seedlings for the first 4 d (until radical emergence). Seedlings for replications one and two grew for 10 d, from 26 Sept 2019 to 6 Oct 2019 and 3 Nov 2019 to 13 Nov 2019, until seedlings had two true leaves and were ready for transplant.

Small chamber trial. Four chambers were fabricated from 1.3-cm diameter polyvinyl chloride pipe and four opaque, 1.3-cm thick insulation sheets, and placed on aluminum benches inside a glass-glazed research greenhouse (42.7° N lat.) (Fig. IV-1A). Each chamber was 107 cm wide × 236 cm long × 51 cm tall, with a total volume of 1.3 m^3. A single piece of transparent, 64-mm thick acrylic sheeting functioned as the roof of each chamber. Experimental PC covers were comprised of individual pieces measuring 24 cm × 15 cm and were taped onto the underside of the acrylic sheet roof with black electrical tape. Each south-facing wall had a 6 m^3·min^{-1} fan (Axial 1751, AC Infinity Inc., City of Industry, CA, USA) that exchanged the air volume in each chamber 4.6 times per minute to improve temperature uniformity inside each chamber. To improve light uniformity and minimize shadows cast by the chamber walls, only a 112 cm × 55 cm area (0.62 m^2) in the middle of each chamber functioned as a growing space. Additionally, we painted wall interiors with flat white paint to improve light scattering within chambers. Air temperature and instantaneous PPFD in each chamber were measured by a shielded and aspirated thermocouple (Type E; Omega Engineering, Inc., Stamford, CT, USA) and quantum sensor (LI-190SA; LI-COR, Inc., Lincoln, NE, USA or SQ-500; Apogee Instruments, Inc., Logan, UT, USA). Environmental conditions inside each chamber were measured every 1 min and averaged hourly with a datalogger (CR-1000; Campbell Scientific, Inc., Logan, UT, USA) and multiplexer (AM16/32B; Campbell Scientific, Inc.). Two chambers were covered with a neutral-density or red-fluorescent film. The neutral-density material was identical to the red-fluorescent film but did not include a fluorescent plastic additive. The preparation of both films is described by Shen et al. 2021. Both films were prototype PC coverings that incorporated micro-structures to increase transmission diffusion (increase photon scattering).

Treatment transmission. A portable spectroradiometer (LI-180 Spectrometer; LI-COR, Inc.) was used to measure the transmission through films at canopy height on a cloudless day at solar noon on 7 Nov 2019. The total photon flux density [TPFD (400–750 nm)] transmission of the neutral-density and red-fluorescent experimental films are displayed in Table IV-1 and Fig. IV-1B. The neutral-density film evenly reduced the photon flux density at each nanometer while the red-fluorescent film absorbed B and G light and fluoresced it as R and FR light at a peak wavelength of 648 nm. Compared to the neutral-density film, the red-fluorescent film decreased the transmission of B and G photons by 73% and 88%, respectively, while it increased the transmission of R and FR photons by 58% and 44%, respectively.

Greenhouse environment. Temperature and supplemental lighting were controlled by a greenhouse environmental control system (Integro 725; Priva, De Lier, the Netherlands, Europe) with setpoints at 19 °C and a 16-h photoperiod. Steam heating, roof vents, and exhaust fans regulated air temperature. Supplemental lighting was provided from luminaires (ILM-PG-180-2-300W-ED-FS-60; Rofianda Trading B.V., Tilburg, the Netherlands, Europe) containing broad-band (white) LEDs (SunLike LED STW9C2SB-S; Seoul Semiconductor Co., Gyeonggi-do, South Korea) that emitted a photosynthetic spectrum similar to sunlight. The LEDs provided an average PPFD of 190 ± 15 $\mu mol \cdot m^{-2} \cdot s^{-1}$ at the chamber roof surface.

Mature lettuce culture. Lettuce 'Cherokee' and 'Rex' seedlings were transplanted into each of four experimental chambers inside the greenhouse on 6 Oct 2019 and 13 Nov 2019 for replication one and two, respectively. Both cultivar seedlings were transplanted into a Rockwool hydroponic substrate (Delta 6.5; Grodan) and placed on plastic trays at a density of 310 cm^2 per plant. Plants received sub-irrigation with fertilizer as described previously but at (in $mg \cdot L^{-1}$): 150 N, 50 P, 200 K, 88 Ca, 58 Mg, 47 S, 2.1 Fe, 0.63 Mn, 0.68 Zn, 0.15 B, 0.56 Cu, and 0.15 Mo. Irrigation pH and EC were measured at irrigation events with a handheld meter (HI9814; Hanna Instruments) and averaged 5.7 ± 0.1 and 1.4 ± 0.2 $mS \cdot cm^{-1}$, respectively. Lettuce plants grew in each chamber for 30 d until destructive measurements on 5 Nov 2019 and 13 Dec 2019 for replication one and two, respectively.

Experimental design. The experiment was a randomized complete block design with two replications over time. Each block contained two chambers, one roofed with either the neutral-density or red-fluorescent film. Each chamber was randomly assigned ten 'Cherokee' and ten 'Rex' lettuce plants, for a total of 80 plants per replication.

104

Data collection. During destructive plant measurements, SFM was measured with a digital scale (GR-200; A&D Store, Inc., Wood Dale, IL, USA). Shoots were then dried in a drying oven (Blue M, Blue Island, IL, USA or SMO28-2; Sheldon Manufacturing, Inc., Cornelius, OR, USA) for 4 d at 60 °C and weighed using a digital scale (GX-1000; A&D Store, Inc.). Relative chlorophyll content (SPAD index) and CIELAB color were averaged from three measurements per representative leaf and measured with a chlorophyll meter (MC-100; Apogee Instruments, Inc.) and colorimeter (Chroma Meter CR-400 or BC-10 Plus, Konica Minolta Sensing America, Inc., Ramsey, NJ, USA). The International Commission on Illumination Lab color space values *L**, *a**, and *b** correspond to lightness from black (0) to white (100), green (−) to red (+), and blue (−) to yellow (+), respectively. The projected canopy area (PCA; cm^2) was measured using top-down photos and ImageJ software (National Institutes of Health 2023). Lettuce yield was calculated by dividing SFM by PCA and converted to units of $kg \cdot m^{-2}$. Specific leaf area (SLA) was calculated on a representative leaf by dividing its area (measured with LI-300; LI-COR Biosciences) by its dry mass (g). Radiation use efficiency (RUE) was calculated by dividing shoot dry mass by the total light integral (400–700 nm; $mol \cdot m^{-2}$).

Data analysis. Data were pooled because there were no significant ($P > 0.05$) treatment × replication or treatment × block interactions for any growth parameters measured. Data were analyzed in R software (R Core Team 2023) using ANOVA and Tukey's honestly significant difference test at $\alpha = 0.05$. Highly influential outliers were evaluated for and removed when exceeding Cook's distance = 0.5.

Expt. 2.

Lettuce seedling culture. Lettuce 'Rouxai', 'Dragoon', and 'Butter Crunch' seeds (Johnny's Selected Seeds) were germinated in Rockwool cubes (same as in Expt. 1) in a 23 °C controlled-environment growth room at ambient CO_2 concentration. Seedlings were grown using the same nutrient solution, photoperiod, PPFD, and humidity domes as in Expt. 1. However, a different warm-white LED (RAY22; Fluence, Austin, TX, USA) was used for germination. Seedlings grew for 8 d, from 10 Mar 2022 to 18 Mar 2022, until they had two true leaves and were ready for transplant.

Greenhouse trial. We utilized a larger [7.93 m × 8.64 m (68.5 m^2)] greenhouse and covered the south-facing glass roof with either an external application of neutral-density whitewash (ReduSol; Lumiforte, Baarle-Nassau, the Netherlands, Europe) or an experimental fluorescent film

(similar to that previously described but from a different manufacturing process) adhered to the interior glass glazing (Fig. IV-1C). The south-facing roof area was 7.93 m × 5.92 m (47.0 m^2). The east- and west-facing walls of each greenhouse were painted white to minimize the amount of light not entering through the south-facing roof. Inside each greenhouse, air temperature and instantaneous PPFD were measured at plant height by two shielded and aspirated thermocouples (Type E; Omega Engineering, Inc.) and two quantum sensors (SQ-500; Apogee Instruments, Inc.). Environmental conditions inside were measured every 1 min and averaged hourly with a datalogger (CR-1000; Campbell Scientific, Inc.) and multiplexer (AM16/32B; Campbell Scientific, Inc.).

Greenhouse treatments. The transmitted solar spectrum inside each greenhouse was measured at bench height with a spectroradiometer (LI-180 Spectrometer, LI-COR, Inc.) on a cloudless day at solar noon on 9 Mar 2022 (Table IV-1 and Fig. IV-1C). Compared to Expt. 1, the maximum transmitted TPFD was higher in both the neutral-density and red-fluorescent greenhouses, and the red-fluorescent greenhouse light environment had a greater fraction of B and G photons, a lower fraction of R and FR photons, and a peak wavelength of 640 nm. Relative to the neutral-density greenhouse, the red-fluorescent film decreased the transmission of B and G photons by 40% and 54%, respectively, while it increased the transmission of R and FR photons by 26% and 11%, respectively. The greenhouse air temperature was controlled by an environmental control system (Integro 725; Priva) with a constant air temperature setpoint of 20 °C. Steam heating, roof vents, and exhaust fans regulated air temperature.

Mature lettuce culture. Lettuce 'Rouxai', 'Dragoon', and 'Butter Crunch' seedlings were randomly selected and transplanted into one of the two greenhouse treatments on 18 Mar 2022. Each greenhouse contained four 1.83 m × 3.15 m (5.77 m^2) benches. Plants were placed on each bench at a density of 0.121 m^2 per plant. Lettuce seedlings were transplanted into 15.2-cm round pots filled with a peat-based soilless substrate (Suremix; Michigan Grower Products, Inc., Galesburg, MI, USA) and were irrigated as needed with a solution consisting of reverse osmosis water supplemented with 13N–1.3P–12.5K water-soluble fertilizer that contained (in mg·L^{-1}) 125 N, 13 P, 120 K, 77 Ca, 19 Mg, 1.7 Fe, 0.4 Cu, and Zn, 0.8 Mn, 0.2 B and Mo (MSU Orchid RO Water Special; GreenCare Fertilizers, Inc., Kankakee, IL, USA). Lettuce plants grew for 35 d until destructive measurements were taken on 22 Apr 2022.

Experimental design, data collection, and analysis. The experiment was organized as a completely randomized design with one replication. Each greenhouse was an experimental unit that was randomly assigned the neutral-density or red-fluorescent film treatment (two levels) and randomly assigned lettuce 'Rouxai', 'Dragoon', and 'Butter Crunch' seedlings. Data collection and analysis were as described in Expt. 1 and were analyzed separately for each lettuce cultivar.

Results

Environmental conditions. The average air temperature inside the neutral-density and red-fluorescent film treatments was 19.6 and 19.1 °C in Expt. 1 (Fig. IV-2A) and 20.3 and 20.4 °C in Expt. 2 (Fig. IV-2B), respectively. The average daily light integral (DLI) inside the neutral-density and red-fluorescent treatments was 7.9 and 6.0 $mol \cdot m^{-2} \cdot d^{-1}$ in Expt. 1 (a 24% difference; Fig. IV-2C) and 11.4 and 9.7 $mol \cdot m^{-2} \cdot d^{-1}$ in Expt. 2 (a 15% difference; Fig. IV-2D).

Morphology. Figure IV-3 displays a representative plant from each lettuce cultivar grown in the two experiments under the neutral-density or experimental red-fluorescent film. Figure IV-4 displays the percentage increase or decrease of growth parameters between lettuce grown under the red-fluorescent film relative to a neutral-density shade with a 15–24% greater average DLI at canopy height. For example, regardless of cultivar, the average single-leaf area was 6% to 25% greater under the red-fluorescent film compared to the neutral-density, higher-light environment (Table IV-2; Fig. IV-4A). The red-fluorescent film increased the PCA of lettuce 'Rex', 'Cherokee', and 'Rouxai' by 12–17%, but unexpectedly 'Butter Crunch' PCA decreased by 23% relative to the neutral-density material (Fig. IV-4B). Similarly, the SLA of 'Rex', 'Cherokee', and 'Rouxai' increased by 11–24% under the red-fluorescent film, but SLA decreased by 15–19% for 'Dragoon' and 'Butter Crunch' (Fig. IV-4C).

Biomass accumulation. The red-fluorescent films had varying effects on SFM within and between experiments. In Expt. 1, the SFM of lettuce 'Rex' decreased by 7% but increased by 7% in 'Cherokee' under the red-fluorescent film (Table IV-2; Fig. IV-4D). In Expt. 2, the SFM of 'Rouxai' and 'Dragoon' under the red-fluorescent film increased by 45% and 15%, but 'Butter Crunch' SFM was statistically similar between treatments. The yield ($kg \cdot m^{-2}$) of lettuce decreased under the red-fluorescent film by 9–19% in Expt. 1 and increased by 10–37% in Expt. 2 relative to the neutral-density shade (Fig. IV-4E). The RUE increased by 9–49% for 'Cherokee', 'Rouxai', 'Dragoon', and 'Butter Crunch' compared to the neutral-density materials (Fig IV-4F). However, 'Rex' RUE decreased by 6% under the red-fluorescent film.

Coloration. The differences in pigmentation of lettuce leaves were inconsistent across experiments and cultivars. Specifically, the relative chlorophyll content (SPAD index) of 'Rex', 'Rouxai', and 'Butter Crunch' were similar, while that of 'Cherokee' and 'Dragoon' under the red-fluorescent film decreased by 11% and 13%, respectively (Table IV-2). Under the red-fluorescent film, the L^* value (where greater values indicate lighter leaves) of 'Cherokee', 'Rouxai', and 'Dragoon' increased by 4–7% (Fig. IV-4G). The a^* value (where lower values indicate greener leaves and greater values indicate redder leaves) of 'Rex' increased by 6%, while that of 'Cherokee', 'Dragoon', and 'Butter Crunch' decreased by 6–14% (Fig. IV-4H). On the other hand, the b^* value (where lower values indicate bluer leaves and greater values indicate yellower leaves) decreased by 8–29% for 'Rex' and 'Rouxai' but increased by 8–14% for 'Cherokee', 'Dragoon', and 'Butter Crunch' (Fig. IV-4I). Despite significant differences in SPAD and CIELAB color space values, the effects of the red-fluorescent film on leaf pigmentation were not consistent (Figs. IV-3 and IV-5).

Tip burn. Marginal leaf necrosis (tip burn) was not present in either lettuce cultivar in Expt. 1 (Table IV-2). However, in Expt. 2, tip burn incidence and severity (quantified by the tip-burn index) increased by 10.9 and 2.5 in 'Dragoon' and 'Butter Crunch' when grown under the red-fluorescent film, respectively. Tip burn severity was calculated according to Frantz et al. (2004).

Discussion

Precise comparisons among studies utilizing red-fluorescent materials are challenging because of differences that include: 1) the use of dissimilar concentrations of fluorescent pigments that vary the transmitted PPFD; 2) the type of fluorescent pigment is not consistent and therefore the transmission photon distribution is different; 3) most studies utilized different crops and cultivars; and 4) environmental conditions and cultural practices during experimentation vary and are often insufficiently documented (Hemming et al. 2006; Hidaka et al. 2008; Kang et al. 2023; Minich et al. 2011; Nishimura et al. 2012; Rodríguez et al. 2002; Shen et al. 2021). In this study, regardless of the experiment or lettuce cultivar, the most consistent morphological acclimation response under the red-fluorescent film was increased single leaf area (Fig. IV-4A). Similarly, single leaf area of lettuce, cabbage (*Brassica rapa* ssp. *pekinensis*), two cultivars of cucumber (*Cucumis sativus*), and Welsh onion (*Allium fistulosum*) increased under a red-fluorescent material relative to a neutral-density control in other studies (Kang et al. 2023; Minich et al. 2011; Nishimura et al. 2012; Rodríguez et al. 2002). In contrast, there was no increase in extension

growth in romaine lettuce, radish (*Raphanus raphanistrum*), or strawberry (*Fragaria × ananassa*) (Hemming et al. 2006; Hidaka et al. 2008; Kang et al. 2023). These differences in morphological responses could be attributed to response variation among species and cultivars, different transmitted spectra, and differences in experimental methodology (e.g., air temperature and transmitted PPFD) that introduced additional interactive effects.

Similar to crop morphology, red-fluorescent materials do not always increase the biomass accumulation of crops. Depending on the experiment and lettuce cultivar in the current study, an experimental red-fluorescent film decreased SFM by up to 7% or increased it by up to 45% (Fig. IV-4D). Likewise, red-fluorescent materials had inconsistent effects on crop biomass accumulation (Hemming et al. 2006; Hidaka et al. 2008; Kang et al. 2023; Loik et al. 2017; Minich et al. 2011; Rodríguez et al. 2002). Plant architecture (i.e., the spatial arrangement of above-ground organs) attributes such as leaf area and plant height influence photon interception and consequently biomass accumulation (Fageria et al. 2006). Previous studies have shown positive correlations between increased lettuce leaf area, plant diameter, or PCA and increased dry mass accumulation (Kim et al. 2004; Li and Kubota 2009; Park and Runkle 2017; Snowden et al. 2016; Wang et al. 2016). In those experiments, decreasing B light, or its ratio with other wavebands, increased lettuce leaf area, which increased whole-plant net assimilation and SDM. Similarly, in the current study and others, increased biomass accumulation was correlated to increased single leaf area (Fig. IV-6) (Kang et al. 2023; Shen et al. 2021; Stallknecht and Runkle 2023). This suggests an increase in biomass accumulation of some crops under red-fluorescent materials depends on potential changes to plant architecture, independent of possible changes to photosynthetic efficiency. We speculate that the reduction in B photons under our films, and likely other red-fluorescent materials too, altered plant architecture to increase lettuce SFM and RUE.

Blue light inhibits stem and leaf elongation in various plant species including arabidopsis (*Arabidopsis thaliana*), wheat (*Triticum aestivum*), soybean (*Glycine max*), cucumber, lettuce, poinsettia, pansy, lobelia, campanula, and coreopsis (Clifford et al. 2004; Dougher and Bugbee 2001; Hernández and Kubota 2016; Meng. et al. 2020; Runkle and Heins 2001). Attenuating the photon flux density or fraction of B light typically increases extension growth. This response is mediated through cryptochromes, phototropins, or both and increases the competitiveness of a plant to intercept PAR (Franklin 2008). The experimental red-fluorescent film in this study reduced B light transmission by 40–58%, which likely relieved the inhibition of lettuce extension

growth and increased leaf area. Therefore, increases in plant extension growth in this study and others are likely caused by decreases in transmitted B light under films with fluorescent additives. This is supported by research with sole-source lighting in which decreasing the fraction of B light increased photon interception and biomass accumulation without necessarily increasing the single-leaf photosynthetic rate (Hernández and Kubota 2016; Meng et al. 2020).

Red-fluorescent materials influence single-leaf photosynthesis in a species-dependent manner. Some pepper (*Capsicum annuum*) and strawberry cultivars had greater single-leaf photosynthetic capacity when grown under a red-fluorescent material relative to a neutral-density control (Loik et al. 2017; Yoon et al. 2020). However, photosynthetic capacity did not increase for crops such as tomato (*Lycopersicon esculentum*), cucumber, basil (*Ocimum basilicum*), or several *Citrus* spp. under red-fluorescent films relative to a neutral-density control with a higher average PPFD (Loik et al. 2017). Considering these conflicting responses, some crops morphologically and photosynthetically acclimate more than others under red-fluorescent materials. Developing a better understanding of the magnitude of crop acclimation under red-fluorescent materials, and how responses may depend on other environmental factors (e.g., DLI) would advance the commercial application and further development of red-fluorescent technologies.

Marginal necrosis (leaf tip burn) is a common physiological disorder of lettuce that is caused by insufficient translocation of calcium to the apical meristem (Frantz et al. 2004). The percentage of plants with tip burn and its severity typically increase in environments with a high PPFD, high temperature, low vapor pressure deficit, and insufficient air velocity around the shoot apical meristem. In theory, the experimental red-fluorescent film used in the current study should have reduced the incidence of lettuce tip burn relative to the neutral-density shade with a ~20% greater average DLI. On the contrary, tip burn incidence increased in 'Dragoon' and 'Butter Crunch' grown under the red-fluorescent film compared to under the neutral-density shade. Lettuce tip-burn can increase when transpiration rates are low. Transpiration rate is controlled through the opening and closing of stomata with guard cells, which are regulated primarily by B and R light (Matthews et al. 2020; Sharkey and Raschke 1981). B-light induced stomatal opening begins at a very low flux density (~5–10 $\mu mol \cdot m^{-2} \cdot s^{-1}$) and is about 10 times more effective than R light at opening stomata (Sharkey and Raschke 1981). Additionally, the magnitude of stomatal conductance depends on the flux of B light as well as the ambient CO_2 concentration, whereby decreasing the flux of B photons or increasing the CO_2 concentration attenuates conductance

(Sharkey and Raschke 1981). We speculate a red-fluorescent shade that decreased the flux of B photons increased the incidence of tip-burn in part by limiting transpiration and thus the translocation of calcium to the actively growing meristem. However, few studies directly evaluating tip burn and light quality exist to validate this assumption. While red-fluorescent materials can increase lettuce crop yield, their implementation may be limited if these materials also increase physiological disorders. To prevent tip burn, the implementation of red-fluorescent materials may necessitate harvesting lettuce earlier before symptoms develop, increasing air velocity, or adjusting what cultivars are grown under these films, since sensitivity varies among cultivars in this study and others (Ertle and Kubota 2022).

Red pigmentation is a desirable quality attribute of some horticultural crops including red-leaf lettuce cultivars 'Cherokee' and 'Rouxai'. In part, leaf pigmentation is regulated by the photon distribution and flux density (Meng et al. 2020; Steyn et al. 2002). Generally, increasing the proportion of B, UV-A, and UV-B photons in a spectrum or increasing the PPFD increases leaf pigmentation in a dose-dependent manner (Meng et al. 2020). Increased red pigmentation (i.e., increased anthocyanin concentration) in leaves acts as a defense mechanism against photoinhibition, which can occur when plants are grown under stressful conditions such as a high PPFD (Steyn et al. 2002). In theory, an experimental red-fluorescent film that had fewer transmitted B photons and a lower DLI should have had less red-leaf lettuce pigmentation. However, differences in leaf color of red-leaf lettuce between treatments were too minute to detect (Figs. IV-3 and IV-7).

Incorporating fluorescent pigments into agricultural plastics started in the early 1990s and has continued in a limited capacity since. The implementation of red-fluorescent greenhouse plastics has remained challenging for several reasons including 1) increased cost of pigmented plastics compared to non-pigmented plastics; 2) unpredictable effects on crop morphology and yield; 3) increasing the concentration of fluorescent pigments decreases the transmitted PPFD; 4) transmitted photon distributions vary among films; and 5) fluorescent pigments can photo-oxidize rapidly and become nonfunctional if not designed properly (El-Bashir et al. 2016; Kang et al. 2023; Stallknecht and Runkle 2023; Park and Runkle 2023). While the commercial implementation has been limited thus far, red-fluorescent PC covers have the potential to increase the yield of at least some crops including lettuce, but further research is warranted to determine the economic feasibility of incorporating this technology in various locations.

In summary, PC plastics with red-fluorescent pigment additives convert much of the B and G photons into R and FR photons. Based on this study with lettuce under an experimental red-fluorescent film, a decrease in B photon transmission can increase leaf area and plant diameter, which increase photon interception and ultimately yield (by up to 37%) compared to plants grown under a neutral-density control film with 15–24% greater transmitted PPFD. We did not measure instantaneous photosynthesis to determine if the greater proportion of R photons under the red-fluorescent film contributed to the increase in biomass accumulation, and additional research is merited. In addition, the economics of these films need to be studied on a case-by-case basis. We conclude that red-fluorescent films have potential as a greenhouse covering or shading material when they are stable, economical, and a reduction in PPFD and a change in plant morphology (such as greater extension growth or leaf area) are acceptable or desirable.

LITERATURE CITED

Bugbee B. 1994. Effects of radiation quality, intensity, and duration on photosynthesis and growth. Intl. Lighting in Controlled Env (Wkshp.). NASA-CP-95-3309:39–50.

Bugbee B. 2016. Toward an optimal spectral quality for plant growth and development: the importance of radiation capture. Acta Hortic. 1134:1–12. https://doi.org/10.17660/actahortic.2016.1134.1.

Clifford SC, Runkle ES, Langton FA, Mead A, Foster SA, Pearson S, Heins RD. 2004. Height control of poinsettia using photoselective filters. HortScience. 39:383–387. https://doi.org/10.21273/hortsci.39.2.383.

Dougher TA, Bugbee B. 2001. Differences in the response of wheat, soybean and lettuce to reduced blue radiation. Photochem Photobio. 73:199–207. https://doi.org/10.1562/0031-8655(2001)0730199ditrow2.0.co2.

Edser C. 2002. Light manipulating additives extend opportunities for agricultural plastic films. Plast Addit Compd. 4(3):20–24. https://doi.org/10.1016/s1464-391x(02)80079-4.

El-Bashir SM, Al-Harbi FF, Elburaih H, Al-Faifi F, Yahia IS. 2016. Red photoluminescent PMMA nanohybrid films for modifying the spectral distribution of solar radiation inside greenhouses. Renew Energy 85:928–938. https://doi.org/10.1016/j.renene.2015.07.031.

Ertle, J.M. and Kubota, C., 2022. Tipburn Inductive Conditions for Testing Cultivar-Specific Sensitivity Under Indoor Vertical Farm Conditions (abstr.). Hortscience. 57(9S):S36-S36.

Fageria NK, Baligar VC, Clark R. 2006. Physiology of crop production. Hawthorn Press Inc., Binghampton, NY. https://doi.org/10.1201/9781482277807-5.

Franklin KA. 2008. Shade avoidance. New Phytol. 179:930–944. https://doi.org/10.1111/j.1469-8137.2008.02507.x.

Frantz JM, Ritchie G, Cometti NN, Robinson J, Bugbee B. 2004. Exploring the limits of crop productivity: beyond the limits of tipburn in lettuce. J Amer Soc Hortic Sci. 129:331–338. https://doi.org/10.21273/jashs.129.3.0331.

Heldt HW, Piechulla B. 2021. Plant Biochemistry. Academic Press, The Netherlands. https://doi.org/10.1016/b978-0-12-818631-2.00003-9.

Hemming S, Van Os EA, Hemming J, Dieleman JA. 2006. The effect of new developed fluorescent greenhouse films on the growth of Fragaria × ananassa 'Elsanta'. Eur J Hortic. Sci. 71(4):145–154.

Hemming S. 2009. Use of natural and artificial light in horticulture-interaction of plant and technology. Acta Hortic. 907:25–35. https://doi.org/10.17660/actahortic.2011.907.1.

Hernández R, Kubota C. 2016. Physiological responses of cucumber seedlings under different blue and red photon flux ratios using LEDs. Environ. Expt. Bot. 121:66–74. https://doi.org/10.1016/j.envexpbot.2015.04.001.

Hidaka K, Yoshida K, Shimasaki K, Murakami K, Yasutake D, Kitano M. 2008. Spectrum conversion film for regulation of plant growth. J Fac Agric, Kyushu Univ. 53:549–552. https://doi.org/10.5109/12872.

Hogewoning SW, Wientjes E, Douwstra P, Trouwborst G, van Ieperen W, Croce R, Harbinson J. 2012. Photosynthetic quantum yield dynamics: from photosystems to leaves. Plant Cell 24:1921–1935. https://doi.org/10.1105/tpc.112.097972.

Inada K. 1976. Action spectra for photosynthesis in higher plants. Plant Cell Physiol. 17:355–365. https://doi.org/10.1093/oxfordjournals.pcp.a075288.

Kang JH, Kim D, Yoon HI, Son JE. 2023. Growth, morphology, and photosynthetic activity of Chinese cabbage and lettuce grown under polyethylene and spectrum conversion films. Hortic. Environ Biotech. 1:11. https://doi.org/10.1007/s13580-022-00502-x.

Kim HH, Goins GD, Wheeler RM, Sager J.C. 2004. Green-light supplementation for enhanced lettuce growth under red-and blue-light-emitting diodes. HortScience. 39:1617–1622. https://doi.org/10.21273/hortsci.39.7.1617.

Kusuma P, Bugbee B. 2021. Improving the predictive value of phytochrome photoequilibrium: Consideration of spectral distortion within a leaf. Front Plant Sci. 12:596943. https://doi.org/10.3389/fpls.2021.596943.

Lamnatou C, Chemisana D. 2013a. Solar radiation manipulations and their role in greenhouse claddings: Fluorescent solar concentrators, photoselective and other materials. Renew Sustain Energy Rev. 27:175–190. https://doi.org/10.1016/j.rser.2013.06.052.

Lamnatou C, Chemisana D. 2013b. Solar radiation manipulations and their role in greenhouse claddings: Fresnel lenses, NIR-and UV-blocking materials. Renew Sustain Energy Rev. 18:271–287. https://doi.org/10.1016/j.rser.2012.09.041.

Li Q, Kubota C. 2009. Effects of supplemental light quality on growth and phytochemicals of baby leaf lettuce. Environ Exp Bot. 67:59–64. https://doi.org/10.1016/j.envexpbot.2009.06.011.

Li QH, Yang HQ. 2007. Cryptochrome signaling in plants. Photochem Photobiol. 83:94–101. https://doi.org/10.1562/2006-02-28-ir-826.

Loik ME, Carter SA, Alers G, Wade CE, Shugar D, Corrado C, Jokerst D, Kitayama C. 2017. Wavelength-selective solar photovoltaic systems: Powering greenhouses for plant growth at the food-energy-water nexus. Earth's Future 5:1044–1053. https://doi.org/10.1002/2016ef000531.

Matthews JS, Vialet-Chabrand S, Lawson T. 2020. Role of blue and red light in stomatal dynamic behaviour. J Exp Bot. 71:2253–2269. https://doi.org/10.1093/jxb/erz563.

McCree KJ. 1971. The action spectrum, absorptance and quantum yield of photosynthesis in crop plants. Agr Meteorol. 9:191–216. https://doi.org/10.1016/0002-1571(71)90022-7.

Meng Q, Boldt J, Runkle ES. 2020. Blue radiation interacts with green radiation to influence growth and predominantly controls quality attributes of lettuce. J Amer Soc Hortic Sci. 145:75–87. https://doi.org/10.21273/jashs04759-19.

Minich, AS, Minich IB, Shaitarova OV, Permyakova NL, Zelenchukova NS, Ivanitskiy AE, Filatov DA, Ivlev GA. 2011. Vital activity of Lactuca sativa and soil microorganisms under fluorescent films. Вестник ТГПУ (TSPU Bulletin) 8(110):74–84.

Nishimura Y, Wada E, Fukumoto Y, Aruga H, Shimoi Y. 2012. The effect of spectrum conversion covering film on cucumber in soilless culture. Acta Hortic. 956:481–487. https://doi.org/10.17660/actahortic.2012.956.56.

Ouzounis T, Rosenqvist E, Ottosen CO. 2015. Spectral effects of artificial light on plant physiology and secondary metabolism: a review. HortScience 50:1128–1135. https://doi.org/10.21273/hortsci.50.8.1128.

Park Y, Runkle ES. 2017. Far-red radiation promotes growth of seedlings by increasing leaf expansion and whole-plant net assimilation. Environ Exp Bot. 136:41–49. https://doi.org/10.1016/j.envexpbot.2016.12.013.

Park Y, Runkle ES. 2023. Spectral-conversion film potential for greenhouses: Utility of green-to-red photons conversion and far-red filtration for plant growth. Plos one. 18(2):0281996. https://doi.org/10.1371/journal.pone.0281996.

Pearson S, Wheldon AE, Hadley P. 1995. Radiation transmission and fluorescence of nine greenhouse cladding materials. J Agric Eng Res. 62:61–69. https://doi.org/10.1006/jaer.1995.1063.

Produce Grower. 2019. Cuesta Roble releases 2019 global greenhouse statistics. https://www.producegrower.com/article/cuesta-roble-2019-global-greenhouse-statistics.

R Core Team. 2023. R-4.0.3 for Windows. R Foundation for Statistical Computing, Vienna, Austria. https://cran.r-project.org/bin/windows/base/old/4.0.3/.

Rajapakse NC, Young RE, McMahon MJ, Oi R. 1999. Plant height control by photoselective filters: current status and future prospects. HortTechnology 9:618–624. https://doi.org/10.21273/horttech.9.4.618.

Rasband, W.S., ImageJ, U.S. National Institutes of Health, Bethesda, Maryland, USA, https://imagej.nih.gov/ij/, 1997-2023.

Raviv M. 1988. The use of photoselective cladding materials as modifiers of morphogenesis of plants and pathogens. Acta Hortic. 246:275–284. https://doi.org/10.17660/actahortic.1989.246.34.

Reddy PP. 2016. Sustainable crop protection under protected cultivation. Springer, Singapore. https://doi.org/10.1007/978-981-287-952-3_1.

Rodríguez R, Bañón S, Franco JA, Fernández JA, Salmerón A, Espí E, González A. 2002. Strawberry and cucumber cultivation under fluorescent photoselective plastic films cover. Acta Hortic. 614:407–413. https://doi.org/10.17660/actahortic.2003.614.61.

Runkle ES, Heins RD, Jaster P, and Thill C. 2000. Plant responses under an experimental near infra-red reflecting greenhouse film. Acta Hortic. 580:137–143. https://doi.org/10.17660/actahortic.2002.580.16.

Runkle ES, Heins RD. 2001. Specific functions of red, far red, and blue light in flowering and stem extension of long-day plants. J Amer Soc Hort Sci. 126:275–282. https://doi.org/10.21273/jashs.126.3.275.

Sager JC, Smith WO, Edwards JL, Cyr KL. 1988. Photosynthetic efficiency and phytochrome photoequilibria determination using spectral data. Trans Am Soc Agric Eng. 31:1882–1889. https://doi.org/10.13031/2013.30952.

Sharkey TD, Raschke K. 1981. Effect of light quality on stomatal opening in leaves of Xanthium strumarium L. Plant Physio. 68:1170–1174. https://doi.org/10.1104/pp.68.5.1170.

Smith HL, McAusland L, Murchie EH. 2017. Don't ignore the green light: exploring diverse roles in plant processes. J Expt Bot. 68:2099–2110. https://doi.org/10.1093/jxb/erx098.

Snowden, MC, Cope KR, Bugbee B. 2016. Sensitivity of seven diverse species to blue and green light: interactions with photon flux. PLoS One 11(10):e0163121. https://doi.org/10.1371/journal.pone.0163121.

Sonneveld PJ, Swinkels GL, Kempkes F, Campen JB, Bot GP. 2006. Greenhouse with an integrated NIR filter and a solar cooling system. Acta Hortic. 719:123–130. https://doi.org/10.17660/actahortic.2006.719.11.

Stallknecht EJ, Herrera CK, Yang C, King I, Sharkey TD, Lunt RR, Runkle ES. 2023. Designing plant–transparent agrivoltaics. Sci Rep. 13:1903. https://doi.org/10.1038/s41598-023-28484-5.

Stallknecht EJ, Runkle ES. 2023. Opportunities and challenges with advanced greenhouse glazing materials. Acta Hortic. [in press].

Stamps RH. 2009. Use of colored shade netting in horticulture. HortScience. 44:239–241. https://doi.org/10.21273/hortsci.44.2.239.

Steyn WJ, Wand SJE, Holcroft DM, Jacobs G. 2002. Anthocyanins in vegetative tissues: a proposed unified function in photoprotection. New Phytol. 155:349–361. https://doi.org/10.1046/j.1469-8137.2002.00482.x.

United States Department of Agriculture (USDA). 2019. 2017 census of agriculture. https://www.nass.usda.gov/Publications/AgCensus/2017/Full_Report/Volume_1,_Chapter_1_US/usv1.pdf.

Wang J, Lu W, Tong Y, and Yang Q. 2016. Leaf morphology, photosynthetic performance, chlorophyll fluorescence, stomatal development of lettuce (Lactuca sativa L.) exposed to different ratios of red light to blue light. Front Plant Sci. 7:250. https://doi.org/10.3389/fpls.2016.00250.

Wittwer SH, Castilla N. 1995. Protected cultivation of horticultural crops worldwide. HortTechnology 5:6–24. https://doi.org/10.21273/horttech.5.1.6.

Yoon HI, Kang JH, Kang WH, Son JE. 2020. Subtle changes in solar radiation under a green-to-red conversion film affect the photosynthetic performance and chlorophyll fluorescence of sweet pepper. Photosynthetica 58:1107–1115. https://doi.org/10.32615/ps.2020.057.

Table IV-1. The transmission characteristics through either a neutral-density (ND) material that evenly reduced light transmission at each wavelength or a red-fluorescent (RF) film that absorbed blue [B (400–499 nm)] and green [G (500–599 nm)] light and fluoresced red [R (600–699 nm)] and far-red [FR (700–750 nm)] light. The material transmissions were measured with a spectroradiometer under treatments inside a glass-glazed greenhouse at solar noon. Average total photon flux density [TPFD (400–750 nm)] was measured at canopy height. B, G, R, and FR wavebands are displayed as a percentage of TPFD. Yield photon flux density (YPFD), phytochrome photoequilibrium (PPE), and internal phytochrome photoequilibrium (iPPE) were calculated according to McCree (1971), Sager et al. (1988), and Kusuma and Bugbee (2021), respectively.

	Expt. 1		Expt. 2	
	Covering material			
Transmission characteristic	ND	RF	ND	RF
TPFD (μmol·m^{-2}·s^{-1}; 400–750 nm)	696	543	1041	878
Blue (% of TPFD)	22	8	23	16
Green (% of TPFD)	30	5	31	17
Red (% of TPFD)	32	65	32	48
Far red (% of TPFD)	16	23	15	19
PPE	0.72	0.76	0.73	0.74
iPPE	0.40	0.45	0.42	0.42
YPFD (μmol·m^{-2}·s^{-1})	517	400	788	656

Table IV-2. Growth response of lettuce grown under a neutral-density (ND) material that evenly reduced light transmission at each wavelength or a red-fluorescent (RF) film. Values indicate means (n=40 for 'Rex' and 'Cherokee'; n=24 for 'Rouxai', 'Dragoon' and 'Butter Crunch') and different letters within each row and for each lettuce cultivar are significantly different by Tukey's honestly significant difference test (P < 0.05). The projected canopy area (PCA), specific leaf area (SLA), radiation use efficiency (RUE), and relative chlorophyll content (SPAD) were calculated as described in the materials and methods. The tip burn index was calculated as described by Frantz et al. (2004). Increasing tip burn index values indicate a greater percentage of plants with tip burn and greater tip burn severity.

	'Rex'		'Cherokee'		'Rouxai'		'Dragoon'		'Butter Crunch'	
	Covering material									
	ND	RF	ND	RF	ND	RF	ND	RF	ND	RF
Leaf area (cm^2)	88	94	138 b	150 a	126 b	158 a	144 b	160 a	252 b	268 a
PCA (cm^2)	450 b	513 a	353 b	413 a	388 b	436 a	335	346	616 a	472 b
SLA ($cm^2 \cdot g^{-1}$)	447 b	509 a	450 b	501 a	826 b	1026 a	585 a	495 b	686 a	553 b
Shoot fresh mass (g)	40.3 a	37.5 b	48.7 b	51.9 a	48.4 b	70.0 a	102.0 b	116.5 a	125.0	125.2
Shoot dry mass (g)	1.89 a	1.67 b	1.94	2.02	2.56 b	3.36 a	4.61 b	5.12 a	5.90	5.60
Yield ($kg \cdot m^{-2}$)	0.92 a	0.75 b	1.39 a	1.26 b	1.23 b	1.59 a	3.06 b	3.37 a	2.03 b	2.66 a
RUE ($g \cdot mol^{-1}$)	0.17	0.16	0.23 b	0.25 a	0.16 b	0.22 a	0.34 b	0.43 a	0.23 b	0.34 a
SPAD	24.6	23.6	26.1 a	23.2 b	19.3	19.6	41.9 a	36.4 b	33.7	32.3
L^*	46.7	46.2	44.5 b	47.5 a	31.0 b	32.4 a	38.4 b	40.0 a	39.4	39.9
a^*	−22.0 b	−20.7 a	−17.6 a	−20.0 b	2.3	1.6	−8.3 a	−8.9 b	−8.8 a	−9.4 b
b^*	31.5 a	28.9 b	27.6 b	31.5 a	9.92 a	7.06 b	16.5 b	18.5 a	18.5 b	20.0 a

Table IV-2 (cont'd)

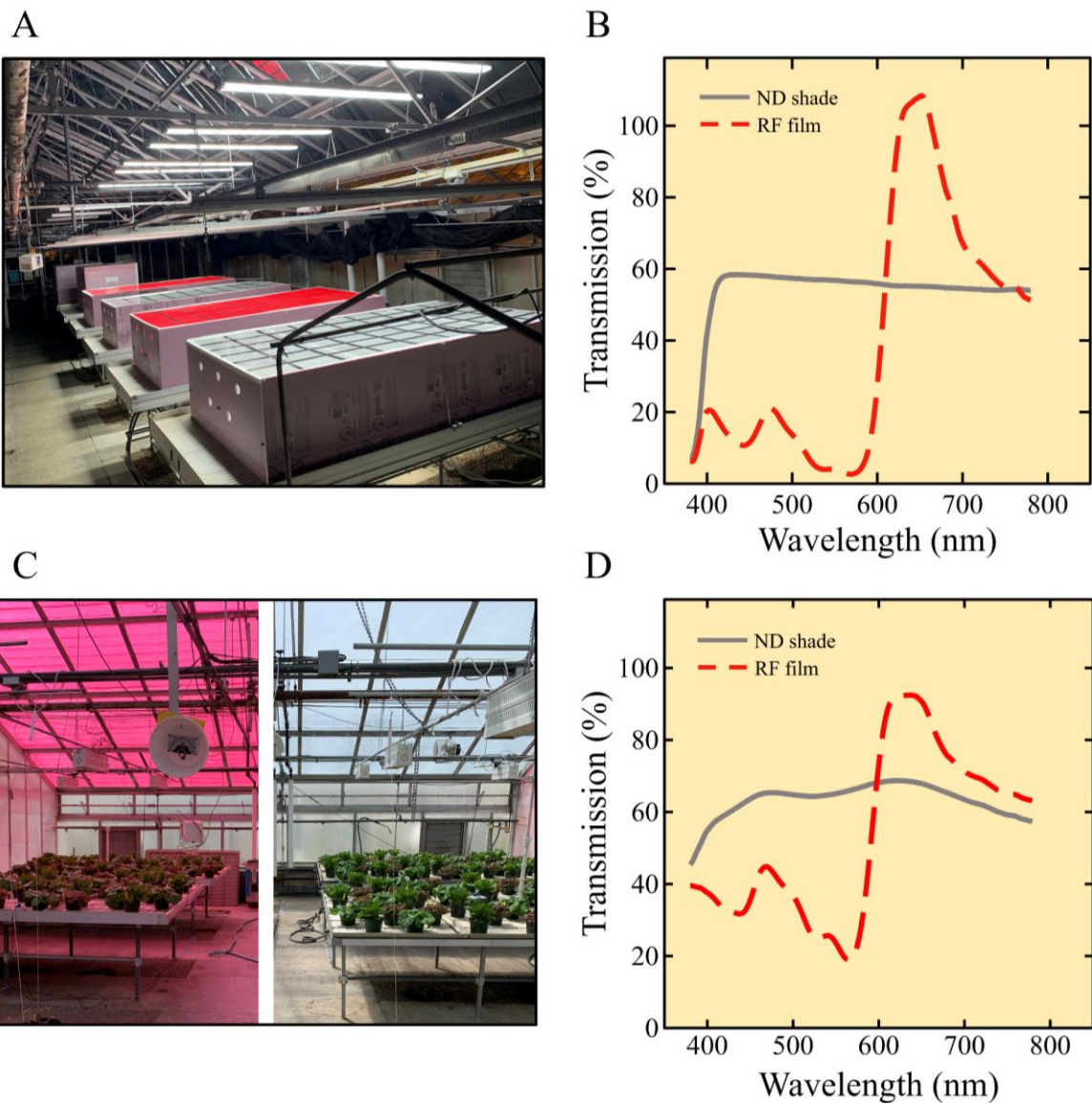| Tip burn index	0	0	0	0	0	0	23.3	34.2	0.8	3.3

Figure IV-1. Experimental setup for the small chamber trial (Expt. 1, Figs. A and B) and greenhouse trial (Expt. 2, Figs. C and D). In Expt. 1, two chambers were covered with a neutral-density (ND) shade or a red-fluorescent (RF) film. In Expt. 2, one greenhouse was covered with whitewash and an identical greenhouse was covered with a similar red-fluorescent film. Transmission spectra in B and D were measured at solar noon.
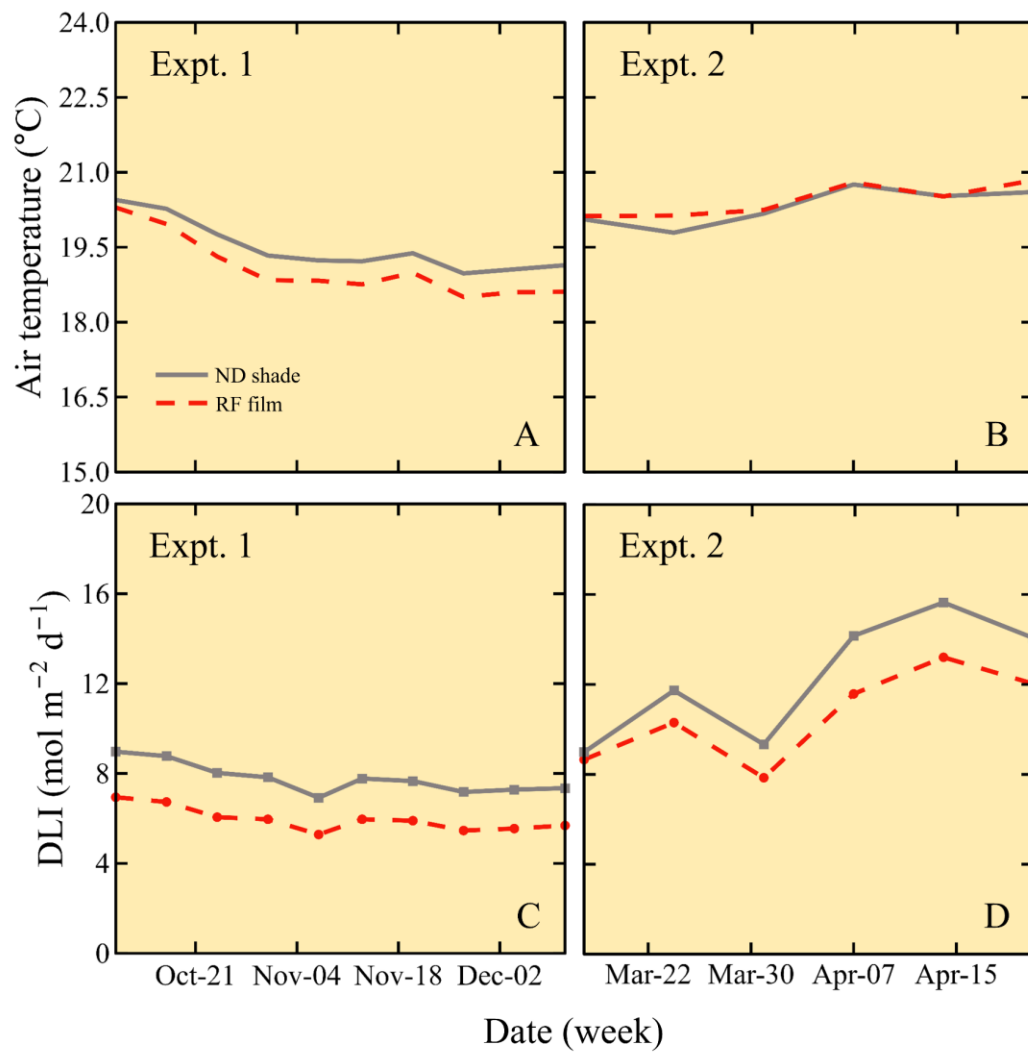
Figure IV-2. Average weekly air temperature (A and B) and daily light integral [DLI (400-700 nm)] (C and D) inside small chambers (Expt. 1) and greenhouses (Expt. 2) covered with a neutral-density (ND) or a red-fluorescent (RF) film.
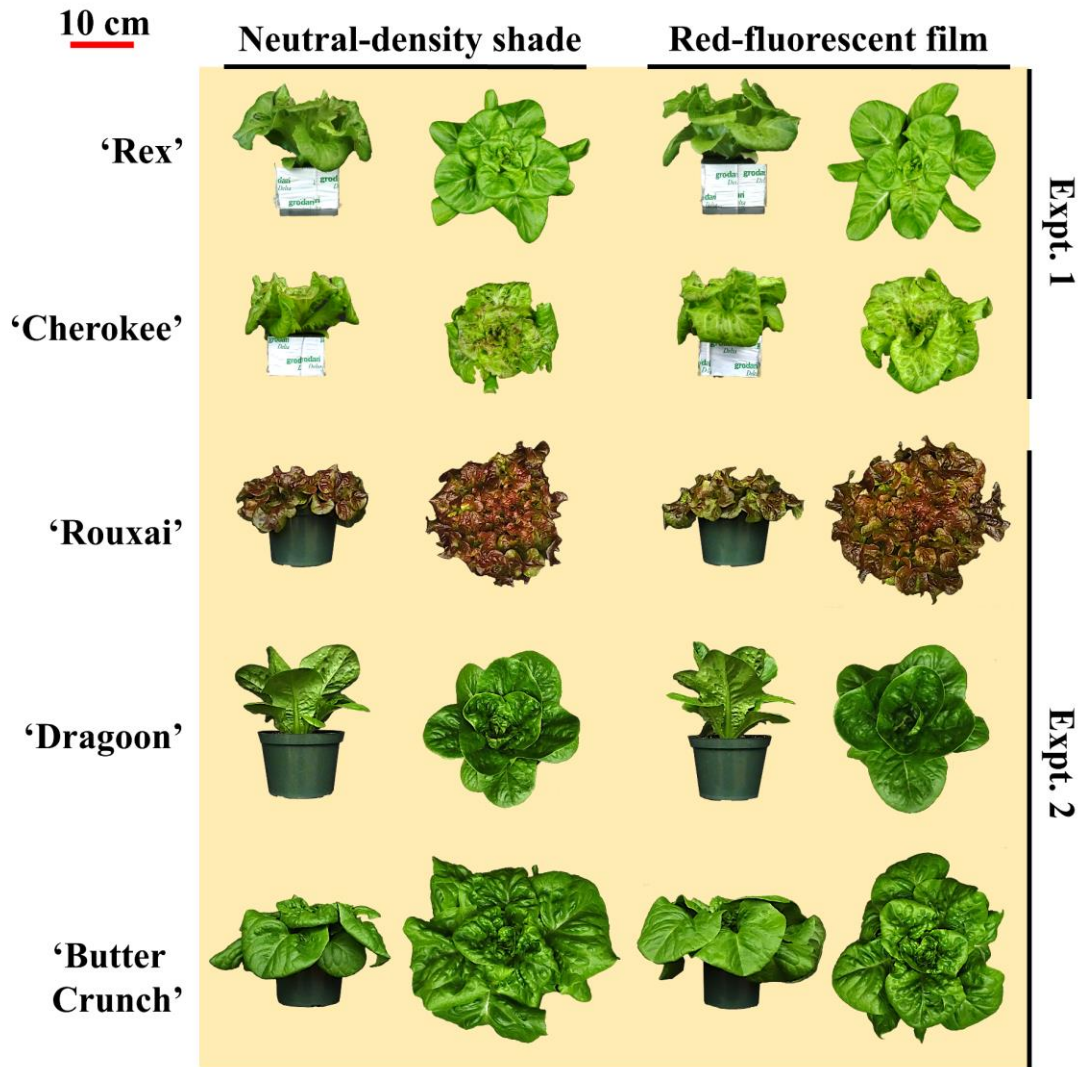
Figure IV-3. Representative plants of lettuce grown under a neutral-density shade or a red-fluorescent film. 'Cherokee' and 'Rex' were grown for 30 d after germination and 'Rouxai', 'Dragoon', and 'Butter Crunch' were grown for 35 d.
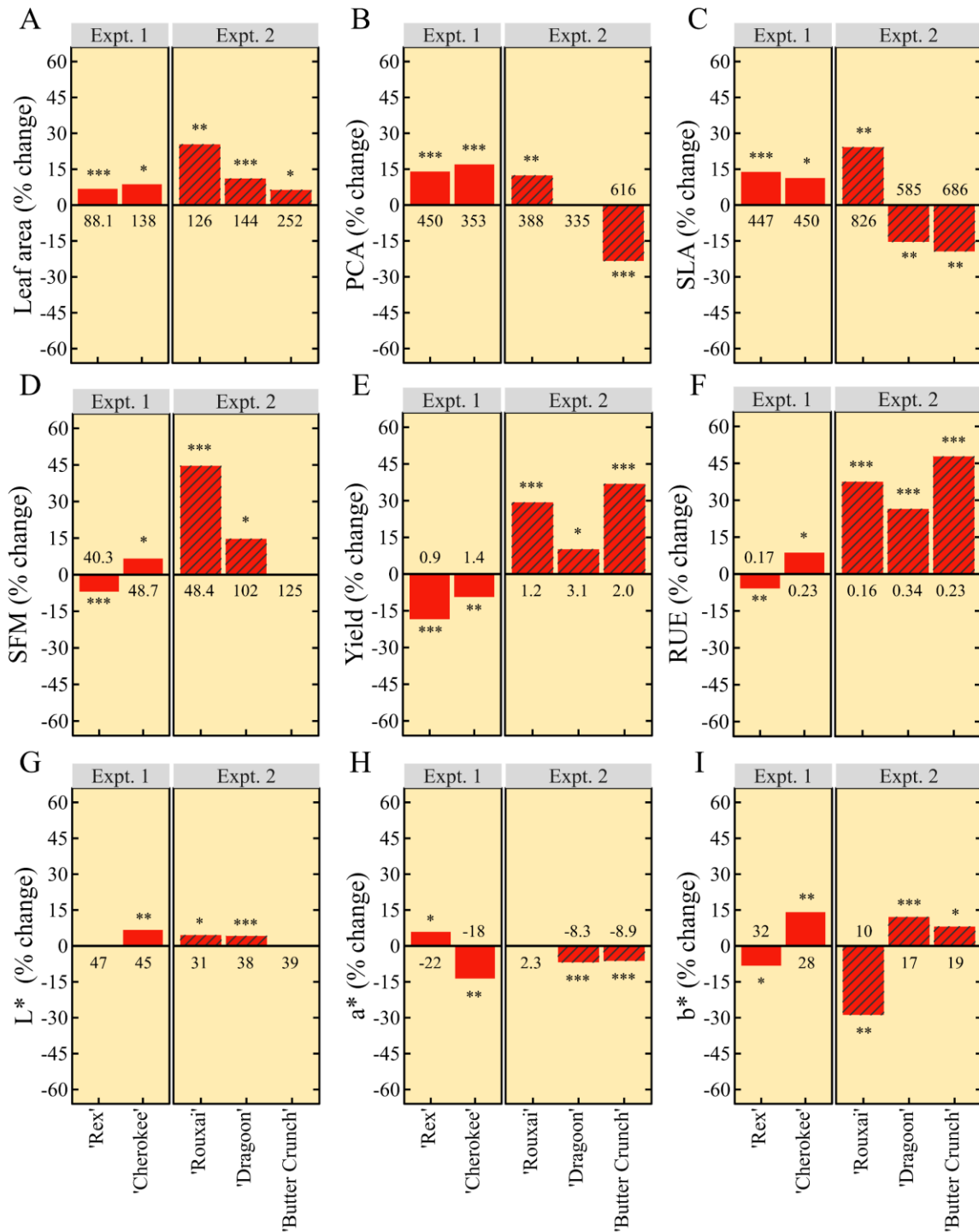
Figure IV-4. The average percentage increase or decrease in growth parameters of lettuce grown under a neutral-density shade or a red-fluorescent film. Projected canopy area (PCA; cm^2), specific leaf area (SLA; cm$^2 \cdot$g^{-1}), shoot fresh mass (SFM; g), yield (kg$\cdot$m^{-2}), and radiation use efficiency (RUE; g$\cdot$mol^{-1}) were calculated as described in the materials and methods. The International Commission on Illumination Lab color space values *L**, *a**, and *b** correspond to lightness from black (0) to white (100), green ($-$) to red ($+$), and blue ($-$) to yellow ($+$), respectively. Asterisks

123

Figure IV-4 (cont'd)

indicate significant differences between treatments for each cultivar, $P < 0.05$, 0.01, and 0.001 are designated by *, **, and ***, respectively. Numerical values indicate the average growth parameter value for each cultivar grown under the neutral-density shade treatment.

Average lettuce leaf color

	Neutral-density shade	Red-fluorescent film
'Rex'	#5C7837	#5A753B
'Cherokee'	#5C723A	#627A3A
'Rouxai'	#52473A	#534A40
'Dragoon'	#575C3E	#5B623F
'Butter Crunch'	#5B623F	#5B623D

Figure IV-5. The average lettuce leaf color measured in the CIELAB color space was converted to hexadecimals. The value inside each colored bar corresponds to the color hexadecimal code.
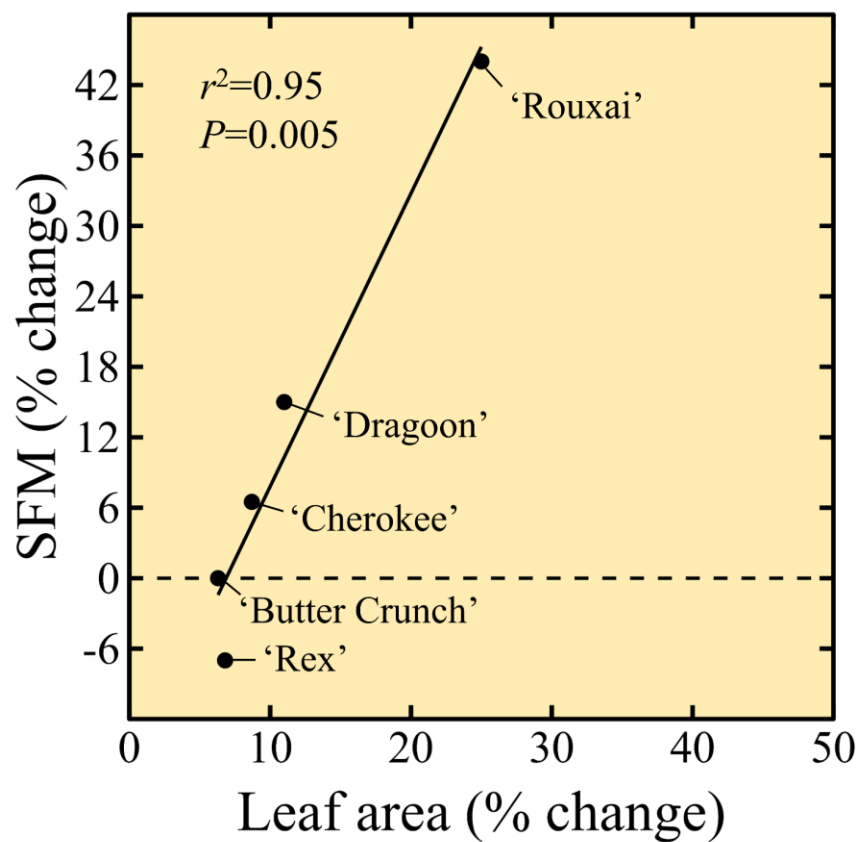
Figure IV-6. The correlation between the average percentage change in lettuce shoot fresh mass (SFM) as a function of percentage change in single leaf area of lettuce grown under a neutral-density shade or a red-fluorescent film.

SECTION V: TOWARDS UNDERSTANDING THE PROMOTION OF PLANT GROWTH UNDER AN EXPERIMENTAL RED-FLUORESCENT PLASTIC FILM

Towards understanding the promotion of plant growth under an experimental red-fluorescent plastic film

Eric J. Stallknecht and Erik S. Runkle[1]

Department of Horticulture, Michigan State University, East Lansing, MI, USA

[1]Corresponding author: runkleer@msu.edu

Index words: tomato, *Solanum lycopersicum*, petunia, *Petunia × hybrida*, lettuce, *Lactuca sativa*, snapdragon, *Antirrhinum majus,* spectral shifting, shading

Abstract

Plastic films containing fluorescent pigments can increase the growth and yield of greenhouse crops, including lettuce (*Lactuca sativa*) and tomato (*Solanum lycopersicum*). These plastics incorporate fluorescent pigment additives that absorb blue (B; 400–499 nm) and/or green (G; 500–599 nm) light to increase red (R; 600–699 nm) and far-red (FR; 700–750 nm) light, but the net transmitted photosynthetic photon flux density (PPFD) is decreased because of imperfect quantum efficiency. The underlying mechanism by which a red-fluorescent plastic can increase plant growth despite a lower PPFD is not understood, but we postulated it can be attributed to a lower blue-light environment that increases leaf expansion and thus, photon capture. To test this hypothesis, we examined photosynthesis and growth responses of vegetable and ornamental crops under a red-fluorescent plastic, plastics with varying transmission percentages of B light (from 6% to 20%), and an uncovered greenhouse control with a 40% greater PPFD. The red-fluorescent film did not increase extension growth parameters such as stem length, leaf area, or projected canopy area compared to a neutral-density cover with a similar average PPFD. However, extension growth under the film was greater than that of plants grown in the uncovered treatment. Under the red-fluorescent film, the maximum rate of photosynthesis (A_{max}) varied by species and cultivar, and did not consistently equate with differences in biomass accumulation. Except for petunia (*Petunia × hybrida*), shoot dry mass (SDM) was similar under the red-fluorescent film and the uncovered

control treatment despite the PPFD difference. However, under the red-fluorescent cover, tomato and lettuce yield (fruit or shoot fresh mass per area) and flower production of snapdragon (*Antirrhinum majus*) and petunia were less than that under the uncovered control. In sum, increased SDM could not be attributed to A_{max} or greater leaf area as a function of the percentage of B light in the transmission spectrum. Additional research is needed to fully understand how red-fluorescent plastics increase crop growth.

Introduction

Protected agricultural systems such as high tunnels and greenhouses can help mitigate undesirable weather conditions, increase water-use efficiency, extend growing seasons, reduce biotic pressure, and in some cases increase crop yield and quality (Wittwer and Castilla 1995). Transparent polyethylene plastics are the most used materials to protect crops, accounting for the vast majority of the approximately 5.6 million hectares of global protected agriculture production in 2019 (Produce Grower 2019). In addition to the well-understood benefits of protected agriculture, there is potential to manipulate the transmission characteristics of various materials. Light transmission characteristics such as photosynthetic photon flux density (PPFD; 400–700 nm), photon distribution, and directionality are controllable and can independently and sometimes interactively impact crop yield and quality.

There is a growing scientific and industry interest in manipulating light quality and quantity when growing ornamental, medicinal, and food crops under protected cultivation. This interest stems from factors including 1) research with light-emitting diodes has improved our understanding of how the light spectrum regulates crop morphology and biomass accumulation; 2) development of covering materials with improved life spans and modified transmission characteristics, including a diversity of incorporated pigments that photoselectively increase or decrease specific light wavebands; and 3) the opportunity to incorporate transparent photovoltaic materials that selectively absorb some of the incident sunlight into protected agriculture (i.e. agrivoltaics) to co-localize energy and agricultural production (Meng et al. 2020; Stallknecht et al. 2023; Ouzounis et al. 2015; Park and Runkle 2023). However, there are still impediments to large-scale commercial implementation of materials that alter the solar spectrum. First, different types of crops grown in protected agriculture may have unique responses to an altered light environment. Second, protected cultivation occurs in diverse geographical locations with dissimilar weather conditions. Third, manipulating the photon distribution decreases the transmitted PPFD. Finally,

129

these novel materials are still developing technologically and are more expensive than an unpigmented counterpart. Therefore, additional research and development are needed to help overcome these barriers and to facilitate large-scale commercial implementation.

One strategy to manipulate the solar spectrum (i.e., alter the transmitted photon distribution) is to incorporate fluorescent additives into plastics that absorb shorter-wavelength ultraviolet (UV; 280–399 nm), blue (B; 400–499 nm), and/or green (G; 500–599 nm) photons and fluoresce longer-wavelength red (R; 600–699 nm) and far-red (FR; 700–799 nm) photons. Various fluorescent materials have increased the biomass accumulation of herbaceous crops such as lettuce (*Lactuca sativa*) and cabbage (*Brassica rapa* ssp. *pekinensis*), a fruiting crop in tomato (*Solanum lycopersicum*), and the woody species Japanese larch (*Larix kaempferi*) (Kang et al. 2023; Parrish et al. 2021; Shen et al. 2021; Shoji et al. 2022; Novoplansky et al 1990). It is often hypothesized these "spectral shifting" materials can increase crop growth by better matching the absorption spectra of isolated and purified chlorophyll (*Chl*) *a* and *b*, or by increasing the flux of R photons that have a higher average quantum yield (mol CO_2 fixed per mol photon) than UV, B, and G photons (Inada 1976; McCree 1971). However, these hypotheses have limitations including 1) plants contain accessory pigments (e.g., carotenoids) that increase light absorption that ultimately contribute to photosynthesis; 2) G photons may be less photosynthetically efficient but can penetrate deeper in individual leaves and plant canopies; 3) quantum efficiency data as a function of wavelength were generated at low PPFDs; and 4) a decrease in B light transmission can alter plant architecture and consequently photon interception and whole-plant photosynthesis (Fageria et al. 2006; Hogewoning et al. 2012; Snowden et al. 2016; Wang and Folta 2013). Currently, few mechanistic studies exist that tested these different hypotheses.

Experiments performed with red-fluorescent films have shown greater extension growth (e.g., increased leaf area or stem length) of crops such as lettuce, cabbage, Welsh onion (*Allium fistulosum*), and cucumber (*Cucumis sativus*) compared to those grown under a neutral-density material (Kang et al. 2023; Minich et al. 2011; Nishimura et al. 2012; Rodríguez et al. 2002; Shen et al. 2021; Stallknecht and Runkle unpublished). However, this response is not consistent; in other studies, the morphology of lettuce, strawberry (*Fragaria* × *ananassa*), and radish (*Raphanus raphanistrum*) were unaffected by red-fluorescent materials (Hemming et al. 2006; Hidaka et al. 2008; Kang et al. 2023). Plants utilize photoreceptors with distinct absorption spectra to perceive the surrounding light environment and mediate photomorphogenesis (Franklin 2008; Ouzounis et

al. 2015). Phytochrome and cryptochrome are photoreceptors that primarily absorb the UV/B and R/FR wavebands, respectively, and can independently or interactively influence plant morphology (Duanmu et al. 2014; Lin and Shalitin 2003). Typically, decreasing the R:FR or the fraction of B photons in a light spectrum increases shade-avoidance or acclimation responses (Franklin 2008; Ouzounis et al. 2015). Red-fluorescent materials typically increase the fraction of R photons more than FR photons, thereby increasing the R:FR and phytochrome photoequilibrium (PPE), which in theory would inhibit extension growth mediated through phytochrome. However, plants grown under red-fluorescent materials often exhibit an increase in extension growth. Thus, Stallknecht and Runkle (unpublished) hypothesized that the primary cause of increased extension growth for some crops under red-fluorescent materials was from a decreased fraction of B photons and was mediated through cryptochromes.

Plant morphology plays an important role in determining the biomass accumulation of individual plants and entire crops (Fageria et al. 2006). Increased extension growth (i.e., increased leaf area and/or internode elongation) can increase biomass accumulation by increasing photon interception, independent of quantum efficiency (Hernández and Kubota 2016; Meng et al. 2020). Stallknecht and Runkle (unpublished) observed a similar trend: there was a positive correlation between increases in lettuce leaf area and shoot fresh mass. Despite the greater lettuce yield, it is unclear if fruiting crops and/or floriculture crops exhibit greater growth and yield under red-fluorescent materials. Moreover, it is also unclear whether a photoselective material that absorbed B photons could have similar effects on crop biomass accumulation and quality compared to a red-fluorescent material.

Researchers have hypothesized that increasing the fraction of R photons in a spectrum from red-fluorescent plastics increases photosynthetic efficiency (i.e., quantum yield), but supporting data are not consistent among crops. The quantum yield of cabbage, sweet pepper (*Capsicum annuum*), and strawberry increased under a red-fluorescent film, but not in basil (*Ocimum basilicum*), tomato and cucumber (Loik et al. 2017; Yoon et al. 2020). Here, we determined how sunlight with decreased percentages of B light regulated plant morphology and area-based net photosynthetic rate for a diverse range of greenhouse crops. We hypothesized decreasing the B light fraction would increase extension growth and biomass accumulation of the leafy green lettuce, the fruiting crop tomato, and the floriculture crops petunia (*Petunia* × *hybrida*) and snapdragon (*Antirrhinum majus*). Additionally, we postulated that the single-leaf photosynthetic

rate (on a leaf area basis) would be independent of the percentage of B light in the modified solar spectrum treatments.

Materials and methods

Seedling growth culture. All seedlings were placed inside a controlled growth room with a 22 °C air temperature, 60% relative humidity, and ambient CO_2 concentration. Sole-source lighting was provided by white, blue, and red light-emitting diodes (RAY 44 Physiospec Indoor; Fluence Bioengineering, Austin, TX). Seedlings were covered with a transparent humidity dome for 4 d until radical emergence. We provided irrigation as needed with deionized water and hydroponic water-soluble fertilizer (12–4–16 RO Hydro FeED; JR Peters, Inc, Allentown, PA), and magnesium sulfate (Epsom salt, Pennington Seed Inc., Madison GA) that provided the following nutrients (in $mg \cdot L^{-1}$): 125 N, 42 P, 167 K, 73 Ca, 49 Mg, 39 S, 1.7 Fe, 0.52 Mn, 0.56 Zn, 0.13 B, 0.47 Cu, and 0.13 Mo. The irrigation solution pH and electrical conductivity (EC) were measured with a handheld meter (HI9814; Hanna Instruments, Woonsocket, RI) and adjusted to a pH of 5.8 and EC of 1.2 mS cm^{-1}. Seeds of red-leaf 'Rouxai' (Rijk Zwaan; Salinas, CA, USA) and green-leaf 'Butter Crunch' lettuce (Johnny's Selected Seeds, Winslow, ME) were sown into 200-cell rock wool sheets (AO 25/40 Starter Plugs; Gordan, Milton, ON, Canada) on 5 Apr 2022 and grew under an 18-h photoperiod at a PPFD of 200 $\mu mol \cdot m^{-2} \cdot s^{-1}$ (DLI = 13.0 $mol \cdot m^{-2} \cdot d^{-1}$) until transplant on 19 Apr 2022 (14 d). Dwarf cherry tomato 'Red Robin' seeds (Park Seed Co., Hodges, SC) were sown into 128-cell trays filled with a peat-based soilless substrate (Suremix; Michigan Grower Products, Inc., Galesburg, MI) on 21 Apr 2022 and grown under an 18-h photoperiod at a PPFD of 250 $\mu mol \cdot m^{-2} \cdot s^{-1}$ (DLI = 16.2 $mol \cdot m^{-2} \cdot d^{-1}$) until transplant on 13 May 2022 (22 d). Petunia 'Madness Pink' and snapdragon 'Snapshot Yellow' seeds (PanAmerican Seed Co., West Chicago, IL) were sown into 288-cell trays filled with a mixture of 50% peat-based soilless substrate and 50% vermiculite on 21 Aug 2022 and grown under a 9-h photoperiod at a PPFD of 200 $\mu mol \cdot m^{-2} \cdot s^{-1}$ (DLI = 6.5 $mol \cdot m^{-2} \cdot d^{-1}$) until transplant on 19 Sep 2022 (30 d).

Chamber design. We constructed four chambers and placed them on aluminum benches inside a glass-glazed research greenhouse at Michigan State University (East Lansing, MI, lat. 43 °N; Fig. V-1A). Each chamber frame was constructed with polyvinyl chloride pipe and provided 2.4 m^2 of growing space with a volume of 2.5 m^3 (Fig. V-2). Each chamber had one 6 m^3 min^{-1} fan (Axial 1751; AC Infinity Inc., City of Industry, CA) installed on the south-facing wall that was

in-line with greenhouse exhaust fans to maintain a similar internal air temperature among chambers.

Treatment transmission. Each chamber was covered with a common neutral-density polyethylene greenhouse plastic (Standard clear 6mil film; Greenhouse Mega Store, Danville, IL), an experimental red-fluorescent film (Shen et al. 2021), or a photoselective film that transmitted 6 or 11% of the photons between 400 and 499 nm (Calcolor 90 Yellow and Cinelux Daffodil; Rosco Laboratories Inc., Stamford, CT). The 6% and 11% B treatments are referred to as "very low blue" and "low blue" henceforth. Varying layers of 11% and 40% neutral-density shading materials (ProtekNet; Johnny's Selected Seeds and Harmony 2047 FR; Ludvig Svensson Inc., Charlotte, NC) were used to cover the chambers so that the PPFD was similar among the four covered treatments. In addition to the four chambers, a greenhouse bench with no chamber or covering material was used as a greenhouse control treatment. We used a spectroradiometer (LI-180 Spectrometer; LI-COR, Inc., Lincoln, NE) to measure treatment transmission spectra on a cloudless day at solar noon (n=10). The photon distribution for each treatment is depicted in Fig. V-1B and Table V-1.

Greenhouse environment and sensing. The research greenhouse was controlled by an environmental control system (Integro 725; Priva, De Lier, the Netherlands) with a constant setpoint of 21 °C and ambient CO_2 concentration. Steam heat, evaporative cooling pads, exhaust fans, and roof vents regulated the greenhouse air temperature. Each greenhouse bench (i.e., an experimental unit) contained one aspirated and shielded thermocouple (Type E; Omega Engineering, Inc., Stamford, CT) and one quantum sensor (LI-190SA; LI-COR, Inc.) maintained at canopy height for the duration of the experiment. Air temperature and instantaneous PPFD were measured every minute with a data logger (CR-1000; Campbell Scientific) and hourly averages were recorded. Average weekly air temperature and daily light integral (DLI; $mol \cdot m^{-2} \cdot d^{-1}$) data are displayed in Fig. V-3A–F and Table V-2. Average weekly air temperature differences among greenhouse benches were <0.5 °C (Fig. V-3A–C). Average DLI values among the four covered treatments were within 0.5 $mol \cdot m^{-2} \cdot d^{-1}$ but the average DLI for the uncovered greenhouse control treatment was 7–12 $mol \cdot m^{-2} \cdot d^{-1}$ greater than the covered treatments (Fig. V-3D–E).

Mature growth culture. Lettuce and tomato seedlings were transplanted into 1800 cm^3 plastic pots filled with a peat-based soilless substrate, and floriculture seedlings were transplanted into 1000 cm^3 plastic pots with the same media. Pots containing lettuce, tomato, and floriculture crops

were placed inside the greenhouse chambers at a density of 22, 12, and 25 plants per m^2, respectively. Plants were irrigated as needed with a solution of reverse osmosis water mixed with a 13N–1.3P–12.5K water-soluble fertilizer that contained (in mg·L^{-1}) 125 N, 13 P, 120 K, 77 Ca, 19 Mg, 1.7 Fe, 0.4 Cu, and Zn, 0.8 Mn, 0.2 B and Mo (MSU Orchid RO Water Special; GreenCare Fertilizers, Inc., Kankakee, IL). The lettuce and tomato received no supplemental lighting. However, floriculture crops received supplemental lighting at an average PPFD of 110 µmol·m^{-2}·s^{-1} at bench height for 16 h·d^{-1} from luminaires (ILM-PG-180-2-300W-ED-FS-60; Rofianda Trading B.V., Netherlands) containing broad-band (white) LEDs with a similar PAR spectrum to sunlight (SunLike LED STW9C2SB-S; Seoul Semiconductor, Gyeonggi-do, South Korea). The LED spectrum consisted of 24% B, 36% G, 34% R, and 6% FR light. The supplemental lighting was controlled with the same environmental control system that managed air temperature inside the greenhouse and operated from 0500 to 2100 h.

Data collection. Lettuce, tomato, and floriculture crops grew until destructive measurements were taken on 10 May, 29 Jul, and 28 Oct 2022 (21, 75, and 40 d in the treatments), respectively. Leaf length and width, chlorophyll concentration (n=3), and CIELAB color space (n=3) were measured on a fully expanded and representative leaf from each plant with a ruler, chlorophyll meter (MC-100; Apogee Instruments, Inc., Logan, UT), and colorimeter (BC-10 Plus; Konica Minolta Sensing), respectively. Specific leaf area (SLA) was calculated by dividing the area of a representative leaf [measured with a leaf area meter (LI-3000C; LI-COR, Inc.)] by its dry mass. The projected canopy area (PCA) was measured with top-down photos and ImageJ software (National Institute of Health 2023). Stem length was measured as the distance from the substrate surface to the apical meristem. Stem diameter was measured with digital calipers (41101 DigiMax; Wiha Switzerland, Monticello, MN, USA) at the substrate surface. Shoot fresh mass (SFM) and shoot dry mass (SDM) per plant were measured for all stems and leaves on a digital scale (GR-200 or GX-1000; A&D Store, Inc., Wood Dale, IL). SDM was measured after drying shoots for 4 d at 60 °C in a dedicated drying oven (Blue M, Blue Island, IL or SMO28-2; Sheldon Manufacturing, Inc., Cornelius, OR). Radiation use efficiency (RUE) was calculated by dividing SDM by the total mol of PAR for each sample. For tomato, ripe and unripe fruit were counted at a single destructive measurement. A tomato fruit was considered ripe when at or past the turning stage (Skolik et al. 2019). Fruit fresh mass (FFM) was measured on all ripe and unripe tomato fruits. For petunia and snapdragon, the time to flower was calculated as the number of days from

transplant to the first fully open flower. Additionally, at the time of harvest, we counted the total number of visible flowers and flower buds and the number of branches > 3 cm long.

Instantaneous photosynthesis. Measurements were made with a portable photosynthesis system (LI-6800; LI-COR, Inc.) using the fluorometer head attachment for each greenhouse crop in each treatment (n=3) to generate light response curves. Measurements were taken on mature, fully-expanded leaves at the top of the canopy ± 3 h from solar noon. The environmental conditions inside the chamber were set at 10,000 rpm fan speed, 500 µmol·s^{-1} air flow rate setpoint (0.85 L·min^{-1}), 50% relative humidity, 400 ppm CO_2 concentration, and 25 °C leaf temperature. Light response curves were generated using light-adapted leaves with descending PPFDs of 1800, 1500, 1200, 900, 600, 300, 150, 50, and 0 µmol·m^{-2}·s^{-1}. The light was provided by the fluorometer head and consisted of 20% B and 80% R photons. Light response data were analyzed in R software (Version 4.2.2, The R Foundation, Vienna, Austria; https://cran.r-project.org) using a non-rectangular hyperbola expressed as:

$$P_N(I) = \frac{\alpha I + P_{NMAX} - \sqrt{(\alpha I + P_{NMAX})^2 - 4\theta I P_{NMAX}}}{2\theta} - R_D$$

where *Pn* (µmol·m^{-2}·s^{-1}) is net photosynthetic rate, α (µmol·µmol^{-1}) is the quantum yield of assimilation, *I* is the PPFD (µmol·m^{-2}·s^{-1}), θ is the convexity of the light response curve, P_{NMAX} (µmol·m^{-2}·s^{-1}) is the maximum rate of photosynthesis, and R_D (µmol·m^{-2}·s^{-1}) is the dark respiration rate according to Marshall and Biscoe (1980).

Stomatal conductance and quantum yield measurements. Leaf temperature, stomatal conductance (g_{sw}), and quantum yield of photosystem II (PhiPSII) survey measurements were taken with a portable fluorometer and porometer (LI-600; LI-COR, Inc.). Survey measurements were taken at solar noon on a cloudless day for each greenhouse crop on light-acclimated leaves near the top of the canopy (n=20). Survey measurements on lettuce, tomato, and floriculture crops were taken on 10 May, 26 Jul, and 24 Oct 2022, respectively.

Experimental design and statistical analysis. The experiment was organized as a completely randomized design where each greenhouse bench was an experimental unit that was randomly assigned the treatment and plants. The lettuce, tomato, and floriculture crop sample size was 20, 24, and 25 plants, respectively. Data were analyzed in R software using analysis of variance and Tukey's honestly significant difference test at $\alpha = 0.05$. Additionally, regression analysis was conducted on plants from the neutral-density and two blue-selective cover treatments as a function

of percentage of B light. The greenhouse control treatment was omitted from regression analysis because the average DLI was ~40% greater than the covered treatments. Additionally, the red-fluorescent treatment was omitted because the transmission of G photons also decreased, which could have interactive effects on crop morphology and biomass accumulation.

Results

Morphology

Lettuce. Fig. V-4 displays representative plants cultivated under four different shading materials with percentages of B photons ranging from 6% to 20% and an uncovered greenhouse control with a 40% higher average DLI. Fig. V-5 depicts important morphological metrics for each crop as a function of the percentage of B photons in the transmission spectrum. The average values and statistical tests for all growth metrics and crops are displayed in Tables V-3–7 and regression analysis in Tables 8–12. The single-leaf area of lettuce decreased linearly as the percentage of B photons decreased from 6% to 20% for red-leaf lettuce 'Rouxai' but not for green-leaf lettuce 'Butter Crunch' (Fig. V-4A). 'Butter Crunch' leaves in the neutral-density treatment had 31% greater area than plants under the uncovered greenhouse control. The projected canopy area (PCA) was between 34–40% and 32–42% smaller in the greenhouse control for 'Rouxai' and 'Butter Crunch' compared to the covered treatments, respectively (Figs. V-4, V-5B). Among the covered treatments, B photon percentage had no effect on the PCA of either lettuce cultivar.

Tomato. Dwarf cherry tomato leaf area and stem length were similar under all covered treatments (Fig. V-5C–D; Fig. V-6). Regardless of the covered treatment, tomato leaves had approximately 20% less surface area and plants were 22% shorter compared to plants under the uncovered control.

Floriculture crops. In general, plants under the covered treatments exhibited greater stem elongation compared to the uncovered control plants, but some species were more responsive to the percentage of B photons. All the covered treatments increased petunia leaf area, but there was no effect on snapdragon leaf area (Fig. V-5E). At the average DLI of 12.7 mol·m^{-2}·d^{-1}, snapdragon leaf area increased by 15% as the percentage of B photons decreased from 20% to 6%, but not in petunia. Unique to petunia, leaf area under the red-fluorescent film was less than plants under the other covered treatments. Among the covered treatments, snapdragon and petunia stem length increased linearly as the percentage of transmitted B photons decreased (Fig. V-5F).

Instantaneous photosynthesis and quantum yield

Fig. V-7 illustrates light response curves developed from sun-acclimated leaves of each crop and each lighting treatment. The average maximum rate of photosynthesis (A_{max}) of lettuce 'Butter Crunch', petunia, and snapdragon under the uncovered treatment was noticeably higher than that under the covered treatments (Fig. V-7B, D, E; Table V-13). Conversely, the A_{max} of lettuce 'Rouxai' and tomato was similar to plants under the covered treatments (Fig. V-7A, C). Among the covered treatments, the relationship between A_{max} and the percentage of B photons in a treatment varied. Lettuce showed a quadratic trend, while tomato showed a linear trend (see Fig. V-8; Table V-13). Generally, A_{max} was lowest in plants grown under the very low blue treatment.

PhiPSII tended to be lower under the uncovered treatment compared to the covered ones. Among the covered treatments, PhiPSII was similar under the neutral-density and red-fluorescent treatments for all species, but PhiPSII was generally lowest under the very low blue treatment (Fig. V-9; Table V-14).

Biomass accumulation

Lettuce. Fig. V-10 displays growth metrics for each crop as a function of the percentage of B photons in the transmission spectrum. Lettuce 'Rouxai' and 'Butter Crunch' grown under the red-fluorescent film had 27% and 17% greater SDM than plants under the neutral-density cover with a similar DLI, and a similar SDM as plants under the uncovered control, which received a 40% higher DLI on a per-plant basis (Fig. V-10A). When the fraction of B photons in the transmitted spectrum increased from 6% to 20%, 'Rouxai' SDM decreased by 17% but there was no trend effect with 'Butter Crunch'. Crop yield considers the harvestable biomass per unit growing area (i.e., shoot fresh mass per m^2) and can be a more appropriate metric for agricultural production systems. Lettuce 'Rouxai' yield increased by 12–28% under the red-fluorescent film compared to the neutral-density and photoselective treatments whereas 'Butter Crunch' yield under the red-fluorescent film was similar to plants under the neutral-density and photoselective treatments (Fig. V-10B). Regardless of the covered spectrum, lettuce 'Rouxai' and 'Butter Crunch' yields were lower than that under the uncovered control.

Tomato. The percentage of B photons and average DLI did not impact tomato SDM (Fig. V-10C). All covered treatments produced less FFM than the uncovered control (Fig. V-10D; Fig. V-6). Among the covered treatments, FFM decreased by 18% as the percentage of B photons increased from 6% to 20%.

137

Floriculture crops. Among the covered treatments, petunia SDM increased linearly as the percentage of B photons decreased, but the trend was not significant in snapdragon (Fig. V-10E). Snapdragon flower number at harvest increased linearly as the percentage of B photons in the spectrum increased (Fig. V-10F). Conversely, petunia had the most flowers under the 6% B light treatment and uncovered greenhouse control, and flower number decreased linearly as the percentage of B photons in the spectrum increased.

Discussion

Although red-fluorescent plastics have increased the growth of various crops in some cases, their effects on crop morphology and biomass accumulation can vary within and between species. Additionally, the mechanism by which red-fluorescent materials enhance biomass accumulation in certain plant species is undetermined. Thus, we conducted a comparative study on the morphology, biomass accumulation, and photosynthetic light response of common and economically important greenhouse crops grown under an experimental red-fluorescent plastic, plastics with varying percentages of B photons in their transmission spectra (ranging from 6% to 20%), and an uncovered greenhouse control with ~40% higher average TPFD.

Morphology

Plants in light-limited environments typically exhibit increased extension growth, such as greater leaf area or stem elongation, as a shade-avoidance or acclimation response to maximize light interception (Casal 2012). The magnitude of extension growth exists in a continuum and is correlated to average PPFD/DLI, albeit not always linearly (Stallknecht et al. 2023). Red-fluorescent materials consistently decrease the transmission TPFD because fluorescent pigments do not always emit photons in the intended direction toward crops. The magnitude of the TPFD decrease depends on factors such as the type of pigment used, pigment concentration, photostability of the pigment, and whether light-extracting microstructures are incorporated (Kang et al. 2023; Loik et al. 2017; Shen et al. 2021; Tokarz et al. 2023; Yoon et al. 2020). In the literature, red-fluorescent materials have varied widely and decreased the average PPFD from <5% to 50%. In the present study and other similar research, red-fluorescent materials can increase extension growth, at least of some species and cultivars, which is indicative of shade-avoidance and acclimation responses (Shen et al. 2021, Stallknecht and Runkle unpublished). In part, greater extension growth under red-fluorescent film is explained by simply lowering the average PPFD, independent of altered light quality.

Decreasing the R:FR/PPE can increase plant extension growth (Casal 2012, Park and Runkle 2017; Park and Runkle 2019). The experimental red-fluorescent material increased the flux of R photons more than FR photons and increased the estimated PPE from 0.72 to 0.74. PPE has an inverse linear correlation with extension growth, and increasing the PPE from 0.72 to 0.74, indoors with electric lights, increased the stem length of snapdragon and petunia by an estimated 4% and 14%, respectively (Park and Runkle 2017). As such, less extension growth would be expected from plants grown under a red-fluorescent film if phytochromes were solely mediating changes to crop morphology. However, the morphology of lettuce, tomato, and snapdragon grown under the red-fluorescent film was similar to that of plants under the neutral-density cover. In contrast, petunia leaf area and stem length were attenuated under the red-fluorescent film relative to the other covered treatments.

In addition to phytochromes, crop morphology is regulated through B-light-absorbing cryptochromes. Red-fluorescent materials commonly absorb photons in the B waveband, which could independently decrease the inhibitory effect that B photons have on extension growth (i.e., increase extension growth) (Casal 2012; Meng et al. 2020). Unlike the relatively small changes to PPE, the experimental red-fluorescent film had 30% fewer B photons compared to the neutral-density cover. Decreasing the percentage of B photons in a spectrum has increased the extension growth of lettuce and some floriculture crops in this study and others (Meng et al. 2020; Runkle and Heins 2001). However, this paradigm is not always consistent, and the effects of B photons can be confounded by other wavelengths (e.g., G and/or R light) (Meng et al. 2020). Our results indicate the effects of red-fluorescent shading materials on plant morphology depend on species sensitivity to PPE and the percentage of B photons. However, light quantity, rather than light quality, predominantly influenced crop morphology.

Photosynthetic light response

The incident PPFD on a leaf is one factor that can influence its maximum photosynthetic capacity, and generally increasing the average DLI increases A_{max} (Masabni et al. 2016). In this study, the A_{max} of green-leaf lettuce 'Butter Crunch', petunia, and snapdragon were greatest under the uncovered treatment. However, the A_{max} of red-leaf lettuce 'Rouxai' and tomato under the uncovered treatment was similar to the A_{max} in the neutral-density treatments despite the average DLI being approximately 9 and 12 $mol \cdot m^{-2} \cdot d^{-1}$ greater, respectively (Fig. V-10A, C). Some plant species upregulate the biosynthesis of anthocyanins that mitigate photoinhibition caused by an

excessive flux of high-energy photons, particularly in the UV and B wavebands, and attenuate A_{max} (Gould 2004; Liakopoulos et al. 2006; Tsormpatsidis et al. 2010). Greater anthocyanin accumulation gives leaves a more reddish appearance, and on average, lettuce 'Rouxai' and tomato leaves under the uncovered treatment were 180% and 13% redder than leaves under the uncovered treatments (Fig. V-4). This suggests that the upregulation of anthocyanins caused by a high PPFD attenuated the A_{max} of red-leaf lettuce and tomato. The magnitude of the A_{max} increase was far less in tomato than that of lettuce 'Rouxai' and does not fully explain the observed decrease in A_{max}. The photosynthetic light response was measured on mature tomato leaves, but the A_{max} of tomato leaves decreases over time (Trouwborst et al. 2011). In addition to increased anthocyanin accumulation, the determinate-type tomato leaves under the uncovered treatment may have been older (i.e., closer to senescence) than those under the covered treatments, which could have a contributed to attenuation of A_{max}.

In other studies, A_{max} differed among several species grown under red-fluorescent materials, and this was at least in part caused by differences in transmitted PPFD. For instance, lettuce and tomato A_{max} were significantly lower when grown under a red-fluorescent material that decreased the PPFD by ~30 to 50% compared to a neutral-density treatment (Loik et al. 2017; Tokarz et al. 2023). However, the A_{max} was similar for a different lettuce cultivar or slightly increased for cabbage and sweet pepper when PPFD under the red-fluorescent material decreased by <5% compared to a neutral-density treatment (Kang et al. 2023; Yoon et al. 2020). Kang et al. (2023) reported differences between A_{max} and the electron transport rate of PSII and PSI of cabbage under a red-fluorescent material compared to a neutral-density control, but we did not (data not presented). Accordingly, A_{max} differences among studies could relate more with PPFD differences between red-fluorescent and neutral-density materials than changes to the light spectrum. Thus, it is still unclear how increasing the flux of R and FR photons while decreasing B and G photons affects A_{max} because red-fluorescent materials always decrease the transmitted PPFD. Whether A_{max} increased or decreased because of PPFD did not necessarily correlate with increased biomass accumulation among studies, suggesting that changes in plant morphology influence light interception and consequently biomass accumulation.

Comparing the photosynthetic light response of crops among studies can be challenging because red-fluorescent materials decrease the PPFD, which independently influences A_{max}. Thus, we grew diverse greenhouse crops under a similar PPFD (~40% shade) with varying percentages

of B photons ranging from 6% to 20% for comparison with the red-fluorescent material. Similar to the current study, decreasing the percentage of B photons from approximately 20% to 5–8% decreased the A_{max} of cucumber, lettuce, and rose (*Rosa × hybrida*) by 26%, 30%, and 19%, respectively (Hogewoning et al 2010; Terfa et al. 2013; Wang et al. 2016). This indicates that our tested hypothesis was incorrect, and at a similar average DLI, decreasing the percentage of B photons lowers the A_{max} of a variety of crops. Furthermore, the A_{max} of plants grown under the red-fluorescent material (14% B) was similar to the A_{max} of plants in the 20% and 11% B-light treatments. It is postulated that decreasing the percentage of B photons limits A_{max} in part by decreasing g_{sw} (Hernández and Kubota 2016; Hogewoning et al. 2010; Matthews et al. 2020). However, g_{sw} was not correlated with A_{max} in the current study for the tested species (Fig. V-11). Additional research is warranted to determine if red-fluorescent materials are influencing g_{sw} and consequently photosynthesis.

Single-leaf photosynthesis measurements do not necessarily equate to biomass accumulation. Although A_{max} was typically lowest under the 6% B-light treatment, SFM was equal to or greater than that of plants grown under the neutral-density cover with 20% B photons. Evaluating the instantaneous photosynthetic response of crops under red-fluorescent materials is useful, but there are also changes to plant architecture, such as increased SLA, petiole elongation, or stem elongation, that can influence whole-plant photosynthesis (Sarlikioti et al. 2011). Thus far, the body of literature evaluating red-fluorescent materials has not identified predictable effects on photosynthesis. Additional studies utilizing whole-plant gas exchange systems are merited to determine how altered plant architecture caused by red-fluorescent materials interacts with single-leaf photosynthesis.

Biomass accumulation

As a general paradigm, a 1% decrease in the PAR received by a plant leads to a 0.75–1% decrease in biomass accumulation (Marcelis et al. 2005). Based on this paradigm, lettuce varieties 'Rouxai' and 'Butter Crunch' would have approximately 40% less SDM when grown under neutral-density treatment compared to the uncovered control. However, the actual decrease in biomass for 'Rouxai' and 'Butter Crunch' was only 19% and 11%, respectively. The relationship between biomass accumulation and average DLI is not entirely linear. As DLI increases, the response in biomass accumulation can reach a saturation point, where further increases in DLI result in diminishing returns, and this is species-dependent. In mature lettuce plants, the saturation DLI is

approximately 15 mol·m^{-2}·d^{-1} (Albright et al. 2000). Our results indicate materials that alter the solar spectrum have the potential to alter the morphology of lettuce without negatively influencing biomass accumulation on a per-plant basis if the average DLI is ≥12 mol·m^{-2}·d^{-1}. As a consequence, a red-fluorescent film that provided roughly 40% shade has the potential to enhance lettuce cultivation in greenhouses when ambient solar radiation is not a limiting factor, while also potentially providing benefits such as modulating greenhouse air temperatures and decreasing evapotranspiration rates.

Contrary to lettuce, fruiting crops such as tomato can utilize a much higher average DLI (e.g., >25–30 mol·m^{-2}·d^{-1}) because they grow more vegetative mass and have fruits acting as sinks for excess photosynthates (Dorais 2003). In Michigan, the average DLI inside a greenhouse in July averages 25–32 mol·m^{-2}·d^{-1} assuming 70% greenhouse transmission (Faust and Logan 2018; Von Elsner et al. 2000). As expected, tomato FFM decreased by 36% as the DLI decreased from approximately 29 to 16 mol·m^{-2}·d^{-1}, which generally follows the PAR-biomass paradigm. Tomato grown under the red-fluorescent material did produce more FFM than under the neutral-density treatment, but this did not fully compensate for the decrease in the average DLI. To mitigate fruiting crop yield losses due to a lower average DLI, a red-fluorescent film may need to be 1) employed in areas with high solar irradiance year-round, such as the Middle East or American Southwest, where the average DLI inside a greenhouse can range from 35–45 mol·m^{-2}·d^{-1} in July; 2) used seasonally when the ambient DLI is high (e.g.,from late spring to early fall); or 3) used seasonally as a retractable shade screen integrated into greenhouse environmental control systems.

Floriculture crops are usually judged on quality metrics such as compactness, branching, and floriferousness rather than biomass accumulation. Like lettuce, snapdragon grown under the red-fluorescent film had a similar SDM as under the uncovered control, but plants were less compact (i.e., increased stem length and PCA) and had fewer flowers. Similar to tomato, petunia grown under a red-fluorescent material had a similar SDM to plants grown under an uncovered control. However, shading generally caused petunia to be less compact, have fewer flowers, and have a 3-d flowering delay. Thus, red-fluorescent film may cause unwanted extension growth and negatively influence flowering metrics of floriculture crops, which could limit the applicability of these materials during light-limiting conditions. This limitation is consistent with previous experiments that utilized materials that absorb FR light to produce more compact potted plants;

despite inhibiting extension growth, FR-absorbing films decreased SDM and in some cases, delayed flowering (Cerny et al. 2003; Demotes-Mainard et al. 2016; Runkle and Heins 2001).

Conclusions

An experimental red-fluorescent material can have varying effects on the morphology, photosynthetic light response, and biomass accumulation of various greenhouse crops. Our experiments indicate that 1) the red-fluorescent film did not increase extension growth more than a neutral-density cover, but did increase extension growth (e.g., increased stem length, leaf area, and/or PCA) compared to plants grown in an uncovered treatment; and 2) the manner in which a red-fluorescent film influenced A_{max} was species- and cultivar-specific, and differences in A_{max} did not always correspond with biomass accumulation. Results of this research do not fully explain the mechanism(s) by which a red-fluorescent film can increase the yield of some crops and not others, but does illustrate the complex interactions between the transmitted spectrum and photon flux density, plant morphology, photosynthetic light response, and biomass accumulation. They also highlight some of the obstacles of utilizing a red-fluorescent film in greenhouse environments considering the broad diversity of crops grown inside, as well as potential benefits for crops such as leafy greens. Further research is needed to understand how modification of the solar spectrum influences stomatal conductance, electron transport, and whole-plant photosynthesis, and to generate fluorescent pigment dose-response curves for different crops to advance the development and application of this technology.

LITERATURE CITED

Albright LD, Both AJ, Chiu AJ. 2000. Controlling greenhouse light to a consistent daily integral. Transactions of the ASAE. 43:421. https://doi.org/10.13031/2013.2721.

Casal JJ. 2012. Shade avoidance. The Arabidopsis book. 10: e0157. ttps://doi.org/10.1199/tab.0157.

Cerny TA, Faust JE, Layne DR, Rajapakse NC. 2003. Influence of photoselective films and growing season on stem growth and flowering of six plant species. J Am Soc Hortic Sci. 128:486–491. https://doi.org/10.21273/jashs.128.4.0486.

Demotes-Mainard S, Péron T, Corot A, Bertheloot J, Le Gourrierec J, Pelleschi-Travier S, Crespel L, Morel P, Huché-Thélier L, Boumaza R, Vian A. 2016. Plant responses to red and far-red lights, applications in horticulture. Environ Exp Bot. 121:4–21. https://doi.org/10.1016/j.envexpbot.2015.05.010.

Dorais M. 2003. The use of supplemental lighting for vegetable crop production: Light intensity, crop response, nutrition, crop management, cultural practices. Canadian Greenhouse Conference. 9.

Duanmu D, Bachy C, Sudek S, Wong CH, Jiménez V, Rockwell NC, Martin SS, Ngan CY, Reistetter EN, Van Baren MJ, Price DC. 2014. Marine algae and land plants share conserved phytochrome signaling systems. Proc Nat Acad Sci. 111:15827–15832.

Fageria NK, Baligar VC, Clark R. 2006. Physiology of crop production. Hawthorn Press Inc., Binghampton, NY. https://doi.org/10.1201/9781482277807-5.

Faust JE, Logan J. 2018. Daily light integral: A research review and high-resolution maps of the United States. HortScience. 53:1250–1257. https://doi.org/10.21273/hortsci13144-18.

Franklin KA. 2008. Shade avoidance. New Phytol. 179:930–944. https://doi.org/10.1111/j.1469-8137.2008.02507.x. https://doi.org/10.1111/j.1469-8137.2008.02507.x.

Gould KS. 2004. Nature's Swiss army knife: the diverse protective roles of anthocyanins in leaves. J Biomed Biotech. 2004:314. https://doi.org/10.1155/s1110724304406147.

Hogewoning SW, Trouwborst G, Maljaars H, Poorter H, van Ieperen W, Harbinson, J. 2010. Blue light dose–responses of leaf photosynthesis, morphology, and chemical composition of Cucumis sativus grown under different combinations of red and blue light. J Exp Bot. 61:3107–3117.

Hogewoning SW, Wientjes E, Douwstra P, Trouwborst G, van Ieperen W, Croce R, Harbinson J. 2012. Photosynthetic quantum yield dynamics: From photosystems to leaves. Plant Cell. 24: 1921–1935.

Inada K. 1976. Action spectra for photosynthesis in higher plants. Plant Cell Physiol. 17:355–365.

Kang JH, Kim D, Yoon HI, Son JE. 2023. Growth, morphology, and photosynthetic activity of Chinese cabbage and lettuce grown under polyethylene and spectrum conversion films. Hortic. Environ Biotech. 1:11. https://doi.org/10.1007/s13580-022-00502-x.

Kusuma P, Bugbee B. 2021. Improving the predictive value of phytochrome photoequilibrium: Consideration of spectral distortion within a leaf. Front Plant Sci. 12:596943. https://doi.org/10.3389/fpls.2021.596943.

Liakopoulos G, Nikolopoulos D, Klouvatou A, Vekkos KA, Manetas Y, Karabourniotis G. 2006. The photoprotective role of epidermal anthocyanins and surface pubescence in young leaves of grapevine (Vitis vinifera). Ann Bot. 98:257–265. https://doi.org/10.1093/aob/mcl097.

Lin C, Shalitin D. 2003. Cryptochrome structure and signal transduction. Ann Rev Plant Bio. 54:469–496. https://doi.org/10.1146/annurev.arplant.54.110901.160901.

Loik ME, Carter SA, Alers G, Wade CE, Shugar D, Corrado C, Jokerst D, Kitayama C. 2017. Wavelength-selective solar photovoltaic systems: Powering greenhouses for plant growth at the food-energy-water nexus. Earth's Future 5:1044–1053. https://doi.org/10.1002/2016ef000531.

Marcelis LFM, Broekhuijsen AGM, Meinen E, Nijs EMFM, Raaphorst MGM. 2005. Quantification of the growth response to light quantity of greenhouse grown crops. Acta Hortic. 711:97–104. https://doi.org/10.17660/actahortic.2006.711.9.

Marshall B, Biscoe PV. 1980. A model for C3 leaves describing the dependence of net photosynthesis on irradiance. J Exp Bot. 31:29–39. https://doi.org/10.1093/jxb/31.1.29.

Masabni J, Sun Y, Niu G, Del Valle P. 2016. Shade effect on growth and productivity of tomato and chili pepper. HortTechnology. 26:344–350. ttps://doi.org/10.21273/horttech.26.3.344.

Matthews JS, Vialet-Chabrand S, Lawson T. 2020. Role of blue and red light in stomatal dynamic behaviour. J Exp Bot. 71:2253–2269. https://doi.org/10.1093/jxb/erz563.

McCree KJ. 1971. The action spectrum, absorptance and quantum yield of photosynthesis in crop plants. Agr Meteorol. 9:191–216. https://doi.org/10.1016/0002-1571(71)90022-7.

Meng Q, Boldt J, Runkle ES. 2020. Blue radiation interacts with green radiation to influence growth and predominantly controls quality attributes of lettuce. J Amer Soc Hortic Sci. 145:75–87. https://doi.org/10.21273/jashs04759-19.

Nishimura Y, Wada E, Fukumoto Y, Aruga H, Shimoi Y. 2012, October. The effect of spectrum conversion covering film on cucumber in soilless culture. Acta Hortic. 956:481-487. 10.17660/ActaHortic.2012.956.56.

Novoplansky A, Sachs T, Cohen D, Bar R, Bodenheimer J, Reisfeld R. 1990. Increasing plant productivity by changing the solar spectrum. Solar Energy Mats. 21:17–23. https://doi.org/10.1016/0165-1633(90)90039-4.

Ouzounis T, Rosenqvist E, Ottosen CO. 2015. Spectral effects of artificial light on plant physiology and secondary metabolism: a review. HortScience. 50(8):1128–1135. https://doi.org/10.21273/hortsci.50.8.1128.

Park Y, Runkle ES. 2017. Far-red radiation promotes growth of seedlings by increasing leaf expansion and whole-plant net assimilation. Environ Exp. Bot. 136:41–49. https://doi.org/10.1016/j.envexpbot.2016.12.013.

Park Y, Runkle ES. 2019. Blue radiation attenuates the effects of the red to far-red ratio on extension growth but not on flowering. Environ Exp Bot. 168:103871. https://doi.org/10.1016/j.envexpbot.2019.103871

Park Y, Runkle ES. 2023. Spectral-conversion film potential for greenhouses: Utility of green-to-red photons conversion and far-red filtration for plant growth. Plos one. 18: e0281996. https://doi.org/10.1371/journal.pone.0281996.

Parrish CH, Hebert D, Jackson A, Ramasamy K, McDaniel H, Giacomelli GA, Bergren MR. 2021. Optimizing spectral quality with quantum dots to enhance crop yield in controlled environments. Comm Bio. 4:124. https://doi.org/10.1101/2020.06.17.157487.

Produce Grower. 2019. Cuesta Roble releases 2019 global greenhouse statistics. 10 Jan. 2020. https://www.producegrower.com/article/cuesta-roble-2019-global-greenhouse-statistics.

R Core Team. 2023. R-4.0.3 for Windows. R Foundation for Statistical Computing, Vienna, Austria. https://cran.r-project.org/bin/windows/base/old/4.0.3/.

Rasband WS. ImageJ, U. S. National Institutes of Health, Bethesda, Maryland, USA, https://imagej.nih.gov/ij/, 1997-2023.

Runkle ES, Heins RD. 2001. Specific functions of red, far red, and blue light in flowering and stem extension of long-day plants. J Am Soc Hortic Sci. 126:275–282. https://doi.org/10.21273/JASHS.126.3.275.

Sager JC, Smith WO, Edwards JL, Cyr KL. 1988. Photosynthetic efficiency and phytochrome photoequilibria determination using spectral data. Trans Am Soc Agric Eng. 31:1882–1889. https://doi.org/10.13031/2013.30952.

Sarlikioti V, de Visser PH, Buck-Sorlin GH, Marcelis LFM. 2011. How plant architecture affects light absorption and photosynthesis in tomato: towards an ideotype for plant architecture using a functional–structural plant model. Ann Bot. 108:1065–1073. https://doi.org/10.1093/aob/mcr221.

Shen L, Lou R, Park Y, Guo Y, Stallknecht EJ, Xiao Y, Rieder D, Yang R, Runkle ES, Yin X. 2021. Increasing greenhouse production by spectral-shifting and unidirectional light-extracting photonics. Nature Food. 2:434–441. https://doi.org/10.1038/s43016-021-00307-8.

Shoji S, Saito H, Jitsuyama Y, Tomita K, Haoyang Q, Sakurai Y, Okazaki Y, Aikawa K, Konishi Y, Sasaki K, Fushimi K. 2022. Plant growth acceleration using a transparent Eu3+-painted UV-to-red conversion film. Sci. Rep. 12:17155. https://doi.org/10.1038/s41598-022-21427-6.

Skolik P, Morais CL, Martin FL, McAinsh MR. 2019. Determination of developmental and ripening stages of whole tomato fruit using portable infrared spectroscopy and Chemometrics. BMC plant Bio. 19:1–15. https://doi.org/10.1186/s12870-019-1852-5

Snowden MC, Cope KR, Bugbee B. 2016. Sensitivity of seven diverse species to blue and green light: interactions with photon flux. PLoS One. 11: e0163121. https://doi.org/10.1371/journal.pone.0163121.

Stallknecht EJ, Herrera CK, Yang C, King I, Sharkey TD, Lunt RR, Runkle ES. 2023. Designing plant–transparent agrivoltaics. Sci Rep. 13:1903. https://doi.org/10.1038/s41598-023-28484-5.

Terfa MT, Solhaug KA, Gislerød HR, Olsen JE, Torre S. 2013. A high proportion of blue light increases the photosynthesis capacity and leaf formation rate of Rosa × hybrida but does not affect time to flower opening. Physiol Plant. 148:146–159. https://doi.org/10.1111/j.1399-3054.2012.01698.x.

Tokarz KM, Makowski W, Tokarz B, Muszyńska E, Gajewski Z, Mazur S, Kunicki E, Jeremiasz O, Sobik P, Nowak P, Miernicka K. 2023. Performance of the photosynthetic apparatus under glass with a luminophore modifying red-to-far-red-light ratio—a case study. Cells. 12:1552. https://doi.org/10.3390/cells12111552.

Trouwborst G, Sander WH, Harbinson J, Wim Van I. 2011. The influence of light intensity and leaf age on the photosynthetic capacity of leaves within a tomato canopy. J Hortic Sci Biotech. 86:403–407. https://doi.org/10.1080/14620316.2011.11512781.

Tsormpatsidis E, Henbest RGC, Battey NH, Hadley P. 2010. The influence of ultraviolet radiation on growth, photosynthesis and phenolic levels of green and red lettuce: potential for exploiting effects of ultraviolet radiation in a production system. Ann App Bio. 156:357–366. https://doi.org/10.1111/j.1744-7348.2010.00393.x.

Von Elsner B, Briassoulis D, Waaijenberg D, Mistriotis A, Von Zabeltitz C, Gratraud J, Russo G, Suay-Cortes R. 2000. Review of structural and functional characteristics of greenhouses in European Union countries: part I, design requirements. J Ag Eng Res. 75:1–16. https://doi.org/10.1006/jaer.1999.0502.

Wang J, Lu W, Tong Y, Yang Q. 2016. Leaf morphology, photosynthetic performance, chlorophyll fluorescence, stomatal development of lettuce (Lactuca sativa L.) exposed to different ratios of red light to blue light. Front Plant Sci. 7:250. https://doi.org/10.3389/fpls.2016.00250.

Wang Y, Folta KM. 2013. Contributions of green light to plant growth and development. Amer J Bot. 100:70–78. https://doi.org/10.3732/ajb.1200354.

Wittwer SH, Castilla N. 1995. Protected cultivation of horticultural crops worldwide. HortTech. 5:6–24. https://doi.org/10.21273/horttech.5.1.6.

Yoon HI, Kang JH, Kang WH, Son JE. 2020. Subtle changes in solar radiation under a green-to-red conversion film affect the photosynthetic performance and chlorophyll fluorescence of sweet pepper. Photosynthetica 58:1107–1115. https://doi.org/10.32615/ps.2020.057

APPENDIX F: TABLES AND FIGURES

Table V-1. The average radiation parameters for each chamber covered with either a neutral density, red fluorescent, or photoselective covering. The average total photon flux density (TPFD; 400–750 nm) was measured at canopy height at solar noon on a cloudless day. Blue (400–499 nm), green (500–599 nm), red (600–699 nm), and far-red (700–750 nm) wavebands are displayed as a percentage of TPFD. The phytochrome photoequilibrium (PPE) and internal phytochrome photoequilibrium (iPPE) were calculated according to McCree (1971) and Sager et al. (1988), and Kusuma and Bugbee (2021), respectively.

Radiation parameter	Chamber covering material				
	No cover (23% blue)	Neutral density (20% blue)	Red fluorescent (14% blue)	Low blue (11% blue)	Very low blue (6% blue)
Transmission (% of TPFD)	100	60	60	60	60
Blue (% of TPFD)	23	20	14	11	6
Green (% of TPFD)	31	30	14	34	35
Red (% of TPFD)	32	33	52	37	39
Far red (% of TPFD)	15	17	21	19	20
Red:Far red	2.16	2.03	2.62	2.05	2.07
PPE	0.72	0.71	0.74	0.72	0.72
iPPE	0.40	0.39	0.42	0.39	0.39

Table V-2. The average air temperature and daily light integral (DLI; 400–700 nm) at canopy height for each treatment and crop type. The leafy greens were lettuce 'Rouxai' and 'Butter Crunch'; tomato was 'Red Robin'; and floriculture crops were petunia 'Madness Pink' and snapdragon 'Snapshot Yellow'. Chamber covering material radiation parameters are displayed in Table V-1.

	Crop	Chamber covering material				
		No cover (23% blue)	Neutral density (20% blue)	Red fluorescent (14% blue)	Low blue (11% blue)	Very low blue (6% blue)
Air temperature (°C)	Leafy greens	22.0	22.7	22.3	22.7	22.0
	Tomato	24.0	23.6	23.9	24.0	23.6
	Floriculture	20.6	20.2	20.5	20.6	20.2
DLI (mol·m^{-2}·d^{-1})	Leafy greens	21.3	12.4	12.5	12.2	12.4
	Tomato	28.5	16.5	16.4	16.2	16.2
	Floriculture	19.5	12.7	12.7	12.8	12.6

149

Table V-3. The growth parameter averages for lettuce 'Rouxai' grown in an uncovered greenhouse control, or one of four chambers that altered the fraction of blue (400–499 nm) photons. The transmission characteristics of each covering material are displayed in Table V-1. Values indicate means (n=20) and different letters within each row are significantly different by Tukey's honestly significant difference test ($P < 0.05$). Chlorophyll concentration (*Chl*), projected canopy area (PCA), specific leaf area (SLA), and radiation use efficiency (RUE) were calculated as previously described.

Growth parameter	Chamber covering material				
	No cover (23% blue)	Neutral density (20% blue)	Red fluorescent (14% blue)	Low blue (11% blue)	Very low blue (6% blue)
Fresh mass (g)	54.8 b	50.8 b	66.6 a	53.5 b	62.6 a
Dry mass (g)	2.46 a	1.99 c	2.52 a	2.13 bc	2.32 ab
Plant height (cm)	9.33 b	12.0 a	11.7 a	11.9 a	11.54 a
Leaf length (cm)	14.01 c	17.5 ab	16.6 b	18.2 a	17.2 ab
Leaf width (cm)	15.6 d	16.1 cd	17.1 bc	17.4 b	18.9 a
Leaf area (cm^2)	170 c	186 bc	197 b	194 b	219 a
Leaf $L*$	29.3 c	38.5 b	39.9 b	39.1 b	44.6 a
Leaf $a*$	1.96 a	−1.68 b	−2.66 b	−1.95 b	−5.46 c
Leaf $b*$	4.94 c	17.4 b	18.7 b	18.8 b	24.9 a
Chl (μmol·m^{-2})	140 a	103 bc	122 ab	93.1 c	82.2c
PCA (cm^2)	245 c	369 b	380 ab	393 ab	408 a
SLA (cm^2·g^{-1})	799 c	985 bc	1185 b	906 c	1604 a
Yield (kg·m^{-2})	2.11 a	1.38 c	1.77 b	1.37 c	1.54 c
RUE (g·mol^{-1})	0.233 b	0.228 b	0.274 a	0.234 b	0.232 b

Table V-4. The growth parameter averages for lettuce 'Butter Crunch' grown in an uncovered greenhouse control, or one of four chambers that altered the fraction of blue (400–499 nm) photons. The transmission characteristics of each covering material are displayed in Table V-1. Values indicate means (n=20) and different letters within each row are significantly different by Tukey's honestly significant difference test (P < 0.05). Chlorophyll concentration (Chl), projected canopy area (PCA), specific leaf area (SLA), and radiation use efficiency (RUE) were calculated as previously described.

Growth parameter	Chamber covering material				
	No cover (23% blue)	Neutral density (20% blue)	Red fluorescent (14% blue)	Low blue (11% blue)	Very low blue (6% blue)
Fresh mass (g)	69.1 b	65.8 b	79.8 a	68.4b	72.0 b
Dry mass (g)	3.05 ab	2.70 c	3.17 a	2.67 c	2.74 bc
Plant height (cm)	10.5 c	16. ab	15.3 b	16.3 ab	17.7 a
Leaf length (cm)	16.3 b	22.6 a	22.3 a	23.3 a	22.5 a
Leaf width (cm)	13.4 b	15.2 a	15.4 a	15.0 a	15.0 a
Leaf area (cm^2)	164 b	207 a	223 a	218 a	212 a
Leaf $L*$	39.3 c	41.7 b	42.3 b	41.9 b	43.5 a
Leaf $a*$	−9.21 a	−9.62 b	−9.38 a	−9.93 c	−9.27 a
Leaf $b*$	18.9 c	20.9 b	20.3 b	22.6a	21.1 b
Chl ($\mu mol \cdot m^{-2}$)	338 a	238 bc	258 b	231 c	225 c
PCA (cm^2)	317 c	478 b	550 a	507 ab	465 b
Yield ($kg \cdot m^{-2}$)	2.19 a	1.40 c	1.47 bc	1.37 c	1.59 b
SLA ($cm^2 \cdot g^{-1}$)	496 c	576 b	583 b	676 a	665 a
RUE ($g \cdot mol^{-1}$)	0.239	0.243	0.249	0.231	0.258

Table V-5. The growth parameter averages for tomato 'Red Robin' grown in an uncovered greenhouse control, or one of four chambers that altered the fraction of blue (400–499 nm) photons. The transmission characteristics of each covering material are displayed in Table V-1. Values indicate means (n=24) and different letters within each row are significantly different by Tukey's honestly significant difference test ($P < 0.05$). Chlorophyll concentration (*Chl*), projected canopy area (PCA), specific leaf area (SLA), and radiation use efficiency (RUE) were calculated as previously described.

Growth parameter	Chamber covering material				
	No cover (23% blue)	Neutral density (20% blue)	Red fluorescent (14% blue)	Low blue (11% blue)	Very low blue (6% blue)
Shoot FM (g)	202 a	200 a	192 a	188 a	197 a
Shoot DM (g)	28.0 a	26.3 a	24.8 a	25.1 a	25.3 a
Fruit FM (g)	715 a	486 c	559 bc	522 bc	573 b
Ripe fruit (no.)	35.7 a	16.4 c	21.2 bc	24.1 b	24.8 b
Unripe fruit (no.)	27.0 a	27.9 a	30.1 a	25.1 a	29.3 a
Stem diameter (mm)	13.5 a	12.6 bc	13.0 ab	11.5 d	12.2 cd
Stem length (cm)	20.3 b	26.1 a	24.9 a	26.6 a	26.7 a
Chl (μmol·m^{-2})	427 a	343 b	332 b	393 a	346 b
Leaf *L**	33.4 b	34.9a	33.2b	32.5 bc	31.6 c
Leaf *a**	−5.95 a	−6.75 b	−6.81 b	−6.56 b	−6.86 b
Leaf *b**	9.54 b	11.4 a	11.2 a	9.83 b	11.5 a
Leaf length (cm)	18.7 b	21.3a	21.0 a	21.2 a	21.5 a
Leaf width (cm)	15.7 b	18.5 a	18.8 a	18.6 a	19.3 a
Leaf area (cm^2)	158 b	203 a	204 a	187 a	198 a

Table V-5 (cont'd)

PCA (cm^2)	413 c	418 bc	450 abc	482 a	470 ab
Yield (kg·m^{-2})	17.5 a	11.8 b	12.5 b	11.1 b	12.4b
SLA (cm^2·g^{-1})	201 d	284 bc	301 ab	269 c	309 a
RUE (g·mol^{-1})	0.659 c	0.838 a	0.808 ab	0.744 bc	0.798 ab

Table V-6. The growth parameter averages for petunia 'Madness Pink' grown in an uncovered greenhouse control, or one of four chambers that altered the fraction of blue (400–499 nm) photons. The transmission characteristics of each covering material are displayed in Table V-1. Values indicate means (n=25) and different letters within each row are significantly different by Tukey's honestly significant difference test ($P < 0.05$). Chlorophyll concentration (*Chl*), projected canopy area (PCA), specific leaf area (SLA), and radiation use efficiency (RUE) were calculated as previously described.

	Chamber covering material				
Growth parameter	No cover (23% blue)	Neutral density (20% blue)	Red fluorescent (14% blue)	Low blue (11% blue)	Very low blue (6% blue)
Shoot FM (g)	67.2 bc	69.8 b	62.9 c	70.3 b	77.5 a
Shoot DM (g)	5.63 a	4.79 c	4.70 c	5.19 b	5.37 ab
Flowers (no.)	54.2 a	42.5 b	43.6 b	43.5b	51.7 a
Days to flower (no.)	28.0 b	31.8 a	30.5a	30.5 a	32.3 a
Leaf length (cm)	5.04 d	6.11 ab	5.57c	5.89 bc	6.35 a
Leaf width (cm)	3.02 c	3.95 a	3.52 b	3.81 ab	4.11 a
Leaf area (cm^2)	25.1 d	37.9 ab	30.9 c	36.0 b	40.5 a
Flower $L*$	38.8 a	38.1 a	38.4 a	38.7 a	38.5 a
Flower $a*$	−7.78a	−8.73b	−8.46 b	−8.33 b	−8.60 b
Flower $b*$	15.2 b	17.7 a	16.5 ab	17.0 a	17.5 a
Chl ($\mu mol \cdot m^{-2}$)	407 a	291 b	318 b	330 b	290 b
Stem length (cm)	13.1 bc	13.9 b	12.4 c	13.5 bc	15.9 a
Branches (no.)	8.76 a	8.28 ab	7.76 b	8.13 ab	7.84 b
PCA (cm^2)	198 d	258 b	234 c	267 b	307 a

Table V-6 (cont'd)

Yield (kg·m^{-2})	3.40 a	2.71 b	2.69 b	2.65 b	2.54 b
SLA (cm^2·g^{-1})	444 c	645 a	580 b	615 ab	647 a
RUE (g·mol^{-1})	0.389 bc	0.390 bc	0.424 a	0.407 ab	0.374 c

Table V-7. The growth parameter averages for snapdragon 'Snapshot Yellow' grown in an uncovered greenhouse control, or one of four chambers that altered the fraction of blue (400–499 nm) photons. The transmission characteristics of each covering material are displayed in Table V-1. Values indicate means (n=25) and different letters within each row are significantly different by Tukey's honestly significant difference test ($P < 0.05$). Chlorophyll concentration (Chl), projected canopy area (PCA), specific leaf area (SLA), and radiation use efficiency (RUE) were calculated as previously described.

	Chamber covering material				
Growth parameter	No cover (23% blue)	Neutral density (20% blue)	Red fluorescent (14% blue)	Low blue (11% blue)	Very low blue (6% blue)
Shoot FM (g)	60.0 ab	56.7 ab	61.1 a	53.3 b	54.7 ab
Shoot DM (g)	8.05 a	6.78b	7.98 a	6.82 b	7.72 ab
Flowers (no.)	76.3 a	58.0 bc	50.2 cd	62.4 b	39.6 d
Days to flower (no.)	31.8 ab	32.5 a	31.0 b	31.0 b	30.9 b
Leaf length (cm)	5.60 ab	5.63 ab	5.50 ab	5.35 b	5.76 a
Leaf width (cm)	1.90 ab	1.81 b	1.87 ab	1.77 b	2.05 a
Leaf area (cm^2)	16.3 c	18.2 bc	18.4 b	16.4 bc	21.0 a
Flower $L*$	39.1 c	42.7 ab	43.0 a	41.6 b	42.9 a
Flower $a*$	−8.72 a	−9.91 bc	−9.61 b	−9.90 bc	−10.1 c
Flower $b*$	12.0 c	13.9 ab	13.71 b	14.4 ab	15.1 a
Chl (μmol·m^{-2})	422 a	364 bc	382 ab	370 bc	331 c
Stem diameter (mm)	5.85 a	5.56 a	5.86 a	5.56 a	5.51 a
Stem length (cm)	23.7 c	26.2 b	28.1 b	27.1 b	33.2 a
Branches (no.)	19.6 a	19.8 a	19.9 a	20.2 a	19.7 a
Yield (kg·m^{-2})	5.29 a	3.84 c	4.55 b	4.07 bc	3.81 c

Table V-7 (cont'd)

PCA (cm^2)	115 b	146 a	135b a	133 ab	145 a
SLA (cm^2·g^{-1})	349 d	499 a	441 c	464 bc	483 ab
RUE (g·mol^{-1})	0.840 d	0.891 cd	1.13 a	0.975 bc	1.02 ab

Table V-8. Growth metrics of lettuce 'Rouxai' as a function of percent blue (400–499 nm) photons in the transmission total photon flux density (400–750 nm). Significance was tested at P < 0.05 using a linear regression model.

	Equation	P	r^2
Fresh mass (g)	$y = -0.0775 * x + 65.2$	<0.001	0.29
Dry mass (g)	$y = 0.0229 * x + 2.43$	<0.001	0.22
Plant height (cm)	-	NS	-
Leaf length (cm)	-	NS	-
Leaf width (cm)	$y = -0.190 * x + 19.8$	<0.001	0.45
Leaf area (cm^2)	$y = -2.14 * x + 226$	<0.001	0.26
Leaf $L*$	$y = 0.0820 * x + 45.6$	<0.001	0.27
Leaf $a*$	$y = 0.242 * x - 6.01$	<0.001	0.37
Leaf $b*$	$y = -0.475 * x + 26.2$	<0.001	0.33
Chl ($\mu mol \cdot m^{-2}$)	$y = 1.41 * x + 75.2$	0.003	0.13
PCA (cm^2)	$y = -2.80 * x + 424$	0.003	0.13
SLA ($cm^2 \cdot g^{-1}$)	$y = 94.3 * \exp(95.4 * 0.420\text{^}x)$	<0.001	0.59
Yield ($kg \cdot m^{-2}$)	$y = -0.00996 * x + 1.55$	0.008	0.11
RUE ($g \cdot mol^{-1}$)	-	NS	-

Table V-9. Growth metrics of lettuce 'Butter Crunch' as a function of percent blue (400–499 nm) photons in the transmission total photon flux density (400–750 nm). Significance was tested at $P < 0.05$ using a linear regression model.

	Equation	P	r^2
Fresh mass (g)	$y = -0.352 * x + 73.4$	0.02	0.09
Dry mass (g)	-	NS	-
Plant height (cm)	-	NS	-
Leaf length (cm)	-	NS	-
Leaf width (cm)	-	NS	-
Leaf area (cm^2)	-	NS	-
Leaf $L*$	$y = -0.120 * x + 43.8$	<0.001	0.19
Leaf $a*$	$y = -0.0170 * x - 9.39$	0.03	0.06
Leaf $b*$	-	NS	-
Chl (μmol·m^{-2})	$y = 1.03 * x + 219$	0.03	0.07
PCA (cm^2)	-	NS	-
SLA (cm^2·g^{-1})	$y = -6.91 * x + 724$	<0.001	0.25
Yield (kg·m^{-2})	$y = -0.0121 * x + 1.60$	0.02	0.01
RUE (g·mol^{-1})	-	NS	-

Table V-10. Growth metrics of tomato 'Red Robin' as a function of percent blue (400–499 nm) photons in the transmission total photon flux density (400–750 nm). Significance was tested at $P < 0.05$ using a linear regression model.

	Equation	P	r^2
Shoot FM (g)	-	NS	-
Shoot DM (g)	-	NS	-
Fruit FM (g)	$y = -5.95 * x + 601$	0.003	0.12
Ripe fruit (no.)	$y = -0.627 * x + 29.4$	<0.001	0.25
Unripe fruit (no.)	-	NS	-
Stem diameter (mm)	-	NS	-
Stem length (cm)	-	NS	-
Chl ($\mu mol \cdot m^{-2}$)	-	NS	-
Leaf L^*	$y = 0.2356 * x + 30.1$	<0.001	0.42
Leaf a^*	-	NS	-
Leaf b^*	-	NS	-
Leaf length (cm)	-	NS	-
Leaf width (cm)	-	NS	-
Leaf area (cm^2)	-	NS	-
PCA (cm^2)	$y = -4.07 * x + 507$	0.01	0.09
Yield (kg$\cdot$m^{-2})	-	NS	-
SLA (cm$^2 \cdot$g^{-1})	$y = -1.40 * x + 305$	0.04	0.06
RUE (g$\cdot$mol^{-1})	-	NS	-

Table V-11. Growth metrics of petunia 'Madness Pink' as a function of percent blue (400–499 nm) photons in the transmission total photon flux density (400–750 nm). Significance was tested at $P < 0.05$ using a linear regression model.

	Equation	P	r^2
Shoot FM (g)	$y = -0.491 * x + 79.6$	0.001	0.14
Shoot DM (g)	$y = -0.424 * x + 5.64$	<0.001	0.24
Flowers (no.)	$y = -0.594 * x + 53.2$	<0.001	0.24
Days to flower (no.)	-	NS	-
Leaf length (cm)	-	NS	-
Leaf width (cm)	-	NS	-
Leaf area (cm^2)	-	NS	-
Flower L*	-	NS	-
Flower a*	-	NS	-
Flower b*	-	NS	-
Chl (μmol·m^{-2})	-	NS	-
Branch length (cm)	$y = -0.164 * x + 22.2$	0.002	0.12
Branches (no.)	-	NS	-
PCA (cm^2)	$y = -3.18 * x + 317$	<0.001	0.28
Yield (kg·m^{-2})	$y = 0.0117 * x + 2.49$	0.01	0.08
SLA (cm^2·g^{-1})	-	NS	-
RUE (g·mol^{-1})	-	NS	-

Table V-12. Growth metrics of snapdragon 'Snapshot Yellow' as a function of percent blue (400–499 nm) photons in the transmission total photon flux density (400–750 nm). Significance was tested at $P < 0.05$ using a linear regression model.

	Equation	P	r^2
Shoot FM (g)	-	NS	-
Shoot DM (g)	$y = -0.0589 * x + 7.83$	0.03	0.07
Flowers (no.)	$y = 1.04 * x + 41.0$	0.05	0.12
Days to flower (no.)	$y = 0.121 * x + 30.0$	<0.001	0.18
Leaf length (cm)	-	NS	-
Leaf width (cm)	$y = -0.0150 * x + 2.05$	0.005	0.11
Leaf area (cm^2)	$y = -0.147 * x + 20.3$	0.04	0.06
Flower $L*$	-	NS	-
Flower $a*$	-	NS	-
Flower $b*$	-	NS	-
Chl (μmol·m^{-2})	$y = 2.01 * x + 331$	0.04	0.06
Stem diameter (mm)		NS	
Stem length (cm)	$y = -0.448 * x + 34.3$	<0.001	0.40
Branches (no.)	-	NS	-
PCA (cm^2)	-	NS	-
Yield (kg·m^{-2})	-	NS	-
SLA (cm^2·g^{-1})	-	NS	-
RUE (g·mol^{-1})	$y = -0.00937 * x + 1.08$	<0.001	0.15

Table V-13. The average initial slope, convexity, maximum rate of photosynthesis (A_{max}), and dark respiration rate of light response curves for each crop according to Marshall and Biscoe (1980). Values represent the average of three measurements.

	Light response curve parameter	Chamber covering material				
		No cover (23% blue)	Neutral density (20% blue)	Red fluorescent (14% blue)	Low blue (11% blue)	Very low blue (6% blue)
Lettuce 'Rouxai'	A_{max} ($\mu mol \cdot m^{-2} \cdot s^{-1}$)	14.3	13.5	15.1	14.9	11.7
	Initial slope	0.0403	0.0423	0.0492	0.0457	0.0421
	Convexity	0.877	0.921	0.962	0.798	0.912
	Dark respiration ($\mu mol \cdot m^{-2} \cdot s^{-1}$)	1.90	1.53	1.97	1.54	1.43
Lettuce 'Butter Crunch'	A_{max} ($\mu mol \cdot m^{-2} \cdot s^{-1}$)	33.3	18.6	19.9	20.4	17.1
	Initial slope	0.0617	0.0534	0.0488	0.0574	0.0542
	Convexity	0.689	0.953	0.838	0.946	0.835
	Dark respiration ($\mu mol \cdot m^{-2} \cdot s^{-1}$)	3.87	2.30	1.93	2.57	2.33
Tomato 'Red Robin'	A_{max} ($\mu mol \cdot m^{-2} \cdot s^{-1}$)	21.3	20.5	19.8	17.9	17.1
	Initial slope	0.0669	0.0628	0.0804	0.0521	0.0584
	Convexity	0.694	0.638	−0.117	0.812	0.806
	Dark respiration ($\mu mol \cdot m^{-2} \cdot s^{-1}$)	3.25	2.35	2.60	1.90	2.16

163

Table V-13 (cont'd)

Petunia 'Madness Pink'	A_{max} ($\mu mol \cdot m^{-2} \cdot s^{-1}$)	26.9	21.2	21.9	20.6	18.4
	Initial slope	0.0565	0.0587	0.0688	0.0542	0.0490
	Convexity	0.850	0.941	0.642	0.962	0.985
	Dark respiration ($\mu mol \cdot m^{-2} \cdot s^{-1}$)	2.47	2.17	2.06	1.48	1.47
Snapdragon 'Snapshot Yellow'	A_{max} ($\mu mol \cdot m^{-2} \cdot s^{-1}$)	39.0	20.8	21.3	21.5	20.0
	Initial slope	0.114	0.0588	0.0678	0.0750	0.0607
	Convexity	−1.76	0.883	0.674	0.0751	0.754
	Dark respiration ($\mu mol \cdot m^{-2} \cdot s^{-1}$)	2.89	1.69	1.72	1.52	1.67

Table V-14. The average leaf temperature, quantum yield of photosystem II (PhiPSII), and stomatal conductance to water (g_{sw}) for each crop grown under different fraction of B photons. Measurements were taken at solar noon on a cloudless day on leaves near the top of the canopy. Values indicate means (n=20) and different letters within each row are significantly different by Tukey's honestly significant difference test (P < 0.05).

		Chamber covering material				
		No cover (23% blue)	Neutral density (20% blue)	Red fluorescent (14% blue)	Low blue (11% blue)	Very low blue (6% blue)
Lettuce 'Rouxai'	Leaf temperature (°C)	30.4 a	28.5 b	27.5 c	29.0 b	28.7 b
	PhiPSII	0.586 bc	0.674 a	0.653 ab	0.681 a	0.568 c
	g_{sw} (mol·m^{-2}·s^{-1})	0.24 ab	0.201 b	0.300 a	0.257 ab	0.210 b
Lettuce 'Butter Crunch'	Leaf temperature (°C)	27.4 a	26.7 a	25.7 b	27.5 a	26.5 ab
	PhiPSII	0.390 c	0.648 a	0.612 ab	0.647 a	0.550 b
	g_{sw} (mol·m^{-2}·s^{-1})	0.293 a	0.228 ab	0.273 a	0.272 a	0.156 b
Tomato 'Red Robin'	Leaf temperature (°C)	29.6 a	27.7 c	28.6 b	28.9 ab	28.9 b
	PhiPSII	0.406 c	0.678 a	0.655 ab	0.655 ab	0.618 b
	g_{sw} (mol·m^{-2}·s^{-1})	0.570 a	0.500 a	0.551 a	0.520 a	0.515 a
Petunia 'Madness Pink'	Leaf temperature (°C)	27.1 a	23.6 cd	23.7 c	23.2 d	25.0 b
	PhiPSII	0.658 b	0.739 a	0.755 a	0.736 a	0.741 a
	g_{sw} (mol·m^{-2}·s^{-1})	0.370 a	0.249 bc	0.307 ab	0.256 bc	0.180 c
Snapdragon 'Snapshot Yellow'	Leaf temperature (°C)	26.4 a	24.3 c	24.0 c	25.0 b	25.0 b
	PhiPSII	0.695 b	0.723 a	0.722 a	0.701 b	0.613 c
	g_{sw} (mol·m^{-2}·s^{-1})	1.389 a	1.135 bc	1.182 b	1.170 b	0.960 c
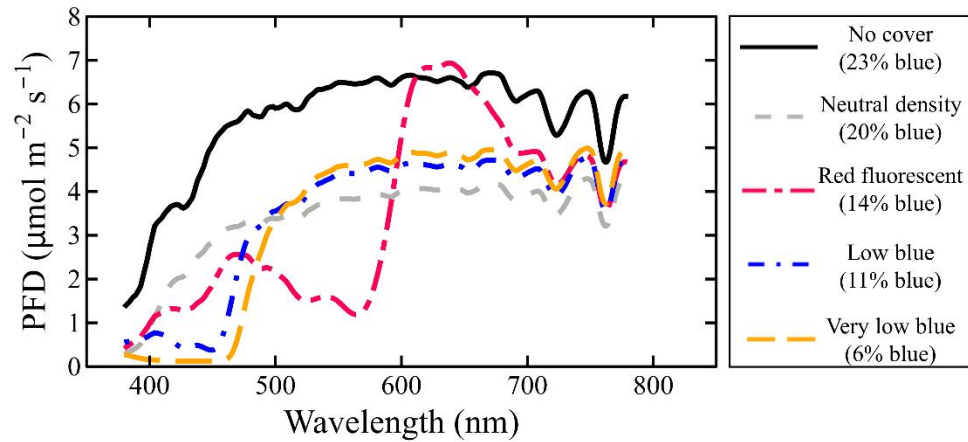
Figure V-1. A) Chambers covered with either a neutral density, red fluorescent, or photoselective covering located in a glass-glazed greenhouse at Michigan State University. B) The photon distribution between 380 and 780 nm of the four covered treatments and one uncovered greenhouse control. The neutral-density cover evenly reduced transmission at each nanometer, the red-fluorescent material absorbed blue (B; 400–499 nm) and green (G; 500–599 nm) photons and fluoresced red (R; 600–699 nm) and to a lesser extent far-red (FR; 700–750 nm) photons, and the photoselective materials absorbed different percentages of B photons. The percent B value indicates the percentage of B photons relative to the total photon flux density (TPFD; 400–750 nm). The spectral characteristics are displayed in Table V-1.
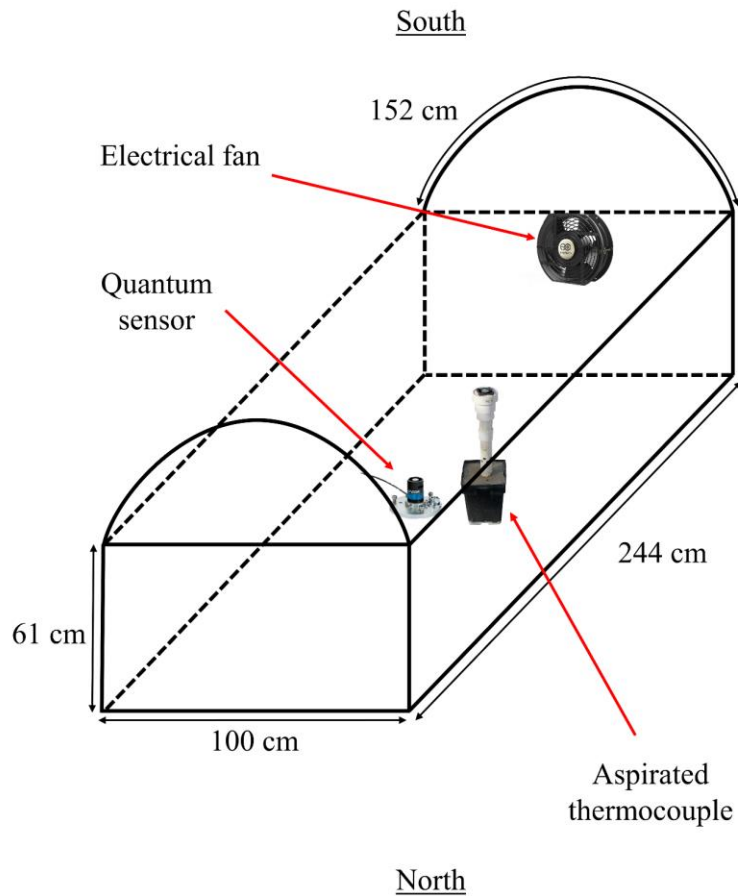
Figure V-2. Schematic for chambers that were covered with either a neutral-density, red-fluorescent, or photoselective materials. The spectral characteristics of each treatment are displayed in Fig. V-1B and Table V-1. Each chamber was oriented north to south. The electric fan had its air flow placed in-line with the greenhouse air flow. Each chamber contained a quantum sensor and aspirated thermocouple that measured the photosynthetic photon flux density (400–700 nm) and air temperature at crop canopy height.
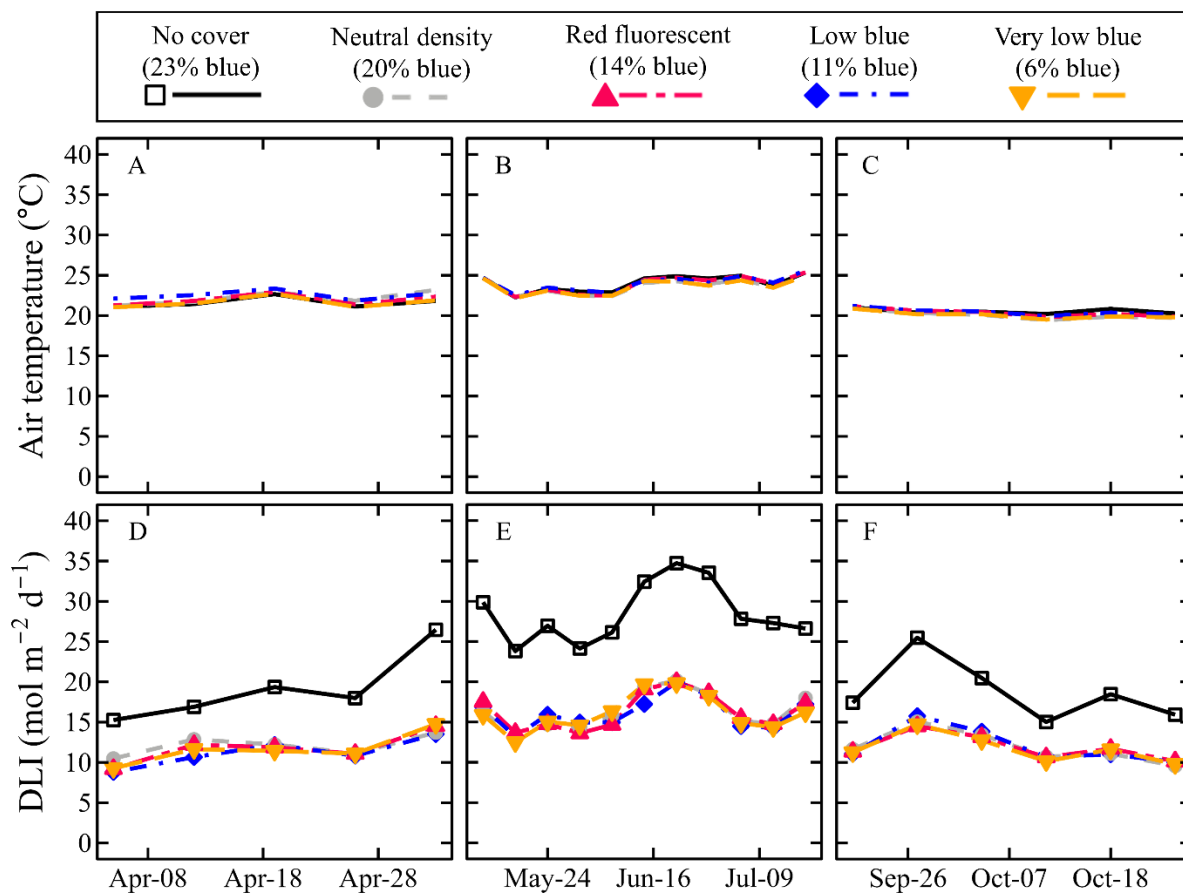
Figure V-3. Average weekly air temperature (A–C) and daily light integral (DLI; D–F) for each treatment. Environmental conditions were measured at canopy height. Treatment spectral characteristics are displayed in Fig. V-1B and Table V-1.

Chamber covering material

Figure V-4. Representative plants grown under various films with different spectral transmissions or no cover. The spectral characteristics under each treatment are in Fig. V-1B and Table V-1. Representative photos of lettuce, tomato, and floriculture crops were taken after 21, 75, and 40 d after transplant into chambers, respectively.
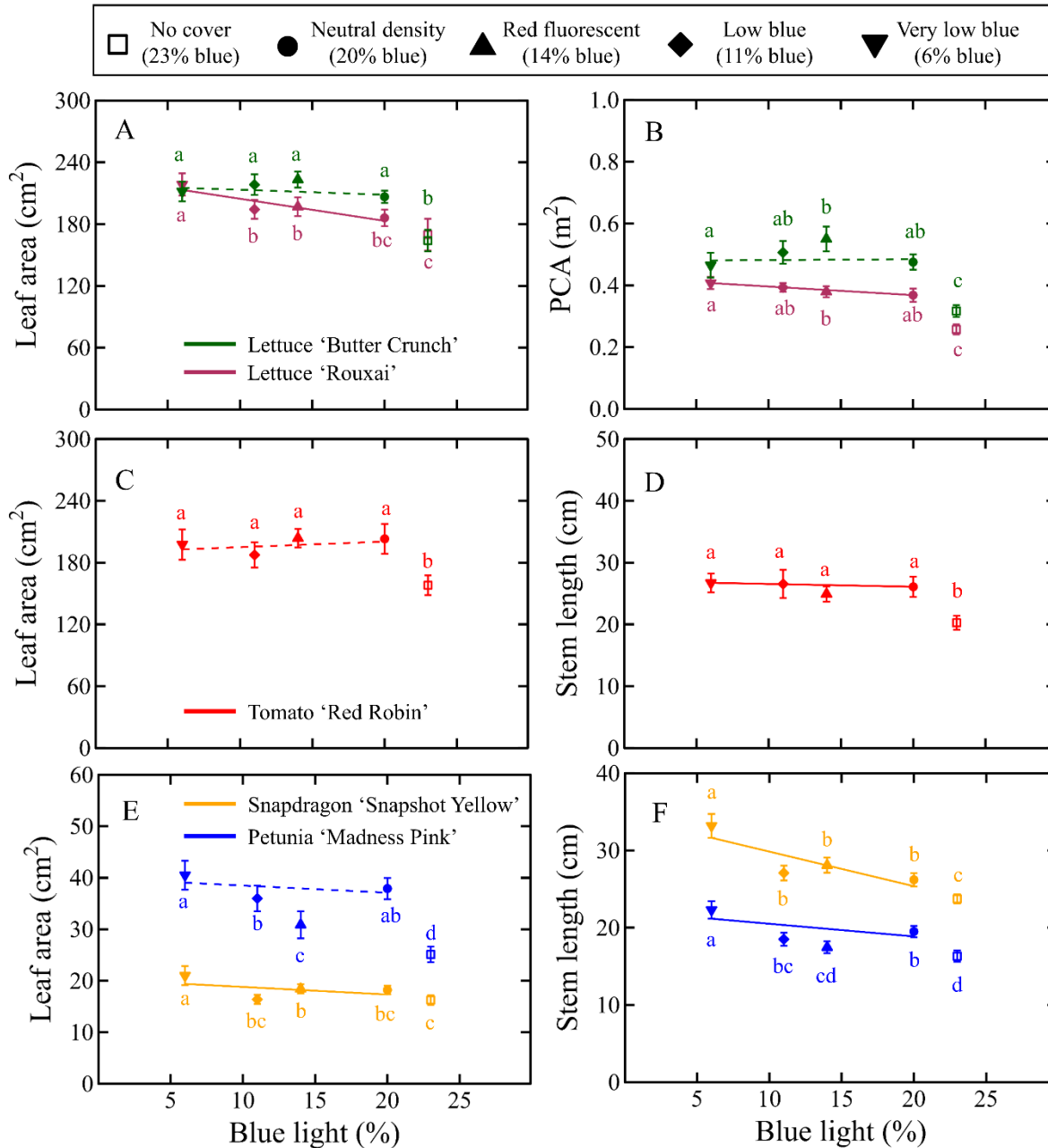
Figure V-5. Key growth metrics for lettuce 'Rouxai' and 'Butter Crunch' (A and B), tomato 'Red Robin' (C and D), and petunia 'Madness Pink' and snapdragon 'Snapshot Yellow' (E and F) as a function of the percentage of blue (400–499 nm) light in the transmitted spectrum of each treatment. Values indicate means ± 95% confidence intervals. The sample size for lettuce, tomato, and floriculture crops were 20, 24, and 25, respectively. Different letters within each crop are significantly different by Tukey's honestly significant difference test ($P < 0.05$). Regressions were fit through the neutral-density and two photoselective treatments (i.e., the red-fluorescent and greenhouse control treatments were omitted from the regression analysis). Regression equations are displayed in Tables V-8–12. Regressions with solid lines are significant at $P < 0.05$ and dashed lines are not.

Chamber covering material

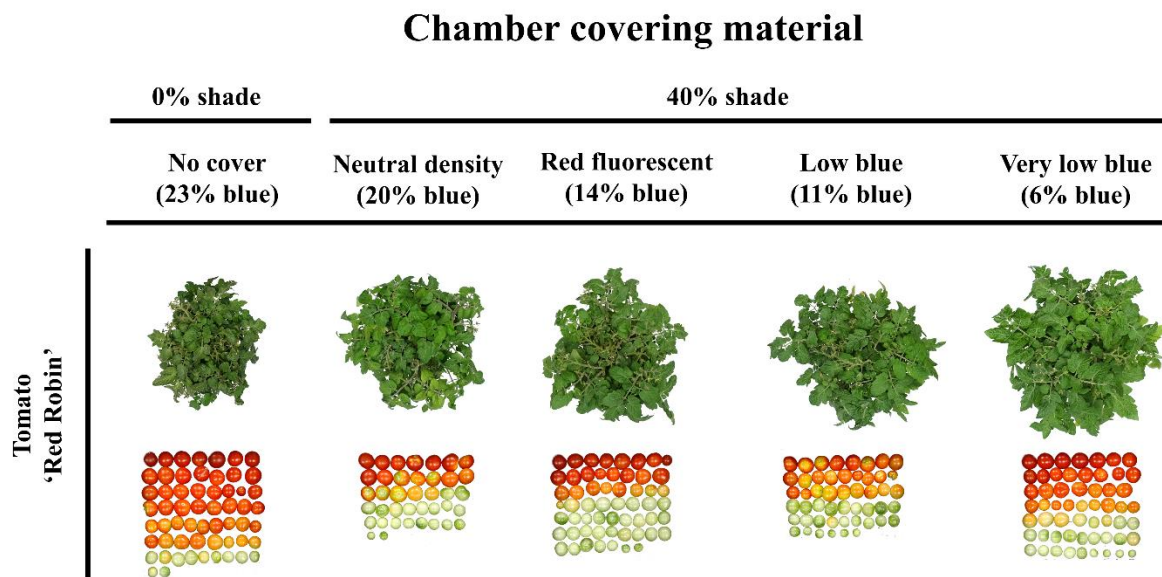| 0% shade	40% shade			
No cover (23% blue)	**Neutral density (20% blue)**	**Red fluorescent (14% blue)**	**Low blue (11% blue)**	**Very low blue (6% blue)**

Figure V-6. Representative tomato plants and fruits grown under various covers with different spectral characteristics or no cover. The spectral characteristics of each treatment are displayed in Fig. V-1B andTable V-1.
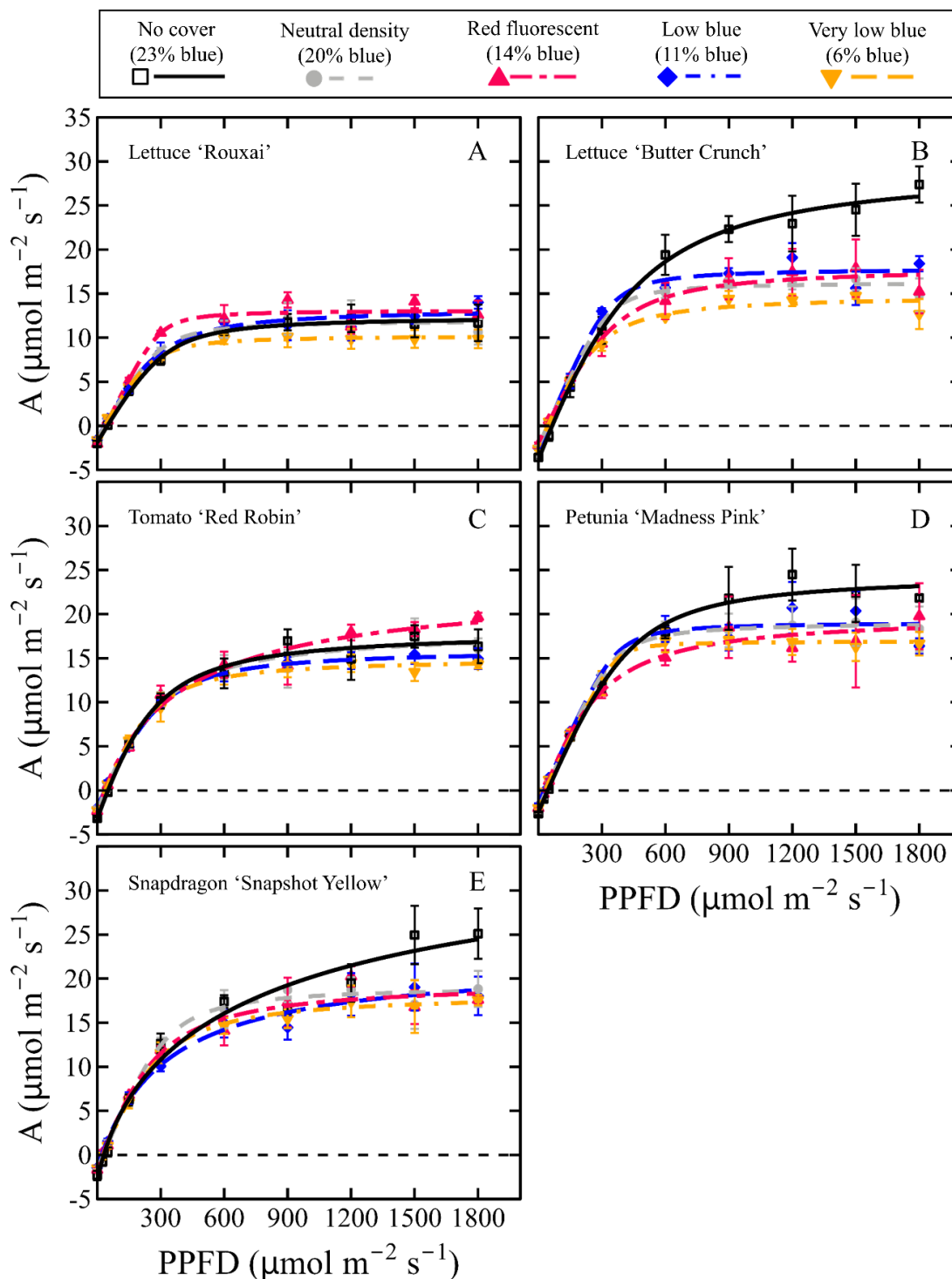
Figure V-7. Instantaneous photosynthesis measurements were used to generate light response curves for each crop. Each plot is photosynthetic rate (A) as a function of photosynthetic photon flux density (PPFD; 400–700 nm). Values represent averages ± 95% confidence intervals (n=3). Regressions were fit according to the model by Marshall and Biscoe (1980). Regression parameters are displayed in Table V-1.
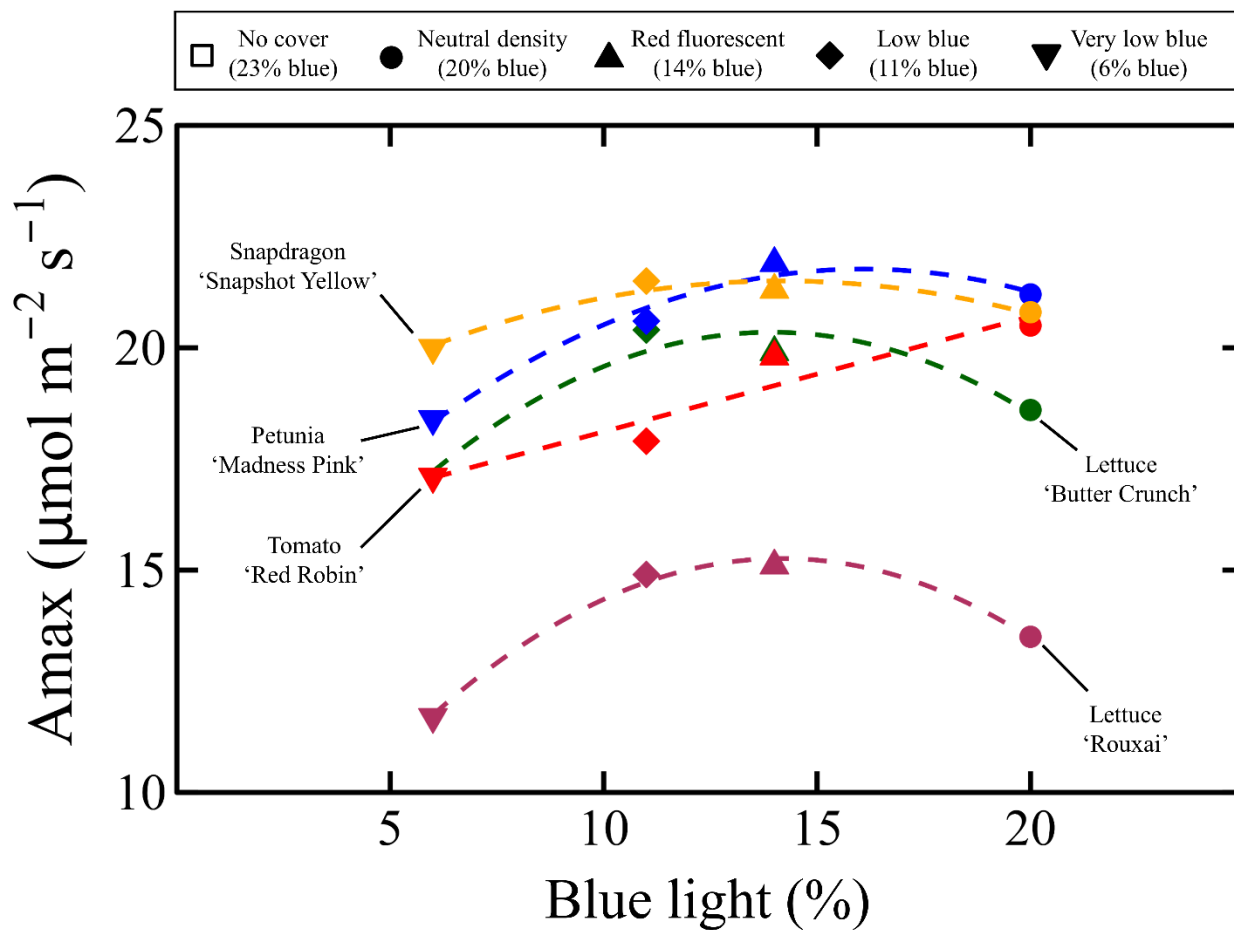
172

Figure V-8. Maximum photosynthetic rate (A_{max}) for lettuce 'Rouxai' and 'Butter Crunch', tomato 'Red Robin', and petunia 'Madness Pink' and snapdragon 'Snapshot Yellow' as a function of the percentage of blue (400–499 nm) photons in the transmission spectrum of each treatment. Amax was derived from light response curves displayed in Fig. V-5 and Table V-1.
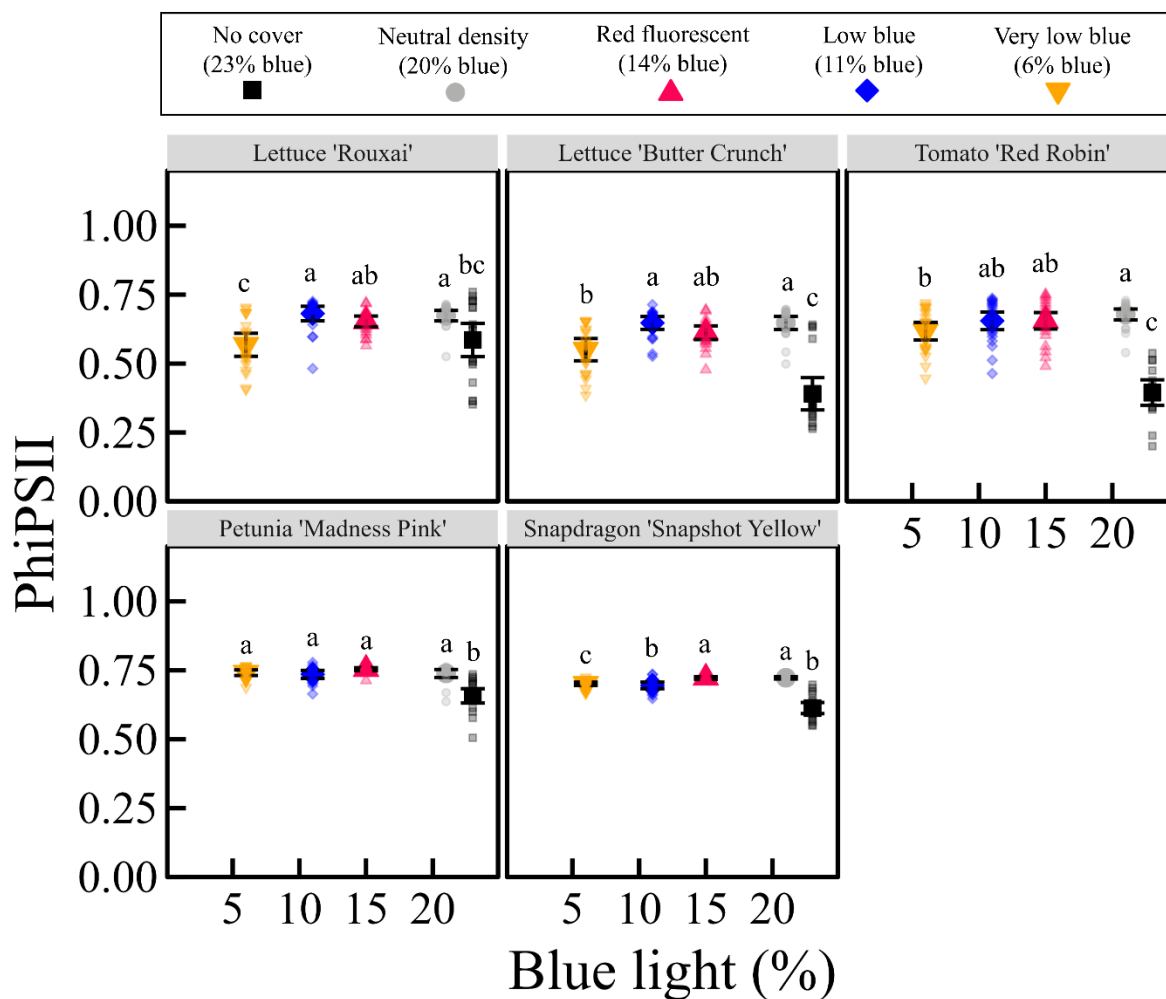
Figure V-9. The average quantum yield of photosystem II (PhiPSII) of leaves near the top of the canopy on a cloudless day at solar noon (n=20) as a function of the percentage of blue (400–499 nm) in the transmission spectrum of each treatment. The spectral characteristics of each treatment are displayed in Fig. V-1B and Table V-1. Different letters within each crop are significantly different by Tukey's honestly significant difference test $P < 0.05$. Average values are displayed in Table V-14.
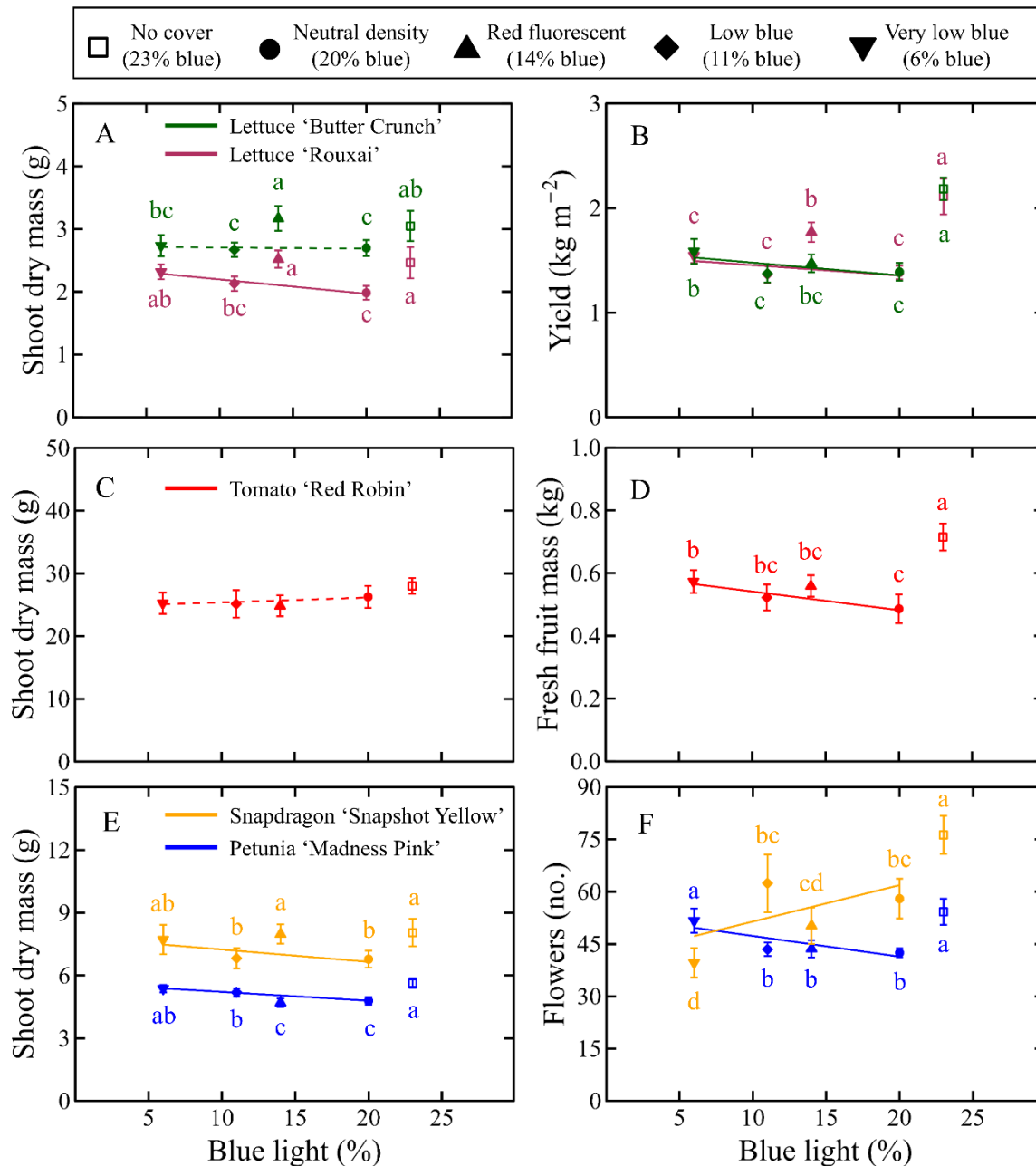
Figure V-10. Key growth metrics for lettuce 'Rouxai' and 'Butter Crunch' (A and B), tomato 'Red Robin' (C and D), and petunia 'Madness Pink' and snapdragon 'Snapshot Yellow' (E and F) as a function of the percentage of blue (400–499 nm) light in the transmitted spectrum of each treatment. Values indicate means ± 95% confidence intervals. The sample size for lettuce, tomato, and floriculture crops were 20, 24, and 25, respectively. Different letters within each crop are significantly different by Tukey's honestly significant difference test ($P < 0.05$). Regressions were fit through the neutral-density and two photoselective treatments (i.e., the red-fluorescent and greenhouse control treatments were omitted from the regression analysis). Regression equations are displayed in Tables V-8–12. Regressions with solid lines are significant at $P < 0.05$ and dashed lines are not.
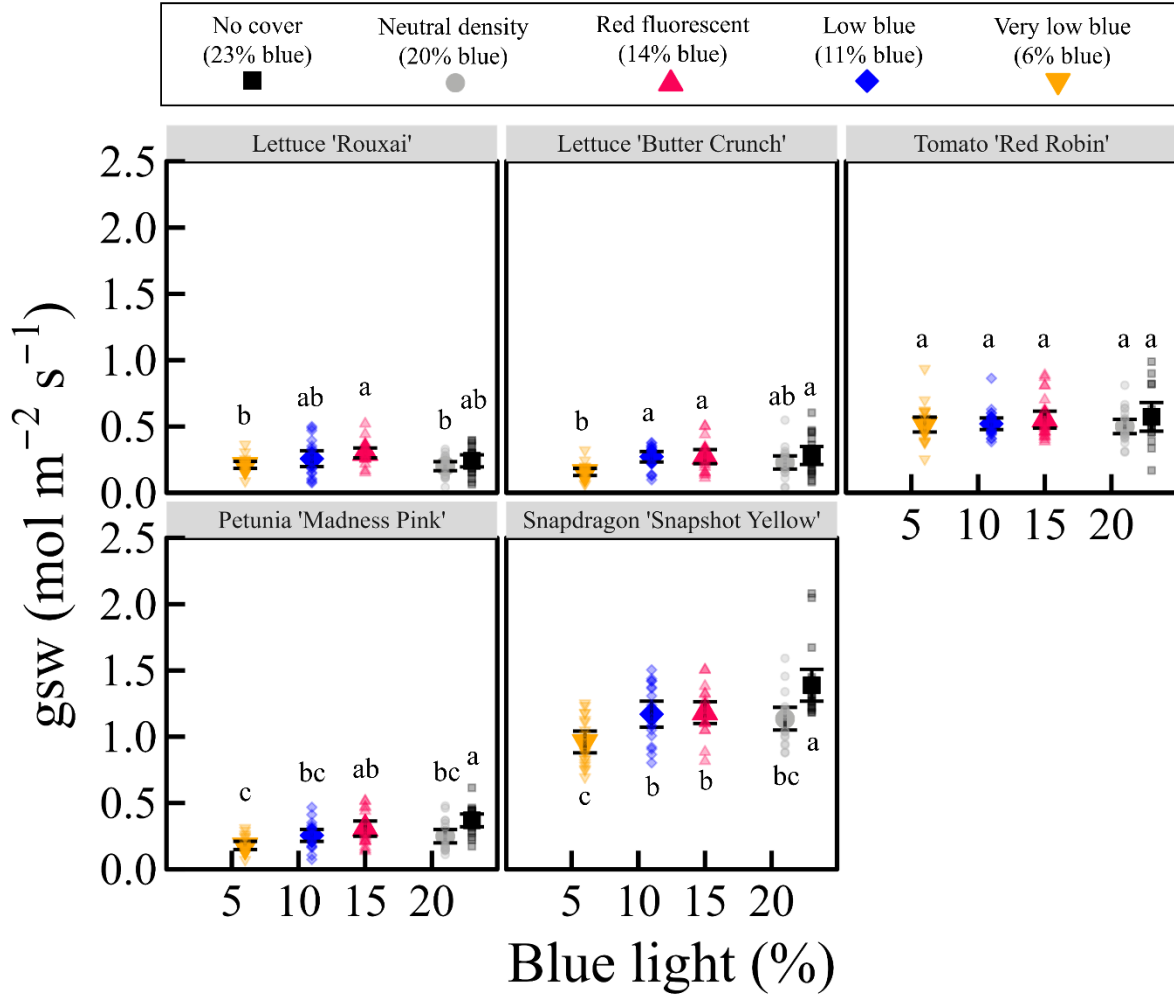
175

Figure V-11. The average stomal conductance (g_{sw}) of leaves near the top of the canopy on a cloudless day at solar noon (n=20) as a function of the percentage of blue (400–499 nm) in the transmission spectrum of each treatment. The spectral characteristics of each treatment are displayed in Fig. V-1B and Table V-1. Different letters within each crop are significantly different by Tukey's honestly significant difference test $P < 0.05$. Average values are displayed in Table V-14.